

5-2016

Identification of host factors required for *Yersinia pestis* macrophage intracellular survival and their impact on vacuole maturation, acidification and trafficking.

Michael Graylin Connor
University of Louisville

Follow this and additional works at: <https://ir.library.louisville.edu/etd>

Part of the [Bacteriology Commons](#), [Cell Biology Commons](#), [Pathogenic Microbiology Commons](#), and the [Systems Biology Commons](#)

Recommended Citation

Connor, Michael Graylin, "Identification of host factors required for *Yersinia pestis* macrophage intracellular survival and their impact on vacuole maturation, acidification and trafficking." (2016). *Electronic Theses and Dissertations*. Paper 2378.
<https://doi.org/10.18297/etd/2378>

This Doctoral Dissertation is brought to you for free and open access by ThinkIR: The University of Louisville's Institutional Repository. It has been accepted for inclusion in Electronic Theses and Dissertations by an authorized administrator of ThinkIR: The University of Louisville's Institutional Repository. This title appears here courtesy of the author, who has retained all other copyrights. For more information, please contact thinkir@louisville.edu.

IDENTIFICATION OF HOST FACTORS REQUIRED FOR
YERSINIA PESTIS MACROPHAGE INTRACELLULAR SURVIVAL
AND THEIR IMPACT ON VACUOLE MATURATION,
ACIDIFICATION AND TRAFFICKING

Dissertation by:

Michael Graylin Connor

B.S., Lees-McRae College, 2010

M.S., University of Louisville, 2012

A Dissertation

Submitted to the Faculty of the

School of Medicine of the University of Louisville

In partial fulfillment of the requirements for the degree of:

Doctor of Philosophy in Microbiology and Immunology

Department of Microbiology and Immunology

University of Louisville School of Medicine

Louisville, KY

May 2016

Copyright 2016 by Michael Graylin Connor
All rights reserved

IDENTIFICATION OF HOST FACTORS REQUIRED FOR
YERSINIA PESTIS MACROPHAGE INTRACELLULAR SURVIVAL
AND THEIR IMPACT ON VACUOLE MATURATION,
ACIDIFICATION AND TRAFFICKING

Dissertation by:

Michael Graylin Connor

B.S., Lees-McRae College, 2010

M.S., University of Louisville, 2012

A Dissertation Approved on

April 1, 2016

by the following Dissertation Committee:

Dissertation Director
Matthew B. Lawrenz

Donghoon Chung

Yousef Abu-kwaik

Micah Worley

Jill Suttles

DEDICATION

Over my life I have been challenged by my family, friends and coaches to pursue the highest caliber of competition and life pursuits. From these experiences I have learned dedication, work ethic and perseverance. Of the greatest experiences, I was taught failure is but a measure of will, work, and resilience. The works to follow are a testament to those people throughout my life that have witnessed both my triumphs and failures with equal passion to inspire me to accomplish my dreams.

ACKNOWLEDGEMENTS

First off, I would like to thank Matt Lawrenz for allowing me the opportunity to study plague in his lab, and dealing with my excited personality. I genuinely appreciate Matt's mentorship and the opportunities he has given me to develop as a scientist. Matt was not only an excellent scientific mentor, but a great friend over the years and I am humbled to consider him as such. The Lawrenz lab members Jarrod Pennington, Tiva VanCleave, and Amanda Pulsifer are great friends and my adoptive family. Finally, Marlene Steffen for making the research resources at my disposal work; even at odd hours and in the snow.

I would like to thank my committee members, especially Hoon and Yousef for their conversations. I also would like to thank Tom Mitchell, Carolyn Casella, Jim Graham, Rob Hancock, Chris Price, Jeremy Camp, Jared and Cortney "Mushill", Nikki Warner, and Maria Gutierrez. Your friendships, conversations, and time have been some of the greatest experiences of my life.

Finally, I would like to thank my family. Through everyone's endless patience, support and the occasional push, I have accomplished what began as merely a thought fifteen years ago.

ABSTRACT

YERSINIA PESTIS EXPLOITS HOST ENDOCYTIC RECYCLING AND VESICULAR TRAFFICKING FOR INTRACELLULAR SURVIVAL

Michael G. Connor

April 1, 2016

Y. pestis is a facultative intracellular pathogen and the causative agent of plague. This bacterium, while most noted for the Black Death during the European 14th century, is not a historic pathogen but a re-emerging pandemic with both domestic and global impact. *Y. pestis* is capable of colonizing the macrophage, and actively subverts phagolysosome maturation to establish a replicative niche known as the *Yersinia* containing vacuole (YCV). The exploited host factors required to support the YCV are unknown. Here we identified a comprehensive list of host factors required for *Y. pestis* survival through a genome-wide RNAi high-throughput screen. We further identify that avoidance of the phagolysosome requires early recruitment of Rab1b and Rab4a on the YCV. Finally, we show that during intracellular infection *Y. pestis* sequesters Rab11b to the YCV to stall host cell recycling and support bacterial replication after 8 hours post-infection. These data identify the first host factors required for *Y. pestis* survival within the macrophage, avoidance of phagolysosome maturation, and a novel role for exploiting the host recycling pathway for bacterial replication.

TABLE OF CONTENTS

DEDICATION	iii
ACKNOWLEDGEMENTS	iv
ABSTRACT	v
LIST OF FIGURES.....	x
LIST OF TABLES.....	xi
Chapter 1:	1
<i>YERSINIA PESTIS</i> AND THE PLAGUE	1
INTRODUCTION	2
IMMUNE EVASION BY <i>Y. PESTIS</i>	5
<i>Y. PESTIS</i> INTERACTIONS WITH PROFESSIONAL PHAGOCYTES	6
SUBVERSION OF THE PHAGOLYSOSOME BY OTHER PATHOGENS.....	8
<i>Rab GTPases Modulation by Mycobacterium tuberculosis</i>	9
<i>Rab GTPase Modulation by Legionella pneumophila</i>	9
RNAI SCREENS IDENTIFY NOVEL PATHOGENESIS MECHANISMS	10
PRINCIPLES OF RNAI SCREENING	11
<i>Screen Class</i>	11
<i>Species of Screen</i>	12
<i>RNAi Method</i>	12
<i>Screen Format</i>	12
<i>Readout</i>	12
PROPOSED RESEARCH	13
FIGURES AND FIGURE LEGENDS	15
TABLES.....	17
Chapter 2:	18
DEVELOPMENT OF BIOLUMINESCENT BIOREPORTERS FOR <i>IN VITRO</i> AND <i>IN VIVO</i>	
TRACKING OF <i>YERSINIA PESTIS</i>	18
OVERVIEW	19
INTRODUCTION	19
RESULTS	22
<i>Construction of a chromosomal luciferase reporter system in Y. pestis</i>	22
<i>Using the Y. pestis Lux reporters as bioreporters</i>	23
<i>Differentiation between bacterial phenotypes in vitro using Y. pestis Lux bioreporters</i>	24
<i>In vivo imaging of bubonic plague</i>	25
<i>In vivo imaging of pneumonic plague</i>	26
<i>Differences in phenotypes can be detected in vivo using the Lux_{P_{cys}ZK} bioreporter</i>	26
DISCUSSION.....	27
MATERIAL AND METHODS	33
<i>Bacterial strains, plasmids, and growth conditions</i>	33
<i>Survival of Y. pestis in the presence of antimicrobial compounds</i>	34

<i>Intracellular survival assays</i>	35
<i>In vivo imaging</i>	35
FIGURES AND FIGURE LEGENDS	37
TABLES	48
Chapter 3:	49
YERSINIA PESTIS REQUIRES HOST RAB1B FOR SURVIVAL IN MACROPHAGES	49
AUTHOR SUMMARY	50
OVERVIEW	50
INTRODUCTION	51
RESULTS:	55
<i>Rab1b is required for Y. pestis survival in macrophages</i>	55
<i>Rab1b is not required for Y. pestis invasion of macrophages</i>	56
<i>Rab1b is required for Y. pestis to avoid YCV acidification</i>	57
<i>Rab1b is necessary for Y. pestis to avoid fusion with the lysosome</i>	58
<i>Rab1b is not required for early Y. pestis association with LC3</i>	59
<i>Rab1b is recruited to the YCV during macrophage infection</i>	59
<i>Disruption of the secretory pathway does not alter Y. pestis survival or inhibition of YCV acidification</i>	60
<i>Rab1b inhibition results in increased acidification of the Legionella containing vacuole</i>	61
DISCUSSION.....	61
MATERIALS AND METHODS.....	66
<i>Bacterial strains, plasmids, and macrophages</i>	66
<i>Transfection of macrophages</i>	66
<i>Bacterial infection of macrophages</i>	67
<i>Immunofluorescent staining and confocal microscopy</i>	67
<i>Statistics</i>	67
FIGURE AND FIGURE LEGENDS	69
SUPPORTING INFORMATION	79
TABLES	82
Chapter 4:	83
GENOME-WIDE RNAI HIGH-THROUGHPUT SCREEN IDENTIFIES THAT YERSINIA PESTIS EXPLOITS THE HOST ENDOCYTIC RECYCLING PATHWAY FOR INTRACELLULAR SURVIVAL	83
INTRODUCTION	84
RESULTS	87
<i>Development of a high throughput assay to monitor the impact of host gene RNAi on Y. pestis intracellular survival</i>	87
<i>Genome-wide siRNA screen identifies host cell signal transduction, transport and localization pathways are required for Y. pestis intracellular survival</i>	88
<i>Host cell recycling is essential for Y. pestis survival</i>	90
<i>Y. pestis requires Rab4a of the recycling pathway to avoid YCV acidification</i>	91
<i>The Yersinia containing vacuole acquires recycling endosome markers</i>	92
<i>Y. pestis infection stalls host recycling</i>	93
<i>Stalling host cell recycling is required for Y. pestis replication</i>	94
DISCUSSION.....	95
MATERIALS AND METHODS:.....	100

<i>Bacterial strains, plasmids, siRNA and transfection of macrophages.</i>	100
<i>qRT-PCR, Western blot and Cell Viability</i>	100
<i>Bacterial infection of macrophages.</i>	101
<i>Bioinformatic analysis.</i>	101
<i>TfR recycling and Acidification assay, Immunofluorescent staining, and confocal microscopy</i>	101
<i>Statistics.</i>	102
FIGURES AND FIGURE LEGENDS	104
TABLES.....	123
Chapter 5:	128
GENOME-WIDE RNAI HIGH-THROUGHPUT SCREEN IDENTIFIES POTENTIAL GENES IMPACTING <i>Y. PESTIS</i> INVASION.....	128
INTRODUCTION	129
RESULTS:	132
<i>Elevated RLU at 20 min post-infection indicates a defect in Y. pestis invasion.</i>	132
<i>Identifying invasion dataset from the Genome-wide RNAi HTS</i>	133
DISCUSSION.....	133
MATERIALS AND METHODS.....	138
<i>Bacterial strains, siRNA transfection of macrophages.</i>	138
<i>Cytochalasin D treatment.</i>	138
<i>Bacterial infection of macrophages</i>	138
<i>Bioinformatics Analysis</i>	139
<i>Statistics</i>	139
FIGURES AND FIGURE LEGENDS	140
TABLES.....	142
Chapter 6:	166
DISCUSSION AND FUTURE DIRECTIONS	166
RESEARCH SUMMARY.....	167
IMPLICATIONS OF MY RESEARCH AND FUTURE DIRECTIONS.....	167
<i>Developing new pathway analysis techniques for RNAi screens through mapping</i> <i>interactions</i>	167
<i>Are Rab1b and Rab4a only required to avoid YCV acidification?</i>	168
<i>Does the Timing of Rab Recruitment Impact YCV Maturation?</i>	169
<i>How does Y. pestis recruit Rab GTPases to the YCV?</i>	170
<i>How do Y. pestis interactions with the host cell recycling pathway contribute to intracellular</i> <i>survival?</i>	171
<i>Extending our Rab11b studies suggests a universal mechanism for intracellular pathogens</i>	172
<i>Does stalling of host recycling potentially impact pro-inflammatory responses?</i>	172
<i>Does Y. pestis use eukaryotic receptors to target the recycling pathway?</i>	174
<i>Is spatial location within the cell important for intracellular survival?</i>	175
<i>Potential Biological Impact of Y. pestis Low Calcium Response in Macrophages</i>	176
FIGURES AND FIGURE LEGENDS	178
TABLES.....	179
REFERENCES.....	180

APPENDIX	197
CHAPTER II	197
<i>Acknowledgements</i>	197
CHAPTER III	197
<i>Acknowledgements</i>	197
DEPARTMENT OF MICROBIOLOGY AND IMMUNOLOGY CHAIRMAN'S CITATION.....	198
CURRICULUM VITAE.....	199

LIST OF FIGURES

FIGURE 1—1 SUMMARY OF <i>Y. PESTIS</i> INTRACELLULAR SURVIVAL.....	15
FIGURE 1—2 RNAI SCREEN DEVELOPMENT WORKFLOW.....	16
FIGURE 2—1 SENSITIVITIES OF CHROMOSOMAL LUX REPORTERS.....	37
FIGURE 2—2 CORRELATION BETWEEN BIOLUMINESCENCE AND BACTERIAL NUMBER.....	38
FIGURE 2—3 LUX REPORTERS DO NOT IMPACT FITNESS OF <i>Y. PESTIS</i>	39
FIGURE 2—4 USE OF LUXPTOLC TO MONITOR SURVIVAL OF <i>Y. PESTIS</i> IN THE PRESENCE OF ANTIMICROBIAL COMPOUNDS.....	40
FIGURE 2—5. SURVIVAL OF <i>Y. PESTIS</i> LUX REPORTERS IN MACROPHAGES.....	41
FIGURE 2—6. DISSEMINATION OF <i>Y. PESTIS</i> DURING BUBONIC INFECTION.....	42
FIGURE 2—7. CONTINUED BIOLUMINESCENCE FROM INOCULATION SITE.....	44
FIGURE 2—8. PROGRESSION OF PNEUMONIC INFECTION.....	46
FIGURE 2—9. EXTENDED IMAGING OF ANIMALS INTRANASALLY INFECTED WITH Δ PLA.....	47
FIGURE 3—1. RAB1B KNOCKDOWN INHIBITS THE SURVIVAL OF <i>Y. PESTIS</i> WITHIN MACROPHAGES.....	69
FIGURE 3—2. RAB1B KNOCKDOWN DOES NOT IMPACT <i>Y. PESTIS</i> INVASION OF MACROPHAGES.....	71
FIGURE 3—3. RAB1B KNOCKDOWN ALTERS YCV ACIDIFICATION.....	72
FIGURE 3—4. RAB1B KNOCKDOWN INCREASES YCV ASSOCIATION WITH LAMP1.....	74
FIGURE 3—5. RAB1B KNOCKDOWN DOES NOT AFFECT YCV ASSOCIATION WITH LC3.....	75
FIGURE 3—6. RAB1B IS RECRUITED TO THE YCV.....	76
FIGURE 3—7. INHIBITION OF THE SECRETORY PATHWAY DOES NOT INHIBIT <i>Y. PESTIS</i> INTRACELLULAR SURVIVAL.....	77
FIGURE 3—8. KNOCKDOWN OF RAB1B INCREASES <i>L. PNEUMOPHILA</i> LCV ACIDIFICATION.....	78
FIGURE 3—9. S1 TRANSFECTION WITH RAB1B siRNA IN MACROPHAGES.....	79
FIGURE 3—10. S2 GROWTH AT 37°C DOES NOT ALTER INTRACELLULAR SURVIVAL OF <i>Y. PESTIS</i>	80
FIGURE 3—11. S3 RAB1B KNOCKDOWN INHIBITS THE SURVIVAL OF ENTERIC <i>YERSINIA</i> WITHIN MACROPHAGES.....	81
FIGURE 4-1. RNAI-BASED ASSAY TO IDENTIFY HOST FACTORS REQUIRED FOR <i>Y. PESTIS</i> INTRACELLULAR SURVIVAL.....	105
FIGURE 4-2. IDENTIFICATION OF HOST FACTORS REQUIRED FOR <i>Y. PESTIS</i> INTRACELLULAR SURVIVAL.....	106
FIGURE 4-3. CLUEGO CLUSTERING OF VALIDATED GENES IMPACTING <i>Y. PESTIS</i> INTRACELLULAR SURVIVAL.....	107
FIGURE 4-4. IDENTIFICATION OF RAB GTPASE INTERACTIONS WITHIN PRIMARY SCREEN HITS.....	109
FIGURE 4-5. HOST RECYCLING INHIBITS <i>Y. PESTIS</i> INTRACELLULAR SURVIVAL.....	111
FIGURE 4-6. RNAI INHIBITION OF RAB4A AND RAB11B DOES NOT IMPACT THE PHAGOLYSOSOME.....	112
FIGURE 4-7. RAB4A OF THE RECYCLING PATHWAY IS ESSENTIAL FOR <i>Y. PESTIS</i> TO AVOID THE PHAGOLYSOSOME.....	114
FIGURE 4-8. <i>Y. PESTIS</i> ACQUIRES RECYCLING ENDOSOME MARKERS RAB4A AND RAB11B.....	115
FIGURE 4-9. RECYCLING ASSAY MEASURES TFR KINETICS.....	117
FIGURE 4-10. <i>Y. PESTIS</i> INFECTION STALLS HOST CELL RECYCLING.....	119
FIGURE 4-11. ANT-TFR ANTIBODY DOES NOT IMPACT <i>Y. PESTIS</i> INTRACELLULAR GROWTH.....	120
FIGURE 4-12. STALLING HOST CELL RECYCLING IS REQUIRED FOR <i>Y. PESTIS</i> REPLICATION.....	122
FIGURE 5-1. ELEVATED RLU IS CONSISTENT AND PROMOTER INDEPENDENT.....	140
FIGURE 5-2. ELEVATED RLU IS AN INVASION DEFECT.....	141
FIGURE 6-1. SUMMARY MODEL OF OUR FINDINGS.....	178

LIST OF TABLES

TABLE 1-1. PATHOGENS SCREENED USING RNAI	17
TABLE 2-1. STRAINS AND PLASMIDS USED IN THIS WORK.....	48
TABLE 3--1. TABLE S1 BACTERIAL STRAINS USED IN THESE STUDIES.....	82
TABLE 4-1. 135 VALIDATED GENES	123
TABLE 4-2. BACTERIAL STRAINS	125
TABLE 4-3. siRNA.....	126
TABLE 4-4. QRT-PCR PRIMERS.	127
TABLE 5-1. ALL PUTATIVE INVASION TARGETS.	142
TABLE 5-2. PANTHER IDENTIFIED RECEPTOR/RECEPTOR ACTIVITY HITS.	163
TABLE 6-1. RAB11 (A/B) PATHOGEN & TOXIN ASSOCIATION.....	179

CHAPTER 1:
YERSINIA PESTIS AND THE PLAGUE

Introduction

Yersinia pestis is the etiological agent of the disease known as plague. *Y. pestis* has caused three major plague pandemics throughout human history. The three pandemics are the “Justinian Plague”, the “Black Death”, and the “Modern Pandemic”. Of the three, the most noted is the Black Death of the 14th century. This outbreak killed one third of the European population, and took over 100 years for the population to recover [1-3]. *Y. pestis* is a zoonotic pathogen, cycling between the rodent (reservoir host) and the flea transmission vector [1]. The bacterium is endemic throughout rodent populations around the world, including the western United States [4, 5]. Incidence of human plague has been increasing, suggesting that plague is a re-emerging pathogen, and not a historic disease [5, 6]. *Y. pestis* has been used as a biological weapon and is considered by the U.S. federal government as a high risk for future use as a bioterrorism agent (*Y. pestis* is a Tier 1 Category A Select Agent) [7].

Human plague manifests in one of three forms: bubonic, septicemic, or pneumonic plague [8-11]. Bubonic plague is the most common and naturally occurring form of disease. During bubonic plague, bacteria are transmitted to humans through an infectious bite from a flea. From the site of inoculation *Y. pestis* traffics to the draining lymph node. Here the bacteria colonize and replicate to high titer. Infected lymph nodes swell into the hallmark “bubo”, a fist-sized lump that resembles a cyst [1]. Bubonic plague is 40-60% lethal between 5-10 days post exposure without antibiotic treatment. Untreated bubonic plague can progress to septicemic plague as the bacteria disseminate throughout the host lymphatics and enter the bloodstream [12, 13]. During a septicemic infection the bacteria rapidly spread throughout the host colonizing the spleen, liver and lungs [11]. Lung colonization results in development of pneumonic plague [1], where the bacteria can be transmitted person to person via aerosolized bacteria. Person to person transmission results in primary pneumonic plague and death can occur within 72 hours. Pneumonic and septicemic plagues are 100% lethal at the onset of symptoms [1, 14]. In all three forms of disease the minimum infectious dose is believed to be 1-100 bacteria [6, 15].

The genus *Yersinia* includes *Y. pestis*, *Y. pseudotuberculosis* and *Y. enterocolitica* [16-19]. In the genus, *Y. pestis* is the only species that causes an acute highly fatal infection in the absence

of timely diagnosis and treatment [14, 20]. Out of the three species *Y. pestis* is the only vector-borne (flea) pathogen [1, 19]. *Y. pestis* began its pathogenic evolution from *Y. pseudotuberculosis* through the acquisition of two additional plasmids (pMT1 & pPCP) and genomic rearrangement approximately 1,000 to 20,000 years ago [16, 18]. There are three biovars of *Y. pestis*, Antiqua, Orientalis and Medievalis [1, 19]. Of these biovars only Orientalis strains are widespread. Each biovar was once believed to represent pandemic outbreaks of plague throughout human history; with Antiqua representing the Justinian Plague, Medievalis the Black Death (14th century), and Orientalis the current pandemic - which began in China [21]. However, given the recent sequence data from victims of the Black Death, and Justinian plagues show that an Orientalis strain is the culprit of all plague outbreaks throughout human history [21-23]. The *Y. pestis* strain "Colorado 92" (CO92) is a clinical isolate representing the Orientalis biovar [9].

By comparing the genomic sequences of *Y. pestis* across the genus, it was determined that the bacterium is currently undergoing genome reduction and the evolutionary niche it now occupies is potentially filled [16, 18]. The genome of *Y. pestis* has exchanged genes for various enteric adhesion, invasion and dissemination effectors in favor of genes to maintain transmission between the flea and mammal, such as plasminogen activator (*pla*) and murine toxin (*ymt*) [1, 16, 18, 19]. However, *Y. pestis* still maintains the pCD1 encoded Ysc type three secretion system (T3SS), which is conserved across the genus [1, 16, 18, 19]. Two of the major genes lost in *Y. pestis* are *yadA* and *invasin*. The *yadA* gene is an adhesion that interacts with the extracellular matrix to promote attachment of *Y. pseudotuberculosis* and *Y. enterocolitica* to the host cell [24-26]. *Invasin* is a highly efficient molecule that binds β 1-intergrins to facilitate uptake of both *Y. pseudotuberculosis* and *Y. enterocolitica* by the host through "outside-in" signaling [26-29]. Even though *Y. pestis* lost these conserved factors the bacterium acquired additional virulence factors that contribute heavily to the organism's life cycle. To highlight this, the Plasminogen activator, *pla*, is protease that is capable of cleaving C3 complement and degrading T3SS effector Yersinia outer membrane proteins (Yops). These functions allow for *Y. pestis* dissemination throughout the host, and dampening of Yop activation of innate immune responses [30-34]. *Pla* is encoded on pPCP [1, 16, 18, 19, 35, 36]. The Murine toxin, *ymt*, is required for transmission from the flea vector to in

mice, and resides on pMT1 [1, 16, 18, 19, 37, 38]. Mutants of *ymt* result in a 10-fold attenuation in LD₅₀ when mice are intraperitoneally challenged [39-42]. Together, this highlights that *Y. pestis* is a young bacterium of *Y. pseudotuberculosis* descent that is undergoing genomic flux to further streamline its genome to adapt to both the flea and mammalian host.

Plague is not a historical pathogen, but rather a re-emerging disease of great health concern domestically and globally. Globally, plague naturally occurs in the rodent population on every inhabited continent except Australia [5]. The World Health Organization estimates ~2,000 to 4,000 cases of human plague occur annually [5, 6, 14]. A recent review by Butler T et al., 2013, ranked the top twelve countries by human plague cases; China and the United States are seven and eleven, respectively [5]. In both cases the countries have high populations, modern health care, and extensive urbanization. The highly developed nature of these countries highlights the potential for a devastating plague outbreak, and stresses the necessity to understand early pathogenesis to enhance our preventative measures.

To date, there is no Federal Drug Administration (FDA) approved vaccine for *Y. pestis* [5, 6, 14, 19, 20, 43]. There are three vaccine candidates that target LcrV, the tip of the pCD1 encoded type-three secretion system, and/or the F1 capsule, encoded by *caf1* on the pMT1 plasmid. The first two vaccines are subunit vaccines using F1 and LcrV independently and the third is a recombinant fusion protein of rF1/LcrV [19, 20, 43, 44]. These vaccine candidates are currently being comprehensively tested for their efficacy in both bubonic and pneumonic plague in multiple mammalian models. While these vaccines have previously been tested in various animal models, the robustness of lasting T and B cell responses remain undetermined (for review see [20, 43, 44]). Vaccine development is slow, in part, because of the *Y. pestis* life cycle. A major concern with current vaccines is isolation of F1 and pCD1 negative strains naturally from the environment [1, 19, 43]. These strains spontaneously lose the capsule and the T3SS. Additionally, capsule negative strains still remain lethal in the mammalian host [1, 19].

Y. pestis is naturally maintained through reoccurring transmission cycles between the flea vector and rodents [1, 45]. Humans become infected with *Y. pestis* by their contact with infected

animals and are accidental hosts in the bacterium's life cycle [1, 8, 9, 11]. Human plague progression is rapid, between 3-10 days, and outpaces the adaptive immune response (see reviews [1, 5, 13, 14]). The swift pathogenesis is a hallmark of plague and highlights the critical role innate immunity plays in controlling disease. The natural progression of disease begins with the inoculation of the bacteria from an infected flea bite into the sub-dermis of the host [1, 42, 46-48]. From this initial site of infection, *Y. pestis* disseminates to the draining lymph node and throughout the lymphatic system [49]. During this process, *Y. pestis* rapidly suppresses the immune system, turns on several temperature dependent virulence factors, and replicates within the host.

Y. pestis has several well-characterized, mammalian-specific, antiphagocytic virulence factors, like the T3SS, secreted Yop effectors, lipopolysaccharide (LPS), and Caf1 capsule (see review [1]). Interestingly, at initial colonization of the mammalian host these virulence factors are down regulated [1]. Without these antiphagocytic tools *Y. pestis* is easily engulfed by macrophages and neutrophils during initial colonization [49-52]. Neutrophils are readily capable of killing the bacteria, however uptake of *Y. pestis* by a macrophage results in the survival of the bacterium [51, 53-62]. *Y. pestis* rapidly subverts the innate immune defenses within these cells and establishes a replicative niche termed the *Yersinia* containing vacuole (YCV) [54, 55, 57, 59].

Immune evasion by *Y. pestis*.

Y. pestis uses several virulence determinants to establish infection [1, 33, 60, 63]. The best studied of these are the *Yersinia* outer membrane proteins (Yops), which are secreted by the T3SS [32, 33, 63]. The T3SS forms a channel in the membrane of host cells that the effector Yops (Yop O, H, M, T, J and E) are translocated through [33]. Once in the cytosol, the Yops interact with host signaling pathways to prevent phagocytosis and induction of a pro-inflammatory response [32]. *Y. pestis* has been shown to selectively target macrophages, neutrophils and dendritic cells for Yop intoxication [64, 65]. Bacterial targeting of neutrophils in particular has been demonstrated to be dependent on the bacterial recognition of the host complement receptor 3 [66]. However, the T3SS of *Y. pestis* is temperature dependent and not actively expressed during initial transmission from the flea vector (26°C) into a mammalian host (37°C) [1].

A second important virulence factor for *Y. pestis* to evade the immune response is LPS [1, 67, 68]. LPS is normally recognized by TLR4 (toll-like receptor 4), a pathogen recognition receptor, found on phagocytic cells, such as dendritic cells and macrophages. LPS recognition by TLR4 triggers signaling through the TRIF and MyD88 adaptor complexes initiating pro-inflammatory innate immune responses [69-71]. This signaling cascade activates the transcription factor NF κ B and initiates production and secretion of pro-inflammatory cytokines, such as IL-1 β and IL-18 [69-71]. However, during plague infection, *Y. pestis* alters the structure of its LPS and expresses a tetra-acylated form of LPS that does not activate TLR4 [67, 68]. Furthermore, data from studies with human TLR4 indicate that *Y. pestis* LPS antagonizes TLR4 signaling, actively dampening the pro-inflammatory response, though the exact mechanism remains unclear [67, 68]. Here again, the LPS modification is temperature dependent and not present at the time of transmission.

Lastly, *Y. pestis* has an atypical capsule encoded by the *caf* operon [1, 72-74]. This capsule is comprised mainly of helical proteins that are loosely attached to the outer membrane of the bacterium [1, 72-74]. Caf1 is an antiphagocytic virulence factor which prevents phagocytosis by macrophages and monocytes [75, 76]. However, studies have demonstrated that capsule mutants are no less virulent than their wildtype counterparts, and at best display only a modest increase in LD₅₀ in mice (summary of strain LD₅₀ table 2 [1]; [39, 77]). Furthermore, *caf1* expression is regulated by temperature and active only at 37°C [78, 79].

All three of these virulence factors are specialized for the mammalian host and required for *Y. pestis* to avoid phagocytosis by innate immune cells. However, they are not expressed in the flea vector, and are temperature regulated (flea 26°C to mammal at 37°C) [1]. Because of this *Y. pestis* during colonization from the flea vector is highly susceptible to uptake by innate immune phagocytes.

Y. pestis interactions with professional phagocytes

During colonization of the mammal *Y. pestis* is inoculated into the dermis, sub-dermis or directly into the blood stream via a capillary during a flea bite [1, 42, 46]. At the site of infection there is an influx of neutrophils and macrophages [51]. These professional phagocytes are the innate immune

system's first responders to infection, and are tasked with controlling infection and priming an immune response. At the site of colonization *Y. pestis* interacts with both neutrophils and macrophages. However, neutrophils are better capable of killing the bacteria at this transitional stage in the bacteria's early pathogenesis [53, 58, 80, 81]. In contrast, when a macrophage or monocyte phagocytizes *Y. pestis*, the bacterium prevents killing within these cells and is capable of establishing an intracellular niche [51, 54, 55, 57, 59, 82, 83]. In further support of this, *Y. pestis* infected rodents and nonhuman primates show bacteria association with macrophages, but to a lesser extent neutrophils from within the same infected host [49, 53, 58, 84].

Y. pestis taken up by macrophages remain within a phagosomal compartment, but the bacteria inhibit the normal maturation of this phagosome to survive within the macrophage [57, 59, 60, 62, 63, 83, 85, 86]. While the mechanisms are not well understood, *Y. pestis* is able to actively inhibit the acidification of this YCV [59]. The YCV does not acidify and the pH remains between pH 6.5 – 7.5 throughout intracellular survival [59, 87]. In contrast to live bacteria, paraformaldehyde killed *Y. pestis* is rapidly degraded in an acidified YCVs [59, 87]. Studies have colocalized Rab7 and Cathepsin D, markers for stages of phagolysosome maturation, to ~30% of all nascent YCVs, indicating that the majority of the bacteria are not in a mature phagolysosome [86, 87]. In contrast, Rab5 and EEA1, markers for the early endosome have not been colocalized to the YCV, either due to lack of these markers on the YCV or the biogenesis of the YCV is too rapid. Approximately eight hours post infection, the phagosome is further modified, and expands into a spacious vacuole in which *Y. pestis* is able to replicate [59]. At this point in YCV biogenesis, the spacious vacuole is clearly observed in light and electron micrographs [55, 59, 62, 86]. Studies to characterize the spacious YCV have indicated this compartment acquires LC3-II, a marker of autophagosomes, as early as four hours post-infection, and autophagy potentially contributes to the metabolism of the bacteria [59, 88, 89]. Studies by Ligeon et al., using *Y. pseudotuberculosis*, show the YCV acquires VAMP3 within 30 mins post-infection and is exchanged for VAMP7 within 3 to 24 hours [89]. They further demonstrated VAMP3 and 7 dynamics are required for YCV LC3-II single/double membrane formation [89]. Additional works submit that the YCV is a phagolysosome [55]. However, unpublished data by Bliska and colleagues indicate the spacious phagolysosome potentially retains

Lamp1, a lysosomal marker, and/or LC3-II [59, 87]. In either case, the spacious phagolysosome or autophagosome have been both identified, but whether *Y. pestis* requires autophagy for replication remains to be determined.

Several *in vivo* studies indicate that intracellular survival in macrophages is important for colonization of the mammalian host [52, 62, 90]. Ye et al. demonstrated selective depletion of Gr1⁺ macrophage and dendritic cells in transgenic MaFIA mice lessens the severity of plague infection [52]. St. John and colleagues further highlight the importance of these innate cells, as chemical inhibition impacts the ability of *Y. pestis* to disseminate from the draining lymph node in a Sphingosine-1-phosphate dependent manner [49]. Additionally, macrophages from canines (a species relatively resistant to plague infection) are better equipped to kill intracellular *Y. pestis* than rodent macrophages (the natural reservoir for plague) [62, 91]. Finally, *in vivo* infection studies with *Y. pestis phoP* mutants, which are defective for intracellular survival, have reported extended times to death for the *phoP* mutant compared to wildtype *Y. pestis* [90]. These data suggest intracellular survival of *Y. pestis* also contributes to early immune evasion and pathogenesis.

Biogenesis of the YCV highlights the importance of exploited host-pathogen interactions to facilitate survival of *Y. pestis* within the macrophage. The current model of *Y. pestis* intracellular survival within the macrophage based on all peer-reviewed publications is summarized in Fig. 1-1

Subversion of the Phagolysosome by other pathogens

Phagolysosome maturation is a well-documented cellular process that requires subsequent recruitment and dissociation of Rab GTPases to coordinated vesicle trafficking and ultimately fusion with the lysosome [92-94]. Rab5, Rab7, and Rab9 are key contributors to the phagosome maturation pathway [94-101]. Initially, Rab5 is recruited to the early endosome and is exchanged with Rab7 on the intermediate phagosome [94, 97-101]. From here, Rab7 is required for the recruitment of Rab9, which completes the fusion of the maturing phagosome with the lysosome [94, 98-101]. At this point, the mature phagolysosome has Cathepsin D and vATPase markers and is actively acidifying to pH 4.0 in order to degrade the vacuole contents [95]. Subtle

disruptions in the recruitment of the Rab proteins can stall or even terminate trafficking of these endocytic vesicles and many intracellular pathogens hijack this process [102, 103].

Vesicular trafficking has become an area with increased research efforts in the context of pathogenesis (for review see [93, 102-104]). Pathogens such as *Mycobacterium tuberculosis* and *Legionella pneumophila* have developed mechanisms to modulate host Rab GTPase machinery and prevent their destruction within the phagolysosome [93, 102, 103].

Rab GTPases Modulation by *Mycobacterium tuberculosis*

Mycobacterium tuberculosis (M. tb) is an intracellular pathogen that causes tuberculosis in humans [105]. The bacterium has developed the ability to exploit host trafficking to prevent degradation in the phagolysosome. Studies dissecting the recruitment and retention of host Rab GTPases to the *Mycobacteria* containing vacuole (MCV) show the bacterium arrests phagolysosome maturation through disruption of the sequence/order of Rab GTPases [93, 106-110]. Briefly, once *M. tuberculosis* is engulfed, the MCV acquires 22 different Rab GTPases [108]. Of these Rabs, differential recruitment of Rab22a and Rab14 to the early endosome stalls the conversion of Rab5 to Rab7, preventing the maturation of the phagolysosome [107, 109, 110]. Further investigation by Seto and colleagues showed Rab7, Rab20, and Rab39 regulated the acidification of the MCV [108]. In contrast, Rab7, Rab20, Rab22b, Rab32, Rab34, Rab38 and Rab43 impacted the recruitment of cathepsin D to these phagosomes [108]. Of note, Seto and colleagues' work highlights speculation that *M. tuberculosis* does not actively target host Rab GTPases, but rather acquires Rab GTPases that normally modulate the process of phagolysosome maturation as a byproduct of how *M. tuberculosis* is trafficked upon uptake [108]. In support of this, recruitment of Rab22a, a Rab GTPase normally found on recycling endocytic vesicles, is associated and retained on the MCV [93, 106].

Rab GTPase Modulation by *Legionella pneumophila*

Legionella pneumophila is a facultative intracellular pathogen and the causative agent of Legionnaire's disease [111, 112]. *Legionella* has a type 4 secretion system (T4SS) and translocates over 300 effector proteins to modulate the host cell upon engulfment [111, 112]. The bacterium

establishes a *Legionella*-containing vacuole (LCV) within the host cell and remodels this niche into a hospitable environment for replication. One of the best studied host targets for *Legionella*'s bacterial effectors is the host Rab1 GTPase (further detailed in the discussion of Chapter 3). Briefly, *L. pneumophila* secretes several effectors that actively modulate the activity of host Rab1 on the LCV [113-126]. This process relies on bacterial modification of the host Rab GTPases' ability to hydrolyze GTP to GDP through cycling of bacterial effectors that, 1) increase Rab1 hydrolysis, 2) AMPylation of Rab1, 3) de-AMPylation of Rab1, and 4) ubiquitination of Rab1 [115-117, 121-129]. The outcome of these modifications on Rab1, results in *L. pneumophila* modulation of LCV acidification and blocking of phagolysosome maturation.

RNAi Screens Identify Novel Pathogenesis Mechanisms

To date, there have been multiple genome-wide RNAi high-throughput screens to identify novel targets and pathways exploited by various bacterial and viral pathogens (Table 1-1; [130-142]). This tool has been exceptionally useful for bacterial and viral pathogens that are naturally difficult to perform traditional genetic screens in, such as *Coxiella burnetii*, West Nile Virus, and *Mycobacterium tuberculosis* [131, 136, 137, 139]. This method is amenable to suitable surrogate infection models and completely rests on the impact of a host gene upon the survival of the pathogen in question. The first genome-wide RNAi screen by Agaisse et al., demonstrated the power of RNAi screen approaches to identify host requirements for survival by *Listeria monocytogenes* and *Mycobacterium fortuitum* [141]. Their results compared *L. monocytogenes* to *M. fortuitum* to identify individual host components required for both vacuole escape and pathogen-containing vacuole (PCV) maturation. They utilized the advanced tools for *Drosophila* cell RNAi and network/gene homologies to identify 160 targets specifically impacting *L. monocytogenes* survival and 91 targets that impacted both organisms' intracellular survival [141]. A major finding from their data was the identification of several Rab GTPases, such as Rab1, 5, 7, and 35, and cellular trafficking components, such as Cop β 1, that altered survival. These data eventually lead to discoveries of autophagy modulation and the exploitation of host genes to arrest phagosome maturation by various pathogens. While Agaisse et al. pioneered the use of RNAi screens to identify novel genes, it was Kumar et al., who truly established the power of bioinformatic analysis

of these types of data. Using *M. tuberculosis* they developed a complex screening system to validate primary screen hits in subsequent secondary and tertiary screens through matching phenotypes and library deconvolution [136]. From their stringent screening process they applied GO ontology and network clustering criteria for the 329 validated hits. Their results demonstrated modular clustering of required host factors for *M. tuberculosis* that was isolate dependent [136]. Furthermore, they show enrichment for biological networks, such as “Metabolism” and “Immune and Inflammation”, that inhibit and regulate survival of *M. tuberculosis* from the same datasets [136]. A highlight from their studies was bioinformatic identification and biological validation of interacting components with the autophagy cascade that dynamically regulated *M. tuberculosis* survival through modulation of IFN γ host responses [136]. Overall, genome-wide screening has successfully identified valuable networks exploited by other pathogens. However, development of an RNAi platform requires meticulous optimization and validation before it is implemented in the screening of a pathogen.

Principles of RNAi Screening

In order to complete an RNAi screen, one must develop and optimize a screening platform to specifically address their hypothesis. Fundamentally, the process of development can be broken down into five parts, 1) class of screen, 2) species of screen or cell type, 3) RNAi method, 4) screen format, and 5) readout (Fig. 1-2; [143, 144]).

Screen Class

In developing a screening platform to address your initial hypothesis one must either select a genome-wide or a functional category class of host targets (Fig. 1-2). A genome-wide screen uses a library comprised of targets from the known coding sequences of the species genome (e.g., *Drosophila*, Mouse or Human). A functional category class screen is a small subset of host targets and can be a class of protein, such as Kinases or Rab GTPases, or a known pathway, such as JAK/STAT or Ubiquitin.

Species of Screen

The next stage is to select the species you will conduct the RNAi in, *Drosophila*, Mouse or Human (Fig. 1-2). This selection is primarily driven by the ability to achieve knockdown of the target transcript using your chosen RNAi method [144].

RNAi Method

The RNAi delivery method can either be long dsRNA, esiRNA, siRNA, or shRNA (Fig 1-2; [143, 144]). Long dsRNA use the host machinery by Dicer to cleave the molecule into pools of siRNA [143]. This method of delivery works best for *C. elegans* and *Drosophila*, because the dsRNA does not activate the type-I interferon response as it would in mammalian cells [143, 145]. The synthetic esiRNA and siRNA are developed to mimic the sequences after Dicer processing of the molecule, and are used mainly for mammalian cells and immortal cell lines [143, 146]. Finally, shRNA are designed to mimic the pre-microRNA substrate of Dicer and are expressed via Retroviral or Lentiviral vectors in transduced cells [143, 147]. The use of shRNA has been shown effective for primary mammalian cells, such as human macrophages [143]. Ultimately, the optimal degree of knockdown to achieve is 70 – 95% of the target [143, 144].

Screen Format

Screening formats are either arrayed or pooled [143]. In an arrayed setup the user screens individual RNAi's with the ability to deconvolute individual results via statistical analysis of their readout [143]. This arrayed approach provides individual data for each of the RNAi's being tested, but can be cost, time and labor prohibitive at the genome-wide level. In a pooled approach, the user combines the individual RNAi's (usually 3-6) and screens them for an effect, then statistically analyzes the results and chooses a subset of targets to further evaluate [143, 144]. A pooled approach lends itself to rapid and cost effective genome-wide screening.

Readout

The final step to platform development is generating a 'readout'. The readout encompasses both the phenotypic reporter system as well as the technique/equipment used to discern the phenotype [143]. The two common phenotypic reporters are fluorescent and

luminescent. While there are several means to analyze a high-throughput screen (HTS), the most common are either high-content imaging or plate reader based [143, 144, 148]. In both instances, the equipment requires optimization much like the rest of the platform and will briefly be summarized. High-content imaging requires the user to determine the autofocus, image quality minimums, segmentation, threshold, and regions-of-interest (ROI) of the image using software analysis tools [148]. From here, the user can quantify a range of phenotypes based on the amount of fluorescent reporter being imaged. A basic example of this for RNAi pathogen screens is number of bacteria or bacterial total intensity per cell [133, 135, 141]. To date, there has not been a multiplexed approach to determine both pathogen survival and relationship to either an overexpressed protein or antibody stained protein. As for a screen using a plate reader there is less to optimize, as the user is mainly concerned with dynamic range of the reporter's intensity (fluorescent or luminescent) and the separation of controls. Here, the optimization of dynamic range is key to determine the limit of detection for the phenotypic response. As for the separation of controls, the user will account for the phenotypes using a Z' factor per plate, Z' score, or B score [149, 150]. These statistical approaches are based on the separation of a positive and negative control being 3σ (standard deviations) apart. For Z' factor in particular, a score >0.5 is highly robust, <0.5 to >0.3 is acceptable, and <0.03 is unacceptable [149].

Proposed Research

Y. pestis is a facultative intracellular pathogen capable of surviving within macrophages. Macrophages are innate immune cells normally capable of killing bacteria, however increasing data show *Y. pestis* prevents this process and survives within these host cells. Survival within macrophages is a potential protective niche for *Y. pestis* during transition from the flea (26°C) to mammalian (37°C) host. During this transition the bacteria is not expressing temperature dependent mammalian specific virulence factors, such as the T3SS, and is easily killed by neutrophils. *Y. pestis* $\Delta phoP$ mutants are defective for intracellular survival and exhibit a higher LD₅₀ with an extended time to death [56, 83, 90, 151]. The role of macrophages during pathogenesis is further emphasized by findings that *Y. pestis* predominately associates with

macrophages and not neutrophils in infected rodents and nonhuman primates [49, 53, 58, 84]. Depletion of macrophages prior to infection with *Y. pestis* dampens bacterial burden [52].

Y. pestis survives within macrophages in a phagosomal compartment known as the YCV. *Y. pestis* actively subverts the phagolysosome maturation by inhibiting acidification of the YCV. After eight hours post-infection, the YCV expands in conjunction with bacterial replication [54, 55, 57, 59, 61, 62, 152, 153]. While the fate of *Y. pestis* within the macrophage is known, the mechanisms exploited by *Y. pestis* to inhibit phagolysosome maturation and establish the YCV have not been defined.

The use of genome-wide RNAi screens for comprehensive identification of required factors exploited by various intracellular pathogens for survival suggests the successful adaptation of this technology to *Y. pestis*. With this, we hypothesize that *Y. pestis* actively exploits host pathways/factors to avoid YCV acidification and support YCV biogenesis. To address this, we:

- 1) Developed a bioluminescent system capable of monitoring bacterial burden within macrophage cells.
- 2) Optimized, established, and completed a genome-wide RNAi screen in the biologically relevant murine macrophage cell line (RAW264.7 cells).
- 3) Performed bioinformatic analysis for identified genes and validation of phenotypes from bioinformatic networks.
- 4) Identified host factors impacting *Y. pestis* intracellular survival, altering YCV biogenesis and avoidance of the phagolysosome.

The following chapters represent the first steps toward comprehensive identification of required host factors and the mechanisms necessary to support *Y. pestis* survival within the macrophage.

Figures and Figure Legends

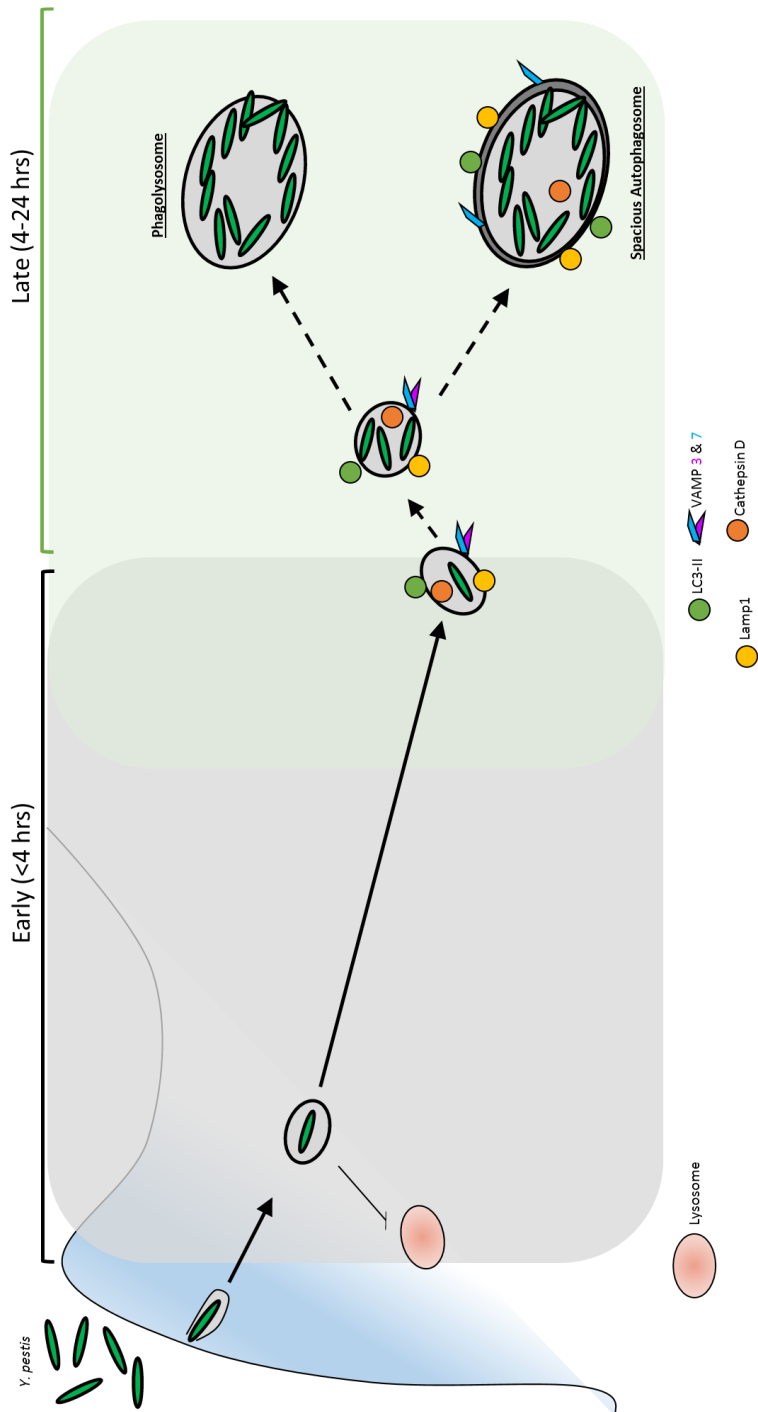


Figure 1—1 Summary of *Y. pestis* intracellular survival

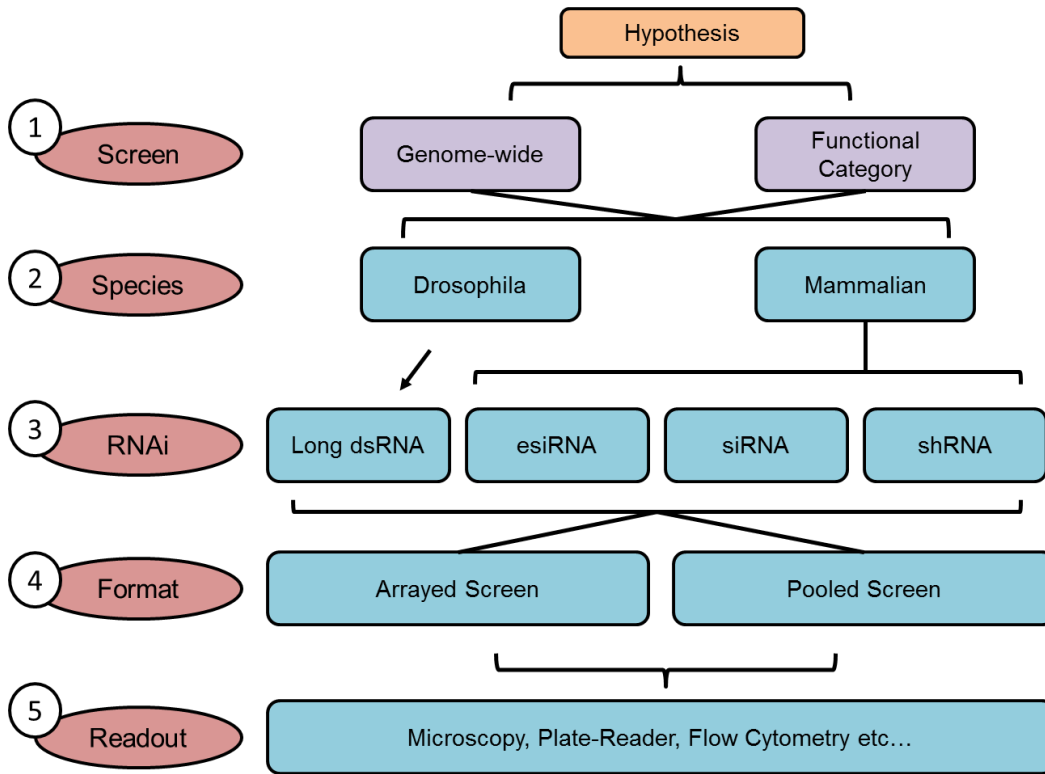


Figure 1—2RNAi Screen Development Workflow

Tables

Table 1-1. Pathogens Screened Using RNAi

Pathogen	Cell Type	Year	Reference
<i>L. monocytogenes</i>	HeLa CCL-2	2015	Kuhbacher [130]
<i>C. burnetti</i>	HeLa	2013	McDonough [131]
Chikungunya virus	U-2 OS	2013	Ooi [132]
Eastern Equine Encephalitis virus	U-2 OS	2013	Ooi [132]
<i>S. typhmuri</i>	MCF-7	2012	Thornbrough [133]
<i>F. tularensis</i>	Human Monocyte-like THP-1; HMDMs; Human Alveolar Macrophages	2012	Zhou [134]
<i>F. tularensis</i>	<i>Drosophila</i> S2R+	2010	Akimana [135]
<i>M. tuberculosis</i>	Human Monocyte-like THP-1	2010	Kumar [136]
<i>M. tuberculosis</i>	Murine Macrophage-like J774.1	2010	Jayaswal [137]
<i>B. melitensis</i>	<i>Drosophila</i> SL2	2008	Qin [138]
West Nile virus	HeLa	2008	Krishnan [139]
<i>C. caviae</i>	<i>Drosophila</i> SL2	2007	Derre [140]
<i>L. monocytogenes</i>	<i>Drosophila</i> SL2	2005	Agaisse [141]
<i>M. fortuitum</i>	<i>Drosophila</i> SL2	2005	Agaisse [141]
<i>M. fortuitum</i>	<i>Drosophila</i> SL2	2005	Philips [142]

CHAPTER 2:
DEVELOPMENT OF BIOLUMINESCENT BIOREPORTERS FOR *IN VITRO*
AND *IN VIVO* TRACKING OF *YERSINIA PESTIS*¹

¹ Sun Y, Connor MG, Pennington JM, Lawrenz MB. Development of bioluminescent bioreporters for in vitro and in vivo tracking of *Yersinia pestis*. PLoS one. 2012;7(10):e47123. PubMed PMID: 23071730.

Overview

Yersinia pestis causes an acute infection known as the plague. Conventional techniques to enumerate *Y. pestis* can be labor intensive and do not lend themselves to high throughput assays. In contrast, bioluminescent bioreporters produce light that can be detected using plate readers or optical imaging platforms to monitor bacterial populations as a function of luminescence. Here we describe the development of two *Y. pestis* chromosomal-based *luxCDABE* bioreporters, Lux_{P_{tolC}} and Lux_{P_{cysZK}}. These bioreporters use constitutive promoters to drive expression of *luxCDABE* that allow for sensitive detection of bacteria via bioluminescence in vitro. Importantly, both bioreporters demonstrate a direct correlation between bacterial numbers and bioluminescence, which allows for bioluminescence to be used to compare bacterial numbers. We demonstrate the use of these bioreporters to test antimicrobial inhibitors (Lux_{P_{tolC}}) and monitor intracellular survival (Lux_{P_{tolC}} and Lux_{P_{cysZK}}) in vitro. Furthermore, we show that *Y. pestis* infection of the mouse model can be monitored using whole animal optical imaging in real time. Using optical imaging we observed *Y. pestis* dissemination and differentiated between virulence phenotypes in live animals via bioluminescence. Finally, we demonstrate that whole animal optical imaging can identify unexpected colonization patterns in mutant-infected animals.

Introduction

Bioreporters are engineered microbes that produce a detectable signal that can be used to monitor cell populations or responses to environmental stimuli. The bacterial *luxCDABE* operon, which produces light through bioluminescence, has been adapted for use as a bioreporter in many species of bacteria [154]. Unlike eukaryotic luciferase systems, the *luxCDABE* operon produces both the luciferase enzyme and the substrates required for light production, removing the requirement for supplemental exogenous substrates for luminescence [155]. By replacing the native *luxCDABE* promoter with a promoter from a gene of interest, researchers can monitor changes in gene expression as a function of bioluminescence. *luxCDABE* reporters driven by constitutive promoters, in which bacterial density directly correlates to luminescence, provide a system to monitor bacterial growth. Furthermore, because bioluminescence is only produced by viable bacteria, bacterial survival can also be monitored with a *luxCDABE* reporter [155]. The ease

of detecting bioluminescent signal from *luxCDABE* without the addition of substrates or inactivation of the bacterium makes this an ideal reporter for real time monitoring of bacteria and high throughput biology technologies.

Yersinia pestis causes the acute infection known as the plague. Human plague can manifest as three different forms. Bubonic plague arises in individuals who have been fed upon by an infected flea. The bacteria are regurgitated into the bite site by the flea and rapidly colonize the proximal lymph nodes. In these tissues, *Y. pestis* evades the immune system and replicates to high numbers. Without treatment, the bacteria can eventually colonize the bloodstream, leading to the development of septicemic plague. Cases of primary septicemic plague can also arise if *Y. pestis* is directly inoculated into the blood by the flea. From the blood, *Y. pestis* disseminates to other tissues in the host. Colonization of the lungs results in the development of pneumonia (called secondary pneumonic plague). Pneumonic plague patients can directly transmit *Y. pestis* to naïve individuals via contaminated aerosols, resulting in primary pneumonic plague [156]. Direct aerosol transmission of *Y. pestis* has also raised concerns about the potential use of plague as a biological weapon [14].

Several examples of the use of bioreporters in *Yersinia* have been reported. Two independent high throughput screens for inhibitors of the *Yersinia* type III secretion system have used bioluminescent bioreporters. The first screen monitored changes in *yopE* transcription with a *PyopE::luxAB* reporter [157], while the second used a *lux* operon driven by a constitutive promoter to monitor bacterial growth [158]. Other groups have engineered *luxCDABE* reporters to be under the transcription control of promoters of virulence genes to monitor expression patterns of these genes [159-161]. In addition to these in vitro assays, a limited number of studies in *Yersinia* using bioluminescent reporters for optical imaging of whole animals have been reported. Trcek et al. developed an inducible *luxCDABE* reporter in *Y. enterocolitica* to monitor oral and IV infection [162]. The authors observed luminescent signal from the abdomen of live animals during oral infection, but due to the nature of the gastrointestinal tract, specific tissue localization required necropsy. However, whole animal imaging revealed unexpected colonization of the cervical lymph nodes that

has been overlooked using conventional models. In *Y. pseudotuberculosis*, Thorslund et al. were able to differentiate infection by wild type (WT) or mutant bacteria using the pCD1-Xen4 reporter [163]. More recently, Nham et al. infected animals subcutaneously with WT *Y. pestis* harboring a plasmid-based luciferase reporter and demonstrated that bioluminescence could be used to localize bacteria to lymph nodes via whole animal imaging. They were also able to use bioluminescence to monitor the development of systemic disease [164].

Whole animal optical imaging has also been used to study pneumonic infection by several Select Agent pathogens. Independently, two groups demonstrated that experimental melioidosis could be visualized in the mouse model [165, 166]. Furthermore, Warawa et al. were able to visualize both upper and lower respiratory tract colonization, differentiate between colonization patterns of mutant bacteria, and show that luminescence detection from the thoracic cavity strongly correlated to bacterial numbers in the lung. Bina et al. developed a plasmid-based *luxCDABE* bioreporter in *Francisella tularensis* [167]. Using this system, they demonstrated that the volume of the bacterial suspension administered to mice could affect whether the bacteria were delivered to the lung [168]. These studies demonstrate the potential for use of bioluminescent-based optical imaging to monitor pneumonic plague.

Several animal models of human plague have been characterized to study *Y. pestis* pathogenesis and develop potential therapeutics [169]. Conventional models to study microbial pathogenesis use separate groups of animals to determine the survival of animals (e.g., LD₅₀ and/or time to death analysis) or dissemination rate of the pathogen (by enumerating bacteria from specific tissues of subsets of animals sacrificed at various time points). In contrast, optical imaging models allow for temporal and spatial analysis of the infection and survival data to be acquired from the same animal. Potential advantages of optical imaging models are: 1) smaller number of animals required for studies, 2) ability to follow the course of the disease in the same animal over time, and 3) potential to identify unexpected dissemination routes.

Here we describe the development of two chromosomally-based *luxCDABE* reporters for use in *Y. pestis*. We demonstrate that these reporters can serve as sensitive bioreporters to monitor *Y.*

pestis growth and survival under different conditions during in vitro growth. We also demonstrate that both bubonic and pneumonic plague infection can be monitored in live animals using these reporters via optical imaging. Finally, we show that the *luxCDABE* bioreporter can be used to compare and differentiate virulence phenotypes in animals without the need to sacrifice animals.

Results

Construction of a chromosomal luciferase reporter system in *Y. pestis*

Our preliminary data demonstrated that in *Yersinia* a *luxCDABE* based-reporter was >200-fold more sensitive than equivalent fluorescent reporters using dsRED or EGFP (data not shown). Therefore, we developed a bioreporter using the *lux* operon in *Y. pestis*. Using a Tn7-based system, we integrated the entire *luxCDABE* operon driven by the EM7 promoter from pGEN-*luxCDABE* into the *Y. pestis* chromosome [170, 171]. Integration of the reporter into the chromosome greatly reduced the amount of bioluminescence produced per bacterium compared to *Y. pestis* with pGEN-*luxCDABE* (likely due to a decrease in copy number), resulting in an average limit of detection of 2.84×10^5 CFU (range = 1.30×10^4 to 6.23×10^6 CFU) for the chromosomal reporter (Fig. 2-1A and B). To increase the sensitivity, we replaced the EM7 promoter with one of two different promoters. We selected the *toIC* promoter from *Burkholderia pseudomallei*, which was used in a similar reporter in *B. pseudomallei* [165], and the *cysZK* promoter from *Y. pestis*, which was identified as a strong constitutive *Y. pestis* promoter [172]. Expression of the luciferase operon from the *toIC* promoter increased the chromosomal reporter sensitivity by ~100-fold (average limit of detection = 2.5×10^3 CFU, range = 1.09×10^3 to 5.86×10^3 CFU) and approached the sensitivity of pGEN-*luxCDABE* (Fig. 2-1C). The *cysZK* promoter further increased the sensitivity by an additional 10-fold, establishing an average limit of detection of 3.06×10^2 CFU (range = 1.08×10^2 to 5.76×10^2 CFU) (Fig. 2-1D). As reported by Bland et al., we also observed increased expression of P_{*cysZK*} at 37°C, but importantly, the LUX_{P_{*cysZK*}} strain maintained a direct correlation between bacterial numbers (CFU) and light production (RLU) during continuous growth at both temperatures (Fig. 2-2). LUX_{P_{*toIC*}} activity did not appear to be influenced by temperature and maintained a strong direct correlation between CFU and RLU at both temperatures (Fig. 2-2).

To ensure that expression of the *lux* operon did not affect growth of *Y. pestis*, we determined the growth rate of the *Y. pestis* reporter strains in vitro (Fig. 2-3A). No significant differences were observed between WT *Y. pestis* (no reporter) or strains carrying the three chromosomal reporters. We further examined whether the Lux reporters impacted fitness of *Y. pestis* in the macrophage model. As seen in broth culture, the Lux reporters did not negatively impact the survival/replication of *Y. pestis* in macrophages, and we observed similar levels of replication by the reporter strains in RAW264.7 macrophages as WT *Y. pestis* without a reporter (Fig. 2-3B). Together these data demonstrate that integration of the *lux* operon driven by either *P_{tolC}* or *P_{cysZK}* generated a sensitive luciferase reporter that does not appear to impact *Y. pestis* growth and whose light production directly correlates to bacterial number.

Using the *Y. pestis* Lux reporters as bioreporters

Due to the requirement for a constant supply of O₂, FMNH₂, and aldehydes for the Lux system to produce light, bioluminescence only occurs in actively growing bacteria [155]. This property, in conjunction with the direct correlation between bioluminescence and bacterial numbers for the Lux_{*P_{tolC}*} and Lux_{*P_{cysZK}*} reporters, suggests that these reporters can be used to monitor *Y. pestis* survival in real time. To test this hypothesis, we incubated *Y. pestis* Lux_{*P_{tolC}*} with decreasing concentrations of a chemical disinfectant (MicroChem-Plus), and then monitored bacterial survival as a function of bioluminescence (Fig. 2-4A). At 6 mins post-exposure, samples were harvested, washed and plated to determine if bioluminescence readings correlated with bacterial numbers (Fig. 2-4B). Within 2 mins of exposure to MicroChem-Plus at concentrations ≥0.05%, we were unable to detect bioluminescence from the *Y. pestis* cultures. This correlated with viable bacteria, as at these concentrations, viable bacteria were below the level of detection of the Lux_{*P_{tolC}*} reporter. At levels of MicroChem-Plus <0.05% we observed a dose dependent reduction in bioluminescence that directly correlated to the number of bacteria recovered after six mins of incubation.

To further demonstrate that bioluminescence can differentiate bacteria survival, *Y. pestis* Lux_{*P_{tolC}*} was incubated in 96-well plates with increasing concentrations of carbenicillin or gentamicin. Plates were incubated for 12 hrs at 26°C, and bioluminescence was detected every hr.

These readings indicated a dose dependent bacterial growth inhibition, with lower bioluminescence readings observed as antibiotic concentrations increased (Fig. 2-4C and E). To confirm that bioluminescence readings correlated with bacterial numbers, a subset of samples was harvested at 4, 8, and 12 hrs and bacterial CFUs were determined by conventional enumeration (Fig. 2-4D and F). As seen for bioluminescence, we also observed a dose dependent response in bacterial CFU. Together these data demonstrate that bioluminescence can be used to monitor changes in bacterial survival.

Differentiation between bacterial phenotypes in vitro using *Y. pestis* Lux bioreporters

To further demonstrate that the *Y. pestis* Lux bioreporters can be used to monitor bacterial numbers in a biological system, we infected macrophages with WT *Y. pestis* pCD1(-) or a mutant defective in macrophage survival ($\Delta phoP$) carrying our reporter constructs. RAW264.7 macrophages were infected with the reporter strains and extracellular bacteria were killed with gentamicin. At several time points post-infection, bioluminescence was measured using a plate reader. In addition, at 1.5, 8, and 24 hrs post-infection, samples were also harvested to determine bacterial numbers by conventional bacterial enumeration techniques. CFU data demonstrated that all three of the WT *Y. pestis* reporter strains survived within the macrophages, but the $\Delta phoP$ mutant strains were attenuated and bacterial numbers differed from WT by approximately two orders of magnitude over the course of the assay (Fig. 2-5A-C). The sensitivity of the bioluminescence signal produced by the Lux_{P_{tolC}} and Lux_{P_{cysZK}} reporter strains allowed for easy differentiation between WT and $\Delta phoP$ phenotypes (Fig. 2-5E-F). In contrast, the lower sensitivity of the Lux_{PEM7} reporter made it more difficult to differentiate the $\Delta phoP$ phenotype (Fig. 2-5D). While RLU data from the WT Lux_{PEM7} strain correlated with CFU data, the bioluminescent signal of the $\Delta phoP$ Lux_{PEM7} strain quickly dropped below the limit of detection of the reporter, resulting in a loss of correlation between bacterial CFU and RLU for this assay. These data demonstrate that the Lux_{P_{tolC}} and Lux_{P_{cysZK}} bioreporters can be used to monitor changes in bacterial populations in biological systems in vitro.

In vivo imaging of bubonic plague

The high sensitivity of the Lux_{P_{cysZK}} bioreporter that we observed in vitro suggested that it could also be used to monitor plague infection in vivo. Bubonic plague is the most common form of human plague and results from flea transmission. In the laboratory, bubonic plague can be modeled by intradermal or subcutaneous inoculation of mice with *Y. pestis*. After inoculation, the bacteria disseminate to the draining lymph node. Eventually the bacteria enter into the bloodstream to cause a systemic infection. To determine if the Lux_{P_{cysZK}} bioreporter could be used to monitor bubonic infection, specifically lymph node colonization, mice were challenged with the WT CO92 Lux_{P_{cysZK}} strain, and infection was monitored using whole animal optical imaging (Fig. 2-6). Mice were inoculated at the base of the tail with approximately 200-400 CFU of the bioreporter strain. The sensitivity of the bioreporter strain allowed us to detect bioluminescent signal from the inoculation site as early as 8 hrs post-inoculation. Furthermore, signal increased over time at the inoculation site, indicating that *Y. pestis* survives and replicates at the inoculation site over the course of the infection (Fig. 2-7A).

Previous work has defined the lymphatic drainage basin for the base of the tail to be the subiliac (also referred to as the inguinal) and the axillary lymph nodes (LN) [173, 174]. We began to detect luminescent signal from the subiliac LN starting between 48 and 72 hrs post-inoculation (Fig. 2-6A, white arrows). Approximately 8-15 hrs after first detection in the subiliac LN, signal began to be detected in the axillary LN, indicating bacterial dissemination to these nodes (Fig. 2-6A, red arrows). For both lymph nodes, the bioluminescent signal continued to increase in the tissues over the course of the infection, indicating bacterial proliferation. By 72 hrs post-inoculation, we began to detect bioluminescence from other regions, indicating systemic infection. The animals succumbed to infection by 96 hrs post-inoculation.

To further demonstrate that our bioreporter can be used to monitor bubonic plague dissemination, an additional group of mice was infected in the footpad with the WT CO92 Lux_{P_{cysZK}} strain. Previous work has demonstrated that dyes can disseminate from this site via two different drainage basins in mice [173, 174]. The first basin drains to the popliteal LN, followed by the sciatic

and renal LNs. Alternatively, drainage to the same basin as from the base of the tail can occur. In these studies we observed *Y. pestis* disseminating only through the former drainage basin from the footpad (Fig. 2-6B). Bioluminescent signal was first detected in the popliteal LN at about 72 hrs post-inoculation. Signal was detected 24 hrs later from regions corresponding to the sciatic and renal LNs. At this time we also were able to detect signal from the spleen. Together these data demonstrate that lymph node colonization and dissemination of *Y. pestis* can be tracked in live animals via optical imaging using the Lux_{P_{cysZK}} bioreporter.

In vivo imaging of pneumonic plague

Primary pneumonic plague occurs when aerosols containing *Y. pestis* are inhaled by a naïve individual. This form of disease can also be modeled in the mouse using the intranasal route of infection [175]. To determine if the Lux_{P_{cysZK}} bioreporter can be used to monitor pneumonic infection, we challenged mice intranasally with the WT CO92 Lux_{P_{cysZK}} strain and followed the progression of pneumonic plague by optical imaging. Bioluminescent signal could be detected from the thoracic cavity of all mice as early as 24 hrs post-inoculation and increased throughout the course of infection (Fig. 2-8A and B). To demonstrate that the bioluminescence signal directly correlated with bacterial numbers, lungs were harvested from a subset of animals after the 24, 48, and 72 hrs imaging sessions. The tissues were imaged and bacterial numbers in the lungs were determined. Bioluminescent signal from imaging of the thoracic cavity directly correlated to lung CFU (Fig. 2-8C; R²=0.8323). The significance of the correlation increased further when comparing signal directly from harvested lungs to CFU (Fig. 2-8D; R²=0.9684). Animals infected with the Lux_{P_{cysZK}} strain succumbed to infection between 60 and 80 hrs post-infection, a similar time to death as seen for *Y. pestis* without a reporter [175, 176].

Differences in phenotypes can be detected in vivo using the Lux_{P_{cysZK}} bioreporter

To demonstrate that whole animal imaging using the Lux_{P_{cysZK}} bioreporter can differentiate between virulence phenotypes, we transferred the reporter into a *Y. pestis*Δ*pla* mutant. *Pla* is required for the development of bubonic plague, and a *pla* mutant is unable to disseminate from the inoculation site to the draining LN [177-179]. In the bubonic model, we observed bioluminescent

signal from the inoculation site of *Y. pestis* $\Delta p/a$ $Lux_{P_{cysZK}}$ infected animals as early as 8 hrs post-infection (Fig. 2-7A). Signal increased at the inoculation site at a rate comparable to WT infected animals until 36 hrs post-infection. After 36 hrs, signal from WT infected animals continued to increase, but the signal from $\Delta p/a$ infected animals plateaued, remaining about 1-2 logs lower than WT signal for the remainder of the experiment. No signal was observed from the draining LN from $\Delta p/a$ infected animals (Fig. 2-7B), supporting previous data that the mutant is unable to disseminate to the LN after intradermal infection [179]. However, one $\Delta p/a$ infected animal (n=9) appeared to develop primary septicemic plague, as no signal was detected from the lymph nodes prior to systemic signal (data not shown).

In the model for pneumonic plague, the $\Delta p/a$ mutant colonizes the lungs but is unable to proliferate in these tissues [176]. As expected, we observed low levels of bioluminescence from the thoracic cavity of mice infected intranasally with *Y. pestis* $\Delta p/a$ $Lux_{P_{cysZK}}$, correlating with low levels of bacteria in these tissues (Fig. 2-8). Importantly, compared to WT infected mice, luminescence from the $\Delta p/a$ infected animals was significantly lower at all time points, except at the 72 hr time point when there were not enough WT animals to calculate significance (Fig. 2-8B). While the $\Delta p/a$ mutant does not proliferate within the lungs during pneumonic infection, the LD₅₀ of the mutant is similar to WT *Y. pestis*, likely due to the development of septicemic plague [176]. The sensitivity of the $Lux_{P_{cysZK}}$ bioreporter allowed us to observe the development of septicemic plague in $\Delta p/a$ infected animals (Fig. 2-9A). Furthermore, as we monitored the $\Delta p/a$ infected animals, we also observed that a subset of animals developed bioluminescent signal near the ears which we did not observe in WT infected animals (Fig. 2-9). Together these data demonstrate that whole animal imaging with the $Lux_{P_{cysZK}}$ bioreporter can differentiate between bacterial phenotypes during both bubonic and pneumonic plague infection.

Discussion

The bacterial *luxCDABE* operon produces a bioluminescent signal that can be used as a bioreporter to monitor bacterial numbers in real time. We developed two *luxCDABE* reporters for use in *Y. pestis* to monitor bacterial survival. We demonstrated that these reporters can be used to

monitor bacterial numbers in the presence of antimicrobial compounds, during intracellular infection, and in animal models for plague infection. Unlike plasmid-based systems previously used in *Yersinia* spp. [160, 162-164], these reporters are integrated into the chromosome. A chromosomal-based system has several characteristics that may be advantageous for future applications. First, integration of the reporter into the chromosome does not require antibiotic selection for maintenance and will likely be more stable than a plasmid-based system. Second, while plasmid reporters may be maintained without antibiotics for a period of time, especially with integrated toxin-anti-toxin maintenance mechanisms [164], [180], the plasmid still confers resistance for the selectable marker carried by the plasmid. Consequently, that marker is not available for further use (for example, to maintain other plasmids). The chromosomal reporters described here were engineered using a system that allows for the antibiotic marker to be removed after integration [171]. Therefore, the marker (in this case Kan) can be reused in downstream applications.

One advantage of a plasmid-based reporter system is that plasmids are often maintained at increased copy numbers compared to the chromosome, which can increase the sensitivity of the reporter. In fact, we observed a dramatic decrease in sensitivity when we moved the *luxCDABE* operon from a plasmid to the chromosome. To overcome this problem we removed the promoter from the original construct and replaced it with a promoter we hypothesized would increase the expression of the *lux* operon. We chose two different promoters to test. The first promoter was from *B. pseudomallei* (*P_{tolC}*) and had been used to successfully develop a similar chromosomal reporter for this bacterium [165]. This promoter increased the sensitivity to the levels of the original plasmid-based reporter. The second promoter was originally identified by Bland et al. as being a strong constitutive promoter in *Y. pestis* (*P_{cysZK}*) [172]. This promoter further increased the sensitivity to a level approximately 10-fold higher than the *LUX_{P_{tolC}}* or *pGEN-luxCDABE*. Importantly, we saw no deleterious impact of increased *luxCDABE* expression from our reporters on *Y. pestis* fitness during growth in vitro, in cell culture, or in the animal models. Therefore, we successfully engineered a chromosomal luciferase reporter that is 10-fold more sensitive than a widely used plasmid-based reporter, without attenuating growth of *Y. pestis*.

For both the $\text{Lux}_{P_{\text{tolC}}}$ and $\text{Lux}_{P_{\text{cysZK}}}$ reporters we observed a direct correlation between bioluminescence and *Y. pestis* numbers. This characteristic is important and demonstrates that bioluminescence readings from these reporters can be used to quantify bacterial numbers. Furthermore, the sensitivity of the reporter and easy detection methods allow these bioreporters to be used in large scale formats. For example, we demonstrated that we could use the $\text{Lux}_{P_{\text{tolC}}}$ bioreporter to monitor bacterial growth in a 96-well format in the presence of antimicrobial compounds. Using this format we were able to easily determine the MIC for both carbenicillin and gentamicin. Furthermore, because we could monitor the bacteria in real time, we were also able to observe differences in growth patterns of *Y. pestis* in these two antibiotics. For example, *Y. pestis* incubated in inhibitory concentrations of carbenicillin (12.5 and 25 $\mu\text{g}/\text{ml}$) did not begin to decrease in bioluminescence until after 8 hrs into the assay, indicating that while bacterial growth might be inhibited, the bacteria were not killed by the antibiotic until after that time (Fig. 2-4C). In contrast, bioluminescence signal from bacteria incubated with inhibitory concentrations of gentamicin (2, 4, and 8 $\mu\text{g}/\text{ml}$) steadily decreased over the course of the assay, suggesting that bacterial death occurred much earlier (Fig. 2-4E). These hypotheses are supported by the CFU data that demonstrated that bacterial numbers did not begin to decrease in the carbenicillin samples until between 8 and 12 hrs, compared to between 4 and 8 hrs in gentamicin samples (Fig. 2-4D and F). These phenotypes can be explained by the mechanisms of action of the two antibiotics. Gentamicin blocks protein synthesis and quickly inhibits bacterial growth, whereas carbenicillin targets the bacterial peptidoglycan, which over time weakens the cell wall, leading to osmotic lysis, but allows for a short period of proliferation. The sensitivity and correlation between bioluminescence and bacterial numbers indicate that the bioreporters can be used to monitor *Y. pestis* survival in high throughput screens for new anti-*Y. pestis* compounds.

While we saw a consistent correlation between bioluminescence and bacterial CFU in all of the assays we reported, macrophages infected with ΔphoP $\text{Lux}_{P_{\text{cysZK}}}$ demonstrated a decrease in bioluminescence between 8 and 24 hrs without a significant difference in CFU between these two time points. The same phenotype was not observed in the WT $\text{Lux}_{P_{\text{cysZK}}}$ strain or in the $\text{Lux}_{P_{\text{tolC}}}$ strains, all of which maintained correlation between RLU and CFU (Fig. 2-5). These observations

demonstrate that depending on the specific experimental assay, one bioreporter may more accurately represent bacterial numbers than the other. Furthermore, while the *Y. pestis* Lux_{P_{cysZK}} bioreporter was more sensitive than the Lux_{P_{tolC}} bioreporter in our initial studies (Fig. 2-1), sensitivities of the bioreporters may change under different experimental conditions. For example, we observed that Lux_{P_{cysZK}} is more active at 37°C than 26°C. Therefore, optimization and validation of the bioreporters must be performed for each new assay as it is being developed.

Nham et al. recently reported the use of a plasmid-based bioluminescent bioreporter to follow the progression of bubonic plague in mice [164]. Using this bioreporter they demonstrated that spread of *Y. pestis* to the draining lymph nodes could be visualized in live animals via optical imaging. Furthermore, the authors were able to identify spread to the liver and spleen during disseminated (septicemic) plague. Similarly, we demonstrate here that the Lux_{P_{cysZK}} bioreporter could be used in optical imaging of bubonic infection. The sensitivity of the Lux_{P_{cysZK}} bioreporter allowed detection of bacteria at the inoculation site as early as 8 hrs post-infection, and we observed distinct dissemination patterns of *Y. pestis* Lux_{P_{cysZK}} from two different inoculation sites that followed the predicted lymphatic drainage basins. As the infection progressed, we were able to identify the transition to systemic infection when bioluminescence was detected from the spleen. Eventually bioluminescence was detected from more peripheral sites, such as the feet and tail, demonstrating that bacterial concentrations reached levels in the blood that could be detected by optical imaging prior to the animals succumbing to infection.

Our data also demonstrate that WT bacteria are not cleared from the inoculation site over the course of the infection, and continuous increase of bioluminescence at the site indicates that the bacteria proliferate. It is still unclear whether secondary septicemic plague initiates from bacteria disseminating from the lymph nodes or the inoculation site, but our data suggest that viable bacteria remain at the inoculation site as a possible reservoir for septicemic spread. Interestingly, while the Δ *pla* mutant did not appear to proliferate to WT levels at the inoculation site, we continued to detect bioluminescent signal from this site for as long as 14 days post-inoculation (unpublished data). These data indicate that the mutant can survive at the inoculation site for an extended period of

time, but survival at this site was not sufficient to lead to septicemic plague. However, one of the nine animals infected with the $\Delta p/a$ mutant developed septicemic plague during our studies. The lack of detectable signal from the draining lymph nodes suggests that the bacteria disseminated into the bloodstream without first colonizing the lymph nodes. A similar rate of septicemic infection by the $\Delta p/a$ mutant was previously reported by Sebbane et al. [179]. While these data may suggest septicemic plague arises from the inoculation site, we agree with Sebbane et al. that it is more likely that sepsis resulted from direct inoculation of the bacteria into the bloodstream during the infection and not from escape from the inoculation site. Additional studies are needed to further understand the dissemination of *Y. pestis* into the bloodstream.

In addition to bubonic infection, we also demonstrate that the $\text{Lux}_{P_{cysZK}}$ bioreporter is sensitive enough to monitor infection of deeper tissues colonized during pneumonic plague. Importantly, through enumeration of bacterial CFU in the lungs, we demonstrated that bioluminescence from the thoracic cavity directly correlates to bacterial numbers in the lungs. This correlation supports the use of bioluminescence to estimate bacterial burden in the lungs. Furthermore, we were easily able to differentiate between WT and $\Delta p/a$ infected animals, suggesting that this bioreporter can be used to differentiate between mutant phenotypes in the animal. The ability to monitor the entire progression of plague in an individual animal via optical imaging allows for dissemination kinetics and survival data to be obtained from the same group of animals, resulting in smaller number of animals per experiment. Furthermore, optical imaging of plague with the $\text{Lux}_{P_{cysZK}}$ bioreporter may benefit therapeutic research, as it will allow researchers to observe the resolution of an established infection after treatment is initiated.

Optical imaging with the $\text{Lux}_{P_{cysZK}}$ bioreporter will also allow researchers to identify unexpected dissemination patterns that might be missed in conventional models. For example, in a subset of animals intranasally infected with the $\Delta p/a$ mutant, we observed bioluminescence from a region near the ears, which we did not observe in WT infected animals. The precise tissues infected in these animals have yet to be identified, but colonization of tissues in this region would not have been detected without the whole animal imaging data. These data raise the possibility that systemic

infection by the Δpla mutant may arise from colonization of the upper respiratory tract as opposed to dissemination directly from the lungs. However, additional experiments to determine the frequency of this phenotype, correlation to systemic infection, and identity of infected tissues are required to test this hypothesis.

Material and Methods

Bacterial strains, plasmids, and growth conditions

The bacterial strains and plasmids used in this study are listed in Table 2-1. *E. coli* was grown in Luria-Bertani (LB) broth at 37°C. *Y. pestis* was grown in Brain Heart Infusion (BHI) broth at 26 or 37°C (with 2.5 mM CaCl₂). When appropriate, antibiotics were used at the following concentrations: kanamycin, 50 µg ml⁻¹ (*E. coli*), 25 µg ml⁻¹ (*Yersinia*); carbenicillin, 50 µg ml⁻¹.

The *Y. pestis* *phoP* mutant was generated using lambda red recombinase as previously described [181]. Briefly, regions flanking the *phoP* gene were amplified by PCR with primers DNA418 (5'-GAT TTC TAC ACC GTC GTG GG-3') and DNA419 (5'-GAA GCA GCT CCA GCC TAC AC CAT ACA CCA ATC CTT GAT AAA ACG TTA AC-3') for the 5' fragment and primers DNA420 (5'-GGT CGA CGG ATC CCC GGA ATAG ACA CTA TGC TCA GAA AAA ATA ATA AAC CC-3') and DNA421 (5'-GGT GAG TTG AGG TAA ACG AGA G-3') for the 3' region. The resulting products were gel purified and combined with a *kan* cassette flanked by FRT sites via overlapping extension PCR using primers DNA418 and DNA421. The resulting fragment was transformed into YPA035 expressing lambda red recombinase, followed by excision of the *kan* cassette, to generate YPA047.

The chromosomal *luxCDABE* reporters (Lux) were generated by first amplifying the *lux* operon, including the EM7 promoter, from pGEN-*luxCDABE* by PCR using primers DNA398 (5'-G GAG CTCTCT TGT CAT TTT CTG AAA CTC TTC ATG CTG-3') and DNA399 (5'-G GAG CTCCCG CAT CAA CTA TCA AAC GCT TCG-3') (engineered *SacI* restriction sites are underlined) [170]. The PCR product and pUC18r6k-mini-Tn7(*kanEW*) (a derivative of pUC18r6k-mini-Tn7 [171] in which the original *kan* cassette was replaced with the *kan* cassette from pKD13) were digested with *SacI* and ligated together to generate pLOU027. The EM7 promoter was subsequently removed from pLOU027 by digesting the plasmid with *KpnI*, which excised the promoter. The *toI/C* promoter was amplified by PCR using primers DNA408 (5'-G GGT ACCGCC ACT CAT CGC AGT GTG-3') and DNA409 (5'-G GGT ACCAGG ATC GTC AAA AAC CGA TAT AAG ACG-3') and the *cysZK* promoter using primers DNA406 (5'-G GGT ACC ACT CTC GCC AAT ATT ATT GCG G-3') and

DNA407 (5'-G GGT ACCCGC CAA AAT ACG TCC GTT G-3') (engineered KpnI restriction sites are underlined). PCR products were digested with KpnI and ligated into KpnI-digested pLOU027. Proper orientation of the promoters was confirmed by DNA sequencing. Reporters were integrated into the *Y. pestis* chromosome through site specific transposition as described previously to generate the LUX_{PEM7}, LUX_{P_{to}C}, and LUX_{P_{cys}ZK} bioreporter strains [171]. The antibiotic resistance cassette was excised from MBLYP-043 and MBLYP-045 as described previously [181].

To compare the sensitivity of the reporters, reporter strains YPA022, YPA038, YPA039, and YPA040 were inoculated in BHI broth in triplicate and grown for 15 hrs at 26°C. Serial 10-fold dilutions of the cultures were made in sterile 1X PBS, and the bacterial concentration of the dilutions was determined by enumerating on BHI agar. 100 µl aliquots were also transferred to a 96-well white plate and bioluminescence for each dilution was determined using a Synergy HT plate reader (BioTek, Winooski, VT) (1 sec read, sensitivity of 135). Linear regression analysis of the log transformed data was used to calculate the trend line, R² values, and limit of detection.

To determine growth profiles and correlation between CFU and bioluminescence, YPA035, YPA038, YPA039, and YPA040 were grown for 15 hrs in BHI at 26°C. Bacteria were diluted into fresh medium to a concentration of 0.03 to 0.05 OD₆₀₀/ml and grown for 12 hrs at either 26 or 37°C. Samples were harvested at various time points during growth to determine OD₆₀₀, bioluminescence using a Synergy HT plate reader (1 sec read, sensitivity of 135), and bacterial numbers by serial dilution and enumeration on BHI agar. Linear regression analysis of the log transformed data was used to calculate the trend line and R² values. To compare expression between 26 and 37°C, RLU per CFU was determined for each sample over the entire growth curve. Statistical significance was determined using the Mann-Whitney *t* test with a two-tailed nonparametric analysis.

Survival of *Y. pestis* in the presence of antimicrobial compounds

To monitor survival of *Y. pestis* in antimicrobial compounds, YPA039 was grown for 15 hrs at 26°C. The OD₆₀₀ of the culture was determined and bacteria were diluted to 1 OD₆₀₀/ml. Bacteria were further diluted 100-fold in BHI to a final concentration of ~10⁶ CFU/ml. 100 µl of bacteria were added to wells of a white 96-well plate. Bioluminescence for each well was determined with a

Synergy HT plate reader (1 sec read, sensitivity of 135) to establish a baseline and then 100 µl of indicated dilutions of MicroChem-Plus (National Chemical Laboratories, Philadelphia, PA) or antibiotics (diluted in BHI) were added to each well. For MicroChem-Plus, the first reading was taken 2.5 mins after addition and every 1.3 mins thereafter until 14 mins. At 6 mins, a subset of samples was harvested, washed once with 1X PBS, and 10-fold serial dilutions of bacteria were spot plated on BHI agar. For antibiotics, the first reading was taken 10 mins after addition of antibiotics and every hr thereafter for 15 hrs. Plates were incubated at 26°C in the plate reader between reads. Samples were blanked against BHI only wells. At 4, 8, and 12 hrs, 100 µl of bacteria were harvested from each concentration and 10-fold serial dilutions were spot plated on BHI agar to determine CFU.

Intracellular survival assays

RAW264.7 macrophages (ATCC, Manassas, VA) were seeded into white 96-well tissue culture plates and infected with 10⁶ CFU (MOI=10) of the *Y. pestis* reporter strains YPA035, YPA038, YPA039, YPA040, YPA073, YPA048, or YPA049, as described previously [182]. Extracellular bacteria were killed by incubation with gentamicin (16 µg/ml) for 1 hr, followed by three washes with 1X PBS. Medium was replaced with DMEM+10% FBS containing 2 µg/ml gentamicin and plates were incubated at 37°C with 5% CO₂ for 24 hrs. Bioluminescence was determined at various time points using a Synergy HT plate reader (1 sec reading, sensitivity of 135). For CFU determinations, cells were lysed with 1% Triton 100 and bacteria were enumerated by serial dilution and plating on BHI agar.

In vivo imaging

All animal studies were approved by the University of Louisville Institutional Animal Care and Use Committee (protocol 10-117). Five-to 7-week-old female B6(Cg)-Tyr^{c-2J}/J (albino C57Bl/6) mice (The Jackson Laboratory, Bar Harbor, ME) were maintained in the ABSL-3 vivarium with sterilized food and water *ad libitum* at the University of Louisville's Center for Predictive Medicine Regional Biocontainment Laboratory and imaging was performed in conjunction with the Center for Predictive Medicine BIO-Imaging Core. Hair was removed with clippers on the dorsal and ventral

sides of the mice two days prior to infection. Mice were anesthetized using a ketamine-xylene mixture for infections and isoflurane for imaging. Mice were infected with MBLYP-043 (WT) or MBLYP-045 ($\Delta p/a$). For bubonic studies, mice were infected via injection of 200-400 CFU at the base of the tail or in the hind foot. For pneumonic infections, mice were infected via intranasal infection of 10^4 - 10^5 CFU. Beginning after infection, mice were monitored for disease symptoms twice daily and moribund mice were euthanized. For imaging, mice were anesthetized and images were taken using the IVIS Spectrum imaging system (Caliper Life Sciences, Hopkinton, MA). Average radiance (photons/sec/cm²) was calculated for regions of interest of infected animals and similar regions were analyzed from uninfected animals or tissues to determine background luminescence (used as the limit of detection). Statistical significance was determined using the Mann-Whitney *t* test with a two-tailed nonparametric analysis.

Figures and Figure Legends

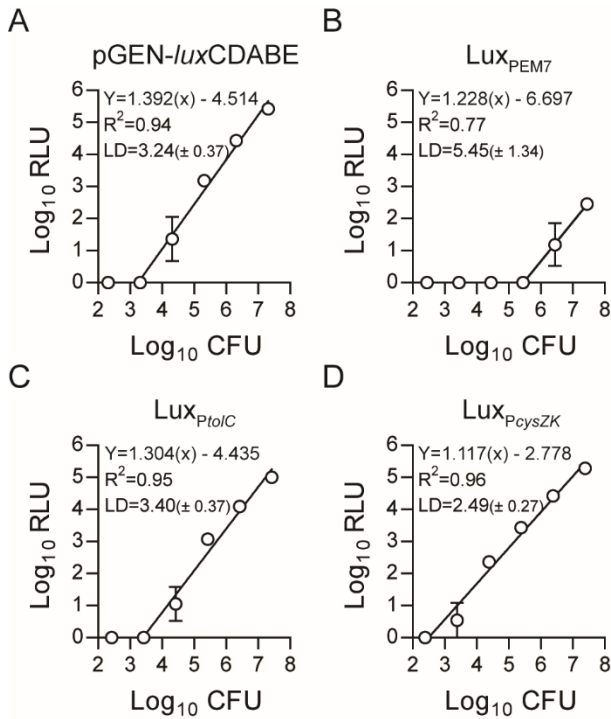


Figure 2—1 Sensitivities of chromosomal Lux reporters.

The *luxCDABE* operon driven by different promoters was integrated into the *Y. pestis* chromosome using Tn7 transposition. Sensitivities of the Lux reporters were determined by making serial dilutions of the *Y. pestis* Lux strains (grown for 15 hrs) and determining the number of bacteria (CFU) and bioluminescence (RLU) in each dilution ($n=3$). Linear regression analysis of the Log transformed data was used to calculate the trend line, R^2 values, and the limit of detection [LD= $\text{Log}_{10}\text{CFU} (\pm \text{standard deviation})$]. (A) pGEN-*luxCDABE*, (B) Lux_{PEM7} , (C) $\text{Lux}_{\text{P}_{\text{toIC}}}$, (D) $\text{Lux}_{\text{P}_{\text{cysZK}}}$.

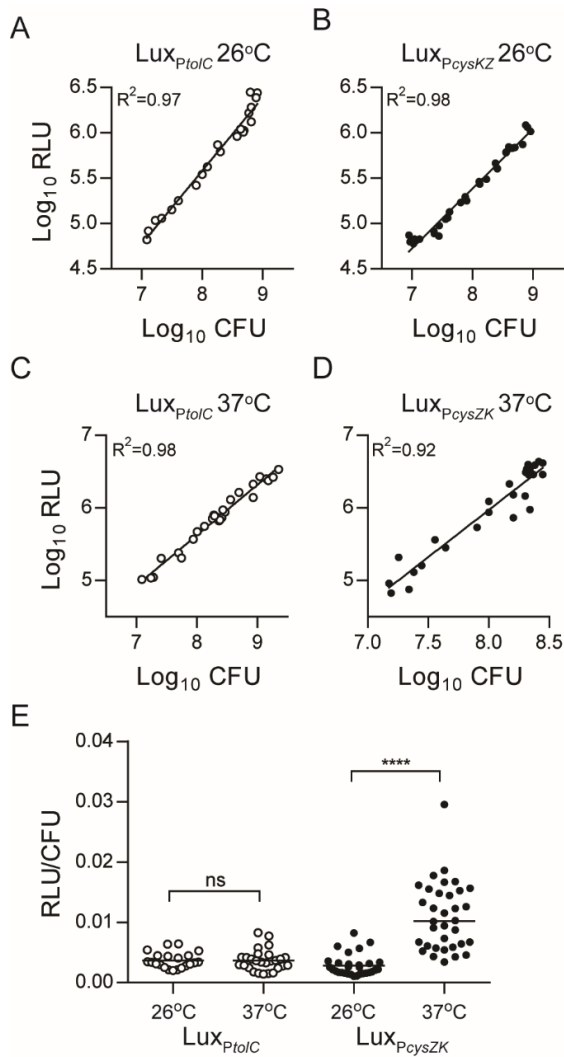


Figure 2—**Correlation between bioluminescence and bacterial number.**

Y. pestis $\text{Lux}_{P_{tolC}}$ and $\text{Lux}_{P_{cysZK}}$ were diluted in BHI broth (n=3) and grown at 26°C (A and B) or 37°C (C and D) for 12 hrs. Samples were harvested at multiple time points during growth to determine bioluminescence (RLU) and bacterial numbers (CFU). Linear regression analysis of the Log transformed data was used to calculate the trend line and R^2 values. (E) To determine if temperature impacted expression of the $\text{Lux}_{P_{tolC}}$ (white circles) or $\text{Lux}_{P_{cysZK}}$ (black circles) reporters, we calculated the RLU/CFU for each sample in A-D and compared the ratios. Black bars represent median values and statistical significance was determined using the Mann-Whitney *t* test with a two-tailed nonparametric analysis (****=p<0.0001, ns=not significantly different)

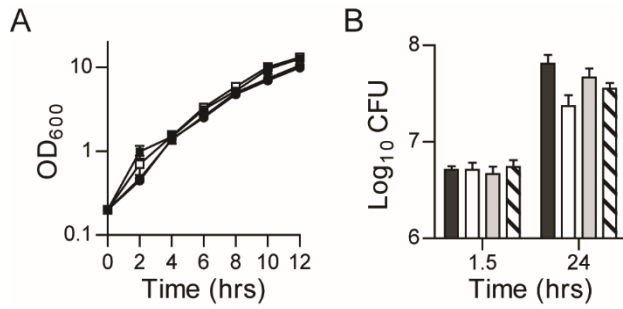


Figure 2—3Lux reporters do not impact fitness of *Y. pestis*.

To determine if carriage of the Lux reporters impacted *Y. pestis* fitness, (A) growth of the *Y. pestis* Lux bioreporter strains (n=3), and (B) survival in macrophages (n=3) were compared to WT *Y. pestis* without a Lux reporter. WT (no reporter) = ● or black bar; LUX_{PEM7} = ○ or white bar; LUX_{PtolC} = □ or gray bar; LUX_{PcysZK} = ■ or hatched bar.

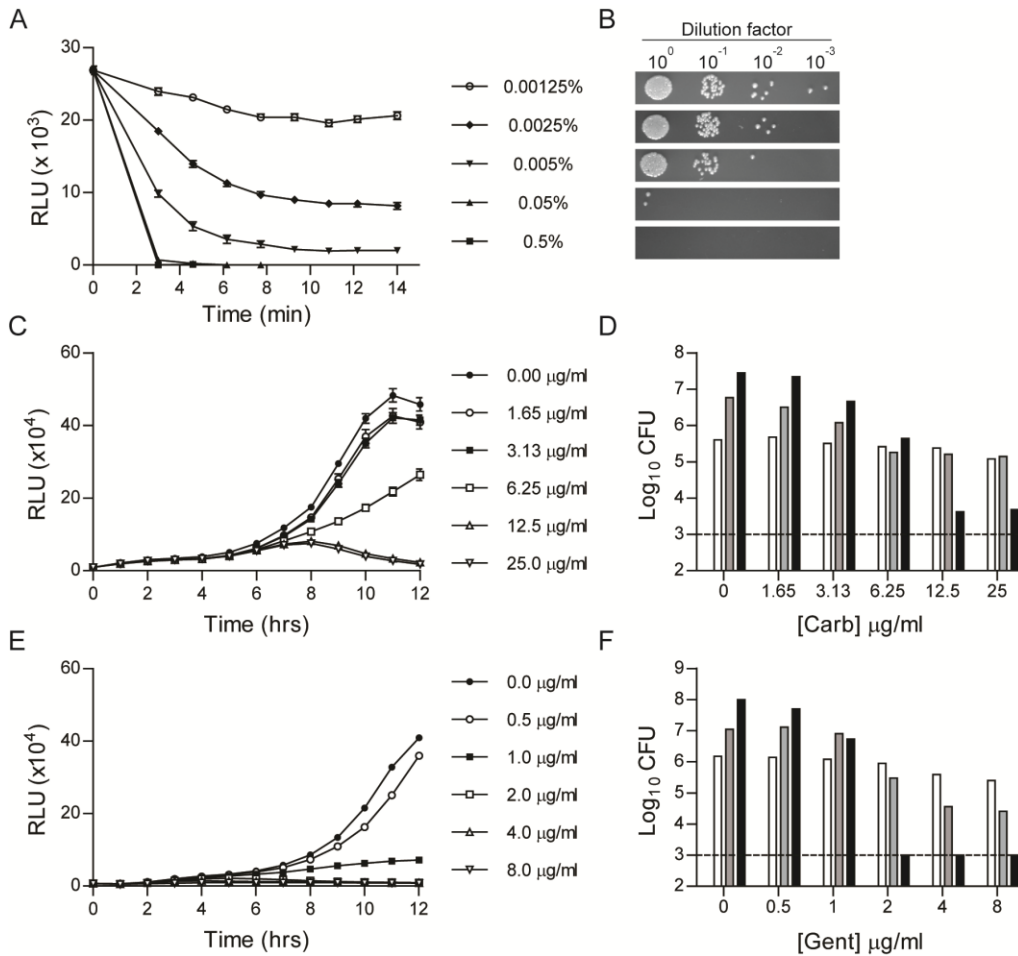


Figure 2—4 Use of LuxPtoIC to monitor survival of *Y. pestis* in the presence of antimicrobial compounds.

Y. pestis LuxPtoIC was incubated with increasing concentrations of antimicrobials (n=9) in a 96-well format and bacterial survival was monitored by measuring bioluminescence. (A) Bioluminescence readings (RLU) from *Y. pestis* LuxPtoIC incubated with MicroChem-Plus for 14 mins. (B) At 6 mins during incubation with MicroChem-Plus, bacteria were harvested from a subset of wells, washed, serially diluted, and spot plated on agar to determine bacterial CFU. (C) Bioluminescence readings (RLU) from *Y. pestis* LuxPtoIC incubated with carbenicillin for 12 hrs. (D) At 4 (white), 8 (gray), and 12 (black) hrs during incubation with carbenicillin bacteria were harvested from a subset of wells to determine bacterial CFU. (E) Bioluminescence readings (RLU) from *Y. pestis* LuxPtoIC incubated with gentamicin for 12 hrs. (F) At 4 (white), 8 (gray), and 12 (black) hrs during incubation with gentamicin, bacteria were harvested from a subset of wells to determine bacterial CFU. For D and F, the dotted line represents the limit of detection.

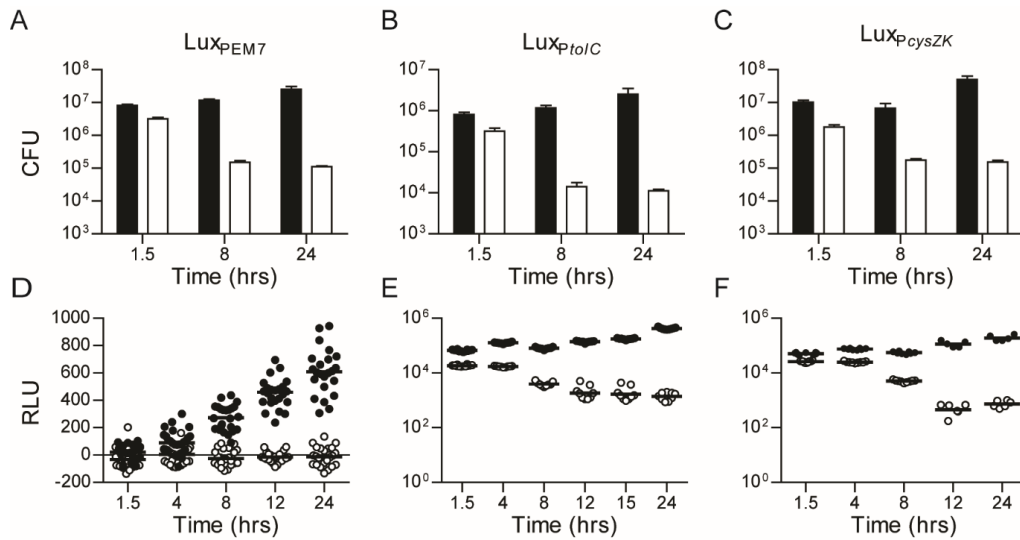


Figure 2—5. Survival of *Y. pestis* Lux reporters in macrophages.

RAW264.7 macrophages were infected with *Y. pestis* Lux reporter strains, extracellular bacteria killed by gentamicin, and bacterial survival monitored by CFU determination (A-C) or bioluminescence (D-F). Data from WT *Y. pestis* is represented by black symbols and from an attenuated $\Delta phoP$ mutant by white symbols. (A and D) are strains with the Lux_{PEM7} reporter (n=3 for CFU, n=24 for RLU), (B and E) are strains with the Lux_{PtolC} reporter (n=3 for CFU, n=12 for RLU), and (C and F) are strains with the Lux_{PcysZK} reporter (n=3 for CFU, n=12 for RLU).

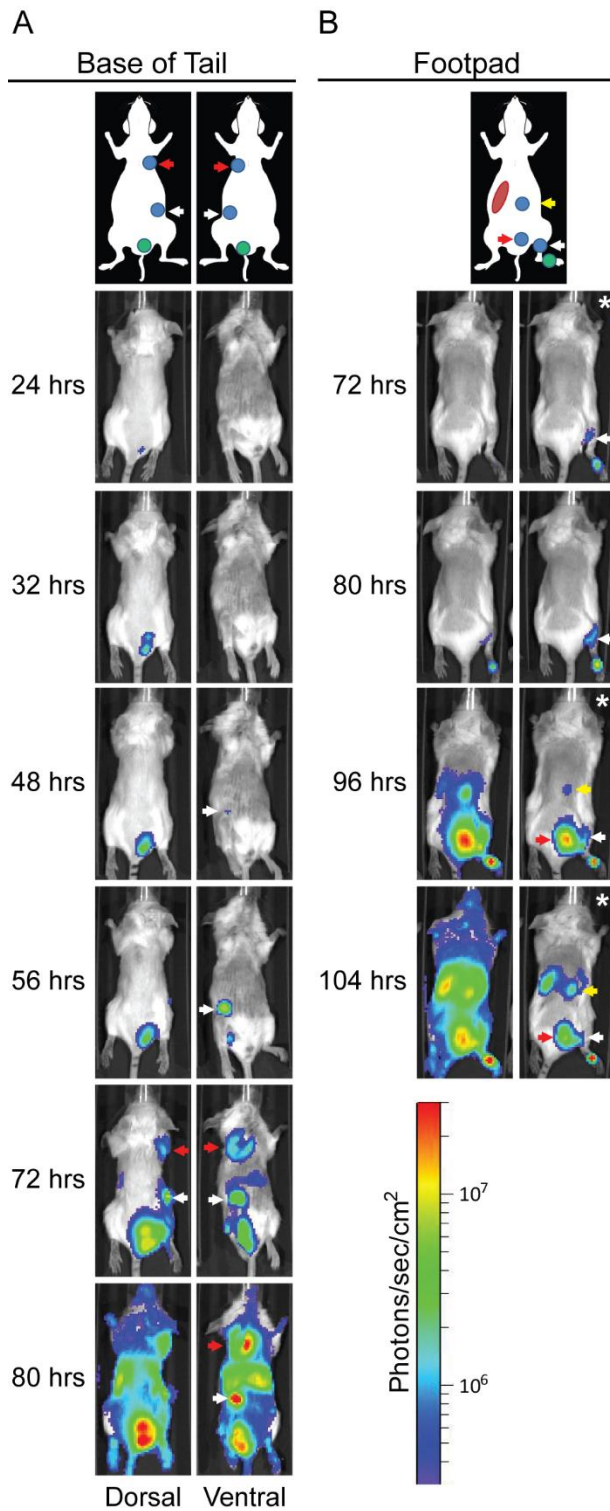


Figure 2—6. Dissemination of *Y. pestis* during bubonic infection.

Mice were infected with ~200 CFU of *Y. pestis* LuxP_{cysZK} subcutaneously at the base of the tail (A) or in the footpad (B) and imaged using an IVIS Spectrum. The lymph node drainage basin for each

inoculation site is diagrammed above the images [173, 174]. Location of the inoculation site is shown as a green circle, lymph nodes as blue circles, and the spleen as a red oval. For (A), the white arrow denotes the subiliac LN and the red arrow the axillary LN. For (B), the white arrow denotes the popliteal LN, the red arrow the sciatic LN, and the yellow arrow the renal LN. All images were adjusted to the radiance scale shown, except for the images in (B) marked with * in upper right corners. For these each image was adjusted to a different radiance to allow for visualization of specific tissues.

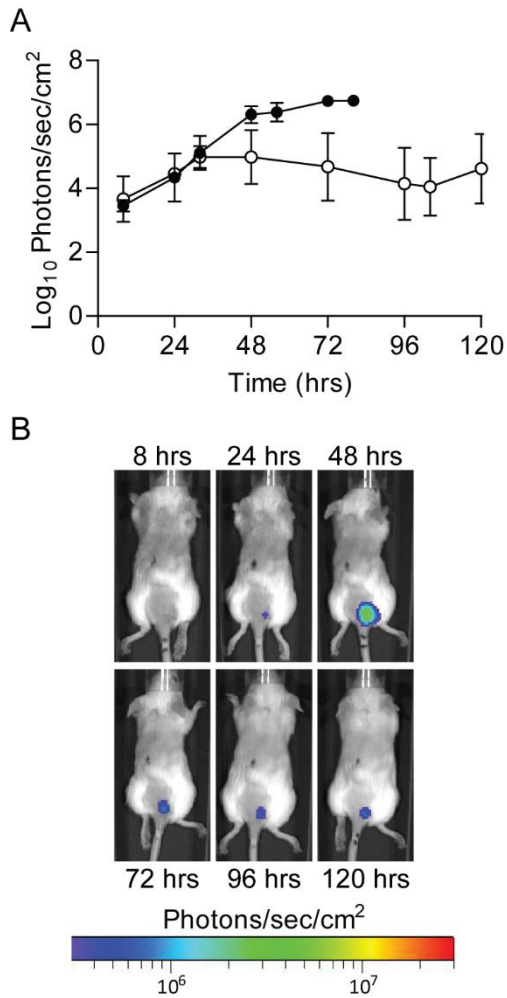


Figure 2—7. Continued bioluminescence from inoculation site.

Mice were infected with ~200 CFU of WT (n=5) or Δpla (n=5) *Y. pestis* Lux_{P_{cysZK}} subcutaneously at the base of the tail and imaged using an IVIS Spectrum. (A) The average bioluminescence detected from the inoculation site was determined over the course of the infection. Black and white symbols represent animals infected with WT or $\Delta pla Y. pestis$, respectively. (B) Sequential images from a representative animal infected with $\Delta pla Y. pestis$ Lux_{P_{cysZK}}.

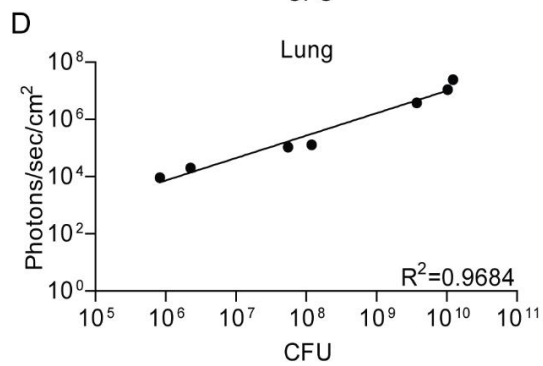
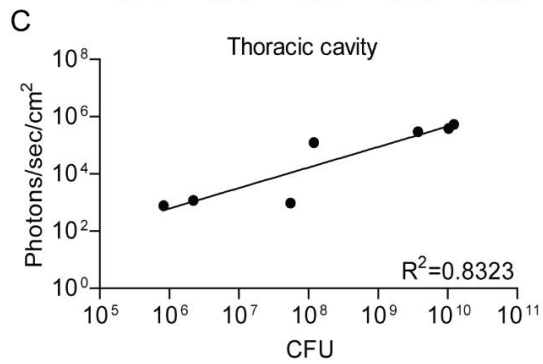
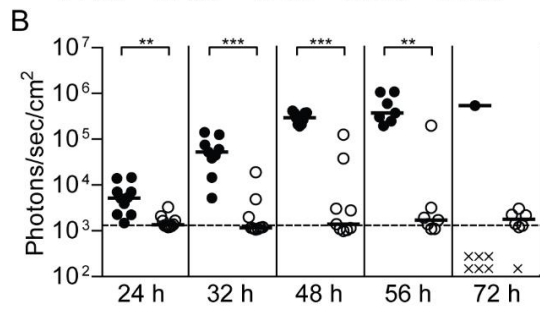
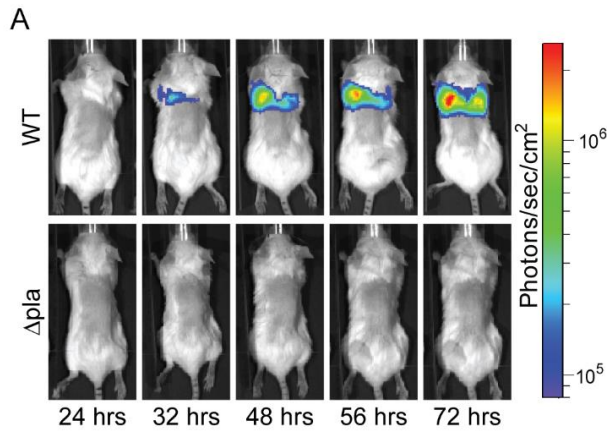


Figure 2—8. Progression of pneumonic infection.

Mice were infected with 5×10^4 – 1×10^5 CFU of *Y. pestis* LuxP_{cysZK} intranasally and imaged using an IVIS Spectrum. (A) Sequential images from representative animals. (B) For each animal, average bioluminescence was calculated for the thoracic cavity using the ROI tool in Living Image 3.2 software package. Black and white symbols represent animals infected with WT or $\Delta plaY$. *pestis*, respectively. Dotted line represents the limit of detection based on images from uninfected animals. ** = $p < 0.005$, *** = $p < 0.001$. At various time points, lungs were harvested from a subset of animals to determine bacterial loads (CFU) and compared to bioluminescence from the thoracic cavity (C) or from the lungs ex vivo (D).

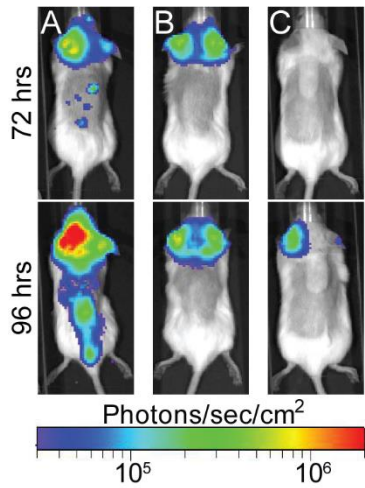


Figure 2—9. Extended imaging of animals intranasally infected with Δpla .

30% of animals infected intranasally with the Δpla mutant in Figure 6 developed bioluminescence signal from regions corresponding to the head. A, B, and C represent three individual animals. Animal A also represents an example of a Δpla infected animal that developed septicemic plague.

Tables

Table 2-1. Strains and plasmids used in this work

<i>Bacterial Strains</i>		
MBLYP-001	<i>Y. pestis</i> CO92; one passage from YP003-1	[9]
MBLYP-043	MBLYP-001 with Lux _{P_{cysZK}} reporter	This work
MBLYP-010	<i>Y. pestis</i> CO92 Δ <i>pla</i> ; one passage from YP102	[176]
MBLYP-045	MBLYP-010 with Lux _{P_{cysZK}} reporter	This work
YPA035	MBLYP-001 pCD1 ⁽⁻⁾	This work
YPA038	YPA035 with Lux _{P_{EM7}} reporter	This work
YPA039	YPA035 with Lux _{P_{tolC}} reporter	This work
YPA040	YPA035 with Lux _{P_{cysZK}} reporter	This work
YPA047	YPA035 Δ <i>phoP</i>	This work
YPA073	YPA047 with Lux _{P_{EM7}} reporter	This work
YPA048	YPA047 with Lux _{P_{tolC}} reporter	This work
YPA049	YPA047 with Lux _{P_{cysZK}} reporter	This work
YPA022	YPA035 with pGEN- <i>luxCDABE</i> plasmid	This work
<i>Plasmids</i>		
pGEN- <i>luxCDABE</i>	<i>Lux</i> operon with EM7 promoter	[170]
pUC18r6k-mini-Tn7(kanEW)	pUC18r6k-mini-Tn7 w/ modified Kan cassette	[171]
pLOU027	pUC18r6k-mini-Tn7(kanEW):: Lux _{P_{EM7}}	This work
pLOU034	pUC18r6k-mini-Tn7(kanEW):: Lux _{P_{tolC}}	This work
pLOU037	pUC18r6k-mini-Tn7(kanEW):: Lux _{P_{cysZK}}	This work
pTNS2	Tn7 transposase helper plasmid	[171]
pSKIPPY	pLH29 w/ Cat cassette replaced with Kan cassette	[183]

CHAPTER 3:
YERSINIA PESTIS REQUIRES HOST RAB1B FOR SURVIVAL IN
MACROPHAGES²

² Connor MG, Pulsifer AR, Price CT, Abu Kwaik Y, Lawrenz MB. *Yersinia pestis* Requires Host Rab1b for Survival in Macrophages. *PLoS pathogens*. 2015;11(10):e1005241. doi: 10.1371/journal.ppat.1005241.

Author Summary

Yersinia pestis is the bacterial agent that causes the human disease known as plague. While often considered a historic disease, *Y. pestis* is endemic in rodent populations on several continents and the World Health Organization considers plague to be a reemerging disease. Much of the success of this pathogen comes from its ability to evade clearance by the innate immune system of its host. One weapon in the *Y. pestis* arsenal is its ability to resist killing when engulfed by macrophages. Upon invasion of macrophages, *Y. pestis* actively manipulates the cell to generate a protective vacuolar compartment, called the *Yersinia* containing vacuole (YCV) that allows the bacterium to evade the normal pathogen killing mechanisms of the macrophage. Here we demonstrate that the host protein Rab1b is recruited to the YCV and is required for *Y. pestis* to inhibit both the acidification and normal maturation of the phagosome to establish a protective niche within the cell. Rab1b is the first protein, either from the host or *Y. pestis*, shown to contribute to the biogenesis of the YCV. Furthermore, our data suggest a previously unknown impact of Rab1b recruitment in the phagosome maturation pathway.

Overview

Yersinia pestis is a facultative intracellular pathogen that causes the disease known as plague. During infection of macrophages *Y. pestis* actively evades the normal phagosomal maturation pathway to establish a replicative niche within the cell. However, the mechanisms used by *Y. pestis* to subvert killing by the macrophage are unknown. Host Rab GTPases are central mediators of vesicular trafficking and are commonly targeted by bacterial pathogens to alter phagosome maturation and killing by macrophages. Here we demonstrate for the first time that host Rab1b is required for *Y. pestis* to effectively evade killing by macrophages. We also show that Rab1b is specifically recruited to the *Yersinia* containing vacuole (YCV) and that *Y. pestis* is unable to subvert YCV acidification when Rab1b expression is knocked down in macrophages. Furthermore, Rab1b knockdown also altered the frequency of association between the YCV with the lysosomal marker Lamp1, suggesting that Rab1b recruitment to the YCV directly inhibits phagosome maturation. Finally, we show that Rab1b knockdown also impacts the pH of the *Legionella pneumophila* containing vacuole, another pathogen that recruits Rab1b to its vacuole.

Together these data identify a novel role for Rab1b in the subversion of phagosome maturation by intracellular pathogens and suggest that recruitment of Rab1b to the pathogen containing vacuole may be a conserved mechanism to control vacuole pH.

Introduction

Yersinia pestis is a facultative intracellular pathogen and causative agent of the disease known as plague. There have been three human plague pandemics in history; the most notable being the Black Death in the 14th century [1, 5]. *Y. pestis* can infect humans either through the bite of an infected flea or inhalation of contaminated aerosols. Flea inoculation can lead to the development of bubonic plague, a form of plague highlighted by bacterial dissemination to, and replication within, lymph nodes [1]. Inhalation of *Y. pestis* contaminated aerosols can result in rapid colonization of the lungs and development of pneumonic plague [1]. Both forms of plague are associated with acute disease progression and high mortality rates in the absence of timely antibiotic treatment. Furthermore, the potential for person-to-person transmission and use as a biological weapon in the absence of a vaccine highlights the risks associated with this pathogen [14].

During its natural life cycle, *Y. pestis* cycles between two different hosts, the mammal and the flea. The bacterium requires different virulence factors to colonize each host, and coordinates the expression of these factors accordingly [1]. *Y. pestis* has several well characterized antiphagocytic mammalian virulence factors, such as the Ysc type three secretion system (T3SS), secreted Yop effectors and the Caf1 capsule [1]. However, these virulence factors are down regulated in the flea vector and at the time of initial colonization of the mammalian host [1]. During this transitional period, *Y. pestis* is highly susceptible to phagocytosis by macrophages and neutrophils [51, 54]. Initial colonization of *Y. pestis* induces a rapid and early influx of neutrophils to the site of infection [51, 184]. Upon phagocytosis by neutrophils, *Y. pestis* is readily killed by these professional phagocytes [53, 58, 80]. However, *Y. pestis* has demonstrated an increased ability to survive phagocytosis by monocytes and macrophages [51, 54, 57, 59, 82]. Upon entry into the macrophage, *Y. pestis* actively circumvents the natural maturation of the phagolysosome by remodeling the phagosome into a hospitable replicative niche called the *Yersinia* containing

vacuole (YCV) [55, 57, 59, 83, 86]. *In vitro* studies have highlighted three key characteristics of the biogenesis of the YCV. First, *Y. pestis* is able to actively inhibit the normal acidification of the phagosome and maintain a pH between 6.5 - 7.5 within the YCV throughout the course of intracellular infection [59]. Second, a significant portion of YCVs appear to become autophagosomes, which is highlighted by colocalization with LC3-II and the presence of double membranes surrounding the bacteria [59, 88]. While the contribution of autophagy to intracellular survival is unclear, data indicates that autophagy contributes to the metabolism of intracellular bacteria [88, 89]. Finally, approximately eight hours after phagocytosis, the tight fitting vacuolar membrane of the YCV begins to expand in size to form a spacious vacuolar compartment that can be observed by both light and electron microscopy [54, 59, 62, 86]. Bacterial replication within the YCV usually coincides with spacious vacuole formation. Importantly, while the fate of *Y. pestis* in the macrophage has been characterized, the mechanisms used to generate the YCV and avoid macrophage killing have not been defined.

The ability of *Y. pestis* to survive within macrophages also appears to impact virulence of the bacterium. *In vivo*, intracellular *Y. pestis* are recovered from macrophages isolated from both infected nonhuman primates and rodents, but rarely from neutrophils isolated from the same animals [49, 58, 84]. Ye and colleagues further showed lower bacterial burdens in transgenic MaFIA mice selectively depleted of macrophage/dendritic cell populations, suggesting that macrophages are required to establish acute infection [52]. *Y. pestis* *phoPQ* mutants, which are defective for intracellular survival, are also attenuated during subcutaneous infection of BALB/c (75-fold change in LD₅₀) and Swiss Webster mice (no change in LD₅₀ but a significant delay in time to death for mutant infected animals) [56, 90]. Moreover, macrophages isolated from canines, a species that are relatively resistant to plague [91], are significantly more capable in killing *Y. pestis* than macrophages isolated from laboratory mice, a species highly susceptible to plague, suggesting that the ability of macrophages to kill *Y. pestis* may contribute to resistance to infection [62]. Together, these data highlight the importance of *Y. pestis* survival within the macrophage during pathogenesis

Rab GTPases are the largest member of the Ras Superfamily of small guanine triphosphatases and are central mediators of vesicle trafficking within eukaryotic cells [102, 185]. These GTPases mediate vesicle trafficking by cycling through active GTP-bound and inactive GDP-bound conformations [102, 185]. When bound to GTP, the Rab protein integrates into specific vesicle membranes to mediate the trafficking of that vesicle through interactions with other trafficking proteins. Hydrolysis of the bound GTP to GDP results in extraction of the Rab from the membrane. While approximately 60 different Rab proteins have been identified, the contributions of only a few Rabs to specific vesicle trafficking steps have been experimentally described. For example, Rab5, Rab7, and Rab9 have been well studied as key mediators of important steps in the phagosome maturation process [94-96, 98, 100, 101]. Rab5 is recruited to the early endosome/phagosome and is required for phagocytosis [94-96, 98, 100, 101]. Following phagocytosis, Rab5 disassociates from the early endosome and Rab7 is recruited to the endosome to facilitate recruitment of Rab9 and subsequent fusion with the lysosome [94-96, 98, 100, 101]. A single disruption in the recruitment of a Rab protein to the maturing vesicle can stall and even terminate trafficking of that particular endocytic vesicle to its intended destination.

Due to the central role of Rab proteins for endosome sorting and phagosome maturation, many intracellular pathogens target Rab proteins to subvert these processes (see [102] for review). A classic example of Rab manipulation is seen in *Mycobacterium* infection of macrophages. *M. avium* and *M. tuberculosis* alter the normal distribution of Rab5 and Rab7 on their vacuole – retention of Rab5 and exclusion of Rab7 – to inhibit phagosomal fusion with the lysosome and subsequent killing of the bacteria [93, 107, 109, 110, 186, 187]. More recently, Rab1 has emerged as a common target required for the intracellular survival of many pathogens [107, 115, 117, 118, 188-195]. Rab1 has two isoforms, Rab1a and Rab1b, which share 92% amino acid similarity and are thought to be functionally redundant [196, 197]. Both isoforms have been shown to be involved in ER-to-Golgi trafficking [191, 198]. More recently Rab1a has been associated with proper endosome sorting during receptor mediated endocytosis and Rab1b has also been linked to autophagosome formation [192, 199-202]. Several pathogen containing vacuoles (PCVs) have been shown to associate with Rab1, and this recruitment is essential for subsequent survival of the

pathogens contained within the PCV [115, 117, 118, 188-193, 203]. *Coxiella burnetii* requires Rab1 for the *Coxiella* replicative vacuole (CRV) to expand in both Chinese hamster ovary (CHO) and RAW264.7 macrophage cells [188]. This expansion is significantly hindered in the presence of a GTP restricted form of Rab1 [188]. Similarly, *Anaplasma phagocytophilum* also recruits Rab1 directly to the *Anaplasma* containing vacuole (APV) and it has been speculated that recruitment of Rab1 to the APV allows the bacteria to hijack endocytic trafficking [191]. Perhaps the best studied subversion of Rab1 by a pathogen comes from *Legionella pneumophila*. Rab1 has been shown to accumulate on the *L. pneumophila* containing vacuole (LCV) as early as 10 min after bacterial uptake and Rab1 knockdown has been shown to inhibit *L. pneumophila* intracellular replication [115, 118, 189]. Furthermore, several *L. pneumophila* secreted effectors have been identified that specifically target and modify Rab1 to alter its localization [115, 118, 120, 121, 124, 128, 189, 193, 203, 204]. In contrast to the requirement of Rab1 for the survival of these intracellular pathogens that exist within vacuoles, *Shigella flexneri*, which replicates in the host cytoplasm, is hindered by Rab1 [190]. Inactivation of Rab1 by *S. flexneri* is critical for bacterial survival and is mediated by the VirA/EspG secreted effector family [190]. Together, these studies suggest a distinct role for host Rab1 GTPases for intracellular survival of pathogens that replicate within vacuolar compartments.

Since Rab1 appears to be targeted by several pathogens that reside within vacuoles in order to survive intracellularly, we investigated the role of Rab1 in the survival of *Y. pestis* within macrophages. We demonstrate that siRNA knockdown of Rab1b in macrophages infected with *Y. pestis* significantly increases YCV acidification and association with the lysosomal marker Lamp1, resulting in decreased intracellular survival of *Y. pestis*. Furthermore, we show Rab1b is recruited to the YCV, suggesting a direct interaction with Rab1b is required for proper YCV maturation. Importantly, Rab1b is the first host protein to be identified that is required by *Y. pestis* to alter phagosome maturation and YCV acidification and impact the ability of this pathogen to survive within the eukaryotic cell. Finally, we also demonstrate for the first time that Rab1b recruitment to the *L. pneumophila* containing vacuole also impacts vacuole pH, suggesting a conserved mechanism for the recruitment of Rab1b to pathogen containing vacuoles.

Results:

Rab1b is required for Y. pestis survival in macrophages

Since *Y. pestis* exists within a vacuolar compartment within macrophages [54, 55, 57], and Rab1 has been linked to survival of several other intracellular pathogens that exist within vacuoles [117, 118, 188, 189, 191, 192, 194], we sought to determine if Rab1 is required for *Y. pestis* intracellular survival. Toward this goal, we initially screened whether either isoform of Rab1 is required for *Y. pestis* to survive in macrophages. RAW264.7 macrophages were transfected with either Rab1a or Rab1b specific siRNAs (pool of 3 siRNAs targeting each gene). 48 h after transfection, macrophages were infected with *Y. pestis* CO92 pCD1⁽⁻⁾ Lux_{P_{tolC}}, which contains a bioluminescent bioreporter to monitor *Y. pestis* numbers [151]. Extracellular bacteria were killed with gentamicin, and intracellular bacterial survival was monitored via bioluminescent signal (Fig 3-1A). While no change in *Y. pestis* bioluminescence was observed in Rab1a siRNA treated cells compared to scrambled siRNA treated controls, we observed a significant decrease in bioluminescence in Rab1b siRNA treated cells, indicating that Rab1b, but not Rab1a, is required for *Y. pestis* survival within macrophages.

To confirm Rab1b is required for *Y. pestis* intracellular survival, RAW264.7 macrophages were transfected with a single Rab1b siRNA optimized for Rab1b knockdown and cell viability (Fig 3-S1) and infected with *Y. pestis* CO92 pCD1⁽⁻⁾ Lux_{P_{tolC}} 48 h post-transfection. As a positive control, we also infected macrophages transfected with Cop β 1 siRNA. Cop β 1 is a component of the cotamer complex and has been shown to alter both invasion and survival of other intracellular pathogens [141, 205]. As expected, Cop β 1 knockdown resulted in a significant decrease in intracellular *Y. pestis* CO92 pCD1⁽⁻⁾ Lux_{P_{tolC}} bioluminescence at 10 h post-infection as compared to scramble siRNA treated cells (Fig 3-1B; $p \leq 0.0001$). Rab1b knockdown also resulted in a significant decrease in bioluminescent signal; *Y. pestis* CO92 pCD1⁽⁻⁾ Lux_{P_{tolC}} bioluminescence was ~50% less in Rab1b siRNA treated cells (Fig 1B; $p \leq 0.0001$). To confirm that *Y. pestis* CO92 pCD1⁽⁻⁾ Lux_{P_{tolC}} bioluminescence accurately represents viable intracellular bacteria, cells were lysed and bacterial numbers were determined by conventional serial dilution enumeration (Fig 3-1C). Conventional enumeration supported our bioluminescent data and demonstrated a significant

decrease in viable intracellular colony forming units (CFU) in Rab1b siRNA treated cells ($p \leq 0.001$). No differences in survival were observed if bacteria were grown at 37°C prior to infection (Fig 3-S2). Importantly, the direct correlation between bioluminescent signal and bacterial enumeration support the use of bioluminescent data to monitor intracellular *Y. pestis* numbers.

To confirm that the pCD1 encoded Ysc type three secretion system (T3SS) does not impact Rab1b mediated *Y. pestis* survival, Rab1b transfected cells were also infected with *Y. pestis* KIM D-19 $Lux_{P_{tolC}}$, which contains the pCD1 plasmid and the Ysc T3SS, and bacterial survival was monitored by bioluminescence and conventional bacterial enumeration (Fig 3-1E and F). As observed for *Y. pestis* CO92 $pCD1^{(-)}$ $Lux_{P_{tolC}}$, we observed an ~50% decrease in *Y. pestis* KIM D-19 $Lux_{P_{tolC}}$ survival in Rab1b siRNA treated cells ($p \leq 0.001$). We also monitored *Y. pestis* intracellular bioluminescence temporally over the course of the infection to determine how early during infection *Y. pestis* intracellular survival was impacted by Rab1b knockdown. This analysis revealed that intracellular bacterial numbers for both strains were significantly decreased in Rab1b treated cells as early as 2 h post-infection, which is the earliest time point we can monitor after gentamicin removal (Fig 3-1D and G; $p \leq 0.001$). Finally, to determine if the Rab1b impact on intracellular survival is conserved in the *Yersinia* genus, transfected macrophages were infected with *Y. pseudotuberculosis* and *Y. enterocolitica*. As observed for *Y. pestis*, both enteric species were attenuated in survival when Rab1b was knocked down (Fig 3-S1). Together these data demonstrate that Rab1b is required for *Yersinia* intracellular survival, which is independent of the Ysc T3SS, and bacterial survival is impacted by Rab1b very early during the infection process.

Rab1b is not required for Y. pestis invasion of macrophages

We observed a difference in *Y. pestis* intracellular numbers in Rab1b siRNA treated cells within 2 h of macrophage infection (Fig 3-1D and G). The difference in recovered bacteria at this early time point could be due to an inability of *Y. pestis* to avoid phagolysosomal killing in the absence of Rab1b. However, Rab1b may also be required for efficient phagocytosis and the difference in *Y. pestis* numbers at 2 h post-infection could be a result of less bacteria gaining entry into the macrophages prior to gentamicin treatment. Because phagolysosome fusion and bacterial killing can occur within 120 minutes of phagocytosis [94, 102], we could not rely on the conventional

gentamicin protection assay, which requires a 1 h incubation period, to differentiate between invasion and bacterial killing in Rab1b siRNA treated cells. Therefore, we used a differential staining procedure to specifically label extracellular *Y. pestis* and determine if Rab1b knockdown impacted *Y. pestis* invasion of macrophages by confocal microscopy. Rab1b siRNA transfected RAW264.7 macrophages were infected with *Y. pestis* CO92 pCD1⁽⁻⁾pGEN-*P_{EM7}*::DsRED [206], which constitutively expresses the DsRED fluorescent protein. At 20 and 80 min post-infection, cells and total bacteria were fixed with paraformaldehyde. Extracellular bacteria were then specifically labeled with anti-*Y. pestis* polyclonal antibody and Alexa Fluor 488 anti-rabbit secondary antibody (Fig 3-2A). As a positive control, macrophages were treated with Cop β 1 siRNA, which has been previously shown to be required for efficient phagocytosis [141]. As expected, cells treated with Cop β 1 had significantly less intracellular *Y. pestis* than scrambled siRNA treated macrophages at both 20 and 80 min post-infection (Fig 3-2B and C; $p \leq 0.001$). Conversely, we observed no difference in the proportion of intracellular *Y. pestis* in Rab1b siRNA treated cells compared to scrambled siRNA treated cells. These data demonstrate that Rab1b is not required for phagocytosis of *Y. pestis* and suggest that the differences in intracellular bacterial numbers in Rab1b siRNA treated cells is due to a decreased ability of *Y. pestis* to avoid macrophage killing in the absence of Rab1b.

Rab1b is required for Y. pestis to avoid YCV acidification.

A hallmark characteristic of *Y. pestis* infection of the macrophage is that the bacterium is able to rapidly subvert normal acidification of the YCV [59]. Because acidification is one of the earliest steps in phagosome maturation and is required for both efficient lysosomal fusion and degradation of phagolysosomal contents [94], we next investigated whether Rab1b is required for *Y. pestis* to avoid YCV acidification. RAW264.7 macrophages were transfected with Rab1b siRNA and then treated with LysoTracker Red DND-99 prior to infection with *Y. pestis* CO92 pCD1⁽⁻⁾ pGEN222, which constitutively expresses EGFP. LysoTracker Red DND-99 fluorescence is pH dependent (fluoresces below pH 5.5), and therefore, allows for identification of acidified vacuoles. As *Y. pestis* inhibition of YCV acidification is an active process, untransfected cells were infected with paraformaldehyde killed *Y. pestis* CO92 pCD1⁽⁻⁾ pGEN222 to serve as a positive control for YCV

acidification. As previously reported for untransfected macrophages [59], *Y. pestis* CO92 pCD1⁽⁻⁾ pGEN222 efficiently avoided YCV acidification in scramble siRNA treated macrophages, with <25% of *Y. pestis* found within acidified vacuoles by 80 min post-infection (Fig 3-3). This was significantly lower than paraformaldehyde killed *Y. pestis*, which were already within acidified vacuoles >80% of the time by 20 min post-infection ($p \leq 0.01$). The ability of *Y. pestis* to inhibit YCV acidification was greatly attenuated in Rab1b knocked down cells, where ~70% of the bacteria were observed within acidified vacuoles within 20 min post-infection ($p \leq 0.01$). Furthermore, *Y. pestis* remained within acidified vacuoles in Rab1b siRNA treated macrophages at 80 min post-infection. These data demonstrate that *Y. pestis* requires the host Rab1b GTPase to inhibit or avoid YCV acidification.

Rab1b is necessary for Y. pestis to avoid fusion with the lysosome.

Acidification of the phagosome precedes or coincides with fusion to lysosomes and degradation of foreign particles such as bacteria [94]. As Rab1b knockdown resulted in increased acidification of the YCV, we next determined if Rab1b is required for *Y. pestis* to avoid fusion with lysosomes. RAW264.7 macrophages were transfected with Rab1b siRNA and infected with live or paraformaldehyde killed *Y. pestis* CO92 pCD1⁽⁻⁾ pGEN-*P_{EM7}*::DsRED. At 20 and 80 min post-infection, cells were washed, fixed with paraformaldehyde, and stained with anti-Lamp1 antibody, a marker for lysosomal fusion (Fig 3-4A). In scrambled siRNA treated cells, we observed minimal association of live *Y. pestis* with Lamp1 (<25%) at 20 and 80 min post-infection, indicating limited association between the YCV and lysosomes at these time points (Fig 3-4B and C). As observed for YCV acidification, there was a significant increase in the association between Lamp1 and paraformaldehyde killed *Y. pestis* (>60%), supporting an active avoidance of lysosomal fusion by *Y. pestis* during macrophage infection (Fig 3-4B and C; $p \leq 0.001$). Rab1b knockdown also significantly altered Lamp1 association with the YCV compared to scramble siRNA (Fig 3-4B and C; $p \leq 0.001$ and $p \leq 0.01$, respectively). At 20 min post-infection, Lamp1 associated with ~55% of YCVs in Rab1b siRNA treated cells, and was maintained at this elevated level at 80 min post-infection. These data indicate that Rab1b is required not only for *Y. pestis* to inhibit YCV acidification but also to avoid lysosomal fusion. Importantly, the ~2-fold increase in association with Lamp1

directly correlates to a similar 2-fold decrease in *Y. pestis* survival in Rab1b siRNA treated macrophages (Fig 3-1).

Rab1b is not required for early Y. pestis association with LC3

Autophagy has been linked to both *Y. pestis* and *Y. pseudotuberculosis* intracellular infection and may be required for sustained bacterial metabolism within cells [59, 88]. Furthermore, studies have shown a recruitment of LC3, a marker for autophagosomes, to the YCV during *Y. pseudotuberculosis* infection of HeLa cells and BMDMs [88, 89]. Recently, Huang and colleagues demonstrated a potential role for Rab1b in autophagy and intracellular survival of *Salmonella enterica Typhimurium* [192]. Given the link of Rab1b to autophagy and autophagy to *Yersinia* intracellular infection, we next investigated if knockdown of Rab1b impacted early association of LC3 to the YCV during macrophage infection. RAW264.7 macrophages were transfected with Rab1b siRNA and infected with live or paraformaldehyde killed *Y. pestis* CO92 pCD1⁽⁻⁾ pGEN-*P_{EM7}::DsRED*. 20 and 80 min post-infection cells were washed, fixed with paraformaldehyde, and stained with anti-LC3 antibody (Fig 3-5A). In contrast to reported infection of epithelial cells with *Y. pseudotuberculosis* [89], we observed a very low incidence in the association between live or killed *Y. pestis* with LC3 during early stages of macrophage infection (Fig 3-5B and C) and this association was not significantly altered in Rab1b siRNA treated cells (~20% association in all samples). These data support previous data that LC3 association with the YCV is lower in macrophages than epithelial cells [88, 89] and demonstrate that Rab1b knockdown does not alter YCV-LC3 association during the early stages of *Y. pestis* infection when we observe changes in YCV maturation and intracellular survival of the bacteria.

Rab1b is recruited to the YCV during macrophage infection.

Rab GTPases mediate vesicular trafficking through direct interactions with vesicle membranes (see [102, 185] for review). Therefore, we next sought to determine whether Rab1b is recruited to the YCV during *Y. pestis* infection. Because Rab interactions with membranes are transient, we transfected RAW264.7 macrophages with a GFP-labelled, constitutively active form of Rab1b [eGFP-Rab1b(CA)]. eGFP-Rab1b(CA) contains a mutation in the GTP binding domain that inhibits

the hydrolysis of GTP, resulting in retention of the protein in the membrane in which the Rab GTPase is recruited [118, 191, 207, 208]. Twenty-four hours after transfection, macrophages were infected with either live or PFA killed *Y. pestis* CO92 pCD1⁽⁻⁾ pGEN::mCherry or *E. coli* K12 pGEN::mCherry, which constitutively express the mCherry fluorescent protein. Cells were washed and fixed with paraformaldehyde at 20 and 80 min post-infection and analyzed by confocal microscopy to determine localization of eGFP-Rab1b(CA) (Fig 3-6). Less than 25% of *E. coli* or PFA killed *Y. pestis*, which traffic to acidified vacuoles, colocalized with eGFP-Rab1b(CA) at 20 min post-infection (Fig 3-6B). Furthermore, we observed no significant change in colocalization at 80 min post-infection. However, in cells infected with live *Y. pestis*, we observed a significant increase in eGFP-Rab1b(CA) localization to the YCV at both time points (Fig 3-6B and C; ~57%; $p \leq 0.05$). These data demonstrate that while Rab1b is minimally associated with phagosomes containing *E. coli* or dead *Y. pestis*, the GTPase is associated with the YCV containing live *Y. pestis* at a significantly higher frequency, suggesting that Rab1b recruitment or retention to the YCV specifically contributes to *Y. pestis* survival.

Disruption of the secretory pathway does not alter Y. pestis survival or inhibition of YCV acidification

Rab1b has an important role in mediating ER-to-Golgi trafficking [209, 210]. While Rab1b appears to be directly recruited to the YCV, it is also possible that the effect of Rab1b knockdown on *Y. pestis* survival is due to changes in Golgi trafficking. To determine if Golgi trafficking, specifically secretory trafficking, is required for *Y. pestis* to inhibit YCV acidification, we treated RAW264.7 macrophages with Brefeldin A (BFA), which blocks Golgi trafficking independent of Rab1b by targeting Arf1. BFA-treated macrophages were infected with *Y. pestis* CO92 pCD1⁽⁻⁾ Lux_{P_{tolC}} for 20 min, extracellular bacteria were killed with gentamicin, and intracellular bacteria bioluminescence was monitored at 2 and 10 h post infection (Fig 3-7A and B, respectively). At both time points there was no significant difference in the survival of *Y. pestis* between untreated macrophages or cells treated with increasing concentrations of BFA. Macrophages treated with 10 μ M BFA were also incubated with LysoTracker Red DND-99 and subsequently infected with *Y. pestis* CO92 pCD1⁽⁻⁾ pGEN222 to determine if inhibition of the secretory pathway altered YCV

acidification. As a control, a separate group of cells were infected with paraformaldehyde killed *Y. pestis* CO92 pCD1⁽⁻⁾ pGEN222. In agreement with the intracellular bacterial survival, there was no significant difference between YCV acidification in BFA-treated macrophages at 20 or 80 min post-infection compared to untreated cells (Fig 3-7C and D). Furthermore, BFA treatment did not alter the acidification of phagosomes containing paraformaldehyde killed *Y. pestis*. Together these data demonstrate that *Y. pestis* avoidance of the phagolysosome is independent of retrograde endocytic trafficking and suggests that Rab1b impacts YCV maturation independent of its function in Golgi trafficking.

Rab1b inhibition results in increased acidification of the Legionella containing vacuole

Previous studies with *L. pneumophila* demonstrate the cyclic recruitment and release of Rab1b on the LCV within 2 hours post-infection [117]. The release of Rab1b from the nascent LCV coincides with the transition of the LCV from a neutral to acidic pH [211, 212]. Given that *Y. pestis* recruits Rab1b to the YCV to prevent vacuole acidification, we hypothesized that *L. pneumophila* recruitment of Rab1b may also result in arrest of LCV acidification. To test this hypothesis, we transfected RAW264.7 macrophage cells with siRNA targeting Rab1b and treated transfected cells with LysoTracker Red DND-99 prior to infection with *L. pneumophila* to monitor LCV acidification. As previously reported, we observed that the majority of LCVs did not colocalize with LysoTracker in scramble siRNA treated macrophage (only 30% of *L. pneumophila* was found in acidified compartments by 80 min post-infection; Fig 3-8). In contrast, we observed a significant increase in LysoTracker colocalization in macrophages treated with siRNA targeting Rab1b at both 20 and 80 min post-infection (Fig 3-8B and C; $p \leq 0.01$ and $P \leq 0.001$, respectively). These data demonstrate that like *Y. pestis*, *L. pneumophila* requires Rab1b to inhibit LCV acidification during early stages of macrophage infection.

Discussion

Rab proteins are central mediators in vesicular trafficking within the cell. As such, intracellular pathogens often target these GTPases to subvert the normal phagosome maturation pathway and survive within host cells (see [102, 103] for reviews). Rab1 was one of the first identified members

of this family and has been extensively studied for its role in Golgi trafficking in yeast, *Drosophila*, and mammalian cells (see [210, 213, 214] for reviews). More recently, both isoforms of Rab1 have been linked to intracellular infection by several pathogens. *Chlamydial* species [194], *L. pneumophila* [118, 189], *A. phagocytophilum*[191], *Coxiella burnetii*[188], and *S. enterica Typhimurium*[192] have been shown to recruit Rab1 to the PCV. Furthermore, inhibition of Rab1 by either RNAi or expression of dominant negative Rab1 constructs indicate that Rab1 function is required for the survival/growth of *L. pneumophila* [189], *C. burnetii* [188], *S. enterica Typhimurium* [133, 192], and *Brucella melitensis* [138]. Our data demonstrate for the first time that *Y. pestis* also belongs to this group. Specifically, we have demonstrated that *Y. pestis* recruits Rab1b to the YCV during infection of macrophages and that this GTPase is required for intracellular survival. Interestingly, Rab1 has only been shown to be required for the survival of pathogens that exist within vacuolar compartments, suggesting a role(s) for Rab1 in subverting normal phagosome maturation and generation of a protective PCV. In fact, functional Rab1 has been shown to be detrimental to the survival of the cytoplasmic pathogen *Shigella flexnerii* through its interaction with the autophagy system within the host cell [190]. However, *S. flexnerii* has also evolved to target Rab1, through the VirG secreted effector protein, and inactivate the GTPase to inhibit macroautophagy during infection [190].

While Rab1 has been linked to the survival of several intracellular pathogens, the role Rab1 plays in the maturation of individual PCVs is less well understood. In *C. burnetii*, Rab1 has been shown to be required for the massive expansion of the *Coxiella* replicative vacuole (CRV) [188]. This requires the acquisition of new membrane in order for the CRV to grow, and Rab1 recruitment to the vacuole may mediate the interception of vesicles (and their membranes) from the secretory pathway. This hypothesis is supported by studies showing that treatment with BFA, which independently inhibits the secretory pathway, also inhibits the expansion of the CRV [188]. Studies from *A. phagocytophilum* and *Chlamydial* species, which also form a large replicative vacuole, also suggest that Rab1 recruitment is important for formation of a spacious vacuolar compartment [191, 194]. Therefore, a common goal of bacteria that recruit Rab1 to their PCV may be to subvert the secretory pathway in order to remodel the PCV. Furthermore, Rab1b has also been linked to

autophagy [192], which is also associated with the replication of both *C. burnetii* and *A. phagocytophilum* [215, 216]. It is possible that in addition to the secretory pathway, Rab1 recruitment may also contribute to the recruitment of autophagosomal membranes to these PCV, though this has yet to be demonstrated. Since the YCV also expands late during infection (though not to the degree of these former pathogens) to form a spacious vacuole [54, 59, 62], it is possible that Rab1b may contribute to YCV expansion. However, we have not observed changes in spacious YCV formation in Rab1b siRNA treated macrophages. Furthermore, our data also suggest that early association with the autophagosome marker LC3 does not appear to protect YCV from acidification, as we observed no difference in YCV-LC3 association in Rab1b siRNA treated cells. More importantly, our data with *Y. pestis* reveal a potential new benefit of Rab1 recruitment to the PCV, which is to avoid phagosomal acidification and subsequent fusion to the lysosome. While it is currently unclear how Rab1b inhibits YCV acidification, it appears to be independent from its contributions to the secretory pathway, as BFA treatment did not result in similar changes to YCV acidification. Importantly, while knockdown of Rab1B does not alter the expression of Rab 5, 7 or 9, which are required for phagosome maturation (Fig 3-S1A), it is possible that recruitment and retention of Rab1b to the early phagosome inhibits interactions with these Rabs (and/or Rab effector proteins) to inhibit normal phagosome maturation. Rab1 has also been linked to endosomal sorting through direct interactions with the kinesin Kifc1, which in turn affects directional vesicular motility within the cell [201, 202]. Thus, Rab1b recruitment may alter early sorting of the YCV to avoid acidification and lysosomal fusion. Studies to better characterize the early YCV, including differences in Rab composition and vATPase recruitment as compared to the normal phagosome are ongoing and will provide further insight into these mechanisms. Rab1 recruitment to the YCV also occurs significantly earlier than reported for *C. burnetii* (≤ 20 min vs. >12 h, respectively) [188], suggesting that timing of recruitment may indicate which function, inhibition of phagosome maturation or membrane acquisition, is contributing to pathogenesis of various pathogens. It should be noted that *C. burnetii* requires passage through an acidified vacuole to induce the expression of important virulence factors and subsequent intracellular survival [217]. Therefore, our observations that early acquisition of Rab1 inhibits PCV acidification may explain why Rab1 recruitment is

delayed during *C. burnetii* infection. In contrast to *C. burnetii*, *L. pneumophila*, which inhibits LCV acidification early during infection [211, 212, 218], recruits Rab1 in a similar time frame as seen during *Y. pestis* infection (within 10 min) [118]. In support of our hypothesis that early recruitment of Rab1b is a mechanism for pathogens to inhibit phagosome acidification, we demonstrated that knockdown of Rab1b decreased the ability of *L. pneumophila* to inhibit LCV acidification (Fig 3-8). Interestingly, *L. pneumophila* appears to control both recruitment and later release of Rab1 from the LCV (discussed below). The timing of Rab1 modification by *L. pneumophila* coincides with a transition from a neutral to an acidic LCV [211, 212], suggesting that Rab1 inhibition of acidification may be an active process that is reversible upon removal of Rab1 from the vacuolar membrane.

Phagosome acidification has been shown to be a key step in phagosome maturation. Acidification of the phagosome is believed to work in concert with Rab5, Rab7 and Rab9 to mediate phagosome maturation and ultimately fusion with lysosomes [94, 95]. Initially, the early phagosome, highlighted by association with Rab5, is slightly acidic (~pH 6.0). As the phagosome matures, the pH decreases and Rab7 replaces Rab5 on the phagosome. Rab7 subsequently recruits more vATPase complexes, resulting in further acidification of the phagosome and recruitment of Rab9. By the time Rab9 mediates lysosomal fusion, the pH of the phagosome is approaching 4.0, which is the optimal pH to activate hydrolases and proteases delivered to the phagosome by the lysosome. Several lines of evidence indicate that acidification of the phagosome is required in order for efficient lysosomal fusion and function to occur [100, 101, 219-221], which suggest that inhibition of acidification could influence proper lysosomal fusion to the PCV. In line with these hypotheses, we observed a direct correlation between increased YCV acidification with increased Lamp1 association, and subsequent decreased *Y. pestis* survival, in Rab1b siRNA treated cells. This direct correlation makes it difficult to separate the impact of acidification directly on *Y. pestis* survival (acidic killing) from lysosomal fusion, but further supports the importance of inhibiting YCV acidification as mechanism for *Y. pestis* intracellular survival [59].

While Rab1 is important for the intracellular survival of several pathogens, bacterial virulence factors that target Rab1 have only been identified for *Chlamydia* [194] and *L. pneumophila* [116, 117, 119, 122, 125, 129, 193, 222, 223]. In the case of *L. pneumophila*, multiple Dot/Icm

secreted factors have been shown to target Rab1 and modify the protein to manipulate localization to the LCV; cycling the host Rab1 between active (anchored to the LCV) and inactive states. The effectors DrrA/SidM, SidD and LepB work in concert to first recruit Rab1 to LCV, and then later remove it [113, 115, 120, 121, 193]. *L. pneumophila* also manipulates Rab1 independent of recruitment to the LCV through the action of SidC/SdcA, LidA and AnkX [116, 127, 129, 223]. The redundancy in Rab1 targeting proteins indicates that Rab1 manipulation by *L. pneumophila* is extremely important for the intracellular survival of this pathogen. For *Y. pestis*, we have yet to define the virulence factors that mediate Rab1b recruitment to the YCV. However, we have shown that *Y. pestis* does not require the pCD1 plasmid (including the Ysc T3SS) or the high pathogenicity island (pgm locus) to recruit Rab1b and inhibit YCV acidification. These findings are in agreement with previous work that has shown both of these genetic elements are dispensable for intracellular survival [49, 53-55]. Therefore, virulence factors encoded elsewhere in the genome are mediating both Rab1b interactions and intracellular survival. While the PhoPQ two component regulator has been shown to contribute to intracellular survival, likely through the regulation of other genes [56, 83, 86, 90], we speculate that these genes do not regulate survival through Rab1b because *phoPQ* mutants still inhibit YCV acidification during infection [86]. However, defining Rab1b recruitment to the *phoPQ* mutant YCV is needed to confirm this hypothesis. Studies to specifically identify *Y. pestis* factors involved in Rab1b recruitment to the YCV are ongoing.

In summary, we have shown here for the first time that recruitment of Rab1b to the PCV directly correlates to the ability of a pathogen to inhibit acidification of the vacuole. These findings indicate a novel function for Rab1b in inhibiting phagosome maturation and suggest that other pathogens may use a similar strategy to modify the maturation of the PCV. Furthermore, in the context of *Y. pestis* infection, Rab1b is the first factor, either host or bacterial, identified that directly impacts acidification of the YCV. Future studies to define how Rab1b impacts phagosome acidification and to identify additional host factors that contribute YCV biogenesis will be important for us to understand how this pathogen evades killing by macrophages.

Materials and Methods

Bacterial strains, plasmids, and macrophages. All bacterial strains used in this study are listed in Table 3-S1 in the Supplementary Information. *Y. pestis* CO92 [9] pCD1⁽⁻⁾ and KIM D-19(pgm⁽⁻⁾) (BEI Resources) were cultivated at 26°C in Brain Heart Infusion (BHI) broth (Difco). When needed, carbenicillin was used at 50µg/mL. Bioluminescent derivatives were generated using the Lux_{P_{toC}} bioreporter as described previously [151]. To generate fluorescent bacterial strains, *Y. pestis* and *E. coli* K12 DH5α were transformed with pGEN222, pGEN-*P_{EM7}*::DsRED, or pGEN222::mCherry [206]. *E. coli* was cultivated at 37°C in Luria-Bertani (LB) broth (Difco) supplemented with 50µg/mL carbenicillin. *L. pneumophila* AA100, a clinical isolate containing pMIP-GFP, was grown on BCYE agar plates for 3 days at 37°C prior to macrophage infection [224-226]. The pGEN222::mCherry plasmid was generated by replacing the EGFP gene from pGEN222 with the mCherry gene using Gibson Cloning [227]. Constitutive active EGFP-Rab1b was generated by site directed mutagenesis of pEGFP-Rab1b [108] using primers 5'- TGG AAC GGT TCC GGA C-3' and 5'- GGC CCG CTG TGT CC-3' to mutate the Glutamine at residue 67 to a Leucine as previously described [108]. RAW264.7 macrophages were obtained from ATCC and cultured in DMEM, 100 mM glucose + 10% FBS (Hyclone).

Transfection of macrophages. For siRNA transfection, 20 µl of 0.165 µM Silencer siRNA (Life Technologies) diluted in Opti-MEM (Life Technologies) was mixed with 10 µl of 0.03% (v/v) Lipofectamine RNAiMax/Opti-MEM (Life Technologies) as described by the manufacturer. 30 µl of the siRNA-Lipofectamine complex was added to each well of a white flat-bottom 96-well plate (Greiner), incubated at room temperature for 10 min, and then 1x10⁴ RAW264.7 macrophages suspended in 80 µl of DMEM+10% FBS were added. Cells were incubated for 48 h at 37°C with 5% CO₂. For 24-well plates used for microscopy, all reagents were increased by 4-fold. For plasmid transfection, 4 µg of plasmid was transfected into 4.4 x 10⁵ RAW264.7 macrophages using Lipofectamine 2000 (Life Technologies) or 0.5 µg of plasmid with JetPrime (Polyplus) as described by the manufacturers. Luminescence was monitored with a Synergy 4 plate reader (BioTek) (1 sec read with sensitivity set at 150).

Bacterial infection of macrophages. Macrophages were infected with *Y. pestis* strains as previously described [57, 151]. Briefly, bacteria were grown at 26°C in BHI, washed in PBS, and diluted appropriately in prewarmed DMEM+10%FBS. Bacteria were added to macrophages and the infection was synchronized by centrifugation. After 20 min, extracellular bacteria were killed with gentamicin (16µg/mL). One hour after gentamicin treatment, the medium was replaced with DMEM + 10% FBS containing 2µg/mL gentamicin. Intracellular *Y. pestis* numbers were determined by bioluminescence using a Synergy HT plate reader (Biotek) or conventional bacterial enumeration as described previously [151]. For *L. pneumophila*, bacteria were swabbed directly from plates and diluted appropriately in prewarmed DMEM+10%FBS. Bacteria were added to macrophages and the infection was synchronized by centrifugation. At 20 minutes and 80 minutes post-infection cell monolayers were washed three times with PBS and fixed as described below [225, 226]. All MOIs were confirmed by conventional enumeration of the inoculum at the time of infection. For vacuole acidification experiments, 75 nM LysoTracker Red DND-99 (Life Technologies) was added to the cells 1 h prior to fixation. Brefeldin A (Sigma) was added to cells 2 h prior to *Y. pestis* infection and maintained throughout the infection.

Immunofluorescent staining and confocal microscopy. For confocal microscopy, cells were fixed to coverslips with 4% paraformaldehyde for 30 min. For indirect immunofluorescent staining, fixed cells were blocked with 3% BSA overnight and incubated with rabbit anti-*Y. pestis* serum (1:1,000), anti-Lamp1 (0.8µg/ul; Abcam ab24170), or anti-MAP-LC3α/β (1:200; Santa Cruz sc-16756) antibodies for 1 h. Unbound primary antibodies were removed by washing and anti-rabbit Alexa Fluor 488 secondary antibody (1:4000; Life Technologies) was added for 1 h. All coverslips were mounted with Prolong Gold with DAPI (Life Technologies) and imaged on an Olympus FV100 laser or Zeiss LSM 710 laser confocal microscope. Colocalization of LysoTracker Red DND-99 or proteins to the YCV was determined using the Coloc function in the Imaris image analysis software (BitPlane).

Statistics. All data are shown as mean and standard deviation of three to six biological replicates and each experiment was repeated three times to confirm the phenotypes. For microscopy, at least

50 vacuoles per biological replicate were analyzed. p-values were calculated by one-way ANOVA (or t-test for *L. pneumophila* experiments) using GraphPad Prism software.

Figure and Figure Legends

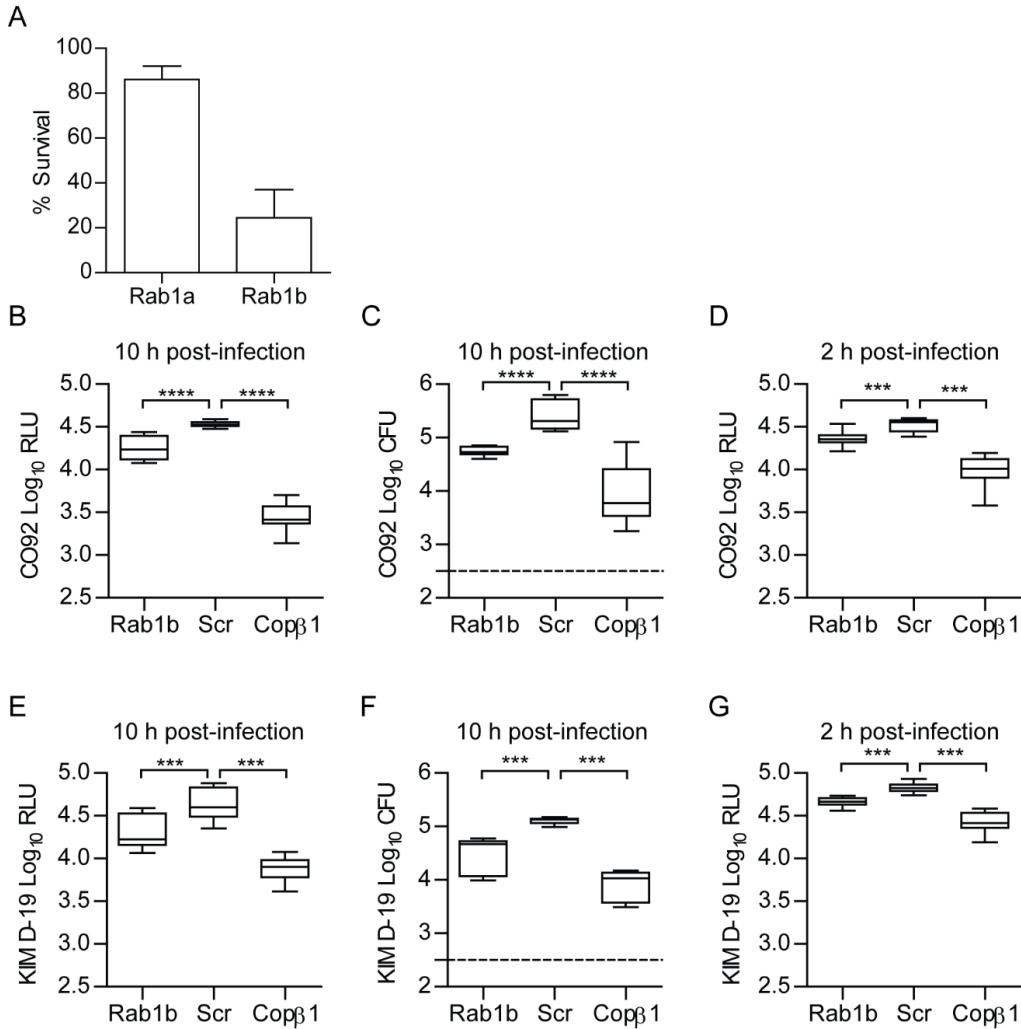


Figure 3—1. Rab1b knockdown inhibits the survival of *Y. pestis* within macrophages.

RAW264.7 macrophages were reverse transfected with Rab1a, Rab1b, scrambled (Scr), or Copβ1 siRNA. 48 h after transfection cells were infected with *Y. pestis* (MOI 10). (A) Percent survival of intracellular CO92 pCD1⁽⁻⁾ Lux_{P_{tolC}} in Rab1a or Rab1b siRNA treated macrophages as compared to Scr siRNA treated macrophages. (B) Bioluminescence of intracellular bacteria from macrophages infected for 10 h with *Y. pestis* CO92 pCD1⁽⁻⁾ Lux_{P_{tolC}}. (C) Conventional enumeration of intracellular bacteria from macrophages infected for 10 h with *Y. pestis* CO92 pCD1⁽⁻⁾ Lux_{P_{tolC}}.

(D) Bioluminescence of intracellular bacteria from macrophages infected for 2 h with *Y. pestis* CO92 pCD1⁽⁻⁾ Lux_{P_{tolC}}. (E) Bioluminescence of intracellular bacteria from macrophages infected for 10 h with *Y. pestis* KIM D-19 Lux_{P_{tolC}}. (F) Conventional enumeration of intracellular bacteria from macrophages infected for 10 h with *Y. pestis* KIM D-19 Lux_{P_{tolC}}. (G) Bioluminescence of intracellular bacteria from macrophages infected for 2 h with *Y. pestis* KIM D-19 Lux_{P_{tolC}}. The limit of detection for conventional enumeration is denoted by the dotted line. RLU = Relative Light Units; CFU = Colony Forming Units. *** = p<0.001, **** =p<0.0001.

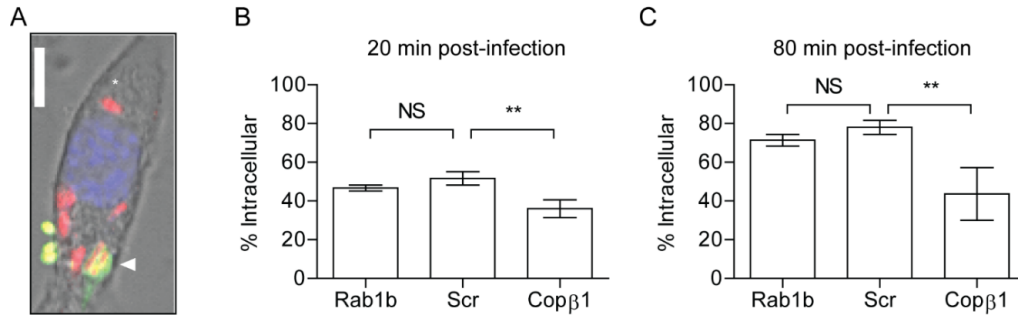


Figure 3—2. Rab1b knockdown does not impact *Y. pestis* invasion of macrophages.

RAW264.7 macrophages were reverse transfected with Rab1b, scrambled (Scr), or Copβ1 siRNA. 48 h after transfection cells were infected with *Y. pestis* CO92 pCD1⁽⁻⁾pGEN-*P_{EM7}*::DsRED(MOI 7.5). 20 or 80 min post-infection cells and bacteria were fixed with paraformaldehyde and extracellular bacteria were stained by indirect immunofluorescence with anti-*Y. pestis* antibody. (A) Representative image showing differential staining of intracellular (red) and extracellular (green or yellow) bacteria. Scale bar is 5μm. Asterisk denotes intracellular *Y. pestis*. (B and C) Percentage of intracellular bacteria calculated at 20 and 80 min post-infection, respectively. ** = p<0.01, ns = not significant.

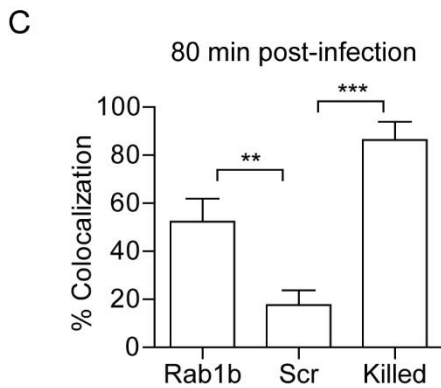
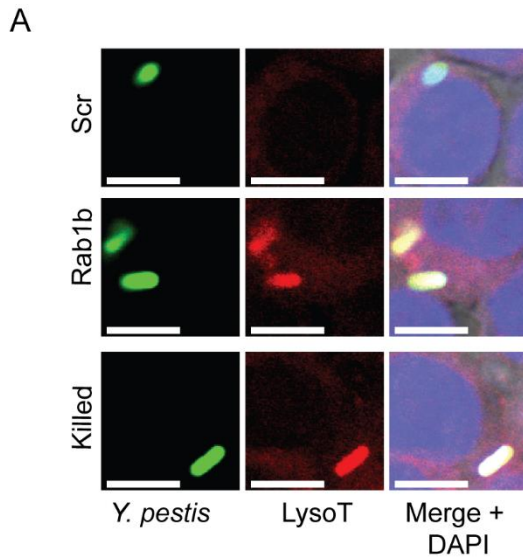


Figure 3—3. Rab1b knockdown alters YCV acidification.

RAW264.7 macrophage cells were reverse transfected with scrambled (Scr), Rab1b or Cop β 1 siRNA. 48 h after transfection cells were incubated with LysoTracker Red DND-99 for 1 h and then infected with live or paraformaldehyde-killed *Y. pestis* CO92 pCD1⁽⁻⁾ pGEN222 expressing EGFP (MOI 7.5). Colocalization of LysoTracker Red DND-99 and *Y. pestis* CO92 pCD1⁽⁻⁾ pGEN222 was

determined by confocal microscopy. (A) Representative images showing colocalization of LysoTracker Red DND-99 and *Y. pestis*. Scale bar is 5 μ m. (B) Percent of YCVs that colocalized with LysoTracker Red DND-99 at 20 min post-infection. (C) Percent of YCVs that colocalized with LysoTracker Red DND-99 at 80 min post-infection. ** = $p < 0.01$, *** = $p < 0.001$.

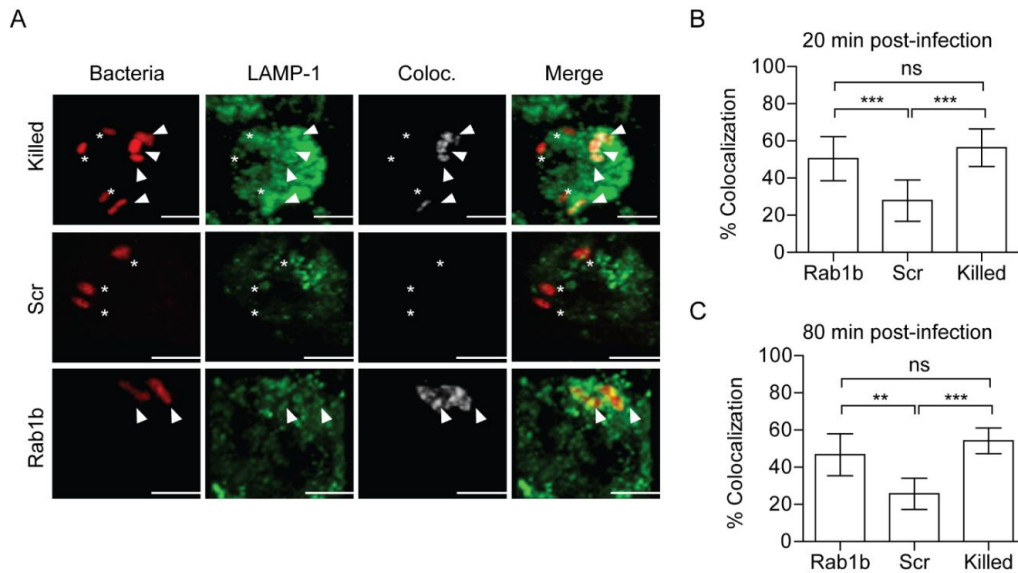


Figure 3—4. Rab1b knockdown increases YCV association with Lamp1.

RAW264.7 macrophage cells were reverse transfected with either scrambled (Scr) or Rab1b siRNA. 48 h after transfection cells were infected with live or paraformaldehyde-killed *Y. pestis* CO92 pCD1⁽⁻⁾pGEN-EM7::DsRED(MOI 3). Cells were stained for Lamp1 and colocalization was determined by confocal microscopy. (A) Representative images showing bacterial colocalization with Lamp1 at 20 min post-infection. Colocalization channel was defined using Imaris software. Asterisks denote bacteria not colocalized with Lamp1; arrowheads denote bacteria colocalized with Lamp1. Scale bar is 5 μ m. (B) Percent of YCVs that colocalized with Lamp1 at 20 min post-infection. (C) Percent of YCVs that colocalized with Lamp1 at 80 min post-infection. ** = $p < 0.01$, *** = $p < 0.001$.

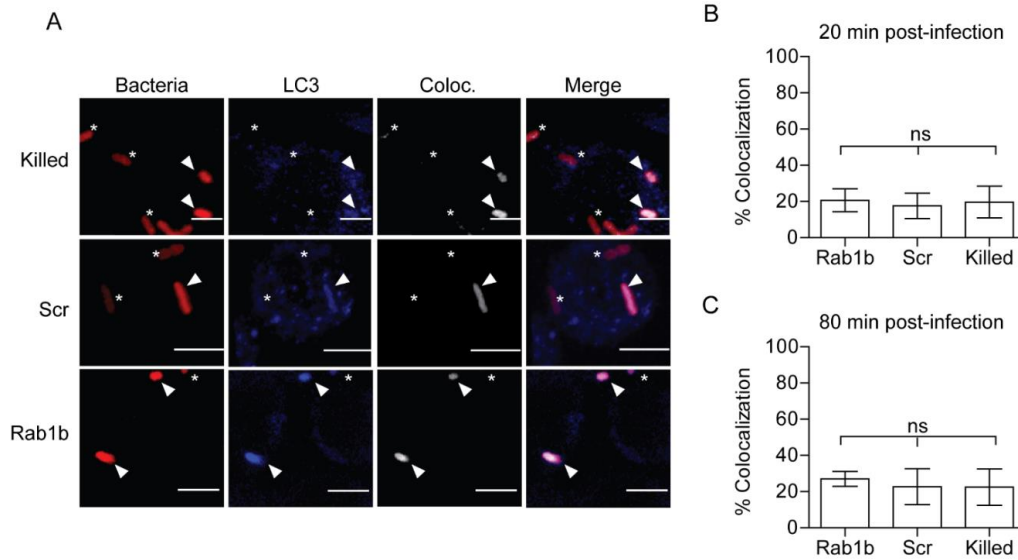


Figure 3—5. Rab1b knockdown does not affect YCV association with LC3.

RAW264.7 macrophage cells were reverse transfected with either scrambled (Scr) or Rab1b siRNA. 48 h after transfection cells were infected with live or paraformaldehyde killed *Y. pestis* CO92 pCD1⁽⁻⁾ pGEN-*P_{EM7}::DsRED* (MOI 7.5). Cells were stained for LC3 and colocalization was determined by confocal microscopy. (A) Representative images showing bacterial colocalization with LC3 at 20 min post infection. The colocalization channel was defined using Imaris software. Asterisks denote bacteria not colocalized with LC3; arrowheads denote bacteria colocalized with LC3. Scale bar is 5 μ m. (B) Percent of YCVs that colocalized with LC3 at 20 min post-infection. (C) Percent of YCVs that colocalized with LC3 at 80 min post-infection. ns = not significant.

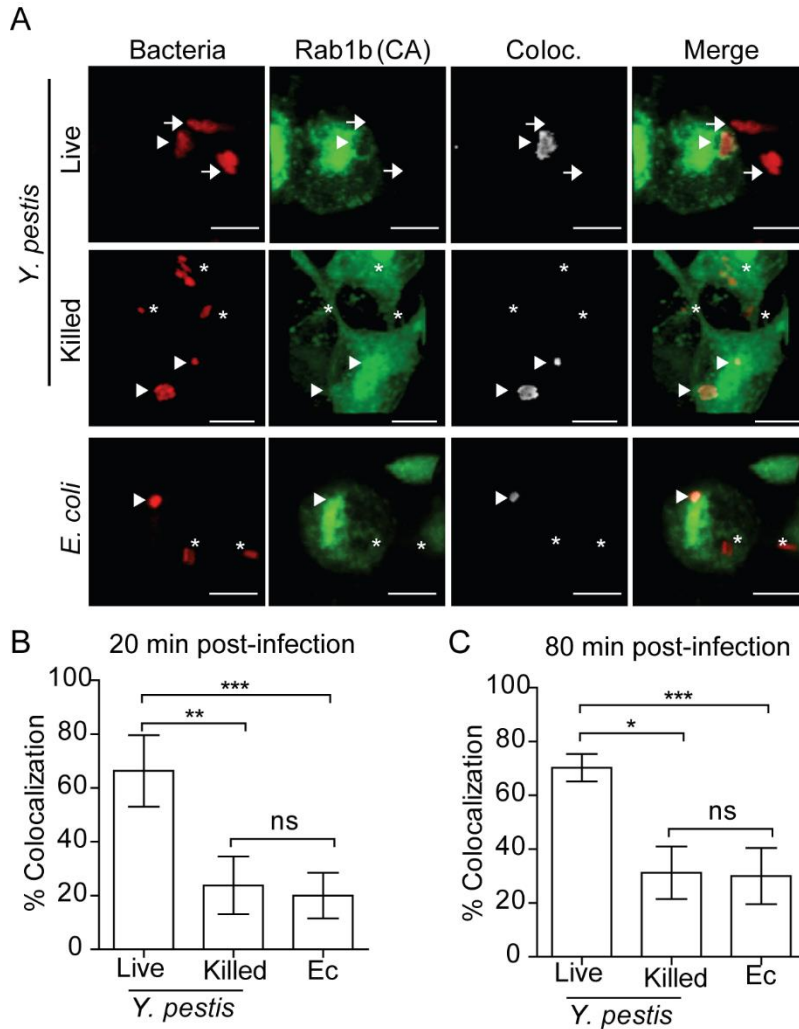


Figure 3—6. Rab1b is recruited to the YCV

RAW264.7 macrophages were transiently transfected with pEGFP-Rab1B(CA). 24 h after transfection cells were infected with either live or paraformaldehyde killed *Y. pestis* pMCherry (MOI 7.5) or *E. coli* pMCherry (MOI 20). Colocalization of EGFP-Rab1b(CA) and bacteria was determined by confocal microscopy. (A) Representative images showing bacterial colocalization with EGFP-Rab1b(CA). Colocalization channel was defined using Imaris software. Asterisks denote bacteria not colocalized with EGFP-Rab1b(CA); arrowheads denote bacteria colocalized with EGFP-Rab1b(CA); arrows denote bacteria in untransfected cells. Scale bar is 5 μ m. (B and C) Percent of bacteria colocalized with EGFP-Rab1B(CA) at 20 and 80 min post-infection. * = $p < 0.05$; ** = $p < 0.01$; *** = $p < 0.001$.

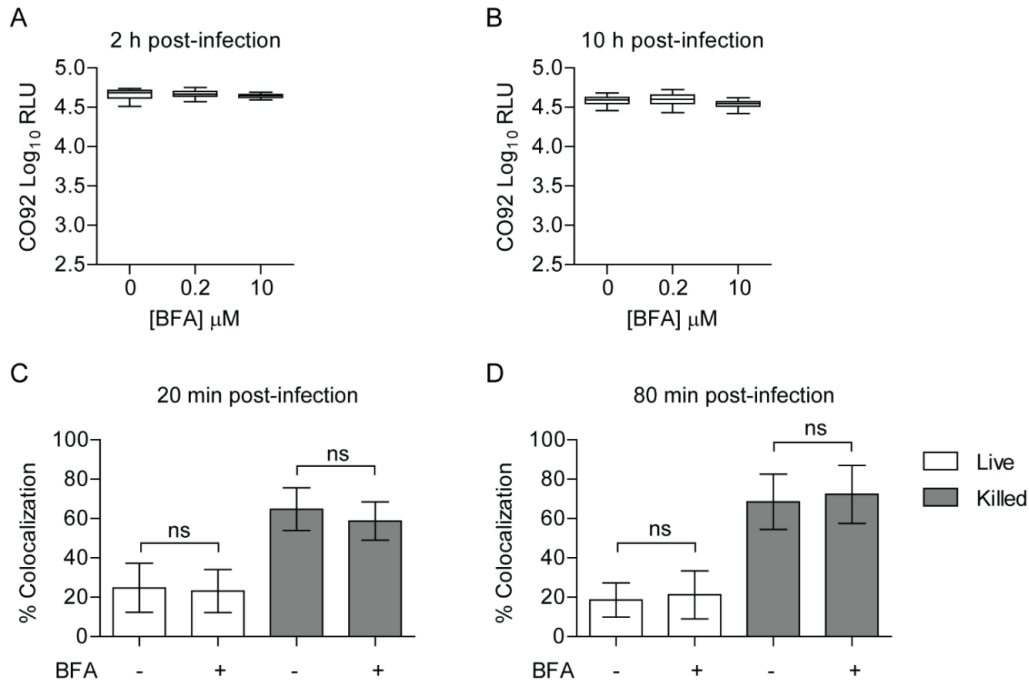


Figure 3—7. Inhibition of the secretory pathway does not inhibit *Y. pestis* intracellular survival.

RAW264.7 macrophages were treated with 0, 0.2 or 10 μ M BFA prior to infection with *Y. pestis* CO92 pCD1⁽⁻⁾ LuxP_{toIC} (MOI 10). Extracellular bacteria were killed with gentamicin and intracellular bacterial numbers were monitored at (A) 2 h and (B) 10 h post-infection by bioluminescence. To determine if BFA treatment impacted the ability of *Y. pestis* to inhibit YCV acidification, macrophages treated with 10 μ M BFA were incubated with LysoTracker Red DND-99 prior to infection with live or paraformaldehyde killed *Y. pestis* CO92 pCD1⁽⁻⁾ pGEN222 (MOI 3). Bacterial Colocalization with LysoTracker Red DND-99 was determined by confocal microscopy at (C) 20 and (D) 80 min post-infection. ns = not significant.

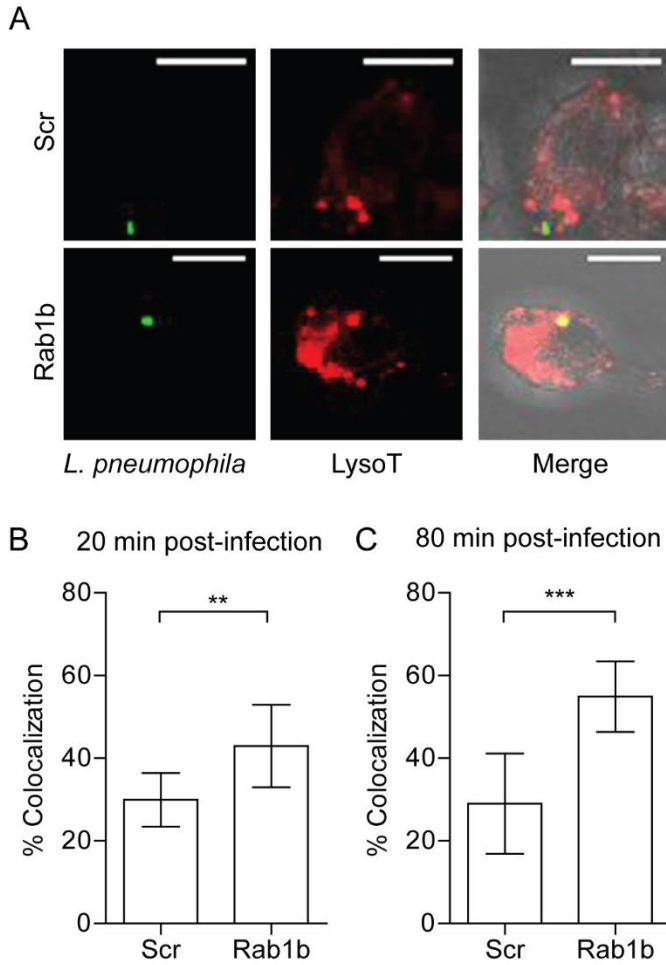


Figure 3—8. Knockdown of Rab1b Increases *L. pneumophila* LCV acidification.

RAW264.7 macrophage cells were reverse transfected with either scrambled (Scr) or Rab1b siRNA. 48 h after transfection cells were incubated with LysoTracker Red DND-99 for 1 h, and infected with *L. pneumophila* pMIP-GFP (MOI 10). Coverslips were fixed and colocalization of LysoTracker was determined by confocal microscopy. (A) Representative images showing colocalization of LysoTracker with *L. pneumophila*. Scale bar is 5 μ m. (B) Percent of LCVs that colocalized with LysoTracker at 20 min post-infection. (C) Percent of LCVs that colocalized with LysoTracker Red DND-99 at 80 min post-infection. **= $p < 0.05$, ***= $p < 0.001$.

Supporting Information

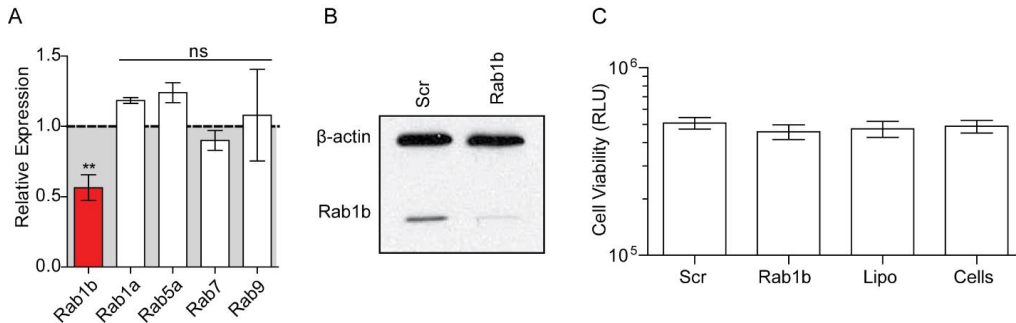


Figure 3—9. S1 Transfection with Rab1b siRNA in macrophages

RAW264.7 macrophages were reverse transfected with either scrambled (Scr) or Rab1b siRNA and incubated for 48 h. (A) Total RNA was isolated from transfected cells (n=5) and Rab1b, Rab1a, Rab5a, Rab7 and Rab9 transcript levels were determined by qRT-PCR (Rab1b primers: 5'-TGCCTTTGTGCTGTCTCTTG -3' and 5'-TCATCCTTTTCCATCTTCCCC -3'; Rab1a primers: 5'-CCTGCCTTCTCCTTAGGTTTG -3' and 5'-TCGAAATCTTTCCTGGCCTG -3'; Rab5a primers: 5'-TGGTCAAGAACGGTATCATAGC -3' and 5'-GCCTTTGAAGTTCTTTAACCCAG -3'; Rab7 primers: 5'-AATAGGAGCGGACTTTCTGAC -3' and 5'-CATCAAACACCAGAACACAGC -3'); Rab9 primers: 5'-CACGGAAGATAGGTCAGAACAC -3' and 5'-CCCTTTAATGCCATCAACAGC -3'); GapDH primers: 5'-AATGGTGAAGGTCGGTGTG -3' and 5'-ACAAGCTTCCCATTCTCGG -3'). Relative expression was calculated using the $\Delta\Delta C_t$ method [228]. Only Rab1b levels were significantly altered in Rab1b siRNA-treated cells compared to scramble treated cells (**=p<0.01; Student's T-test). (B) Whole cell lysates were harvested from transfected cells and Rab1b protein levels (anti-Rab1b(G-20); Santa Cruz sc-599) were determined by Western blot. β -actin (anti- β -Actin; Abcam ab8227) represents loading control. (C) Cell viability of Rab1b siRNA transfected cells was determined using Cell Titer-Glo as described by the manufacturer (Promega). No significant difference in viability was observed between Rab1b siRNA treated cells and scramble siRNA-treated (Scr), untransfected macrophages (Cells), or macrophages treated with Lipofectamine without siRNA (Lipo). RLU = Relative Light Units.

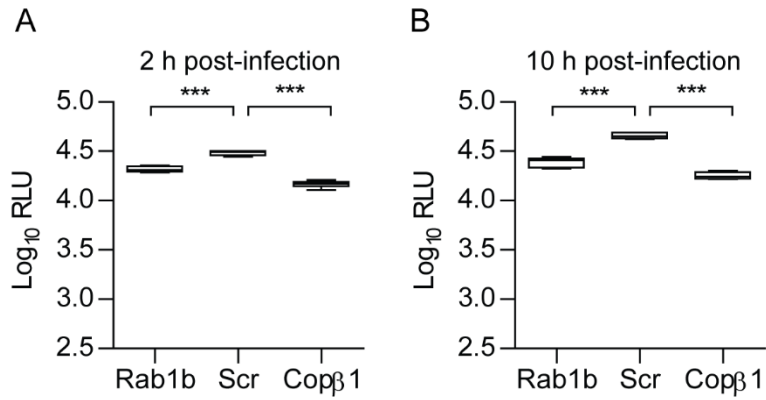


Figure 3—10. S2 Growth at 37°C does not alter intracellular survival of *Y. pestis*.

RAW264.7 macrophages were reverse transfected with Rab1b, scrambled (Scr), or Copβ1 siRNA. 48 h after transfection cells were infected with *Y. pestis* CO92 pCD1⁽⁻⁾ Lux_{P_{tolC}} (MOI 10) grown for 3 h at 37°C prior to infection. (A) Bioluminescence of intracellular bacteria from macrophages infected for 2 h. (B) Bioluminescence of intracellular bacteria from macrophages infected for 10 h. RLU = relative light units. *** = p < 0.001

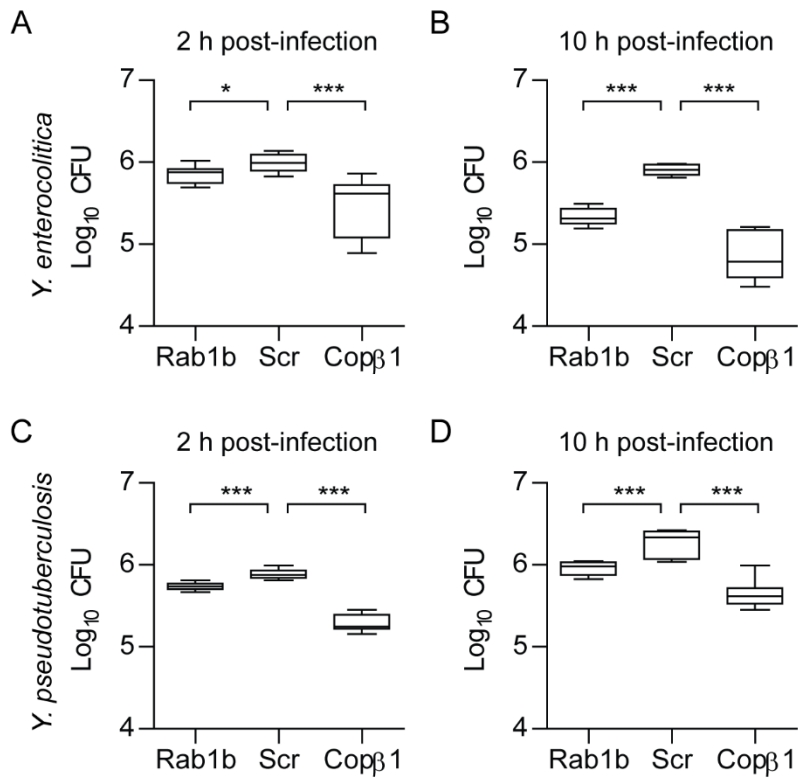


Figure 3—11. S3 Rab1b knockdown inhibits the survival of enteric *Yersinia* within macrophages.

RAW264.7 macrophages were reverse transfected with Rab1b, scrambled (Scr), or Copβ1 siRNA. 48 h after transfection cells were infected with pYV cured *Y. enterocolitica* 8081 [229] or *Y. pseudotuberculosis* IP32952 [17](MOI 10). Extracellular bacteria were killed with gentamicin and at 2 and 10 h post infection intracellular bacteria were determined by conventional enumeration. (A) Intracellular *Y. enterocolitica* at 2 h post infection. (B) Intracellular *Y. enterocolitica* at 10 h post infection. (C) Intracellular *Y. pseudotuberculosis* at 2 h post-infection (D) Intracellular *Y. pseudotuberculosis* at 10 h post-infection. The limit of detection for conventional enumeration is 2.5 log₁₀ CFU. CFU = colony forming units. * = p<0.05, *** = p<0.001

Tables

Table 3--1. Table S1 Bacterial strains used in these studies.

Bacterial Strains	References/sources
<i>Y. pestis</i> CO92 pCD1 ⁽⁻⁾	[9]
<i>Y. pestis</i> KIM D-19 pgm ⁽⁻⁾ pCD1 ⁽⁺⁾	BEI Resources
<i>Y. pseudotuberculosis</i> IP32593 pYV ⁽⁻⁾	[17]
<i>Y. enterocolitica</i> 8081 pYV ⁽⁻⁾	[229]
<i>E. coli</i> DH5 α	New England Biolabs
<i>L. pneumophila</i> AA100	[224]

CHAPTER 4:
GENOME-WIDE RNAI HIGH-THROUGHPUT SCREEN IDENTIFIES THAT
YERSINIA PESTIS EXPLOITS THE HOST ENDOCYTIC RECYCLING
PATHWAY FOR INTRACELLULAR SURVIVAL

Introduction

Yersinia pestis is a facultative intracellular pathogen that causes the human disease known as plague [1, 5]. There have been three major plague pandemics, the most noted being the Black Death during the 14th century [1]. Recent epidemiological data demonstrates that *Y. pestis* is endemic in many countries, including the United States, and have led to the World Health Organization classifying plague as a re-emerging disease [1, 5]. In 2015, the Centers for Disease Control and Prevention (CDC) reported 15 human plague cases in the United States with three fatalities [6]. There are three forms of human plague: bubonic, pneumonic, and septicemic plague. Each form of plague results in an acute infection but is highlighted by the tissues primarily colonized by *Y. pestis*. Bubonic plague is the most common form of human plague and arises after a bite from a *Y. pestis* infected flea. The bacteria rapidly disseminate from the inoculation site through the lymphatic system and colonize the draining lymph node [1, 49, 184]. Eventually the bacteria enter and replicate in the bloodstream, leading to the formation of septicemic plague [1, 6]. In rare cases, *Y. pestis* can be directly inoculated into the blood by a flea or from the bite of an infected animals, resulting in primary septicemic plague without colonization of the lymphatic system [1]. From the blood, *Y. pestis* is distributed throughout the body and colonizes other tissues such as the spleen, liver and lungs. Colonization of the lungs leads to the development of secondary pneumonic plague and the potential for patients to aerosolize *Y. pestis* by coughing and person-to-person transmission. Inhalation of infected aerosols by naïve individuals can result in colonization of the lungs by *Y. pestis* and the development of primary pneumonic plague. All three forms of plague are very rapid infections with high mortality rates in the absence of early antibiotic treatment. [1, 230]. Furthermore, the ability for aerosol transmission of the *Y. pestis* raises the potential for this bacterium to be used a biological weapon [14].

In the environment, *Y. pestis* is maintained through a zoonotic transmission cycle between rodents and fleas [1, 5]. The ability of *Y. pestis* to exist in these two very different hosts is a result of the acquisition of virulence factors required for the mammalian host and transmission factors required for flea colonization [1, 42, 48, 231]. The bacterium regulates these two groups of factors accordingly to ensure expression of appropriate factors only when required [1, 41, 42, 48, 231,

232]. For example, important antiphagocytic factors expressed during mammalian infection, like the Ysc type three secretion system (T3SS), secreted Yop effectors, and the Caf1 capsule, are not required for flea infection and are thus repressed in the flea vector[1]. However, the repression of these antiphagocytic factors in the flea means that during the initial colonization of the mammalian host during bubonic plague, *Y. pestis* is not expressing important virulence factors. Therefore, there is a transition period when the bacteria are highly susceptible to recognition and phagocytosis by macrophages and neutrophils immediately upon flea transmission [51, 54]. This susceptibility is highlighted by intravital microscopy of the infection site by Shannon et al. [233]. Following flea transmission of *Y. pestis* to the dermis of the ear, polymorphonuclear leukocytes (PMNs) are rapidly recruited to the infection site and appear to phagocytosis the bacteria. To a lesser degree, host macrophages are also recruited and engulf bacteria. Interestingly, infected macrophages appeared to migrate away from the infection site. Importantly, growing evidence suggests that these two phagocytes have very different abilities to kill *Y. pestis* [51, 53, 58, 80-82, 233]. Specifically, neutrophils appear to be much more efficient at killing phagocytosed bacteria than macrophages [53, 58, 80]. Moreover, several studies suggest that *Y. pestis* actively inhibits killing by both mouse and human macrophages [54, 55, 57, 59, 82, 83, 86, 152].

Intracellular *Y. pestis* have been isolated from macrophages in both rodent and nonhuman primate models of plague and from plague infected patients [49, 58, 84, 234, 235]. These findings suggest *Y. pestis* intracellular survival may contribute to virulence. Supporting this hypothesis, Ye et al. showed that animals selectively depleted of macrophage/dendritic cell populations exhibited delayed dissemination and subsequently lower bacterial burdens during plague infection [52]. Moreover, the *Y. pestis* *phoPQ* mutant, which is defective for survival within macrophages [56, 83, 86, 90], has a 75-fold attenuation in subcutaneous infection of BALB/c mice and a significant delay in the development of lethal disease in Swiss Webster mice [56, 90]. In contrast, studies with canine macrophages, a species relatively resistant to plague [62], demonstrated that *Y. pestis* is defective in intracellular survival in these cells compared to murine macrophages [62, 91]. These data, combined with studies showing the sensitivity of *Y. pestis* to PMN phagocytic killing [53, 58,

80], suggest that *Y. pestis* infection of macrophages may provide an intracellular niche to avoid killing by PMNs during early stages on infection.

Upon phagocytosis by macrophages, *Y. pestis* quickly and actively inhibits the normal maturation process of the phagosome [54, 55, 57, 59, 83, 86, 152]. A hallmark of this process is the inhibition of phagosome acidification by *Y. pestis* [55, 59]. The bacterium remains within this phagosome throughout the course of the intracellular infection, eventually remodeling it into a compartment called the Yersinia containing vacuole (YCV). In addition to maintaining a neutral pH, a subset of the YCVs eventually mature into autophagosome-like compartments, acquiring both LC3-II and double membranes [88, 89]. During late infection, the YCV begins to expand from a tight fitting vacuole to a spacious vacuole, which coincides with bacterial replication [55, 59, 62, 86, 88, 89]. While autophagy has been noted during *Y. pestis* infection, the extent to which it impacts intracellular survival is not fully understood [59]. However, studies with *Y. pseudotuberculosis* indicate autophagy is important for intracellular bacterial metabolism [88, 89].

Recently we identified the first host factor required by *Y. pestis* for the YCV biogenesis process [61]. We showed that the Rab GTPase Rab1b, which normally mediates ER-Golgi trafficking [209, 210], is rapidly recruited to the YCV and is required for *Y. pestis* to inhibit vacuole acidification and phagosome maturation within macrophages. While Rab1 has been shown to be recruited to the vacuole of several intracellular pathogens [61, 118, 188, 189, 191, 192, 194], these studies were the first to link recruitment to avoidance of the phagosome acidification maturation. Furthermore, inhibition of pathogen-containing vacuole (PCV) acidification by Rab1 recruitment may be a conserved virulence mechanism for intracellular pathogens as RNAi of Rab1 during *Legionella pneumophila* infection also resulted in LCV acidification [61]. These data demonstrate that *Y. pestis* actively targets host factors to subvert macrophage phagosomal maturation and/or to generate a protective replicative niche within the macrophage. Here we attempt to identify additional host factors required for *Y. pestis* intracellular survival by developing an RNAi-based, high throughput assay to monitor the impact of host factors on *Y. pestis* survival in macrophages. Using this assay, we performed a whole genome screen and identified 135 genes contributing to *Y. pestis* intracellular survival. Network analysis of these genes revealed enrichment for factors

involved in host cell recycling pathway. Based on these findings, we demonstrate that *Y. pestis* actively remodels the YCV to resemble host recycling endosomes. Finally, we demonstrate that *Y. pestis* infection also disrupts normal host cell recycling, likely through sequestration of Rab11.

Results

Development of a high throughput assay to monitor the impact of host gene RNAi on Y. pestis intracellular survival

RNAi has been used to identify host factors required for intracellular survival of several pathogens [130-133, 135-142]. However, most of these screens have used *Drosophila* or HeLa cell lines, which may not present the same hurdles to intracellular survival as a pathogen may encounter during infection of macrophages. As macrophages are specifically infected during *Y. pestis* infection, our first goal was to select a macrophage cell line that was amenable to Lipofectamine-mediated transfection/RNAi needed for high-throughput screening. Towards this end, we tested siRNA transfection and knockdown in several human and mouse macrophage cell lines. While robust RNAi was observed in mouse macrophages, we were unable to reproducibly knockdown gene expression in human cell lines (data not shown). Based on these results, we chose RAW264.7 mouse macrophages for further optimization. Using a combination of siRNAs targeting genes of variable expression levels, we optimized Lipofectamine/siRNA concentrations and the transfection time to consistently achieve >70% knockdown of targets (Fig. 4-1A). We also confirmed the transcript knockdown correlated with decreased protein levels for GAPDH and COPB1 (Fig. 4-1B). Next, we established whether we could monitor changes *Y. pestis* intracellular survival in siRNA-treated macrophages. Macrophages were transfected with siRNAs targeting *Rab2A* and *Copβ1*, genes shown to impact the intracellular survival of multiple pathogens [130, 135, 138, 140, 141] and infected with *Y. pestis* CO92 pCD1⁽⁻⁾LUXP_{tolC} [151]. This bioluminescent bioreporter can differentiate as little as a 2-fold difference in macrophage intracellular burdens (Fig. 4-1C) and bioluminescence directly correlates to intracellular bacterial numbers (Fig. 4-1D; R² = 0.89). Transfection with these two siRNAs significantly inhibited *Y. pestis* intracellular survival compared scrambled siRNA treated macrophages (Fig. 4-1E), demonstrating the utility of this

approach to identify host factors required for *Y. pestis* intracellular survival. Finally, using Cop β 1 siRNA as a positive control, we determined the robustness of our assay by establishing a Z' factor. Z' factors between 0.5 and 1 represent highly reproducible assays that are amenable to high throughput analysis [143, 144, 149]. At 2 and 10 hours post infection, we calculated a Z' factor of 0.61 and 0.83, respectively, indicating a highly robust assay (Fig. 4-1F). Together these results indicate a robust assay that can be used for high throughput screening of host factors required for *Y. pestis* intracellular survival (Fig. 4-1G).

Genome-wide siRNA screen identifies host cell signal transduction, transport and localization pathways are required for Y. pestis intracellular survival.

To identify host factors required for *Y. pestis* intracellular survival, RAW264.7 macrophages were reverse transfected with siRNAs targeting 17,370 genes, representing the whole mouse genome, and infected with *Y. pestis* CO92 pCD1⁽⁻⁾Lux_{P_{tolC}}. Each plate also contained control wells transfected with scrambled or COP β 1 siRNAs. Bioluminescence was measured at 2 and 10 h post-infection and Z' factors were calculated from the control wells (the average Z' factor for the screen at 2 and 10 h were 0.57 and 0.66, respectively). Plates with Z' factor less than 0.3 were repeated. At 12 h post-infection cell viability was also determined for 14,203 of the genes. Bioluminescence was normalized for each plate based on control wells and changes in *Y. pestis* intracellular survival were ranked by normalized scores (Fig 4-2A). 302 siRNAs that inhibited bacterial growth and 39 siRNAs that promoted bacterial growth were selected for secondary validation based on selection criteria outlined in the Materials and Methods. 23 additional siRNAs associated with autophagy were also chosen for further validation. For secondary validation, RAW264.7 macrophages were transfected with siRNAs targeting the 364 primary screen hits and subsequently infected with two different *Y. pestis* strains, one with the Ysc T3SS (KIMD19 pCD1⁽⁺⁾ Lux_{P_{tolC}}) and one without (CO92 pCD1⁽⁻⁾ Lux_{P_{tolC}}). Bioluminescence was measured at 2 and 10 h post-infection and normalized scores from each strain were compared (Fig 4-2B). A direct correlation was observed between the two strains ($r_s=0.87$) supporting previous studies that have shown that the T3SS is dispensable for intracellular survival [54, 61, 83, 151]. From the primary hits, we confirmed that 135 siRNAs showed

≥40% inhibition of *Y. pestis* intracellular survival and 7 siRNAs showed a hypervirulent phenotype with ≥20% more growth than scrambled controls (Table 4-1).

To identify specific host pathways that may have been enriched for by our screen, we used a combination of Gene Ontology (GO) clustering and network analyses on our validated data set. ClueGO, a third party Cytoscape app, clusters genes under their GO term in a non-redundant manner, while preserving the highest enrichment of the parent GO term by applying a two sided hypergeometric test and kappa score to generate significance testing (for review see [236, 237]). Using all GO evidence codes, a minimum kappa score of 0.4, and a p-value threshold of 0.05, we observed substantial clustering within the validated dataset (Fig. 4-3A). Of the five enriched groups, the largest clustering enrichment was under Rab protein signal transduction ($pV \leq 0.001$; Fig. 4-3B). Additional enrichment included vesicle-mediated transport, vacuole organization, vesicle docking and mitochondrion organization (Fig. 4-3B). Under the parent GO Term clusters, detailed GO terms significantly focused on host trafficking networks, transport and localization were common themes (Fig. 4-3C).

Based on the significant enrichment for Rab GTPase signal transduction in the GO ontologies, we next determined the degree to which the nine validated Rab GTPases (1b, 2b, 3d, 4a, 19, 20, 23, 30, & 40b) interacted within our validated screen hits. Using the GTPases as focal points, we generated a map of direct interactions from these Rab GTPases within our validated screen hits. These interactions were mapped using a combination of STRING and BioGRID databases to create a Circos plot with known interactions (gray), activators (green), and inhibitors (red) (Fig 4-4A). The Circos plot showed 8% (11 genes) of the validated hits directly interact with these validated Rab GTPases. Next, we sought to identify the degree to which the validated Rab GTPases interacted within the validated and primary hit interactome. To do this, we identified direct interactions between all validated genes, and then expanded this analysis to include direct interactions with all primary screen hits using the STRING and BioGRID databases. These data were used to generate a map of the interactome using Cytoscape (Fig. 4-4B). This interactome showed that 59% of the genes identified in the primary screen and 28% of validated genes directly interacted with one another and that several of the Rab GTPases were part of this interactome.

Together this data suggest that specific Rab-mediated host traffic pathways are targeted by *Y. pestis* in order to subvert phagosome maturation and intracellular survival. Host cell recycling is essential for *Y. pestis* survival

Host cell recycling is essential for *Y. pestis* survival

Rab GTPases are well studied regulators of cellular trafficking and endocytic pathways [185]. Our initial bioinformatic analysis of validated genes emphasized Rab-mediated endocytic trafficking as essential for *Y. pestis* intracellular survival. The Rab GTPases from our validated dataset could be categorized into three trafficking pathways: 1) host cell recycling (Rab4a, 20, 23, & 30); 2) retrograde trafficking (Rab1b & 2b); and 3) the secretory pathway (Rab40b) [99, 101, 102, 185, 238, 239]. As there appeared to be significant enrichment for Rab proteins involved in host cell recycling, we focused on this pathway for further analysis.

Rab4a, Rab11b and Myo5b are well characterized contributors to host cell recycling [238]. While Rab4a was a validated gene in our screen, the other two genes did not pass our primary screen criteria ($\geq 60\%$ inhibition of *Y. pestis* survival; < 50 cytotoxicity) - Rab11b only inhibited *Y. pestis* survival by 50% in the primary screen and Myo5B was cytotoxic (upon subsequent analysis, only one of the three Myo5B siRNAs used in the primary screen was cytotoxic; data not shown). However, because of the importance of these proteins in the recycling pathway, we chose to independently verify the contribution of Rab4a, Rab11b and Myo5b on *Y. pestis* intracellular survival. Toward this end, RAW264.7 macrophages were transfected with single siRNAs targeting each of the three genes. Transfection with each siRNA resulted in $> 60\%$ knockdown on each gene target (Fig. 4-5A) with no significant loss in cell viability (Fig 4-5B). Subsequent infection with *Y. pestis* CO92 pCD1⁽⁻⁾Lux_{P_{tolC}} confirmed that knockdown of all three genes impacted the ability of *Y. pestis* to survive within the macrophage (Fig. 4-5C-F). Knockdown of Rab4a had the largest impact, inhibiting *Y. pestis* survival by 40% at 2 h (Fig. 4-5C; $p < 0.001$) and $> 80\%$ at 10 h (Fig. 4-5D; $p < 0.001$). Interestingly, knockdown of Rab11b and Myo5B had no significant impact on *Y. pestis* survival at 2 h (Fig. 4-5C), but attenuated *Y. pestis* by $> 40\%$ at 10 h (Fig. 4-5D; $p < 0.001$). Bioluminescence data was confirmed at 10 h by conventional bacterial enumeration (Fig. 4-5E). Importantly, knockdown of Rab4a or Rab11b did not alter the expression of Rab GTPases involved

with phagolysosome maturation (Fig. 4-6A & B). Together these data indicate that *Y. pestis* requires the host recycling pathway to avoid killing by macrophages.

Y. pestis requires Rab4a of the recycling pathway to avoid YCV acidification

The decreased *Y. pestis* bioluminescence observed at 2 h for the Rab4a RNAi-treated cells could be attributed to either decreased bacterial uptake or early survival in the phagosome. To differentiate between these two possibilities, RAW264.7 macrophages transfected with siRNA targeting Rab4a or Rab11b were infected with *Y. pestis*-GFP. 20 min post-infection, extracellular bacteria were differential stained and quantified by confocal microscopy (Fig. 4-7A & B). The ratio of extracellular/total bacteria was compared to scrambled and Cop β 1 siRNA treated macrophages. RNAi inhibition of Cop β 1 has been previously shown to prevent RAW264.7 macrophage uptake of *Y. pestis* [61]. Using Cop β 1 as a positive control, we show >35% inhibition of *Y. pestis* invasion (Fig. 4-7B). The data shows there is no significant difference between Rab4a or Rab11b treated cells in comparison to the negative control (Fig. 4-7B). These together suggested that Rab4a inhibition of *Y. pestis* survival was due to events impacting early YCV biogenesis post-invasion.

Similar to Rab4a, we have previously shown that RNAi of Rab1b resulted in significant reduction in *Y. pestis* intracellular survival at 2 h post-infection, which directly correlated to an increase in the frequency of YCV acidification [61]. Therefore, we next determined the impact of Rab4a, Rab11b and Myo5b RNAi on YCV acidification. To monitor YCV acidification, transfected macrophages were pulsed with LysoTracker Red DND-99 prior to infection with *Y. pestis* CO92 pCD1⁽⁻⁾ pGEN222::EGFP. LysoTracker Red DND-99 is a fluorescent probe which accumulates in acidified vacuoles (<pH 5.5). As a positive control, macrophages were also infected with paraformaldehyde killed *Y. pestis* CO92 pCD1⁽⁻⁾ pGEN222::EGFP [59, 61]. As previously shown, *Y. pestis* actively avoided YCV acidification with <20% of YCVs colocalized with LysoTracker Red DND-99 by 80 min post-infection (Fig. 4-7E) [61]. In contrast, YCV containing paraformaldehyde killed *Y. pestis* is acidified as >80% of YCVs were acidified by 80 mins post infection (Fig. 4-7E). As indicated by our RLU data, Rab4a knockdown increased YCV acidification to 55% by 20 min post-infection, and >70% by 80 min post-infection (pV \leq 0.001; Fig. 4-7D & E). Our data shows that Rab4a and Rab11b are not required for *Y. pestis* invasion. However, Rab4a is required *Y. pestis*

to avoid early YCV acidification. In contrast, Rab11b and Myo5b impact YCV acidification later in the process of intracellular survival as inhibition of these host factors impact acidification to a larger degree at 80 mins post-infection.

Interestingly, while there was a statistically significant increase in YCV acidification with the loss of Rab11b at 20 mins post infection (10%; Fig. 4-7D) this did not reflect the 2 h RLU data (Fig. 5C). Moreover, by 80 mins post infection the loss of Rab11b caused a >40% of YCVs to acidify (Fig. 4-7D) which parallels our RLU data at 10 hours post infection (Fig. 4-5D). Finally, the loss of Myo5b had no effect on YCV acidification at 20 mins post infection, but by 80 mins post infection increased YCV acidification by >40% (Fig. 4-7D), which again reflected bioluminescence data at 10 hours post infection (Fig. 4-5D). In summary, our findings demonstrate that Rab4a, Rab11b, and Myo5b are required for efficient avoidance of YCV acidification within the first 80 mins of infection. Furthermore, these data suggest that *Y. pestis* is actively exploiting the recycling endocytic pathway for YCV biogenesis.

The Yersinia containing vacuole acquires recycling endosome markers

Rab GTPases exert their function through coordinated and sequential direct interactions on the vesicle membrane [102, 185]. Recycling endosome maturation/trafficking is initiated by Rab4a for fast recycling back to the plasma membrane on the early endosome [238]. In contrast, Rab4a is exchanged for Rab11b for the maturation/trafficking of slow recycling vesicles that reside spatially close to the Golgi-ERGIC space [238]. Therefore we postulated that *Y. pestis* hijacks the host endocytic recycling pathway by recruiting Rab4a to the early YCV, and then exchanges Rab4a for Rab11b in order to remodel the YCV as a slow recycling endosome. To determine if Rab4a or Rab11b are recruited to the YCV, RAW264.7 macrophages were transfected with plasmids expressing Rab4a or Rab11b fused to EGFP [108] followed by infection with either *Y. pestis* CO92 pCD1⁽⁻⁾ pGEN::mCherry, paraformaldehyde killed *Y. pestis* CO92 pCD1⁽⁻⁾ pGEN::mCherry, or *E. coli* pGEN::mCherry. Association with Rab4a or Rab11b was determined by confocal microscopy (Fig. 4-8A). Rab4a localized to paraformaldehyde killed *Y. pestis* and *E. coli* at 50% and 45% respectively by 20 mins post infection (Fig. 4-8B). In contrast, live 75% of live *Y. pestis* bacteria colocalized with Rab4a at 20 mins post-infection (Fig. 4-8B). The localization of Rab4a, at 20 mins

post infection to both paraformaldehyde killed *Y. pestis* and *E. coli* associate and could reflect the nature of Rab4a on the early sorting endosome [238].

However, by 80 mins post infection there is substantial loss of Rab4a to both paraformaldehyde killed *Y. pestis* and *E. coli*, 30% and 20% colocalization respectively. In contrast, live *Y. pestis* still retains 65% colocalization. Of note, is the significant drop in Rab4a colocalization with live *Y. pestis* by 80 mins post infection. In respect to Rab11b, by 20 mins post-infection 75% of live YCVs colocalized with Rab11b in contrast to 20% for paraformaldehyde killed *Y. pestis* and *E. coli* (Fig. 4-8C). The association of Rab11b with live *Y. pestis* significantly increases to 85% ($p \leq 0.05$) by 80 mins post-infection, whereas paraformaldehyde killed *Y. pestis* and *E. coli* remained at 20% (Fig. 4-8C). These data taken together indicate that *Y. pestis* is actively recruits, and potential retains, Rab4a and Rab11b to the YCV during early stages of infection.

Y. pestis infection stalls host recycling

Our data has shown that Rab4a and Rab11b, and indirectly host cell recycling, are required for *Y. pestis* to actively subvert the maturation of the phagosome. Recruitment of these proteins to the YCV also indicates that *Y. pestis* remodels its phagosome to resemble a recycling endosome. Because of these links to host cell recycling, we next tested whether infection with *Y. pestis* has an impact on host cell recycling of the infected macrophage. Toward this end, we monitored transferrin receptor (TfR) recycling using differential antibody labelling as a measure of global host cell recycling. As a positive control for this assay, Rab4a, which is required for efficient recycling of TfR [240-242], was knockdown by RNAi and compared to scramble siRNA transfected macrophages. In scramble control samples, intracellular TfR peaked at 10 min post-antibody labelling of the TfR and recycling was observed at 20 mins, with a decrease in the intracellular receptor (Fig. 4-9C). In contrast, while intracellular TfR also peaked at 10 min post-antibody labelling in Rab4a siRNA treated cells, the steady state level of intracellular receptor remained significantly elevated as compared the scrambled control ($pV \leq 0.001$; Fig. 4-9C). Importantly, TfR intensity per cell remained significantly ($pV \leq 0.001$) elevated in the Rab4a siRNA treated cells even at 24 h, indicating continued inhibition of recycling.

To determine the impact of *Y. pestis* infection on recycling, RAW264.7 macrophages were treated with anti-TfR antibody and then infected with *Y. pestis* CO92 pCD1⁽⁻⁾pGEN::dsRed, paraformaldehyde killed *Y. pestis* CO92 pCD1⁽⁻⁾pGEN::dsRed, or *E. coli* K12 pGEN::dsRed. At 2 and 24 h post-infection, cells were fixed and intracellular TfR intensity per cell per field was determined by microscopy (Fig.4-10A). Unlike paraformaldehyde killed bacteria, infection with live *Y. pestis* stalled host recycling as early as 2 h post-infection, resulting in significantly higher intracellular TfR intensity per cell per field as compared to uninfected cells, and continued to impact recycling as long as 24 h post-infection (Fig. 4-10). Furthermore, we observed a dose response, with greater MOIs of *Y. pestis* resulting in increased intracellular TfR intensity per cell per field. Importantly, infection with 10-fold higher numbers of *E. coli* K12 did not result in a significant change in TfR retention. Next, we confirmed these results in primary macrophages. As observed for RAW264.7 macrophages, infection of human monocyte derived macrophages (HMDMs) with *Y. pestis* resulted in increased intracellular TfR intensity per cell per field, while infection with paraformaldehyde killed *Y. pestis* or *E. coli* had no impact on recycling (Fig.4-10 C,D,F & G). Finally, HMDMs were also infected with *Salmonella enterica* Typhimurium to determine if infection with another intracellular pathogen impacted the host cell recycling pathway. In contrast to *Y. pestis*, *S. enterica* Typhimurium had no impact on TfR recycling (Fig. 4-10H & I). Importantly, *Y. pestis* intracellular growth was also not impacted by the presence of the TfR antibody (Fig.4-11). Together these data demonstrate that *Y. pestis* actively inhibits host cell recycling (vs. killed *Y. pestis*), inhibition is not just a response by macrophages to bacteria (vs. *E. coli* K12), and inhibition is pathogen specific (vs. *S. enterica* Typhimurium).

Stalling host cell recycling is required for *Y. pestis* replication

Y. pestis infection stalls host recycling as early as 2 h post-infection. Since Rab11b is recruited to the YCV, it is possible that *Y. pestis* infection stalls host cell recycling through sequestration of Rab11b on the YCV. If this is true then overexpression of Rab11b may be able to restore host cell recycling. To test this hypothesis, RAW264.7 macrophages transfected with a plasmid overexpressing wildtype Rab11b-EGFP [108] were infected with *Y. pestis* CO92 pCD1⁽⁻⁾pGEN::mCherry and TfR recycling was monitored. At 2 h post-infection untransfected cells showed

a >2 fold increase in both TfR intensity and endosomes per cell over Rab11b transfected cells (Fig. 12 A & B). By 24 h post-infection Rab11b transfected cells have a 2 fold increase in TfR intensity (Fig. 4-12C), and have a significantly lower level of endosomes per cell ($pV \leq 0.001$; Fig. 4-12D). In contrast, untransfected cells have a significantly higher TfR intensity per cell ($pV \leq 0.01$; Fig. 4-12C), but have a >2 fold increase in endosomes per cell (Fig. 4-12D). Overexpression of Rab11b restored host cell recycling and significantly decreased the amount of TfR endosomes per cell ($pV \leq 0.001$; vs untransfected). Our data showed Rab11b loss significantly impacted *Y. pestis* survival at 10 h post-infection ($p \leq 0.001$; Fig. 4-5D), and through accumulation of Rab11b *Y. pestis* stalled host cell recycling. We therefore, hypothesized that Rab11b overexpression would impact bacterial burden in Rab11b transfected cells. To test this, we quantified bacteria number per cell in Rab11b transfected vs untransfected cells. Overexpression of Rab11b prevents bacterial replication in RAW264.7 macrophages at 24 h (Fig. 4-12 E & F). At 2 h post-infection there are equal numbers of bacteria between transfected and untransfected cells (Fig. 4-12F). However, at 24 h post-infection there >4 fold increase in bacteria in untransfected cells (Fig. 4-12H). These data demonstrate that *Y. pestis* infection disrupts host cell recycling and this is required for bacteria replication.

Discussion

Y. pestis is easily phagocytosed by monocytes/macrophages during the initial transition from the flea to the mammalian host [54]. Once engulfed *Y. pestis* resides in a *Yersinia*-containing vacuole (YCV) that is remodeled by the bacterium to avoid normal phagolysosome maturation and generate a cellular compartment for replication [54, 55, 59]. While paraformaldehyde-killed *Y. pestis* is trafficked to an acidified compartment, and live *Y. pestis* is not [56, 59, 61, 83, 86]. These observations indicate *Y. pestis* actively modulates host-pathogen interactions during infection to avoid YCV acidification and establish a replicative niche within the macrophage. While the fate of *Y. pestis* within the host macrophage is well studied, the mechanisms and cellular processes necessary to support *Y. pestis* intracellular infection are largely unknown.

To better understand the cellular processes required for *Y. pestis* intracellular survival, we designed and conducted the first ever RNAi genome-wide screen to identify essential host

processes necessary for survival of *Y. pestis* inside macrophages. From our screen we identified 135 host targets required by *Y. pestis* during infection of the macrophage. These gene targets enriched for three key cellular processes: vesicular trafficking, transport, and localization within the cell. The ontologies of these cellular processes provide the evidence that *Y. pestis* specifically targets host vesicular trafficking during intracellular infection. Analysis of these GO ontologies revealed overlap between the processes which highlighted the essential role of the host recycling pathway for the dynamic maturation of the YCV. Furthermore, mapping the interactions between the validated and primary screen hits showed enrichment focused on recycling Rab GTPases.

Following up on these findings, we demonstrate that *Y. pestis* recruits recycling markers Rab4a and Rab11b to the YCV to resemble/enter the recycling pathway. RNAi of Rab4a, Rab11b, and Myo5b increased YCV acidification, but two distinct phenotypes were observed. Rab4a knockdown increased YCV acidification within 20 mins post-infection, which was sustained out to 80 mins, whereas, inhibition of Rab11b and Myo5B did not have a dramatic impact on YCV acidification until 80 mins post-infection, and the impact was not to the same extent as Rab4a. From this data, we postulate that Rab4a and Rab1b (identified to be required for rapid inhibition of YCV acidification in a previous study [61]) are recruited to the YCV specifically to arrest YCV acidification and avoid phagolysosome maturation.

Conversely, Rab11b while recruited early to the YCV, plays a dominant role in bacterial replication and is not specifically required to avoid YCV acidification. Rapid recycling via Rab4a occurs off of the early endosome prior to trafficking into a slow recycling arm, which requires Rab11b [238]. Rab11b moves recycling endosomes into the slow recycling pathway through additional trafficking components, such as Myo5b, Rab11fip proteins and Arf6 [238, 243, 244]. Our findings suggest that *Y. pestis* is trafficked into a slow endocytic path as RNAi inhibition of Rab11b and Myo5b have no impact on bacterial survival within 2 h of *Y. pestis* infection of the macrophage. However, by 10 h post-infection both Rab11b and Myo5b attenuate bacterial burden by >50%. Additional analysis of the limited, but growing literature on recycling endosome maturation, we identified additional genes that regulated Rab11b also inhibited *Y. pestis* survival. Known Rab11b interactors are: EHD1, Rab11fip2, 3, & 5, and Arf1 [238]. Two of these components, (EHD1 &

Arf1), inhibited *Y. pestis* survival by ~ 30% at 10 h during primary screening, but did not make cutoff criteria for inclusion in the validation screens. We believe Rab11b and Myo5b are essential for latter stages of YCV biogenesis, potentially through exploitation of the slow endocytic recycling arm. Furthermore, our novel finding that overexpression of Rab11b prevents *Y. pestis* replication suggests that targeting Rab11b is a major regulator separating intracellular *Y. pestis* survival from replication within a spacious YCV.

Intriguingly, inhibition of Rab11 isoforms have been shown to impact the survival of other pathogens that replicate in expanded independent intracellular compartments, such as *Anaplasma phagocytophilum* and *Chlamydia spp* [191, 194]. *A. phagocytophilum* recruits Rab11a to the *Anaplasma phagocytophilum*-occupied vacuole (ApV) within 5 h post-infection (>43% of ApVs), and this is maintained out to 24 h post-infection [191]. Inhibition of Rab11a, using a dominant negative form which cannot tether to the ApV, they attenuate *A. phagocytophilum* intracellular survival by >10% at 5 h post-infection in HL-60 cells [191]. RNAi knockdown of Rab11a in HeLa and HEp-2 cells, prevents *Chlamydia trachomatis* reversion from the metabolically active reticulate body into the inert infectious elementary body by blocking the bacteria's ability to disrupt the Golgi [245-247]. Excitingly, when we re-visited the *Coxiella burnetii* genome-wide RNAi screen data (another pathogen residing in a pathogen containing vacuole termed the CCV) we noticed that inhibition of Rab11b also prevented bacterial replication [131]. While to our knowledge the role of Rab11b in *C. burnetii* has not been fully defined, one suspects it is also recruited to the CCV. This is suggestive that exploitation of Rab11 isoforms is potentially a specific requirement of pathogens that expand their containing vacuoles during bacterial replication. Additional, studies to define the role of Rab11 in vacuole expansion would shed substantial light on how these pathogens acquire the machinery to support vacuole expansion.

Moreover, we show *Y. pestis* infection stalls the host cell recycling by sequestration of Rab11b, making this the first identification of any pathogen to arrest endocytic recycling traffic. While studies have shown various pathogens manipulate host Rab GTPase machinery for survival (for review [102]), no one has demonstrated a living bacterium capable of stalling an entire trafficking pathway. Recently, studies using Anthrax toxin demonstrate disruption of host recycling

endosomes was directly attributed to the toxins impact on Rab11b and Sec15 exocyst assembly [248]. However, through overexpression of Rab11b they were able to restore wildtype *Drosophila* wing structure and normal recycling [248]. Within this context, we were intrigued that during our screen Arf6 RNAi, a well-studied Rab4 effector and a negative regulator of rapid recycling [249-253], had a slight hypervirulent phenotype at 10 h post-infection. This observation could be suggestive, that inhibition of rapid recycling forces cellular compensation by the slow recycling arm and Rab11b through an increase in slow recycling endosomes. Due to this, there is less total free unbound Rab11b available for the cell to manage trafficking of these recycling endosomes, which in turn lowers the threshold needed to be sequestered to stall efficient recycling within the cell, and thusly, a hypervirulent phenotype for *Y. pestis* as more bacteria are capable of establishing a replicative niche. Studies with Anthrax toxin and our *Y. pestis* infection data suggest there are quantifiable finite protein levels for each Rab GTPase within the cell, and disruption/retention of a specific Rab GTPase dilutes the unbound pool available for cellular processes. If true, this would provide a novel insight into general intracellular pathogenesis, as a pathogenic organism, whether it be virus, parasite or bacterial, target host cell Rab GTPases for survival and actively force the infected cell to compensate to the benefit of the pathogen. Through this compensation the infectious agent could create a diversion hiding their presence to the innate host defenses.

Looking deeper into a mechanistic explanation for overexpression of Rab11b inhibition of *Y. pestis* replication we noticed recent findings linking Rab11b to autophagy [254]. Szatmari and colleagues, demonstrate that Rab11b interacts with Hook, a negative regulator of endosome maturation, to facilitate crosstalk between recycling endosomes and induction of autophagy [254]. This peaked our interested as studies have noted that latter stages (>8 h post-infection) of *Y. pestis* replication occurs within a spacious YCV that resembles an autophagosome as it acquires both LC3-II and double membranes [88, 89]. Though the significance of autophagy to *Y. pestis* survival/replication during infection is unknown, findings in *Y. pseudotuberculosis*, the closet ancestral relative within the *Yersinia* genus, suggest that autophagy is required for bacterial replication [88, 89]. Ligeon et al., demonstrate *Y. pseudotuberculosis* acquires VAMP3 within 30 mins post-infection and is exchanged for VAMP7 within 3 to 24 hours, and these VAMP3 and 7

dynamics are required for YCV LC3-II single/double membrane formation [89]. Studies by Moreau and colleagues further show that *Y. pseudotuberculosis* replicates in autophagosomes, and induction of autophagy with rapamycin significantly increased metabolically active bacteria [88]. Additionally, these studies show that Atg4b C74A (enzymatically inactive Atg4b) prevented LC3 recruitment to *Y. pseudotuberculosis* YCV [88]. In this context, our lab observed macrophage infection using *phoPQ* mutants of *Y. pestis*, compensated for bacterial number, survive the first 8-10 h post-infection, have no significant difference in YCV acidification, and the decline in bacterial burden coincides with wildtype replication (MC & ARP unpublished data). Transcriptional studies of Δ *phoPQ* mutants indicate the stress response regulator controls 188 *Y. pestis* genes [86]. The majority of these differentially regulated genes are putative or hypothetical, but appear to be involved with *Y. pestis*' ability to acquire/sense nutrient deprivation and deal with antimicrobial peptides [86]. These studies further conclude that *phoPQ* does not impact trafficking of the YCV but adaption of the YCV to a replicated niche [86]. In either case, the link between Rab11b and autophagy induction is exciting as we show *Y. pestis* stalls host recycling and restoration of this process through overexpression of Rab11b prevents bacterial replication. Perhaps, *Y. pestis* stalls host cell recycling to facilitate entry into autophagosomes, or that autophagy triggers mammalian specific virulence factors for *Y. pestis*. In this sense, one would hypothesize that overexpression of Rab11b would also prevent *Y. pseudotuberculosis* replication as well – provided the end result of stalling host recycling is to induce autophagy within infected cells.

In summary, we completed a genome-wide RNAi HTS to identify required host factors to support *Y. pestis* intracellular survival. From our data, we have demonstrated for the first time that *Y. pestis* remodels the YCV to resemble a recycling endocytic vacuole, and through the sequestration of Rab11b stalls host recycling. We further show that overexpression of Rab11b prevents bacterial replication. Our overexpression data demonstrates for the first time an exploited host protein that differentially separates an intracellular pathogen's survival from replication. Our future goals include defining the role of Rab11b and inhibition of host cell recycling in the context of autophagy and defining the mechanisms used by *Y. pestis* to generate the YCV.

Materials and Methods:

Bacterial strains, plasmids, siRNA and transfection of macrophages. All bacterial strains listed in table 4-1. *Y. pestis* CO92 [9] pCD1⁽⁻⁾ and KIM D-19(pgm⁽⁻⁾) (BEI Resources NR-4681) were cultivated at 26°C in Brain Heart Infusion (BHI) broth (Difco). *E.coli* and *S. typhimurium* was cultivated at 37°C in Luria-Bertani (LB) broth (Difco). Growth media supplemented with Carbenicillin at 50µg/mL when needed. Bioluminescent derivatives were generated using the Lux_{P_{tolC}} bioreporter as described previously [151]. *Y. pestis* and *E. coli* fluorescent derivatives bacterial strains are described previously [61]. *S. enterica Typhimurium* pGEN-*P_{EM7}*::DsRED was generated using Eppendorf protocol # 4308 915.532. RAW264.7 macrophages were obtained from ATCC and cultured in DMEM, 100 mM glucose + 10% FBS (Hyclone). For 96-well RNAi high-throughput screening, RAW264.7 macrophages were forward transfected using Tecan liquid handling robotics (Tecan) to pool 3 siRNAs from the Silencer siRNA Mouse Genome Library v3 (Ambion) at [1µM] final concentration in 20µl Opti-MEM, and then mixed with 10µl of 0.03% (v/v) Lipofectamine RNAiMax/Opti-MEM (Life Technologies) as described by the manufacturer. 30 µl of the siRNA-Lipofectamine complex was added to each well of a white flat-bottom 96-well plate (Greiner), incubated at room temperature for 10 min, prior to addition of 1x10⁴ RAW264.7 macrophages suspended in 80 µl of DMEM + 10% FBS. 24-well plates reagents were increased 4-fold previously described [61]. For plasmid transfection, 4.4 x 10⁵ RAW264.7 macrophages were transfected using 0.5 µg of plasmid with JetPrime (Polyplus) as described by the manufacturers. All single siRNAs used are in Table 4-2.

qRT-PCR, Western blot and Cell Viability. Rab GTPase expression, total RNA from 1.6x10⁵ transfected cells was isolated as previously described [61] and qRT-PCR was performed using SybrGreen (Life Technologies) with primers in Table 4-3. Relative expression was calculated using $\Delta\Delta C_t$ method [228]. Western blot was performed as previously described [61]. For AlamarBlue (Life Technologies) cell viability, 10µl reagent was added directly to macrophages and incubated at 37°C 5% CO₂ for 2 hrs, then read using Synergy 4 (ex: 560: Em: 600).

Bacterial infection of macrophages. Macrophages were infected with *Y. pestis* as previously described [59, 61, 151]. In brief, bacteria cultivated overnight at 26°C in BHI, washed in PBS, and diluted in prewarmed DMEM+10%FBS. Bacteria were added to macrophages and infection synchronized by a 200xg centrifugation for 5 mins. 20 mins post infection extracellular bacteria were killed with gentamicin (16µg/mL) for one hour, and then media was replaced with DMEM + 10% FBS containing 2µg/mL gentamicin for the duration of the experiment. Intracellular *Y. pestis* was quantified using a Synergy HT or Synergy 4 plate reader (Biotek; 1 sec read with sensitivity set at 150) or conventional bacterial enumeration as described previously [151]. *S. enterica Typhimurium* infection of macrophages was done with 200xg centrifugation for 10 mins. 60 mins post infection extracellular bacteria were killed with gentamicin (100µg/mL) for one hour, and then media was replaced with DMEM + 10% FBS containing 10µg/mL gentamicin for the duration of the experiment.

Bioinformatic analysis. Validated and primary screen hits were stored with both Entrez Gene and MGI identifiers. A script was made to pull interacting partners from all experimental evidence codes from BioGRID [255] and STRING [256] databases using MGI and Entrez Gene identifiers. The script stored interactors for the input datasets, validated (135 genes) and primary hits (364 genes), as follows: 1) direct interactions within each individual dataset, and 2) direct interactions from validated to primary hits. These interactions were stored and imported into Cytoscape (v3.30; [257]) to generate interaction maps. For GO Ontology clustering, the validated (135) hits were imported by Entrez Gene identifier to Cytoscape plugins ClueGO [237] and CluePedia [236]. Genes were clustered using all GO evidence codes, a minimum kappa score of 0.4 and a p-value threshold of 0.05. To construct Circos plots, individual gene GO ontologies for validated datasets were generated using Entrez Gene identifier in PANTHER [258]. Circos plots were then overlaid with screening score data and interactions previous stored from BioGRID and STRING databases.

TfR recycling and Acidification assay, Immunofluorescent staining, and confocal microscopy

For confocal microscopy, cells were fixed to coverslips with 2.5% paraformaldehyde for 30 min. Indirect immunofluorescent staining, fixed cells were blocked with 3% BSA overnight and incubated with rabbit anti-*Y. pestis* serum (1:1,000). Unbound primary antibodies were removed by washing

and anti-rabbit Alexa Fluor 594 secondary antibody (1:2000; Life Technologies). For TfR recycling assay using siRNA transfection, 1.6×10^5 were transfected as described above in a 24-well plate (Greiner) and incubated either for 48 h at 37°C 5% CO₂. Prior to kinetic assay using siRNA transfection, cells were washed three times in cell culture grade PBS (Hyclone), left in cell culture PBS and placed on ice for 30 mins. Media was aspirated and replaced with 37°C pre-warmed DMEM, 100 mM glucose + 10% FBS (Hyclone) with anti-TfR (1/1000 dilution; Abcam ab84036). Cells were moved to 37°C waterbath. At desired time points coverslips were removed and placed in acidic stripping buffer (HBSS + 50mM glycine + 150mM NaCl + 0.2% BSA pH 4) on ice. Coverslips were washed thrice with acidic stripping buffer and fixed with 2.5% paraformaldehyde for 15 min at room temperature. Cells were rocked in permeabilization buffer (0.5% Tween 20 + 3% BSA) overnight at 4°C prior to 1 h incubation with staining buffer (0.5% Tween 20 + 3% BSA + anti-rabbit 2,000 Alexa Fluor 488). For TfR recycling during bacterial infection, 1×10^5 RAW264.7 macrophages were seeded in a 24-well plate (Greiner) and incubated overnight at 37°C 5% CO₂. Macrophage media was replaced with 37°C pre-warmed DMEM, 100 mM glucose + 10% FBS (Hyclone) with anti-TfR (1/1,000 dilution; Abcam ab84036). Bacterial strains were diluted to desired MOIs in DMEM, 100 mM glucose + 10% FBS (Hyclone) and added to macrophages. After 1 h gentamicin killing media was replaced with appropriate gentamicin maintenance doses with 1/1,000 anti-TfR antibody. Coverslips were removed at 2 and 24 h post-infection, placed in acidic stripping buffer and processed as described above. Lysotracker Red DND-99 (Life Technologies) acidification experiments were done as previously described [61]. For confocal microscopy, cells were fixed to coverslips and imaged as previously described [61]. All Coverslips were mounted with Prolong Gold with DAPI (Life Technologies), and imaged on a Zeiss LSM 710 laser confocal microscope. Colocalization of Lysotracker Red DND-99 or proteins to the YCV was determined using the Coloc function in Imaris image analysis software (BitPlane). Quantification of TfR recycling was done in Fiji [259].

Statistics. Unless otherwise noted in corresponding figure legend, all data are shown as mean and standard error margin (SEM) of one representative experiment. All experiments were repeated three to six for biological trend and each experiment was repeated three times to confirm the

phenotypes. For microscopy, at least 50 YCVs or 25 fields per biological replicate and experiment were analyzed. P-values calculated by one-way ANOVA or Student's T-Test, with appropriate post-hoc testing when necessary using GraphPad Prism software

Figures and Figure Legends

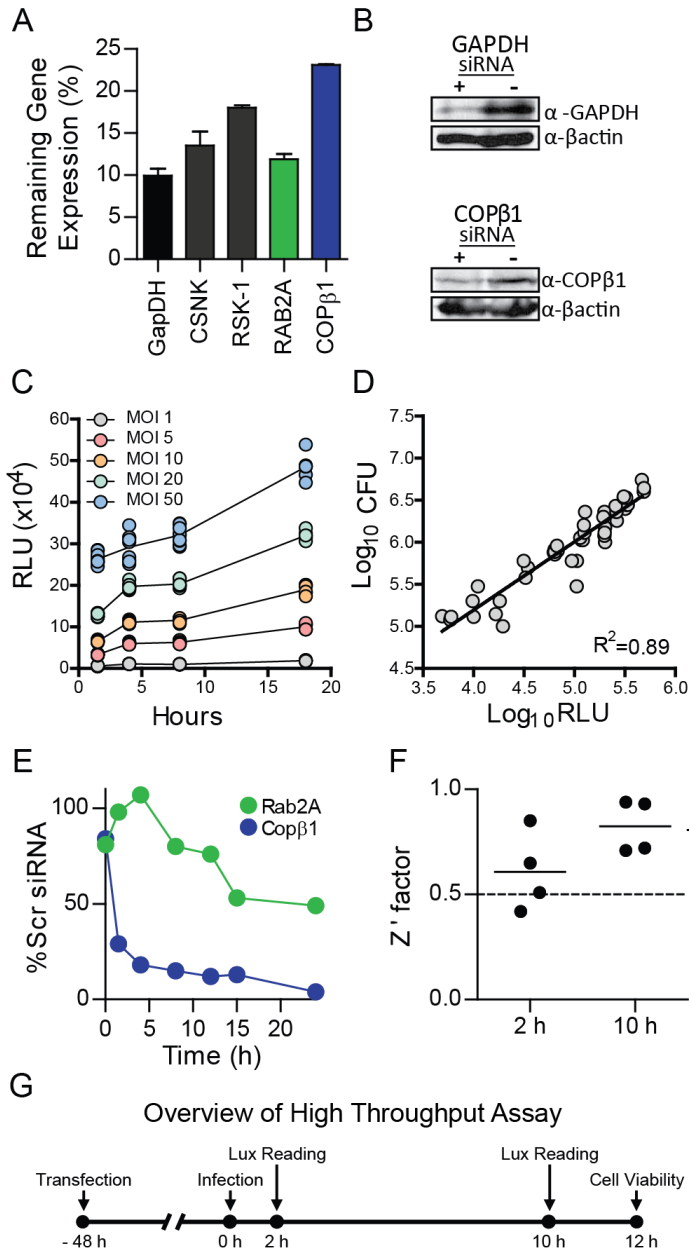


Figure 4-1. RNAi-based assay to identify host factors required for *Y. pestis* intracellular survival.

(A and B) To determine if reproducible RNAi could be achieved in RAW264.7 macrophages, cells were reverse transfected with siRNAs targeting indicated genes. 48 h post-transfection, cells (n=3) were harvested for (A) RNA isolation and qRT-PCR (data represents the level of gene expression compared to scrambled siRNA control) or (B) protein isolation for Western blot analysis (β actin was used as a loading control). (C and D) To demonstrate that the *Y. pestis* CO92 pCD1⁽⁻⁾ Lux_{P_{tolC}} bioreporter accurately represents intracellular bacterial numbers, RAW264.7 macrophages were infected with *Y. pestis* CO92 pCD1⁽⁻⁾ Lux_{P_{tolC}} at indicated MOIs (n=12) and extracellular bacteria were killed with gentamycin. (C) Bioluminescence (RLU) of intracellular bacteria was determined at 1, 4, 8 and 18 h post-infection. (D) At 18 h, cells from each MOI (n=3) were lysed and bacterial numbers (CFU) were determined and compared to 18 h bioluminescence (RLU). (E) To demonstrate that RNAi targeting specific genes could impact *Y. pestis* intracellular survival, RAW 264.7 macrophages were transfected with siRNAs targeting Rab2A or COP β 1. 48 h post-transfection macrophages were infected with *Y. pestis* CO92 pCD1⁽⁻⁾ Lux_{P_{tolC}} (MOI 10). Extracellular bacteria were killed with gentamycin and intracellular bacterial bioluminescence monitored over time. Data is represented as percent RLU of scramble siRNA (scr) control. (E) To demonstrate robustness of the assay, RAW264.7 macrophages (n=48) were reverse transfected with either scrambled siRNA (negative control) or siRNA targeting Cop β 1 (positive control). 48 h post-transfection macrophages were infected with *Y. pestis* CO92 pCD1⁽⁻⁾ Lux_{P_{tolC}} (MOI 10). Extracellular bacteria were killed with gentamycin and intracellular bacterial bioluminescence was determined at 2 and 10 h post-infection. Z' factor from 4 independent experiments are shown (bar = mean). (G) Overview of optimized high throughput assay for RNAi screening.

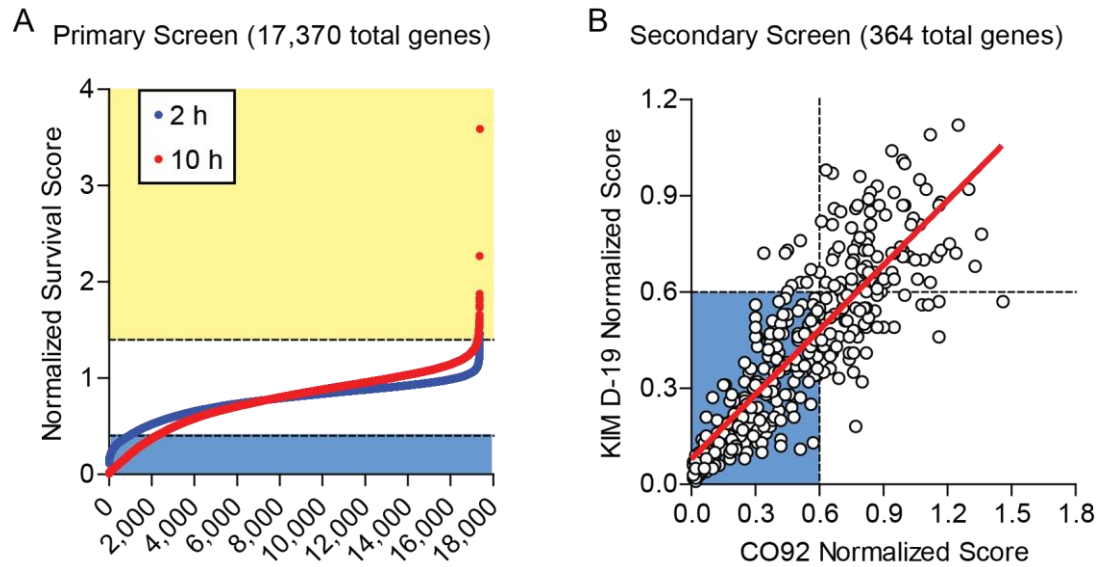


Figure 4-2. Identification of host factors required for *Y. pestis* intracellular survival

To identify host factors required for *Y. pestis* to survive in macrophages, RAW264.7 macrophages were reverse transfected with siRNAs for 48 h. (A) Transfected cells were infected with *Y. pestis* CO92 pCD1⁽⁻⁾ Lux_{P_{tolC}} (MOI 10) and intracellular bacteria bioluminescence (RLU) determined at 2 (blue) and 10 (red) h post-infection. RLU values were normalized to controls [(gene RLU / avg. positive control RLU) / (avg. negative control RLU / avg. positive control RLU)] and ranked from lowest to highest. Normalized scores ≤0.5 are highlighted in blue and ≥1.4 in yellow. (B) For secondary validation, transfected cells were infected with *Y. pestis* CO92 pCD1⁽⁻⁾ Lux_{P_{tolC}} or KIMD19 pCD1⁽⁺⁾ Lux_{P_{tolC}} (MOI 10) and intracellular bacteria bioluminescence (RLU) determined at 10 h post-infection. RLU values were normalized to controls and compared to each other. The red line represents the line of best fit (linear regression). Normalized scores ≤0.6 are highlighted in blue.

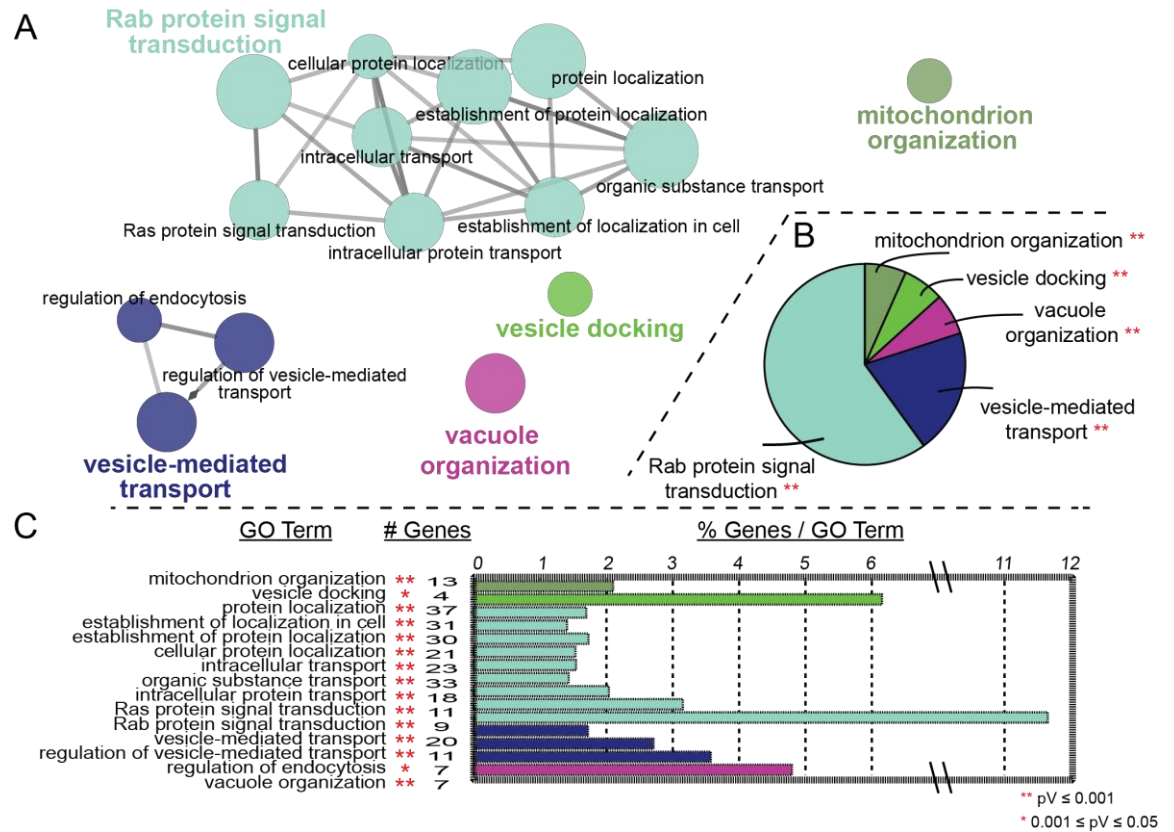


Figure 4-3. ClueGO clustering of validated genes impacting *Y. pestis* intracellular survival.

(A) Cytoscape generated layout for GO term node clusters. Clusters are color coded by highest order parent ontology. (B) Pie chart representing the percent parent ontology represented as a whole within our validated genes. (C) Detailed ontologies within the parent clusters broken down by the number of genes and the percent representation of those genes within the detailed term.

Figure 4-4. Identification of Rab GTPase interactions within primary screen hits.

(A) To determine the Rab GTPases network interactions, we pulled all interactions from the Rab GTPases to the validated screen hits (n=135). The resulting interactions are displayed as a Circos plot as follows. Lines: Gray (interaction), Green (activator) and Red (inhibitor). Each square represents if the target gene met cutoff criteria for inhibition (red) or hypersurvival (green) in the primary (outside ring), CO92 secondary (middle ring) or KIM-D19 secondary (inside ring) screens. Gene symbols are on the outside. (B) Interactome of direct interactions between primary and validated hits. Gray squares are primary hits, blue ovals are validated genes. Rab GTPases are highlighted with red boarder and labeled

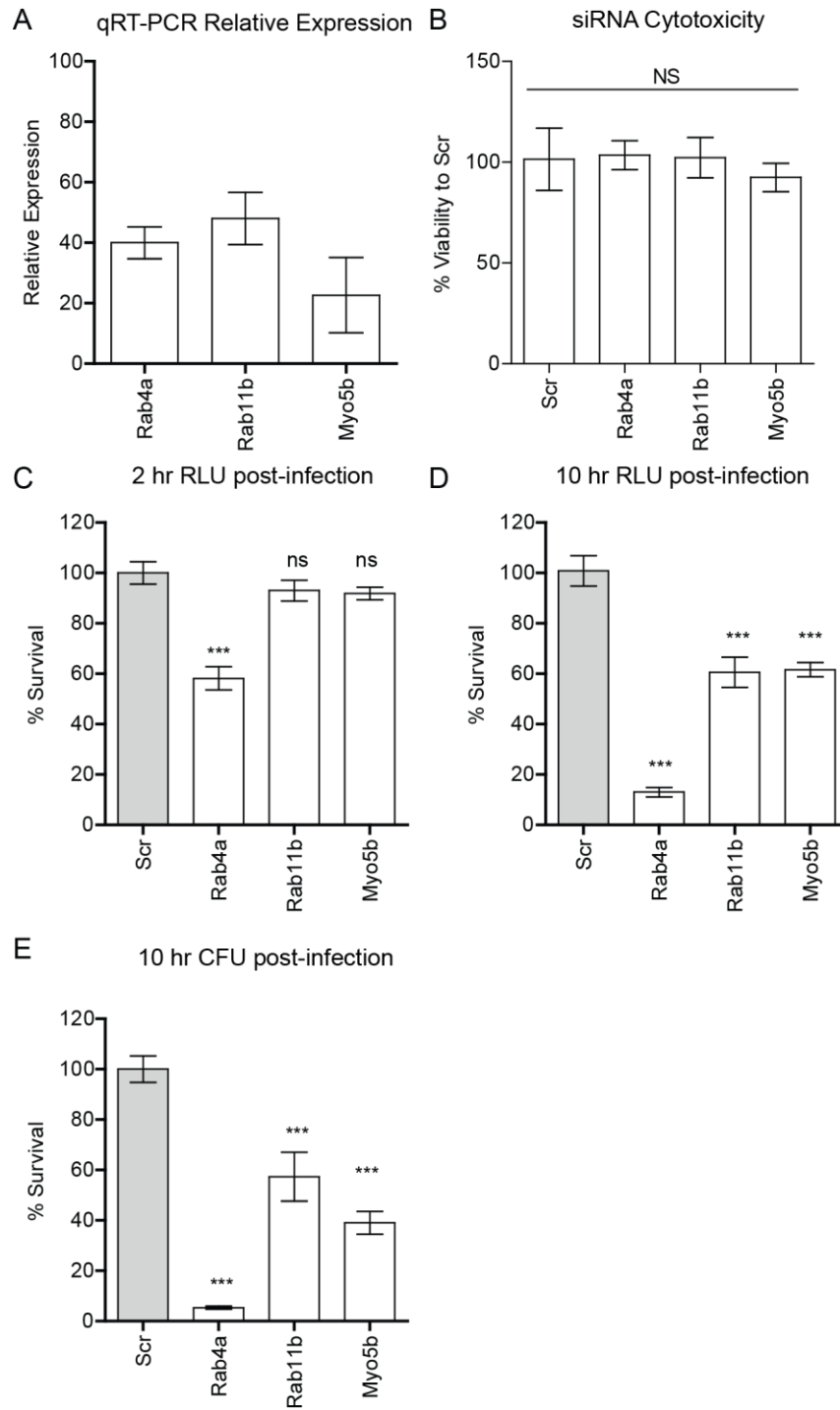


Figure 4-5. Host recycling inhibits *Y. pestis* intracellular survival

RAW 264.7 macrophages were transfected with a single siRNA targeting Rab4a, Rab11b or Myo5B. At 48 h post-transfection (A) RNA samples were harvested for qRT-PCR (n=9) or (B) cell viability was determined (n=5). To determine the impact of RNAi on *Y. pestis* survival, transfected RAW264.7 macrophages (n=8) were infected with *Y. pestis* CO92 pCD1⁽⁻⁾ Lux_{P_{tolC}} (MOI 10) and intracellular bacterial numbers were determined by bioluminescence at (C) 2 h or (D) 10 h post-infection and compared to scrambled (scr) controls. (E) At 10 h post-infection, a subset of samples (n=3) were harvested for convention bacterial enumeration. Statistical significance was calculated by one-way ANOVA with Tukey's Multiple Comparison post hoc. *** = $p \leq 0.001$; ns = not significant.

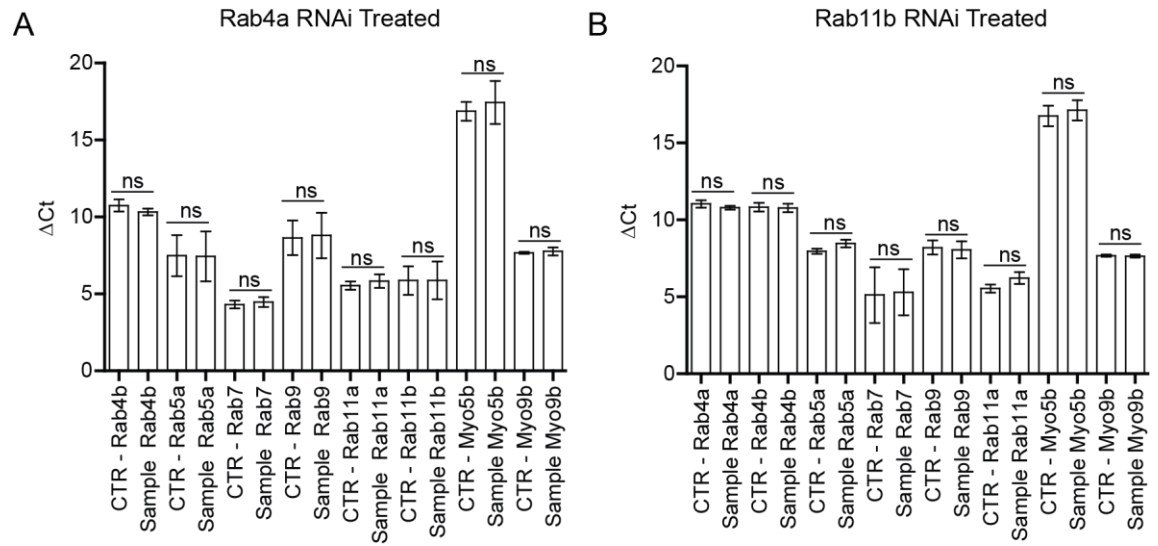
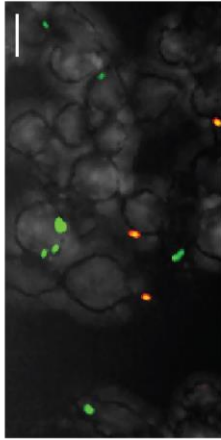


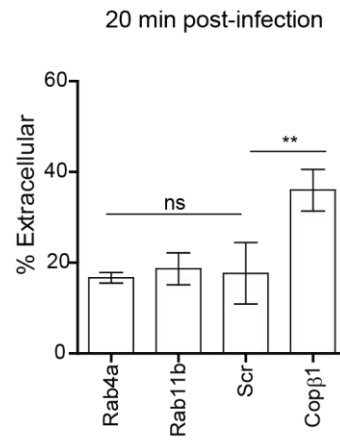
Figure 4-6. RNAi inhibition of Rab4a and Rab11b does not impact the phagolysosome

RAW 264.7 macrophages were reverse transfected for 48 h with single siRNA targeting indicated host genes. Total RNA was isolated after 48 h and Δ Ct (avg. target gene – avg. reference gene) determined for gene targets in either Rab4, Rab11b or scrambled negative control siRNA. (A) Δ Ct of targets in Rab4a treated vs scrambled negative control (CTR; n=9). (B) Δ Ct of targets in Rab11b treated vs scrambled negative control (CTR; n=9).

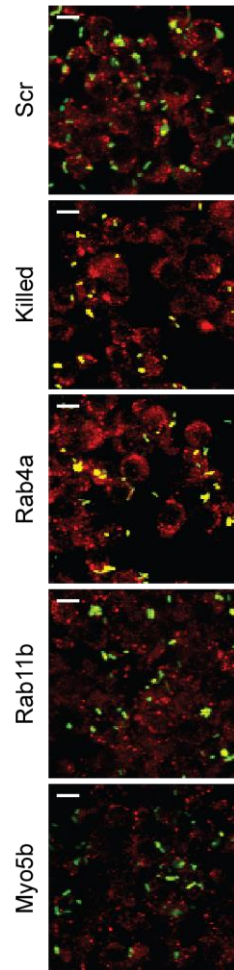
A



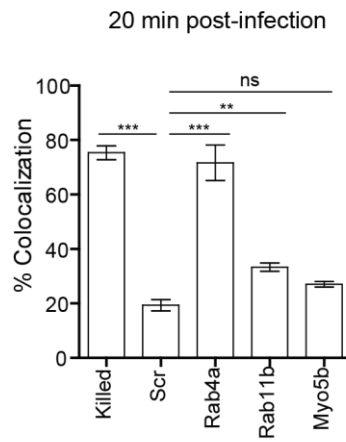
B



C



D



E

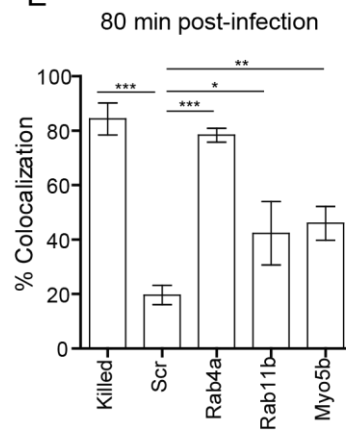


Figure 4-7. Rab4a of the recycling pathway is essential for *Y. pestis* to avoid the phagolysosome

For invasion, cells were infected with *Y. pestis* CO92 pCD1⁽⁻⁾ pGEN222 EGFP (MOI ~3). After 20min infection cells were fixed, and counter stained by indirect immunofluorescence with anti-*Y. pestis* antibody. (A) Representative image of differential staining showing intracellular bacteria (green) and extracellular bacteria (red/yellow). 10µm scale bar. (B) Percent of extracellular bacteria at 20min post-infection, represented as mean ± std (n=3). After transfection cells were incubated with Lysotracker Red DND-99 for 1hr. After 1hr cells were infected with either live *Y. pestis* CO92 pCD1⁽⁻⁾ pGEN222 EGFP or paraformaldehyde killed *Y. pestis* CO92 pCD1⁽⁻⁾ pGEN222 EGFP (MOI ~3). Colocalization determined by confocal microscopy. (C) Representative field images at 20min post-infection. 10µm scale bar. (D & E) Percent colocalization with Lysotracker Red DND-99 at 20 and 80min post-infection, represented as mean ± std (n=3). Significance calculated by one-way ANOVA. ns= not significant, * = pV ≤0.05, ** = pV ≤0.01, *** = pV ≤0.001.

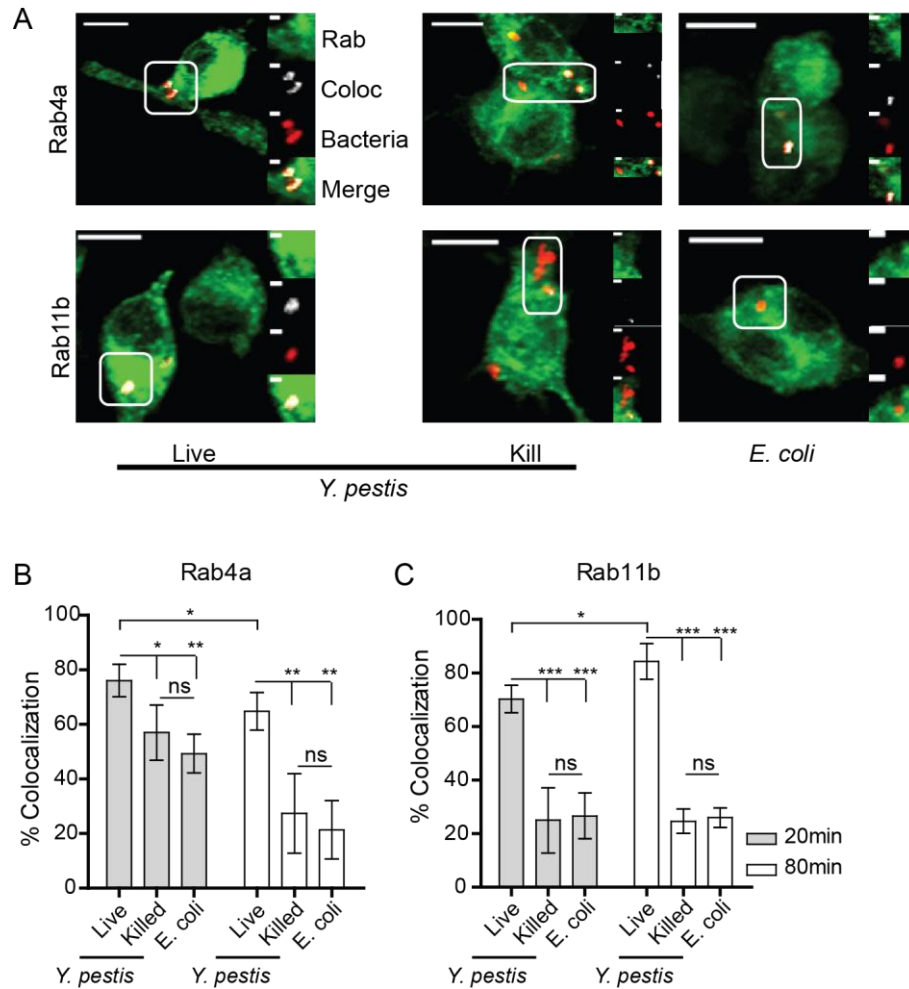


Figure 4-8. *Y. pestis* acquires recycling endosome markers Rab4a and Rab11b.

To determine if the bacteria recruited Rabs 4a and/or 11b, RAW 264.7 cells were transiently transfected with either pEGFP-Rab4a or pEGFP-Rab11b, and infected with either live or paraformaldehyde killed *Y. pestis* CO92 pCD1⁽⁻⁾ mCherry (MOI 3) and *E. coli* mCherry (MOI 20) 24 h later. (A) Representative images at 20 min post-infection with cropped bacteria inserts. (B and C) Rab4a and Rab11b percent colocalization represented as mean \pm std of all biological repeats (n=3). Significance calculated by one-way ANOVA or Student's T-test. * = $pV \leq 0.05$; ** = $pV \leq 0.01$; *** = $pV \leq 0.001$; ns = not significant. Scale bar 10 μ m and insert 2 μ m.

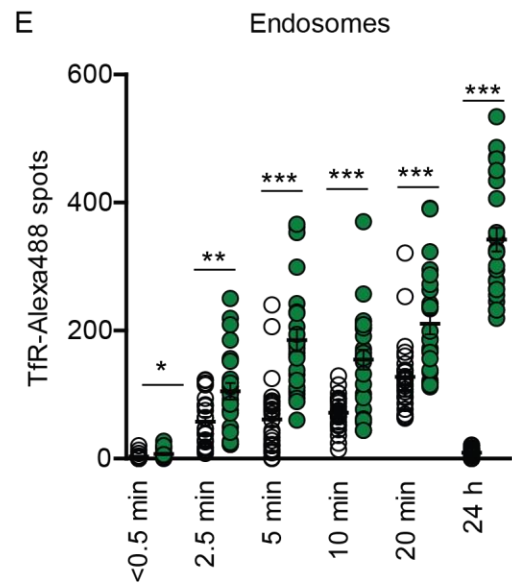
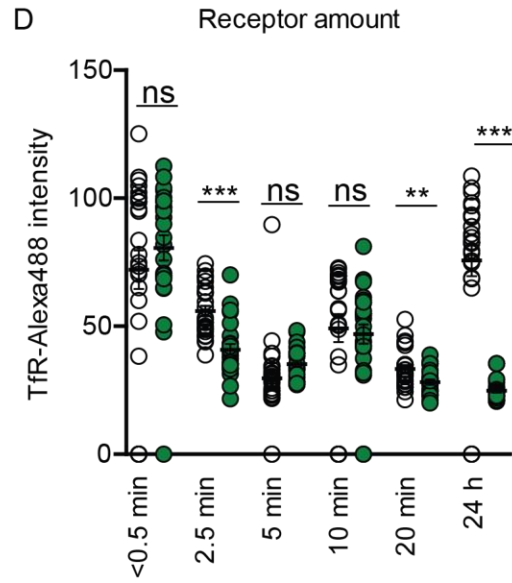
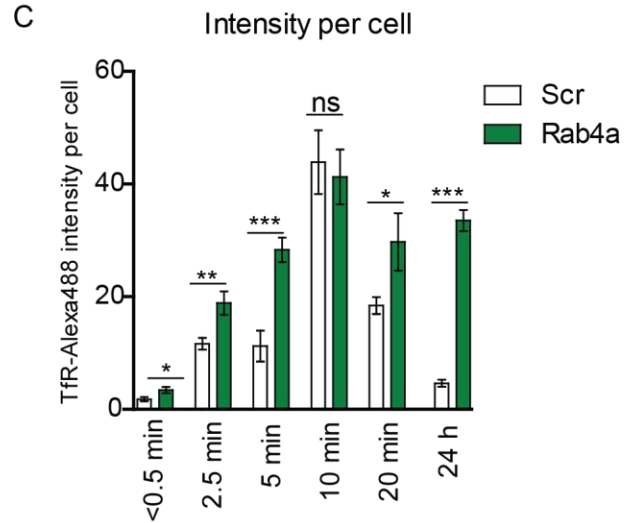
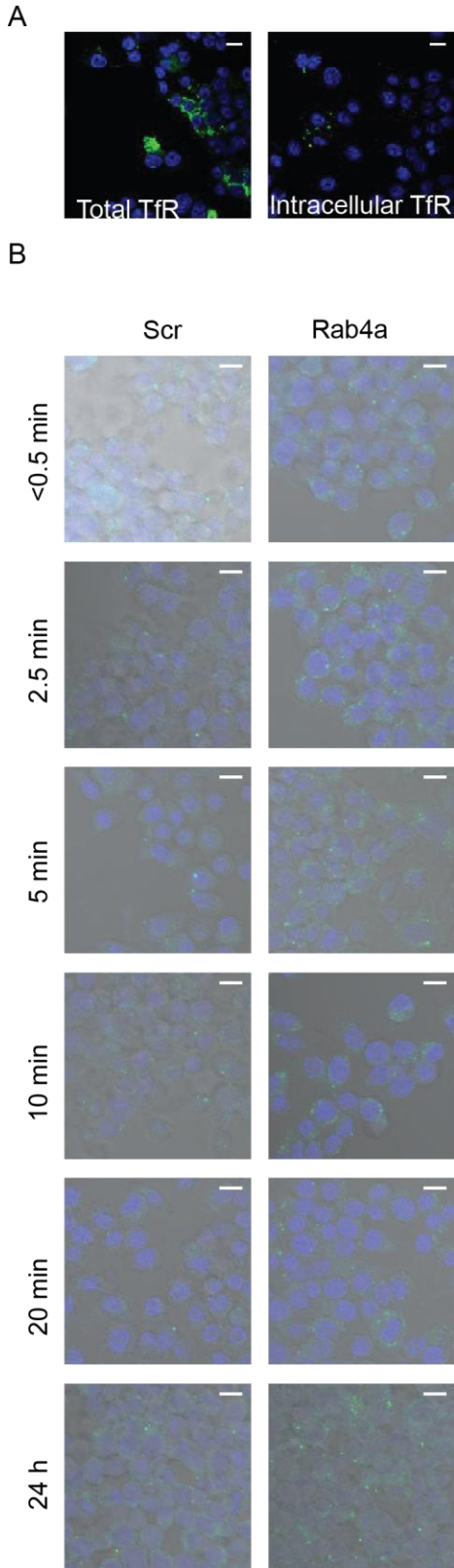
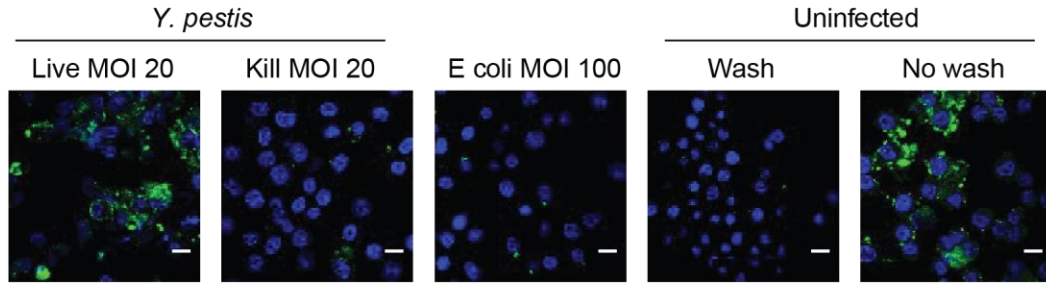


Figure 4-9. Recycling assay measures TfR kinetics.

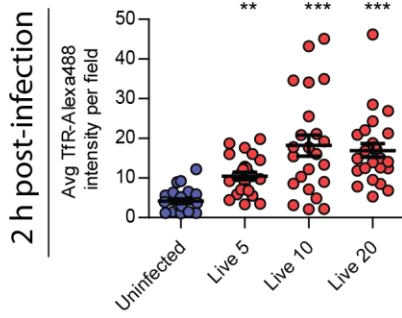
RAW 264.7 cells were transfected with either scrambled (scr) or Rab4a siRNA for 48 h prior to synchronization, pulsing with anti-TfR antibody, fixed and counterstained with Alexa488 secondary antibody (n=25). (A) Representative images of total TfR staining vs only internalized TfR after acidic washing to remove surface and non-specifically bound antibody. (B) Representative images over the kinetic time course for either scr or Rab4a treated cells. (C) Internalized TfR Intensity per cell for either scr or Rab4a treated cells over the kinetic time course ((intensity of TfR x TfR spots)/cell number). (D) Receptor amount (intensity of TfR) from raw intensity of internalized TfR in either scr or Rab4a. (E) Endosome amount (# TfR spots) in either scr or Rab4a. Significance calculated by Student's T-test. Graphed as mean \pm SEM. * = $pV \leq 0.05$; ** = $pV \leq 0.01$; *** = $pV \leq 0.001$; ns = not significant. Scale bar 10 μ m.

A

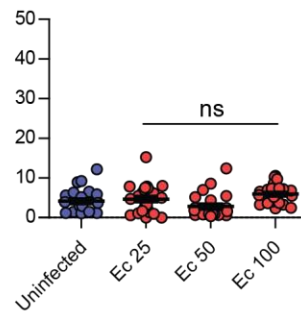
24 h post-infection



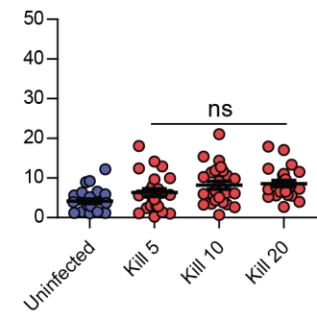
B



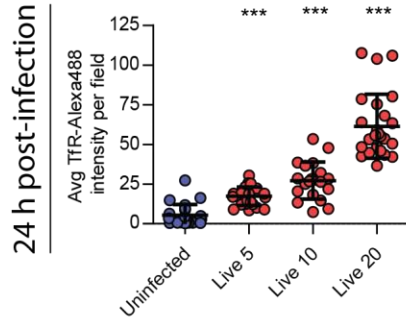
C



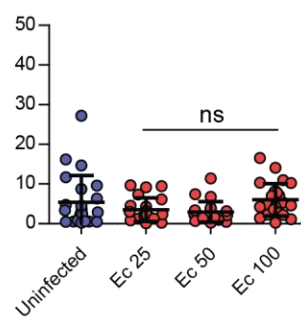
D



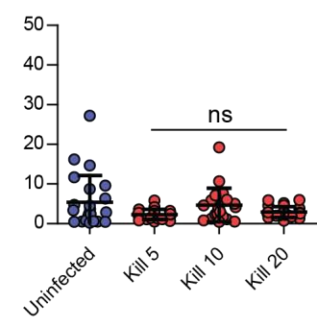
E



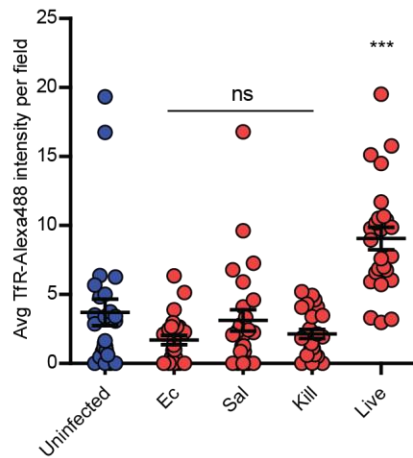
F



G



H HMDMs 2 h post-infection



I HMDMs 24 h post-infection

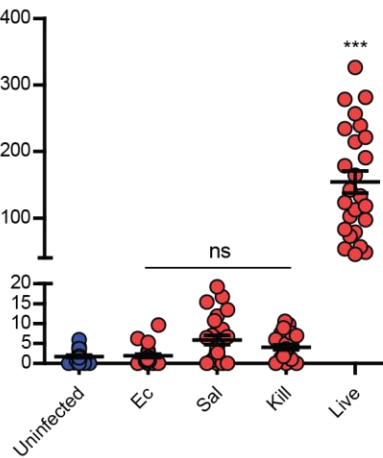


Figure 4-10. *Y. pestis* infection stalls host cell recycling.

(A) Representative images at 24 h post-infection in RAW264.7 cells. (B-G) Avg TfR intensity per field for infected RAW2647 cells with either dsRed live or paraformaldehyde killed *Y. pestis* (MOI 5, 10, 20) or *E. coli* (MOI 25, 50, 100). (H & I) Avg TfR intensity per field for HMDMs infected with either dsRed live or paraformaldehyde killed *Y. pestis* (MOI 10), *E. coli* (100) or *Salmonella* (MOI 100). Significance calculated by one-way ANOVA using Dunnett's multiple comparison test to uninfected control. Graphed as a representative experiment with mean \pm SEM. ** = $pV \leq 0.01$; *** = $pV \leq 0.001$; ns = not significant. Scale bar 10 μ m.

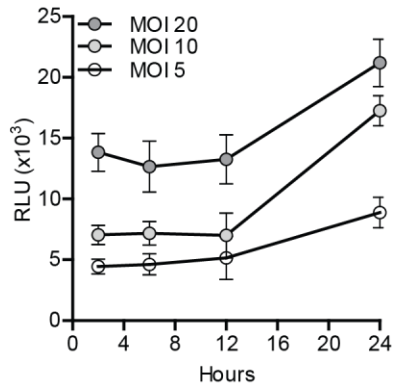


Figure 4-11. Ant-TfR antibody does not impact *Y. pestis* intracellular growth.

RAW264.7 cells were infected with *Y. pestis* CO92 pCD1⁽⁻⁾Lux_{P_{tolC}} (n=8; MOI 5, 10, 20) for 20 mins. Extracellular bacteria were killed, and intracellular bacteria maintained in gentamicin. Anti-TfR antibody was maintained in the media throughout the experiment. Bioluminescence was monitored at 2, 6, 12 and 24 h post-infection.

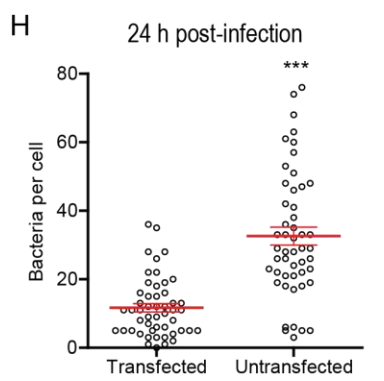
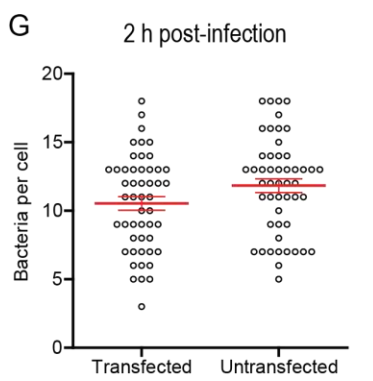
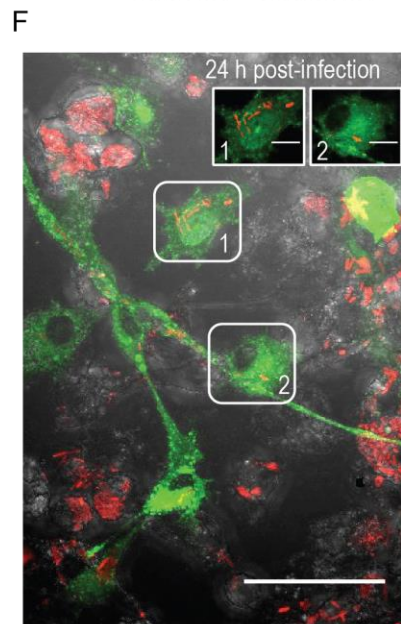
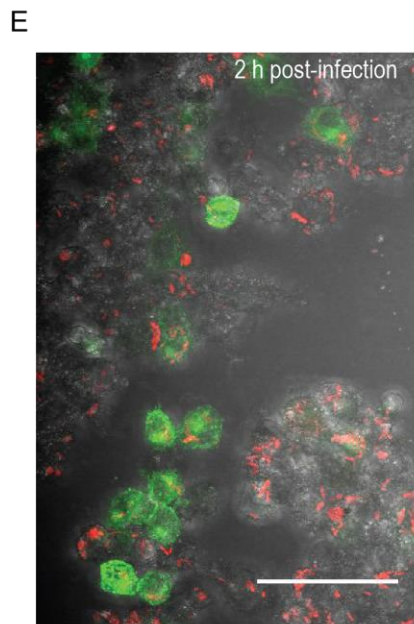
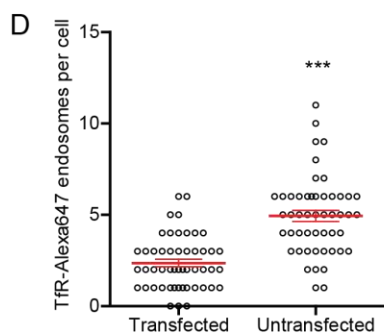
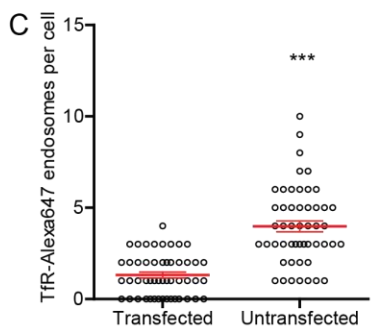
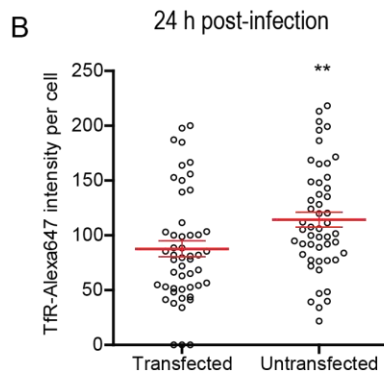
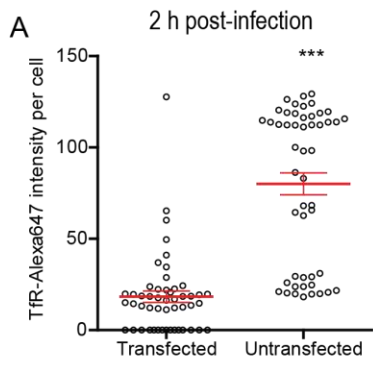


Figure 4-12. Stalling host cell recycling is required for *Y. pestis* replication.

RAW264.7 macrophages were transiently transfected with pEGFP-Rab11b prior to infection with *Y. pestis* CO92 pCD1⁽⁻⁾ pGEN::mCherry (MOI 10) in a recycling assay. (A & B) 2 h post-infection of TfR intensity and endosomes for transfected vs untransfected cells (n=50). (C & D) 24 h post-infection of TfR intensity and endosomes for transfected vs untransfected cells (n=50). (E & F) representative field images at 2 and 24 h post-infection. (G) 2 h post-infection bacteria per transfected vs untransfected cells (n=50). (H) 24 h post-infection bacteria per transfected vs untransfected cells (n=50). Significance calculated by paired Student's T-test. Graphed as a representative experiment with mean \pm SEM. ** = $pV \leq 0.01$; *** = $pV \leq 0.001$; Scale bar field 50 μ m and insert 10 μ m.

Tables

Table 4-1. 135 validated genes

siRNA Gene Target Identifiers				10 Hour Normalized <i>Y. pestis</i> Survival for Genes Meeting Cutoffs		
Entrez Gene ID	Gene Symbol	MGI Gene/Marker ID	Ensembl ID	CO92 Primary	CO92 Secondary	KIM-D-19 Secondary
12266	C3	MGI:88227	ENSMUSG00000024164	0.31	0.45	0.73
14064	F2rl2	MGI:1298208	ENSMUSG00000021675	0.27	0.89	0.60
14635	Galk1	MGI:95730	ENSMUSG00000020766	0.27	0.47	0.62
14676	Gna15	MGI:95770	ENSMUSG00000034792	0.28	0.51	0.76
14967	H2-D4	MGI:95899		0.32	0.73	0.60
14997	H2-M9	MGI:1276570	ENSMUSG00000067201	0.20	0.66	0.41
15002	H2-Ob	MGI:95925	ENSMUSG00000041538	0.21	0.57	0.50
15384	Hnrnpab	MGI:1330294	ENSMUSG00000020358	0.14	0.27	0.35
15387	Hnrnpk	MGI:99894	ENSMUSG00000021546	0.19	0.30	0.56
15482	Hspa1l	MGI:96231	ENSMUSG00000007033	0.34	0.21	0.22
16174	Ii18rap	MGI:1338888	ENSMUSG00000026068	0.29	0.36	0.40
16678	Krt1	MGI:96698	ENSMUSG00000046834	0.24	0.38	0.27
16950	Loxl3	MGI:1337004	ENSMUSG00000000693	0.26	0.55	0.46
17135	Mafk	MGI:99951	ENSMUSG00000018143	0.20	0.82	0.41
17195	Mbl2	MGI:96924	ENSMUSG00000024863	0.01	0.50	0.45
17279	Melk	MGI:106924	ENSMUSG00000035683	0.27	0.47	0.24
17289	Mertk	MGI:96965	ENSMUSG00000014361	0.28	0.43	0.50
17385	Mmp11	MGI:97008	ENSMUSG00000000901	0.12	0.95	0.49
17527	Mpv17	MGI:97138	ENSMUSG000000090262	0.35	0.60	0.53
17540	Mrvi1	MGI:1338023	ENSMUSG00000005611	0.20	0.67	0.43
17896	Myl4	MGI:97267	ENSMUSG000000061086	0.11	0.31	0.29
17904	Myl6	MGI:109318	ENSMUSG000000090841	0.16	0.59	0.40
17907	Mylpf	MGI:97273	ENSMUSG00000030672	0.06	1.00	0.59
17925	Myo9b	MGI:106624	ENSMUSG00000004677	0.09	0.58	0.58
17932	Myt1	MGI:1100535	ENSMUSG00000010505	0.35	0.56	0.25
18007	Neo1	MGI:1097159	ENSMUSG000000032340	0.17	0.54	0.63
18044	Nfya	MGI:97316	ENSMUSG00000023994	0.04	0.69	0.46
18071	Nhlh1	MGI:98481	ENSMUSG000000051251	0.09	0.54	0.45
18082	Nipsnap1	MGI:1278344	ENSMUSG000000034285	0.19	0.34	0.36
18143	Npas2	MGI:109232	ENSMUSG00000026077	0.20	0.37	0.46
18181	Nrf1	MGI:1332235	ENSMUSG000000058440	0.09	0.20	0.27
18201	Nsmaf	MGI:1341864	ENSMUSG000000028245	0.16	0.57	0.35
18209	Ntn3	MGI:1341188	ENSMUSG000000079662	0.35	0.81	0.50
18530	Pcdh8	MGI:1306800	ENSMUSG000000036422	0.17	1.08	0.56
18538	Pcna	MGI:97503	ENSMUSG000000027342	0.17	0.40	0.39
18641	Pfkl	MGI:97547	ENSMUSG000000020277	0.15	0.57	0.52
18690	Phx5	MGI:104521		0.20	0.55	0.38
18720	Pip5k1a	MGI:107929	ENSMUSG000000028126	0.28	0.78	0.46
18744	Pja1	MGI:1101765	ENSMUSG000000034403	0.26	0.37	0.44
18992	Pou3f2	MGI:101895	ENSMUSG000000095139	0.20	0.90	0.49
19053	Ppp2cb	MGI:1321161	ENSMUSG000000009630	0.15	0.72	0.51
19064	Ppy	MGI:97753	ENSMUSG000000017316	0.23	1.16	0.57
19110	Prl4a1	MGI:1206587	ENSMUSG000000005891	0.33	0.27	0.19
19331	Rab19	MGI:103292	ENSMUSG000000029923	0.25	0.42	0.14
19332	Rab20	MGI:102789	ENSMUSG000000031504	0.23	0.53	0.37
19335	Rab23	MGI:99833	ENSMUSG000000004768	0.18	0.41	0.35
19340	Rab3d	MGI:97844	ENSMUSG000000019066	0.27	0.73	0.59
19341	Rab4a	MGI:105069	ENSMUSG000000019478	0.13	0.33	0.10
20195	S100a11	MGI:1338798	ENSMUSG000000027907	1.59	1.12	0.63
20333	Sec22b	MGI:1338759	ENSMUSG000000027879	0.16	0.45	0.51
20336	Exoc4	MGI:1096376	ENSMUSG000000029763	1.50	1.16	0.87
20438	Siah1b	MGI:108063	ENSMUSG000000040749	0.33	0.12	0.20
20610	Sumo3	MGI:1336201	ENSMUSG000000020265	0.32	0.50	0.47
20630	Snrpc	MGI:109489	ENSMUSG000000024217	0.35	0.63	0.58
21454	Tcp1	MGI:98535	ENSMUSG000000068039	0.25	0.62	0.44
21787	Tfg	MGI:1338041	ENSMUSG000000022757	0.34	0.38	0.51
22110	Tsypyl1	MGI:1298395	ENSMUSG000000047514	0.32	0.55	0.50
26394	Lypla2	MGI:1347000	ENSMUSG000000028670	0.27	0.46	0.28
27395	Mrpl15	MGI:1351639	ENSMUSG000000033845	0.11	0.25	0.27
54633	Pqbp1	MGI:1859638	ENSMUSG000000031157	0.27	0.45	0.60
56041	Uso1	MGI:1929095	ENSMUSG000000029407	0.15	0.39	0.31
56096	Plac1	MGI:1926287	ENSMUSG000000061082	0.34	0.58	0.48
56284	Mrpl19	MGI:1926274	ENSMUSG000000030045	0.33	0.29	0.30
56522	Papalb	MGI:1932115	ENSMUSG000000074817	0.26	0.60	0.66
56523	Pmfbp1	MGI:1930136	ENSMUSG000000031727	0.34	0.62	0.43
58220	Pard6b	MGI:2135605	ENSMUSG000000044641	0.36	0.33	0.29

siRNA Gene Target Identifiers				10 Hour Normalized <i>Y. pestis</i> Survival for Genes Meeting Cutoffs		
Entrez Gene ID	Gene Symbol	MGI Gene/Marker ID	Ensembl ID	CO92 Primary	CO92 Secondary	KIM-D-19 Secondary
58234	Shank3	MGI:1930016	ENSMUSG00000022623	0.34	0.31	0.46
64384	Sirt3	MGI:1927665	ENSMUSG00000025486	0.25	0.65	0.40
66409	Rsl1d1	MGI:1913659	ENSMUSG00000005846	0.22	0.33	0.31
66615	Atg4b	MGI:1913865	ENSMUSG00000026280	0.24	0.38	0.20
66681	Pgm1	MGI:97564	ENSMUSG00000029171	0.28	0.44	0.58
67474	Snap29	MGI:1914724	ENSMUSG00000022765	0.37	0.41	0.57
67717	Lipf	MGI:1914967	ENSMUSG00000024768	0.26	0.50	0.46
67832	Brix1	MGI:1915082	ENSMUSG00000022247	0.10	0.35	0.28
68572	Ict1	MGI:1915822	ENSMUSG00000018858	0.20	0.83	0.52
68943	Pink1	MGI:1916193	ENSMUSG00000028756	0.20	0.74	0.39
69902	Mrto4	MGI:1917152	ENSMUSG00000028741	0.25	0.54	0.47
70152	Mettl7a1	MGI:1916523	ENSMUSG00000054619	0.28	0.87	0.49
71306	Mfap3l	MGI:1918556	ENSMUSG00000031647	0.24	1.16	0.46
71472	Usp19	MGI:1918722	ENSMUSG00000006676	1.46	1.33	0.68
71740	Pvrl4	MGI:1918990	ENSMUSG00000006411	0.21	0.40	0.26
71883	Coq2	MGI:1919133	ENSMUSG00000029319	0.28	0.31	0.43
72183	Snx6	MGI:1919433	ENSMUSG00000005656	0.36	0.56	0.67
73419	Armt1	MGI:1920669	ENSMUSG000000061759	0.14	0.55	0.41
74053	Grip1	MGI:1921303	ENSMUSG00000034813	0.35	0.28	0.21
74116	Pi16	MGI:1921366	ENSMUSG00000024011	0.33	0.15	0.31
74143	Opa1	MGI:1921393	ENSMUSG00000038084	0.36	0.32	0.20
74782	Git8d2	MGI:1922032	ENSMUSG00000020251	0.27	0.57	0.56
75292	Prkd3	MGI:1922542	ENSMUSG00000024070	0.30	0.87	0.59
75530	Lym7	MGI:1922780	ENSMUSG00000020268	0.30	0.34	0.30
75985	Rab30	MGI:1923235	ENSMUSG00000030643	0.39	0.19	0.11
76308	Rab1b	MGI:1923558	ENSMUSG00000024870	0.13	0.76	0.35
76338	Rab2b	MGI:1923588	ENSMUSG00000022159	0.14	0.42	0.12
76366	Mtif3	MGI:1923616	ENSMUSG00000016510	0.16	0.21	0.12
77604	Rbm12b2	MGI:1924854	ENSMUSG00000052137	0.13	0.25	0.26
81500	Sil1	MGI:1932040	ENSMUSG00000024357	0.12	0.70	0.60
83672	Sytl3	MGI:1933367	ENSMUSG000000041831	0.14	0.60	0.55
98685	Trmt1l	MGI:1916185	ENSMUSG00000053286	1.88	1.46	0.57
98758	Hnrnpf	MGI:2138741	ENSMUSG00000042079	0.16	0.67	0.53
104776	Aldh6a1	MGI:1915077	ENSMUSG00000021238	0.36	0.43	0.53
108011	Ap4e1	MGI:1336993	ENSMUSG00000001998	0.37	0.26	0.25
108069	Grm3	MGI:1351340	ENSMUSG00000003974	0.29	0.30	0.52
108853	Mtrf1l	MGI:1918830	ENSMUSG00000019774	0.32	0.24	0.21
109323	C1qtnf7	MGI:1925911	ENSMUSG000000061535	0.17	0.40	0.43
140859	Nek8	MGI:1890646	ENSMUSG00000017405	0.28	0.34	0.72
170719	Oxr1	MGI:2179326	ENSMUSG00000022307	0.32	0.25	0.38
192232	Hps4	MGI:2177742	ENSMUSG000000042328	1.48	1.10	0.92
207227	Sxbp5l	MGI:2443815	ENSMUSG00000022829	0.24	0.30	0.31
207920	Esrp1	MGI:1917326	ENSMUSG000000040728	0.17	0.44	0.28
208177	Phldb2	MGI:2444981	ENSMUSG000000033149	0.30	0.41	0.47
209456	Trp53bp2	MGI:2138319	ENSMUSG00000026510	0.30	0.82	0.55
213556	Plekhh2	MGI:2146813	ENSMUSG00000040852	0.32	0.30	0.46
215335	Slc36a1	MGI:2445299	ENSMUSG00000020261	0.33	0.73	0.51
217371	Rab40b	MGI:2183451	ENSMUSG00000025170	0.31	0.55	0.32
218121	Mboat1	MGI:2387184	ENSMUSG00000038732	0.26	0.58	0.45
218952	Fermt2	MGI:2385001	ENSMUSG00000037712	0.28	0.51	0.27
224044	Cyp2ab1	MGI:3644957	ENSMUSG00000022818	0.36	0.62	0.35
224118	0	No associated gene	0	0.37	0.57	0.13
227157	Mpp4	MGI:2386681	ENSMUSG00000079550	0.29	0.80	0.32
228775	Trib3	MGI:1345675	ENSMUSG00000032715	0.30	0.76	0.41
229534	Pbxip1	MGI:2441670	ENSMUSG00000042613	0.32	0.36	0.42
231507	Plac8	MGI:2445289	ENSMUSG00000029322	0.33	0.38	0.29
233489	Picalm	MGI:2385902	ENSMUSG00000039361	1.59	1.25	1.12
234852	Chmp1a	MGI:1920159	ENSMUSG00000000743	0.33	0.58	0.49
235330	Ttc12	MGI:2444588	ENSMUSG00000040219	0.09	0.53	0.37
238831	Ppwd1	MGI:2443069	ENSMUSG00000021713	0.30	0.56	0.51
241035	Pkhd1	MGI:2155808	ENSMUSG00000043760	0.33	0.30	0.49
259100	Olfrc66	MGI:3030500	ENSMUSG00000063582	0.34	0.50	0.54
268294	Zbtb24	MGI:3039618	ENSMUSG00000019826	1.46	1.11	0.56
269198	Nbea1	MGI:2444343	ENSMUSG00000073664	0.33	0.19	0.28
279499	Kctd19	MGI:3045294	ENSMUSG000000051648	0.06	0.69	0.33
327814	Ppfa2	MGI:2443834	ENSMUSG000000053825	0.27	0.65	0.47
380795	Ighg3	MGI:2144790	ENSMUSG00000076615	0.18	0.49	0.39
381827	1700073E17Rik	MGI:1920734	ENSMUSG000000087204	0.09	0.51	0.11
403395	Clec3a	MGI:2685642	ENSMUSG000000008874	0.35	0.71	0.58

Table 4-2. Bacterial Strains

Table 1. Bacterial Strains	
Bacterial Strains	References/sources
<i>Y. pestis</i> CO92 pCD1 ⁽⁻⁾	[9]
<i>Y. pestis</i> KIM D-19 pgm ⁽⁻⁾ pCD1 ⁽⁺⁾	BEI Resources
<i>Y. pestis</i> CO92 pCD1 ⁽⁻⁾ pGEN- <i>P</i> _{EM7} ::DsRED	[61]
<i>S. enterica</i> Typhimurium	ATCC 14028 (LT2)
<i>S. enterica</i> Typhimurium pGEN- <i>P</i> _{EM7} ::DsRED	LOU121; This study
<i>E. coli</i> DH5α	New England Biolabs
<i>E. coli</i> K12 DH5αpGEN- <i>P</i> _{EM7} ::DsRED	[61]
<i>E. coli</i> DH5α pEGFP-Rab4a	[108]
<i>E. coli</i> DH5α pEGFP-Rab11b	[108]

Table 4-3. siRNA

Table 2. siNRA	
Target	Catalog #
Rab1b	103033
Rab4a	64223
<i>Rab11b</i>	63944
<i>Myo5b</i>	63101

Table 4-4. qRT-PCR Primers.

Table 3. qRT-PCR Primers		
Target	5' – Forward – 3'	5' – Reverse – 3'
Rab4a	CATCGTCCTTATCCTCTGCG	AAAGCCTCTTCGACGTTCTC
Rab4b	CAGAAGTGGAAAGGAGCTGAG	TCACCAGGAATTTGAAGAGGAAG
Rab5a	TGGTCAAGAACGGTATCATAGC	GCCTTTGAAGTTCTTTAACCCAG
Rab7	AATAGGAGCGGACTTTCTGAC	CATCAAACACCAGAACACAGC
Rab9	CACGGAAGATAGGTCAGAACAC	CCCTTTAATGCCATCAACAGC
Rab11a	GTGGGCAATAAGAGTGATTTACG	TCTGTTAGAATTGTCTGAAAAGCAG
<i>Rab11b</i>	AAGACCATCAAGGCTCAGATC	CGCTCCACGTTCTCATATGTC
<i>Myo5b</i>	ATTTGAGGAACGGGTCACAG	GGTCAGAGCAGATGGGTTATATG
<i>GapDH</i>	AATGGTGAAGGTCGGTGTG	ACAAGCTTCCCATTCTCGG

CHAPTER 5:
GENOME-WIDE RNAI HIGH-THROUGHPUT SCREEN IDENTIFIES
POTENTIAL GENES IMPACTING *Y. PESTIS* INVASION

Introduction

In order to establish an infection, bacteria must first adhere to, and then invade the host cell. Bacteria mediate adherence to host cells via adhesins that interact with host surface proteins to attach the bacteria to the plasma membrane [260, 261]. In order to invade the host cell bacteria use either a trigger or zipper mechanism [260, 261]. The trigger mechanism is characterized by the activation of signaling cascades below the attached bacteria that “trigger” cytoskeletal rearrangements. These events cause plasma membrane ruffling around the organism, and ultimately lead to its internalization [260, 261]. This mechanism is well studied for *Salmonella enterica* Typhimurium [260, 261]. In this case, the bacteria uses the T3SS to inject effectors that trigger Rho GTPases that promote actin ruffling around the bacteria [260, 261]. The zipper mechanism occurs when bacterial proteins bind host membrane proteins creating an internalization signal (“outside-in”) that induces the bacteria’s uptake [260, 261]. An example of this is Invasin, a conserved molecule between *Y. pseudotuberculosis* and *Y. enterocolitica* that binds β 1 integrins [26, 28, 29, 262, 263]. Through clustering of β 1 integrins on the host cell surface the enteric *Yersinia* induce “outside-in” signaling and invade the host cell through the zipper mechanism [26].

We have observed that *Y. pestis* is rapidly taken up by the macrophage. Within 20 mins of a synchronized infection >65% of total bacterial inoculum is intracellular. The speed and rate of invasion for *Y. pestis* is substantially higher than other well studied intracellular pathogens, such as *S. enterica* Typhimurium. During *S. enterica* Typhimurium infection of macrophages it takes nearly an hour, after synchronization, for roughly ~50% of the inoculum to be intracellular (unpublished data) – an event that is a trigger mechanism mediated by SP1 island of the T3SS [264]. These observations lead us to hypothesize *Y. pestis* invasion is receptor mediated, through the zipper mechanism.

Y. pestis has several known adhesins, such as Ali, YadB, YadC, Pla and pH 6 antigen [1, 26, 265]. Studies of these adhesins in *Y. pestis* demonstrate their importance for adhering to host epithelial cells and professional phagocytes through interactions with host proteins, but clear links indicating their role in *Y. pestis* invasion has not been established [26, 265-267]. Furthermore, the

Y. pestis T3SS is not used for invasion, and is actually well established to be anti-phagocytic [1]. Cowan et al. demonstrated that after a five min centrifugation to initially synchronize bacterial contact, 75% of *Y. pestis* inoculum can invade HeLa cells by 100 min post-infection [27]. These data confirm that *Y. pestis* is capable of invading epithelial cells just as efficiently as the enteric *Yersinia* species. Further, they showed that loss of pPCP (and specifically the Pla adhesin) had a significant impact on invasion, but Pla(-) bacteria were still able to invade. Straley et al. demonstrated that *Y. pestis* lacking defined virulence determinants, such as the T3SS (encoded on pCD1 plasmid) and *caf1* (capsule), are still capable of invading at high titers and survive within macrophages [54]. These studies highlight that an unknown chromosomally encoded effector contributes to bacterial invasion. Importantly, Straley and colleagues also show that opsonization of *Y. pestis* does not prevent bacterial invasion, nor does it significantly impact the ability of the bacteria to survive within these cells [54]. Together, these suggest an unknown interaction of a bacterial adhesin is responsible for *Y. pestis* invasion.

Since these observations, multiple attempts have been made to identify both the bacterial ligand and eukaryotic receptor used by *Y. pestis* for invasion [31, 49, 268-271]. Initially, Ng et al. conducted a microarray analysis of upregulated host genes during *Y. pestis* infection at 26°C in murine macrophages and identified Clec9a receptor [269]. However, Ng and colleagues were not specifically looking for receptors and neither this group nor others have followed up with this receptor. In 2004, two groups followed up on Ccr5 receptor mutation, termed CCR5 Δ 32, which is a European conserved mutation linked to HIV resistance, and proposed to be a result of plague outbreak in the 14th century [268, 271]. In both studies, Ccr5^{-/-} knockout mice had no significant difference in survival when challenged with *Y. pestis* [268, 271]. However, Elvin et al. demonstrate there was a significant difference in bacterial burden within infected Ccr5^{-/-} macrophages [268]. These two studies concluded that *Y. pestis* entry and pathogenesis was more complex than previously thought.

Pla, and multifunctional protein encoded on the pPCP1 plasmid of *Y. pestis*, has been shown to bind to the macrophage receptor DEC-205 (also known as CD205) to promote

dissemination [31]. However, these data failed to demonstrate clear evidence that preventing interactions with Pla were sufficient to perturb intracellular bacterial growth. Studies by Sodeinde and colleagues previously demonstrated the binding of Pla to CD205 found that Pla activity did not play a primary role in *Y. pestis* resistance to innate host defenses, but was important for dissemination of the bacteria, suggesting other factors contributed to *Y. pestis* invasion [177].

DC-SIGN (CD209) and Langrin (CD207) were demonstrated to bind LPS oligosaccharide core of *Y. pestis* [270, 272]. *Y. pestis* does not have an O-antigen, but an oligosaccharide outer core attached to lipid A (for review see [67]). In these studies KIM 10 pCD1 (-) strains were constructed with either a truncated outer core or O-polysaccharide covered core. Using these strains, in a fluorescence flow cytometry platform, they show the LPS core facilitates adherence to both dendritic and Langerhans cells, as mutants where the oligosaccharide core are truncated or covered by the O-polysaccharide are significantly attenuated [270, 273]. With the same strains they demonstrate lower intracellular bacterial burdens after killing extracellular bacteria for 1 h with gentamicin (100µg/mL) [270, 273]. However, the data failed to provide a clear preventative role, as *Y. pestis* LPS is temperature modulated (hexa-acylated (26°C) to tetra-acylated (37°C); discussed in chapter 1). Furthermore, these studies failed to adequately quantify the relationship of bacterial inoculum, to either adherence or intracellular burden during in their flow cytometry assays.

While a few receptors have been identified through links with *Y. pestis* adhesins, the link to *Y. pestis* invasion is not well established in these works. The actual receptor(s) driving *Y. pestis* invasion of macrophages remains to be identified. During the optimization and completion of the Genome-wide RNAi HTS we emphasized our ability to kinetically monitor intracellular growth post-infection. We built our screening assay to have kinetic reads at 20 min, 2 h and 10 h post-infection with the idea that multiple time points might help us identify genes that were either a putative receptor, responsible for spacious YCV formation and bacterial replication, or differentially exploited during early and late YCV biogenesis. We noticed at 20 mins post-infection there was a consistent elevation in bioluminescence (RLU) in our Copβ1 positive control over our scrambled

(scr) negative control. This phenotype peaked our interest due to the consistency of our observations, and thus warranted further characterization. Here we describe the characterization of elevated 20 min RLU as an invasion phenotype from our genome-wide RNAi screen.

Results:

Elevated RLU at 20 min post-infection indicates a defect in Y. pestis invasion.

During the genome-wide RNAi screen to identify host factors required for *Y. pestis* intracellular survival (Chapter 4) we noticed that Cop β 1 siRNA-treated wells had elevated bioluminescence (~10-15% higher) compared to scrambled (scr) negative controls across all screen plates (n=205) (Fig.5-1A). Cop β 1 is a cytosolic component of the cotamer complex implicated in non-clathrin dependent recycling of LDL receptors [274, 275]. This complex is also associated with ADP-ribosylation factors (ARFs) and Golgi vesicle trafficking [274, 275]. Knockdown of Cop β 1 has previously been shown to inhibit uptake of other pathogenic bacteria, such as *L. monocytogenes* [141]. Therefore, the elevated bioluminescence at 20 mins post-infection may indicate an invasion defect in Cop β 1 treated cells. Alternatively, it is possible that the phenotype was an artifact of the promoter driving our bioreporter (*pToIC*). To test if elevated RLU was promoter dependent, we compared macrophage infection with *Y.pestis* CO92 pCD1⁽⁻⁾LUX_{P_{toIC}} to *Y.pestis* CO92 pCD1⁽⁻⁾LUX_{P_{CysZ}}. These two promoters drive the same bacterial luciferase system and have been integrated into the chromosome of *Y. pestis* CO92. Both of the promoters have been characterized previously, and have direct correlation between bioluminescence and bacterial number (see chapter 2) [151]. Bioluminescence was read at 20 mins post-infection, Our results show both promoters have ~ 10-15% elevated bioluminescence at 20 mins post-infection in Cop β 1 treated cells in comparison to scrambled negative control (scr) (Fig. 5-1B). This data shows elevated RLU at 20 mins post-infection is independent of the promoter driving the bacterial luciferase system in *Y. pestis* CO92.

Since the phenotype was not promoter dependent, we next tested whether known inhibitors of *Y. pestis* invasion displayed the same phenotype. Previous studies with *Y. pestis* showed treatment with Cytochalasin D significantly impacts invasion of HeLa cells [27]. This chemical

inhibitor has been demonstrated to prevent a range of cytoskeletal remodeling events to prevent phagocytosis [276]. Cytochalasin D has been extensively used to study bacterial invasion [253, 276-286]. Importantly, while Cytochalasin D treatment inhibits invasion, it has not been shown to not alter subsequent intracellular survival of *Y. pestis*. Therefore, treatment with Cytochalasin D was chosen as a control to determine if inhibition of *Y. pestis* invasion of macrophages recapitulated the 20 min phenotype observed in Cop β 1 siRNA treated cells. Cytochalasin D treated cells were infected with *Y. pestis* CO92 pCD1⁽⁻⁾Lux_{P_{tolC}} for 20 min and bioluminescence was determined and compared to intracellular bacterial burden at 80 min post-infection. A dose dependent elevation in bacterial bioluminescence over our untreated control was observed in the Cytochalasin treated cells (Fig. 5-2A). This elevation correlated to a dose dependent decrease in the RLU of intracellular bacterial burden at 80 mins post-infection (Fig. 5-2B). These data confirm that elevated RLU at 20 mins post-infection is an indicator of invasion defect.

Identifying invasion dataset from the Genome-wide RNAi HTS

Having demonstrating that elevated bioluminescence at 20 mins post-infection is an indicator of an invasion defect, we sought to utilize this phenomena to identify potential invasion defects from the genome-wide RNAi screen. 20 min bioluminescence was normalized for our entire 20 min dataset (n=16,757) by the average percent of the scrambled (scr) negative control on each individual plate. We established a cutoff criteria (materials and methods) and applied this to the entire 20 min dataset. This resulted in the identification of 1,075 genes with an invasion defect based on their elevated RLU at 20 mins post-infection (Table 5-1). To identify potential receptor/receptor activity of these hits we used PANTHER GO ontology database [258, 287]. Of the 1,075 genes identified with an invasion defect, 96 (9%) had direct receptor related functionalities (Table 5-2).

Discussion

Here we demonstrate that elevated bioluminescence (RLU) at 20 mins post-infection is an indication of a defect in *Y. pestis* invasion defects. Through our characterization of this phenotype, we show elevated RLU at 20 mins is: 1) independent of the promoter driving *Y. pestis*

chromosomally integrated bioluminescent bioreporter, 2) using Cytochalasin D, a known invasion inhibitor, we are able to recapitulate a dose dependent elevation in 20 min RLU that is inversely proportional to the bacterial burden at 80 mins, based on intracellular RLU, and 3) our observations mimic previous data of Cowan et al., demonstrating that Cytochalasin D was capable of inhibiting *Y. pestis* invasion in HeLa cells [27]. Furthermore, from our phenotypic characterization we were able to identify a subset of genes from our genome-wide RNAi HTS as impacting *Y. pestis* invasion. This represents the first ever comprehensive list of potential receptors and invasion related components exploited by *Y. pestis* for entry into the host macrophage. Many of the invasion hits that are not classified as receptors, are actually signaling/ trafficking molecules downstream of these receptors, such as the Arfgaps (2, 15, 17, & 18). Interestingly, Arfgap2 interacts with Arf1 to facilitate endocytosis and transport of endocytic cargo to the Golgi-ERGIC space [288]. Arf1 in turn is involved with Rab4a mediated endocytic recycling of receptors [238]. Of note, is the inclusion of Edg1 (Sphingosine 1-phosphate receptor 1) in our identified dataset. This receptor was shown by St. John and colleagues to be required by *Y. pestis* for efficient trafficking through the host lymphatics, and possibly entry into the macrophage (discussed below) [49] (Table 5-2). Moreover, none of the receptors identified impacting adherence of *Y. pestis* to the host cell (DEC 205, CD205, CD207 and CD209) were identified in our invasion dataset. This strongly suggests that while these receptors might contribute to adherence, they do not appear to contribute to *Y. pestis* invasion.

St. John et al. recently identified a requirement of S1P for dissemination from the draining lymph node during a bubonic infection model [49]. Their studies employed the use of chemical and antibody receptor agonists to block the trafficking of *Y. pestis* in the host lymphatics [49]. In their hands, *Y. pestis* was still partially able to colonize the host even without S1P. Furthermore, they demonstrated that from the site of infection there are two waves of infected cells that traffic to the draining lymph node. The first wave is double positive CD11c and CD11b cells, then over the course of 48 hrs the trafficked cells shift to CD11c, CD11b or PMN single positive cell types, which are representative on non-APC and inducible monocyte populations, respectively [49]. This novel observation highlighted that *Y. pestis* pathogenesis is potentially established through multiple innate immune cell types displaying a common receptor that facilitates *Y. pestis* adherence and

invasion. This suggests that potentially the eukaryotic receptor exploited for *Y. pestis* invasion is also the receptor used to drive lymphatic dissemination.

The elevated RLU observed at 20 min post infection could be a result of : 1) Unimpeded light from extracellular bacteria results in the full amount of photons easily reaching the detector. Whereas, the light from intracellular bacteria has to escape both the YCV and the macrophage before reaching the detector, thusly dampening the amount of photons that are read. 2) Internalized bacteria undergo a rapid metabolic change that dampens light production due to substrate and ATP requirements of the luciferase operon. Whereas, extracellular bacteria do not shift their metabolic state. 3) After uptake of the bacteria within the macrophage bacteria that are being actively degraded do not produce light, resulting in decreased intracellular RLU in comparison to their extracellular counterparts. Regardless of the molecular mechanism driving the elevation in RLU from the luciferase system, we demonstrate that this is a strong indicator of a bacterial invasion defect.

There are three possible phenotypic outcomes post-invasion of the bacteria into the macrophage: 1) Elevated RLU is a reflection of strictly an invasion defect at 20 mins post-infection, and intracellular RLU at 80 min/ 10 h is survival 2) Elevated RLU is an invasion defect, and loss of this invasion route forces the bacteria down a phagolysosome maturation pathway. Resulting in kinetically decreasing RLU at both 80 min and 10 h post-infection in comparison to scr control, and 3) Invasion of *Y. pestis* is not completely blocked by knockdown of the receptor, and a subpopulation of bacteria invade the macrophage via the normal mechanism resulting in decreased RLU at 80 min, but survival or growth (same RLU or increased RLU) at 10 h. Either case, elevated 20 min RLU phenotypically indicates an invasion defect. However, we are currently characterizing the relationship between intracellular RLU at 80 min and 10 h post-infection to determine if these post invasion phenotypes reflect a branch point in *Y. pestis* survival due to disruption of the natural invasion route.

Cytochalasin D is an example of a true invasion defect in which there is an elevated RLU read at 20 mins followed by a decrease in RLU at 2 h but either remains stable or increases at the

10 h RLU read (unpublished data). Rab1b is an example of RLU data showing no invasion defect, but a survival defect as RLU continues to decrease at 80 min and 10 h post-infection. We demonstrate that siRNA inhibition of Rab1b has no impact on bacterial invasion as the 20 min RLU is comparable to the scr negative control (unpublished data). Using confocal microscopy we demonstrate that 20-25% of the bacteria are extracellular, but the 80 min and 10 h data show decreasing RLU (chapter 4; [61]). We further show that the RLU decrease is a direct result of increased YCV acidification within 80 mins post-infection [61]. In contrast, RNAi of Cop β 1 is a primary example of both invasion and survival defect. There is an elevated 20 min RLU that correlates with confocal analysis showing 30-40% of the bacteria remain extracellular (chapter 4). However, at 80 min and 10 h the intracellular RLU decreases as a direct result of increased acidification of the YCV at 80 mins post-infection (unpublished data). From our data with Cytochalasin D, Rab1b and Cop β 1 there are three possible explanations for intracellular RLU at 80 mins/ 10 h with an elevated RLU at 20 mins for the *Y. pestis* invasion dataset. In order to test each outcome we would use comparisons of elevated RLU to YCV acidification.

The first outcome is that elevated RLU at 20 min strictly reflects invasion, and intracellular RLU at 80 min (or longer) is a measure of survival post-invasion. To test this hypothesis, we would need to test for acidification of the YCV at 80 mins post-infection for targets that have decreased RLU over time. Then, the results of acidification tests would need to be compared to RLU reads at 20 and 80 mins for a control that forces the bacteria toward the phagolysosome and ultimately degradation. In this instance, one would expect elevated RLU reads at 20 mins to have no correlation with increased YCV acidification or with increased intracellular RLU across a kinetic infection. Furthermore, determining this branching point between invasion and survival at 80 mins would implicate that the mechanism of bacterial entry is directly linked to avoidance of the phagolysosome, and is independent of the dogma that bacteria actively arrest phagolysosome maturation for survival.

The second possibility, is that blocking the natural entry mechanism of *Y. pestis* forces the bacteria toward a phagolysosome maturation pathway and results in bacterial death by 80 mins/

10 h. To determine this, a comparison of acidified YCVs of the target to scrambled negative control siRNA would need to be completed. One would expect to see a significant increase in acidified YCVs by 80 mins post-infection if elevated RLU at 20 mins is related to bacterial survival at 80 mins. Additionally, one would expect a continuous decrease in bacterial survival by RLU over time.

The third outcome that RNAi inhibition incompletely blocks *Y. pestis* invasion, and a subpopulation enters normally. This is based outcome is based on the caveats of RNAi. Firstly, RNAi penetrance is not 100% and the 80 min/ 10 h RLU is reflective of normal *Y. pestis* entry into macrophage cells that did not receive adequate knockdown of the specified host target. Penetrance meaning that one cannot determine expression within a single cell or the amount of siRNA that is distributed among cells. In this case further analysis of these genes would indicate that over time the bacteria that invade through the normal entry mechanism are able to survive and replicate. To address this hypothesis, we would need to test for acidification of the YCV at 80 mins post-infection. If there is no significant difference between YCV acidification of the target gene and the scrambled negative control, the elevated 20 min RLU in respect to decreased, non-acidified 80 min RLU would indicate an invasion defect, but would not indicate if *Y. pestis* invasion mechanism was directly linked to survival.

Overall, demonstrating the elevated RLU at 20 mins post-infection is a measure of *Y. pestis* invasion efficiency provides a powerful tool to dissect bacterial invasion and potentially identify the receptor of *Y. pestis* entry. While we have begun characterizing the various phenotypic results, additional studies are needed to determine the relationship of invasion to survival. A critical experiment for these studies is deciphering the RLU readouts of opsonized *Y. pestis* during macrophage infection, and if *Y. pestis* anti-sera prevents uptake. In regards to opsonization, one would expect to drive *Y. pestis* uptake via the Fc receptor and have no impact on bacterial survival as previously shown [54]. In contrast, using *Y. pestis* anti-sera at 26°C, or live bacteria in a dose dependent response should provide an invasion phenotype or force the bacteria down a phagolysosome maturation pathway. We believe the latter is true, as previous studies elude to a *Y. pestis* specific invasion mechanism that is dependent on a chromosomally encoded protein [27].

That being said, if one saturates the normal binding receptor and forces the bacteria to enter via another mechanism it would be shuttled to the phagolysosome and degraded in an acidified vacuole. Cowan et al., data supports the anti-sera hypothesis as entry of *Y. pestis* was attenuated during 26°C and 37°C temperature shifts due to an unknown chromosomally encoded bacterial protein, however, their data suggests it is due to phagolysosome trafficking [27].

Materials and Methods

Bacterial strains, siRNA transfection of macrophages.

Y. pestis CO92 [9] pCD1⁽⁻⁾ and derivatives (BEI Resources NR-4681) were cultivated at 26°C in Brain Heart Infusion (BHI) broth (Difco). Bioluminescent derivatives were generated using the LUX_{P_{tolC}} or LUX_{PCysZ} bioreporter as described previously [151]. RAW264.7 macrophages were obtained from ATCC and cultured in DMEM, 100 mM glucose + 10% FBS (Hyclone). For siRNA transfection, 20 µl of 0.165 µM Silencer siRNA (Life Technologies) diluted in Opti-MEM (Life Technologies) was mixed with 10 µl of 0.03% (v/v) Lipofectamine RNAi-Max/Opti-MEM (Life Technologies) as described by the manufacturer. 30 µl of the siRNA-Lipofectamine complex was added to each well of a white flat-bottom 96-well plate (Greiner), incubated at room temperature for 10 min, and then 1x10⁴ RAW264.7 macrophages suspended in 80 µl of DMEM+10% FBS were added. Cells were incubated for 48 h at 37°C with 5% CO₂.

Cytochalasin D treatment

Cytochalasin D was two-fold serially diluted from 2mM DMSO stock into DMSO and then diluted to final concentrations of 0.5, 1 and 2µM in DMEM 10% FBS (Hyclone). The DMSO matched control (0µM) was used for analysis. Inhibitor and RAW264.7 murine macrophage cells were incubated for 1 hr at 37°C with 5% CO₂ prior to bacterial infection. Final concentration of DMSO in DMEM 10% FBS was < 3%.

Bacterial infection of macrophages.

Macrophages were infected with *Y. pestis*CO92 pCD1⁽⁻⁾LUX_{P_{tolC}} or *Y.pestis* CO92 pCD1⁽⁻⁾LUX_{PCysZ} (MOI 10) as previously described [59, 61, 151]. In brief, bacteria cultivated overnight at

26°C in BHI, washed in PBS, and diluted in prewarmed DMEM+10%FBS. Bacteria were added to macrophages and infection synchronized by a 200xg centrifugation for 5 mins. 20 mins post infection extracellular bacteria were killed with gentamicin (16µg/mL) for one hour, and then media was replaced with DMEM + 10% FBS containing 2µg/mL gentamicin for the duration of the experiment. Bioluminescence was quantified using a Synergy HT or Synergy 4 plate reader (Biotek; 1 sec read with sensitivity set at 150) at 20 min, 80 min and 10 h post-infection [151].

Bioinformatics Analysis

Using the Genome-wide RNAi HTS dataset, we first normalized the 20 min dataset to the RLU of the avg scr negative control per plate as follows: (x gene RLU / avg scr RLU). We then constructed a 95% confidence interval (CI) around the % elevation seen in the Copβ1 controls per plate. We used the lower 95% CI limit as our cutoff criteria for % elevated RLU to identify genes with an invasion defect per plate. For GO ontology analysis, Entrez Gene identifiers for all 1,075 genes meeting the lower 95% CI limit of Copβ1 controls per plate were ran through PATNHER (<http://www.pantherdb.org/>) for their molecular processes based on GO ontology. Those Entrez Gene identifiers that were sub-classified under Receptor Activity (96) were used to generate a separate dataset.

Statistics

All experiments were repeated in triplicate, and are displayed as single representative experiments. All statistics were calculated in Graph Pad using either Student's T-Test, or one way ANOVA with post-hoc Dunnett's multiple comparison test for significance.

Figures and Figure Legends

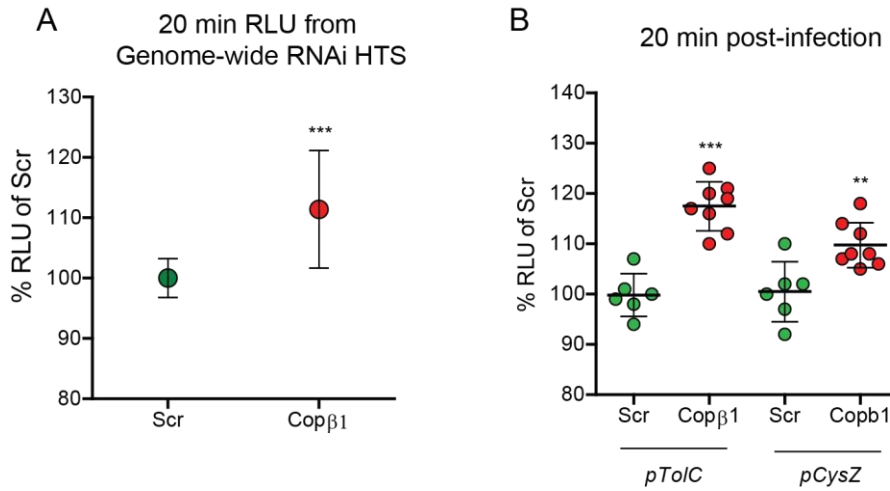


Figure 5-1. Elevated RLU is consistent and promoter independent.

(A) Bioluminescence (RLU) at 20 min post-infection for all genome-wide RNAi HTS plates (n=205).

(B) RAW264.7 macrophage cells transfected with either scrambled (scr; n=6) negative control or Copβ1 (n=8) siRNA for 48 hrs prior to infection with either *Y.pestis* CO92 pCD1⁽⁻⁾LUX_{P_{TolC}} or *Y.pestis* CO92 pCD1⁽⁻⁾LUX_{P_{CysZ}} (MOI 10). Percent RLU compared to scr at 20 min. RLU = Relative Light Units. Significance calculated with Student's T-test; ** = p<0.01, *** = p<0.001.

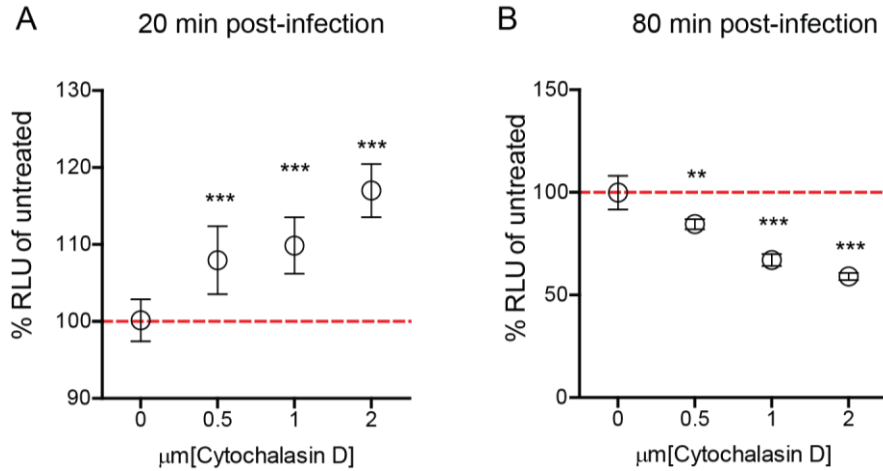


Figure 5-2. Elevated RLU is an invasion defect.

RAW264.7 macrophage cells treated with 0.5, 1, or 2 μm final [Cytochalasin D] (n=6) for 1 hr prior to infection with *Y.pestis* CO92 pCD1⁽⁻⁾Lux_{P_{to}I_C (MOI 10). Bioluminescence (RLU) reads at (A) 20 and (B) 80 mins post-infection. Graphed as percent RLU compared to 0 μm matched DMSO control. Dotted line = 100%. RLU = Relative Light Units. Significance calculated with One way ANOVA post-hoc Dunnett's multiple comparison test to 0 μm matched DMSO control; ** = p<0.01, *** = p<0.001.}

Tables

Table 5-1. All putative invasion targets.

Entrez Gene ID	Gene Symbol	Screen Survival		
		20min	2.0hr	10.0hr
13858	Eps15	1.08	0.75	0.78
13859	Eps15-rs	1.09	0.62	0.73
14163	Fgd1	1.09	0.72	0.78
14469	Gbp2	1.21	0.90	1.09
14704	Gng3	1.13	0.86	0.94
14709	Gng8	1.10	0.81	1.00
330914	Grit	1.16	0.92	0.94
69993	Chn2	1.12	0.62	0.89
78618	Acap2	1.12	0.81	0.83
11539.00	Adora1	1.17	0.74	0.74
67333	Stk35	1.15	0.76	0.92
68556	Uck1	1.21	0.79	0.92
14744	Gpr65	1.12	0.84	0.90
15551	Htr1b	1.12	0.94	1.14
16995	Ltb4r1	1.10	0.88	1.02
216749	Nmur2	1.10	0.84	0.85
227288	Il8ra	1.10	0.77	0.90
387285	Hcrtr2	1.15	0.92	1.00
436440	Gpr31c	1.14	0.79	0.83
64095	Gpr35	1.11	0.68	0.69
80910	Gpr84	1.17	0.97	1.06
84111	Gpr87	1.09	0.87	0.96
12766	Cxcr3	1.08	1.01	1.30
12801	Cnr1	1.10	0.93	1.03
13051	Cx3cr1	1.16	0.94	1.03
13488	Drd1a	1.13	1.15	1.23
13490	Drd3	1.16	1.08	1.20
13491	Drd4	1.16	0.85	1.09
13609	Edg1	1.17	0.99	1.30
13617	Ednra	1.13	0.65	0.70
14062	F2r	1.15	0.96	1.22
14065	F2rl3	1.14	1.04	1.28
14293	Fpr1	1.30	1.23	1.39
14294	Fprl1	1.12	1.00	1.19
14527	Gcgr	1.18	0.78	0.82
14602	Ghrhr	1.09	0.94	0.98
14652	Glp1r	1.11	0.82	0.85
14715	Gnrhr	1.15	0.95	1.03
14747	Cmklr1	1.16	0.87	1.04
170757	Eld1	1.23	0.81	0.87
226278	Prihr	1.12	1.06	1.51
227289	Gpbar1	1.13	0.91	1.02
229323	Gpr171	1.14	0.78	0.93
238252	Gpr135	1.17	0.75	0.79
239853	Gpr128	1.17	0.85	0.85

243277	E230012M21	1.16	0.99	1.42
269053	Gpr152	1.16	0.90	0.98
321019	Ebi2	1.14	0.78	0.85
52389	D7Ertd680e	1.16	0.96	1.29
52614	Emr4	1.11	1.06	1.34
53978	Edg4	1.08	1.08	1.36
56696	Gpr132	1.09	0.96	1.21
78560	Gpr124	1.28	1.10	1.10
94226	Edg8	1.18	1.19	1.53
101533	1200016C12Rik	1.06	0.94	1.01
105501	Abhd4	1.03	0.95	1.18
11434	Acr	1.00	0.74	0.95
11487	Adam10	1.09	0.75	0.77
11488	Adam11	1.43	1.22	1.83
11492	Adam19	1.10	0.93	1.22
11495	Adam2	1.01	0.73	0.77
13983	Esr2	1.01	1.00	1.57
15370	Nr4a1	1.06	0.63	0.77
171234	V1rf3	1.00	0.92	1.57
18227	Nr4a2	1.07	1.06	1.60
18441	P2ry1	1.10	0.45	0.52
19214	Ptgdr	1.13	0.71	0.75
19220	Ptgfr	1.06	0.48	0.59
19222	Ptgir	1.01	0.80	1.15
19228	Pthr1	1.03	0.99	1.39
19401	Rara	1.09	0.86	0.91
20605	Sstr1	1.03	0.76	0.87
20607	Sstr3	1.05	1.04	1.13
20608	Sstr4	1.06	0.68	0.96
20609	Sstr5	1.00	0.78	1.22
21337	Tacr2	1.01	0.86	1.03
21338	Tacr3	1.05	0.63	0.68
213527	Pthr2	1.06	1.05	1.80
215854	Taar5	1.04	0.82	1.11
21833	Thra	1.22	0.87	1.01
21834	Thrb	0.99	0.92	1.16
21907	Nr2e1	1.06	0.44	0.50
22045	Trhr	1.00	1.10	1.56
22337	Vdr	1.11	0.59	0.60
22354	Vipr1	1.04	0.95	1.32
22355	Vipr2	1.03	0.76	0.95
233571	P2ry6	1.02	0.82	1.08
23957	Nr0b2	1.06	1.01	1.41
23958	Nr2e3	1.10	0.49	0.58
243083	Tmprss11f	1.11	0.84	1.06
243084	A030012E10	1.03	0.89	1.27
319757	Smo	1.12	0.91	1.10
329093	Cpa6	1.09	0.90	1.15
56544	V2R2	1.05	0.77	1.13
57385	P2ry4	1.02	0.78	1.12
66286	1810029G24Rik	1.03	0.90	1.04
67168	P2y5	1.06	0.80	0.89
67469	Abhd5	1.06	0.88	1.12
70008	Ace2	1.11	0.77	0.93

70839	P2ry12	1.01	0.86	1.02
72461	2510048K03Rik	1.09	0.76	0.95
73218	3110056O03Rik	1.04	1.07	1.31
76453	2310046G15Rik	1.12	0.71	0.82
77593	4930550B20Rik	1.04	0.81	0.86
84112	Sucnr1	1.02	0.88	1.23
235606	Apeh	1.21	0.59	0.66
23792	Adam23	1.35	0.89	0.98
70835	Prss22	1.27	0.85	0.86
12288	Cacna1c	1.16	0.78	0.82
12298	Cacnb4	1.11	0.86	0.90
319446	Dpep2	1.21	0.96	1.18
11486	Ada	1.08	0.73	0.75
21752	Tert	1.13	0.60	0.61
12299	Cacng1	1.13	0.90	1.08
12337	Capn5	1.09	0.87	0.90
12864	Cox6c	1.07	0.96	1.00
13860	Eps8	1.24	0.95	0.99
18606	Enpp2	1.13	1.10	1.23
353025	Caps2	1.05	0.90	1.07
50766	Crim1	1.21	0.74	0.82
74754	Dhcr24	1.15	0.77	0.92
13074	Cyp17a1	1.03	0.95	1.03
13075	Cyp19a1	0.99	0.93	1.06
217707	Coq6	1.03	0.87	1.10
22034	Traf6	0.99	0.88	1.18
22682	Za20d2	1.04	0.62	0.75
52700	Txnl5	1.04	0.80	0.97
53600	Timm23	0.98	0.91	0.94
69035	Zdhhc3	0.99	0.48	0.67
78903	Wrnip1	1.05	0.80	0.84
209027	Pycr1	1.12	0.75	0.79
102141	Snx25	1.02	0.62	0.75
103724	Tbc1d10a	1.03	0.79	0.81
11848	Rhoa	1.04	0.84	1.01
11853	Rhoc	1.02	0.81	1.08
11858	Rnd2	1.01	0.93	1.22
14787	Rhpn1	1.08	0.51	0.55
19395	Rasgrp2	1.01	0.75	0.90
194590	Reps2	1.08	0.77	0.85
19731	Rgl1	1.04	0.84	1.08
19732	Rgl2	1.16	0.80	0.86
19734	Rgs16	1.12	0.56	0.61
19735	Rgs2	1.17	0.87	0.94
19737	Rgs5	1.12	0.78	0.84
19769	Rit1	1.16	0.66	0.68
20224	Sar1a	1.07	0.82	0.84
20334	Sec23a	1.08	0.86	1.03
20401	Sh3bp1	1.13	0.89	0.94
213391	Rassf4	1.10	0.61	0.62
215653	Rassf2	1.02	0.75	0.76
217463	Snx13	1.07	0.62	0.69
217692	Sipa1l1	1.08	0.58	0.62
21844	Tiam1	1.09	0.91	1.15

225870	Rin1	1.07	0.62	0.76
232441	Rerg	1.04	0.74	0.76
233071	Snx26	1.08	0.93	1.06
233537	4921513O04	1.05	0.77	0.85
24012	Rgs7	1.04	0.73	0.91
246709	Rgs13	1.03	0.75	0.89
50778	Rgs1	1.10	0.81	1.13
51791	Rgs14	1.10	0.60	0.72
56212	Rhog	1.15	0.35	0.35
56437	Rrad	1.02	0.65	0.80
69159	Rhebl1	1.08	0.54	0.60
71330	Rcctb1	1.16	0.80	0.96
72536	Tagap	1.14	0.76	0.85
74156	Cach	1.05	0.84	0.98
74194	Rhoe	1.08	0.84	1.00
75985	Rab30	1.14	0.38	0.39
109904	Mcf2	0.99	0.83	0.83
114713	Rasa2	1.08	0.69	0.75
15463	Hrb	1.03	0.73	0.77
16653	Kras2	1.03	0.62	0.65
18797	Plcb3	1.04	0.74	0.81
19330	Rab18	1.02	0.90	0.97
19337	Rab33a	1.03	0.82	0.84
19338	Rab33b	1.16	0.96	1.11
19414	Rasa3	1.03	0.78	0.88
19415	Rasal1	1.11	0.75	0.84
19416	Rasd1	1.05	0.72	0.80
212285	LOC212285	1.04	0.87	1.05
223864	Rapgef3	1.04	0.93	0.96
231801	Agfg2	1.06	0.88	1.08
270160	Rab39	1.02	0.62	0.66
271457	Rab5a	1.00	0.87	0.92
67844	Rab32	1.02	0.52	0.57
74055	Pice1	0.99	0.72	0.77
103135	Usp52	1.10	0.81	0.87
103694	Tmed4	1.06	0.92	0.97
114886	Cygb	1.07	1.01	1.12
11657	Alb1	1.05	0.64	0.69
13063	Cycs	1.06	0.85	0.96
16803	Lbp	1.13	0.67	0.83
16819	Lcn2	1.08	0.83	0.84
17189	Mb	1.03	0.67	0.73
225651	Mppe1	1.05	0.82	0.96
330260	Pon2	1.10	0.99	1.06
50767	Nte	1.45	1.36	1.61
71701	Pnpt1	1.14	0.89	0.91
74244	Apg7l	1.18	0.50	0.52
78600	Pde6h	1.13	0.74	0.75
12978	Csf1r	1.26	0.84	0.89
16452	Jak2	1.28	0.41	0.50
16590	Kit	1.29	0.59	0.69
57745	Zfp112	1.18	0.87	1.10
13713	Elk3	1.01	0.75	0.75
20254	Scg2	1.06	0.91	0.92

20351	Sema4a	1.05	0.73	0.93
20358	Sema6a	1.03	0.71	1.02
20394	Scg5	1.05	0.45	0.46
22402	Wisp1	1.01	0.77	0.86
224860	Plcl2	1.03	0.86	0.87
24117	Wif1	1.06	0.89	1.01
26456	Sema4g	1.03	0.47	0.49
26556	Homer1	1.03	0.80	0.81
67196	2700084L22Rik	1.08	0.77	0.80
67405	Nts	1.05	0.85	0.95
73318	1700013N18Rik	1.06	0.92	1.00
14609	Gja1	1.09	0.90	0.99
18417	Cldn11	1.06	0.84	0.95
20821	Trim21	1.05	0.79	0.84
22194	Ube2e1	1.06	1.03	1.11
22209	Ube2a	1.10	0.84	0.86
26458	Slc27a2	1.08	0.72	0.76
54419	Cldn6	1.10	0.91	1.06
56228	Ube2j1	1.11	0.95	1.06
58187	Cldn10	1.12	0.91	0.97
66105	Ube2d3	1.07	0.83	0.90
66894	Wwp2	1.05	0.66	0.77
74153	Ube1l	1.06	0.83	0.92
79263	Trim39	1.05	0.83	0.87
100705	Acacb	1.05	0.87	0.87
107885	Mthfs	1.04	0.48	0.55
17237	Mgrn1	1.06	0.65	0.74
18563	Pcx	1.11	0.85	0.87
212085	4921513B05Rik	1.06	0.81	0.94
224826	Ubr2	1.04	0.60	0.84
229487	Pet112l	1.10	0.90	0.96
59004	Pias4	1.12	0.99	1.14
97541	Qars	1.06	0.84	1.12
99152	Anapc2	1.04	0.87	1.01
1E+08	Dnajc3	1.05	0.52	0.63
13418	Dnajc1	1.08	0.79	0.93
14616	Gja8	1.09	0.87	0.93
14617	Gjd2	1.06	0.85	0.91
15507	Hspb1	1.07	0.96	1.16
15528	Hspe1	1.11	0.89	1.14
17475	Mpdz	1.03	1.00	1.00
17714	Grpel2	1.05	0.78	0.87
213539	Bag2	1.04	0.92	0.93
231997	Fkbp14	1.07	0.74	0.97
56354	Dnajc7	1.07	0.59	0.84
56445	Dnaja2	1.03	0.83	1.02
57431	Dnajc4	1.06	0.68	0.87
64010	Sav1	1.03	0.93	1.14
66411	Ckap1	1.07	0.93	1.03
67035	Dnajb4	1.04	0.99	1.02
68598	Dnajc8	1.07	0.75	1.14
76889	Adck4	1.06	0.95	0.99
80888	Hspb8	1.08	0.97	1.00
83945	Dnaja3	1.07	0.80	0.98

93742	Pard3	1.03	0.91	0.94
23970	Pacsin2	1.06	0.61	0.89
386649	Nsfl1c	1.05	0.75	0.76
56440	Snx1	1.04	0.89	0.91
71889	Epn3	1.05	0.82	0.88
11629	Aif1	1.15	0.72	0.78
12813	Col10a1	1.07	0.82	0.88
18125	Nos1	1.11	0.64	0.71
18126	Nos2	1.10	0.60	0.71
18570	Pdcd6	1.11	0.47	0.50
20193	S100a1	1.08	0.72	0.79
20198	S100a4	1.08	0.83	0.86
21926	Tnf	1.09	0.52	0.54
270084	Lpcat2	1.16	0.76	0.92
27062	Cadps	1.09	0.88	0.89
52589	Ncald	1.09	0.72	0.83
67500	Ccar1	1.12	0.71	0.72
70527	Stampb	1.08	0.86	0.90
73316	Calr3	1.11	0.92	0.96
80796	Calm4	1.12	0.81	1.02
12263	C2	1.10	0.83	0.91
14134	Fcnb	1.10	0.64	0.74
14256	Flt3l	1.07	0.51	0.68
14962	Cfb	1.13	0.65	0.87
16168	Il15	1.09	0.56	0.60
20292	Ccl11	1.11	0.92	0.93
50908	C1s	1.08	0.86	0.91
50928	Klrg1	1.09	0.85	0.86
54525	Syt7	1.10	0.79	0.83
14118	Fbn1	1.19	0.91	1.00
16782	Lamc2	1.19	1.06	1.17
17388	Mmp15	1.23	0.99	1.12
17392	Mmp3	1.18	0.88	1.22
17395	Mmp9	1.21	0.99	1.11
18074	Nid2	1.20	1.08	1.31
214766	Mmp21	1.25	0.68	0.92
23948	Mmp17	1.27	0.78	1.10
240047	Mmp25	1.21	0.69	0.92
26561	Mmp23	1.19	0.81	1.06
13433	Dnmt1	1.04	0.92	1.09
13629	Eef2	1.05	0.84	0.94
13685	Eif4ebp1	1.02	0.78	0.93
13690	Eif4g2	1.07	0.72	0.81
13796	Emx1	1.05	0.77	1.08
13797	Emx2	1.02	0.74	0.75
14265	Fmr1	1.01	0.80	1.09
14836	Gsc	1.07	0.82	1.03
14842	Gsh1	1.07	0.73	0.75
14843	Gsh2	1.05	0.93	1.04
14852	Gspt1	1.07	0.86	0.97
15115	Hars	1.06	0.87	0.92
15248	Hic1	1.05	0.85	0.98
212528	Trmt1	1.03	0.97	0.98
226414	Dars	1.03	0.73	0.85

23879	Fxr2	1.02	0.67	0.68
54632	Ftsj1	1.01	0.78	1.00
70791	Hars2	1.07	0.65	0.76
15312	Hmgn1	1.00	0.80	0.84
16589	Uhmk1	1.02	0.88	1.07
171170	Mbnl3	1.05	0.68	0.78
70223	Nars	1.02	0.62	0.70
72199	Mms19l	1.03	0.72	0.82
76936	Hnrpm	1.03	0.82	0.91
94353	Hmgn3	1.01	0.81	0.89
108017	Fxyd4	1.22	0.83	0.96
171209	Accn3	1.19	0.82	0.86
17178	Fxyd3	1.22	0.77	0.82
217356	Tmc8	1.19	0.95	1.06
229927	Clca4	1.20	1.15	1.46
435845	Tmprss11c	1.17	0.73	0.74
56808	Cacna2d2	1.20	0.90	1.04
74270	Usp20	1.18	0.71	0.95
103710	Slc35e4	1.03	0.95	1.16
106039	Gga1	1.01	0.95	1.30
110891	Slc8a2	1.00	0.83	0.93
117591	Slc2a9	1.10	0.81	1.30
140918	Slc7a12	1.05	0.97	1.13
142681	Slc34a3	1.02	0.72	1.27
14664	Slc6a9	1.07	0.95	1.14
16792	Laptm5	1.03	1.02	1.34
18399	Slc22a6	1.00	0.96	1.28
20509	Slc19a1	1.03	1.05	1.25
20536	Slc4a3	1.07	0.95	1.05
207151	Slc22a9	1.00	1.05	1.32
210148	Slc30a6	1.01	0.75	1.17
216867	Slc16a11	1.02	0.90	1.16
224661	Slc26a8	1.01	1.00	1.13
22599	Slc6a20b	1.03	0.94	1.08
227059	Slc39a10	1.03	1.02	1.33
229706	Slc6a17	1.12	0.94	1.04
242773	Slc45a1	1.01	0.91	1.15
260302	Gga3	1.05	0.98	1.25
268512	Slc26a11	1.04	0.97	1.06
54160	Copg2	1.00	0.99	1.36
56358	Copz2	1.02	1.00	1.27
59042	Cope	1.02	0.98	1.27
64454	Slc5a4b	1.01	0.99	1.38
67843	Slc35a4	1.00	0.67	1.19
69089	Oxa1l	1.01	0.89	1.26
71805	Nup93	1.00	1.03	1.53
72027	Slc39a4	1.01	0.94	1.16
72961	Slc17a7	1.01	1.03	1.46
74102	Slc35a5	1.03	0.67	1.24
74338	Slc6a19	1.06	1.07	1.23
77996	D730039F16Rik	1.07	0.88	1.20
98396	Slc41a1	1.00	1.03	1.20
108956	2210421G13Rik	0.99	1.01	1.13
109280	9330176C04Rik	1.05	0.93	1.25

11777	Ap3s1	1.05	0.92	1.36
16531	Kcnma1	1.05	0.96	1.12
16532	Kcnma3	1.01	0.95	1.11
16536	Kcnq2	1.02	0.96	1.10
18669	Abcb1b	1.00	0.63	1.15
18670	Abcb4	1.01	0.68	1.24
192140	Tmc2	1.01	0.93	1.29
193034	Trpv1	1.01	0.90	1.01
20271	Scn5a	1.00	0.97	1.09
20928	Abcc9	0.99	0.56	1.11
210463	BC026439	1.07	1.09	1.19
213603	BC010552	1.07	0.93	1.18
213827	Arcn1	1.00	0.95	1.17
223604	Kcnk9	1.04	0.92	1.11
224742	Abcf1	1.00	0.57	0.91
228993	BC019537	1.00	0.76	0.94
231430	BC038311	1.05	0.97	1.08
232910	Ap2s1	1.00	1.07	1.55
236149	Slc22a26	1.05	0.91	1.23
241612	Slc5a12	0.99	0.70	1.05
241919	BC061928	1.02	0.81	0.81
243813	Leng9	1.05	0.95	1.01
252903	Ap1s3	0.99	0.93	1.23
27061	Bcap31	1.02	1.02	1.22
319800	C730048C13Rik	1.06	0.92	1.18
320590	9430071P14Rik	1.01	0.98	1.36
338363	6030446N20Rik	0.99	0.89	1.19
338365	A230035L05Rik	1.00	0.91	1.35
399548	Scn4b	1.01	0.93	1.17
56325	Abcb9	0.99	0.61	1.25
56334	Tmed2	0.99	0.95	1.09
57776	Ttyh1	1.03	0.92	1.07
67135	2310021H06Rik	1.03	1.15	1.18
68044	2510006C20Rik	0.99	0.97	1.57
68279	Mcoln2	1.00	0.93	1.00
68682	1110028E10Rik	1.02	0.93	1.34
69065	1810008K03Rik	1.00	1.03	1.29
72175	2810423E13Rik	1.00	0.95	1.30
74424	Tmc5	1.00	0.97	1.30
75761	Apol7a	1.00	0.93	0.99
77577	9830002I17Rik	0.99	0.85	1.15
101744	C330005M16Rik	1.05	0.89	0.93
102954	Nudt10	1.00	1.06	1.16
105352	Dusp22	1.04	0.63	1.06
108096	Slco1a5	1.04	0.98	1.04
110074	Dutp	1.02	0.65	1.03
110332	4921523A10Rik	1.02	1.02	1.20
110895	Slc9a4	1.07	0.93	1.14
13853	Epm2a	1.02	0.65	1.13
14198	Fhit	1.04	0.91	1.07
16331	Inpp5d	1.03	1.01	1.11
170835	Pib5pa	1.06	0.96	1.09
18640	Pfkfb2	1.02	1.09	1.24
214901	Chtf18	1.01	0.82	0.88

216152	BC005764	1.01	1.11	1.49
232941	C79127	1.00	1.05	1.25
235534	Acpl2	1.04	0.95	1.15
242291	1110001C20Rik	1.02	1.10	1.28
28248	Slco1a1	1.01	0.94	1.12
28250	Slco1a4	1.03	0.86	1.00
28254	Slco1a6	1.04	1.06	1.12
384619	Ccdc155	1.07	1.05	1.42
52036	Saps3	1.01	0.73	1.32
54561	Nap1l3	1.03	0.96	1.06
57028	Pdpx	1.01	1.00	1.11
58242	Nudt11	1.03	0.98	1.16
58243	Nap1l5	1.01	1.06	1.22
60600	Tsga8	1.02	0.87	0.93
66387	Nudt8	1.02	1.02	1.13
67395	4930403L05Rik	1.01	1.07	1.24
67528	Nudt7	1.00	1.04	1.45
67952	Tomm20	1.00	1.07	1.26
68695	1110033O09Rik	1.02	0.98	1.29
69274	Ctdspl	1.01	0.78	1.24
71474	Ppp6r2	1.00	0.91	1.21
74140	Tm9sf1	1.04	0.93	1.20
74189	Phactr3	1.05	1.10	1.37
74411	4932443D16Rik	1.00	1.00	1.12
75769	4833424O15Rik	1.10	1.05	1.42
77573	Vps33a	1.00	0.87	0.96
13057	Cyba	1.00	0.80	0.82
217864	D12Wsu95e	1.04	0.81	0.84
276829	Smtnl2	1.03	0.77	0.80
319593	D130011D22Rik	1.01	0.91	0.92
320373	D130016K21Rik	1.01	0.76	0.76
330577	D030069K18	1.03	0.95	0.97
442805	D130007C19Rik	1.01	0.87	0.90
52014	Nus1	1.00	0.92	0.97
52668	lfi27l1	1.00	0.79	0.91
52670	Cpsf4l	1.02	0.95	1.11
52717	D10Ert641e	1.03	0.84	0.98
214932	Cecr5	1.04	0.89	1.04
225745	Ccdc5	1.08	0.88	1.10
321022	Cdv3	1.03	0.87	0.91
57912	Cdc42se1	1.04	0.91	0.97
66440	Cdc26	1.07	0.79	0.83
67849	Cdca5	1.06	1.10	1.20
71991	Ckn1	1.07	0.93	1.00
72278	Ccpg1	1.09	1.07	1.08
94040	Clmn	1.14	1.00	1.06
103466	C630002B14Rik	1.05	0.97	1.09
12331	Cap1	1.00	0.86	0.89
231855	Ap5z1	1.09	0.88	0.97
235386	C630028N24Rik	1.03	0.80	0.89
442802	C330011M18Rik	1.01	0.92	0.93
54378	Cacng6	1.02	0.79	0.81
68112	C330016H24Rik	1.04	0.82	0.82
12959	Cryba4	1.07	0.97	1.12

12964	Cryga	1.08	0.85	0.99
12967	Crygd	1.03	1.03	1.05
12970	Crygs	1.04	1.05	1.07
234577	Cpne2	1.06	0.97	1.17
245684	Cnksr2	1.05	0.83	0.92
266692	Cpne1	1.04	1.05	1.13
338337	Cog3	1.08	1.00	1.16
57358	Cmar	1.03	0.94	1.03
66398	Commd5	1.10	1.04	1.18
76524	Cln6	1.09	0.90	0.97
94109	Csmd1	1.04	1.05	1.05
13626	Eed	1.07	0.95	1.03
210757	E430004N04Rik	1.04	0.98	1.01
211305	E330017E16	1.04	1.03	1.12
228598	Ebf4	1.04	0.94	1.03
240754	Lax1	1.07	1.05	1.16
319996	D130060C09Rik	1.12	1.10	1.19
320360	E130307J04Rik	1.06	1.00	1.08
403205	E030025L21Rik	1.05	0.93	1.18
54648	Ccdc120	1.04	1.07	1.20
231630	D5Ertd40e	1.06	0.93	1.01
65111	Dap3	1.06	0.88	0.97
213491	Szrd1	1.09	0.86	0.95
219072	Haus4	1.08	0.86	0.92
232813	D430041B17	1.06	0.85	0.99
27762	Vwa7	1.07	0.97	1.09
319388	D230002A01Rik	1.08	0.97	1.03
319655	Podxl2	1.07	0.99	1.14
52552	D13Ertd275e	1.14	1.01	1.06
52846	D1Bwg0212e	1.05	0.85	0.89
67586	D4Bwg1540e	1.06	0.94	1.10
67948	Fbxo28	1.09	1.04	1.17
78581	D530033C11Rik	1.12	0.99	1.19
107986	Ddb2	1.05	1.02	1.02
112403	Dom3z	1.07	1.05	1.15
116905	Dph2l1	1.15	0.95	1.03
13216	Defa1	1.07	1.09	1.27
13221	Defa-rs12	1.09	1.06	1.18
13238	Defa4	1.07	0.96	1.13
13239	Defcr5	1.07	1.02	1.23
13380	Dkk1	1.13	1.01	1.22
13446	Doc2a	1.08	1.06	1.13
13447	Doc2b	1.06	1.04	1.14
13517	Dspp	1.10	1.01	1.20
13518	Dst	1.08	1.08	1.15
227525	Dclre1c	1.18	1.02	1.11
23853	Def6	1.09	0.93	1.10
23854	Def8	1.09	0.99	1.10
246079	Defb9	1.09	1.02	1.24
360212	Defb38	1.08	0.98	1.00
50722	Dkk1l	1.11	1.20	1.38
54638	DXlmx40e	1.25	1.04	1.44
54722	Dfna5h	1.19	1.18	1.36
56176	Pigp	1.07	0.95	0.99

56455	Dnclc1	1.08	1.19	1.26
56811	Dkk2	1.11	0.95	1.19
58251	Ddc8	1.10	1.00	1.08
66148	Dnajc15	1.06	0.99	1.15
67379	Dedd2	1.11	1.02	1.03
67728	Dph2l2	1.06	1.05	1.14
68184	Denr	1.06	0.99	1.24
68563	Dpm3	1.07	1.20	1.41
68897	Disp1	1.10	1.06	1.07
71804	Dufd1	1.11	1.01	1.06
71972	Dnmbp	1.11	1.04	1.30
73284	Ddit4l	1.13	1.00	1.02
77674	Defb12	1.16	1.06	1.29
94223	Dgcr8	1.08	1.22	1.30
97998	Deptor	1.06	1.08	1.10
102920	Fshprh1	1.12	0.85	1.08
103583	Fbxw11	1.14	0.79	0.89
14154	Fem1a	1.05	0.67	0.73
14210	Fin15	1.10	0.90	0.99
14221	Fjx1	1.09	0.89	1.07
14352	Fv4	1.07	0.68	0.74
17281	Fyco1	1.10	0.91	0.94
213980	Fbxw10	1.10	0.69	0.71
231470	Fras1	1.05	0.97	1.14
239839	Ccdc14	1.21	0.68	0.79
240263	Fem1c	1.06	0.88	0.94
30050	Fbxw2	1.10	0.84	0.95
384061	Fndc5	1.06	0.87	0.98
50759	Fbxo16	1.07	0.79	0.81
50764	Fbxo15	1.16	0.99	1.05
64339	Fndc4	1.08	0.75	0.83
66153	Fbxo36	1.07	0.91	1.08
71313	Fsip1	1.05	0.77	1.04
78938	Fbxo34	1.19	0.75	0.81
219150	F830020C16Rik	1.13	0.82	0.91
320463	F630111L10Rik	1.10	0.93	0.97
50757	Fbxo12	1.17	0.84	0.90
54357	Epb4.1l4b	1.11	0.67	0.67
14585	Gfra1	1.09	1.07	1.11
217648	Gm527	1.05	0.87	0.90
229588	Gm128	1.06	0.95	0.96
23885	Gcl	1.15	0.89	1.10
241950	Gm1805	1.09	0.83	0.87
381334	Gal3st2	1.26	0.80	1.04
68592	Gcipip	1.20	0.67	0.80
70772	Ggnbp1	1.09	0.87	0.97
93683	Glce	1.08	0.91	0.97
16970	Lrmp	1.13	0.80	0.86
211228	Lrrc25	1.56	1.08	1.10
269593	Luzp1	1.13	0.97	0.99
432582	E130309D14Rik	1.11	0.92	0.99
432589	LOC432589	1.11	0.93	0.96
544988	544988	1.12	0.83	0.85
16639	Klra8	1.08	1.08	1.09

67224	Med29	1.06	0.81	0.94
140559	Igsf8	1.14	1.24	1.26
15982	lfrd1	1.02	1.09	1.18
15983	lfrd2	1.04	1.14	1.26
192232	Hps4	1.17	1.42	1.48
382522	Hist3h2bb-ps	1.01	1.18	1.21
66141	lfitm3	1.11	1.39	1.51
66320	Tmem208	0.98	1.14	1.17
66667	Hspbap1	1.06	1.00	1.09
80876	lfitm2	1.01	1.34	1.38
83408	Gimap3	0.99	1.07	1.09
99899	lfi44	1.04	0.84	0.88
13863	Lcn5	1.02	0.80	0.83
16699	Krtap13	1.04	0.74	0.90
212871	LOC212871	1.14	0.81	0.87
268905	Krtap13-1	1.11	0.82	0.86
381806	LOC381806	1.03	0.68	0.72
432555	LOC432555	1.03	0.64	0.71
54135	Lsr	1.08	0.94	1.08
66380	Krtap3-3	1.05	0.87	0.99
66708	Krtap3-2	1.02	0.75	0.88
76893	Lass2	1.05	0.86	0.90
18095	Nkx3-1	1.09	0.69	0.72
18307	Olfr10	1.13	0.90	1.17
213765	BC125332	1.09	0.88	1.00
259015	Olfr1038	1.08	0.84	0.91
433904	Ociad2	1.11	0.66	0.72
67122	Nrarp	1.08	0.58	0.75
68039	Nmb	1.07	0.71	0.72
72310	Nkg7	1.07	0.60	0.73
258925	Olfr20	1.07	0.76	0.81
28028	Mrpl50	1.07	0.72	0.76
434204	MGC51670	1.05	0.90	0.92
68499	Mrpl53	1.04	0.75	0.89
17149	Magoh	1.09	0.69	0.71
17235	Mcsp	1.06	0.60	0.66
66591	Mad2l1bp	1.07	0.94	0.96
170829	Tram2	0.98	0.84	1.01
219024	Tmem55b	0.98	0.62	0.72
21950	Tnfsf9	1.04	0.65	0.73
22031	Traf3	1.01	0.72	0.77
22040	Trex1	0.96	0.82	0.87
22057	Tob1	0.98	0.79	0.81
22157	Tulp1	0.98	0.78	0.87
224840	Trem14	0.97	0.71	0.76
227331	Tnrc15	1.02	0.82	0.85
227606	Tbpl2	0.96	0.73	0.76
231130	Tnip2	1.00	0.79	0.83
252838	Tox	0.98	0.69	0.70
27279	Tnfrsf12a	0.95	0.76	0.79
277414	Trp53i11	0.99	0.73	0.83
30934	Tor1b	0.96	0.86	0.96
64930	Tsc1	0.95	0.83	0.83
66241	Tmem9	0.96	0.65	0.67

67946	Spata6	1.01	0.62	0.66
71326	Trem1	1.00	0.70	0.83
71609	Tradd	1.00	0.72	0.74
72236	Tsnaxip1	1.01	0.74	0.74
72265	Tram1	0.98	0.77	0.82
20939	Sva	0.99	0.81	0.84
20944	Svs5	1.01	0.78	0.82
232811	Suv420h2	0.98	0.61	0.73
237336	Tbpl1	0.98	0.66	0.67
27381	Tcl1b2	0.99	0.65	1.02
387347	Tas2r118	0.97	0.83	0.98
387515	Tas2r144	0.96	0.67	0.70
53878	Svs2	1.01	0.83	0.92
57252	Tas2r105	0.96	0.74	0.89
574417	Tas2r137	0.97	0.65	0.71
67043	Syap1	0.97	0.63	0.65
67923	Tceb1	0.98	0.82	1.17
68416	Sycn	0.98	0.70	0.78
71578	Sval1	0.97	0.68	0.76
93670	Tac4	0.96	0.77	0.83
104871	Spata7	1.03	0.64	0.64
20759	Spr2e	0.99	0.77	0.89
20760	Spr2f	0.96	0.88	1.04
20761	Spr2g	1.02	0.75	0.79
20770	Spt1	0.99	0.85	0.95
225888	Suv420h1	1.04	0.84	1.00
229285	Spg20	0.96	0.65	0.74
278240	Spin2	0.96	0.79	0.87
54402	Stk19	0.97	0.51	0.56
68720	Lce1b	0.98	0.87	0.98
69611	Lce1d	1.02	0.70	0.73
70599	Ssfa2	1.02	0.96	1.07
75956	Srrm2	0.98	0.67	0.76
216395	Tmem5	1.02	0.89	0.96
21667	Tdgf1	1.09	0.91	1.03
219249	Tdrd3	1.02	0.76	0.88
27380	Tcl1b4	1.00	0.88	1.04
27382	Tcl1b5	1.09	0.76	0.76
56351	Tebp	1.02	0.85	0.95
67878	Tmem33	1.00	0.84	0.99
73122	Tgfbrap1	1.02	0.69	0.98
73679	Tex19.1	1.01	0.81	0.84
83559	Tex18	1.04	0.64	0.66
108946	Zzz3	1.04	0.76	0.88
112405	Egln1	1.04	0.95	1.04
112406	Egln2	0.99	0.88	1.21
14204	Ii4i1	1.00	0.93	1.17
15495	Hsd3b4	1.05	0.63	0.77
15496	Hsd3b5	0.98	0.57	0.73
170737	Znrf1	1.02	0.76	1.10
20250	Scd2	1.01	0.79	0.79
20834	Znrf4	1.00	0.70	0.87
22761	Zfpm1	1.05	0.68	0.82
22789	Zp3r	1.01	0.79	0.89

319740	Zfyve27	1.04	0.95	0.97
320951	9030221M09Rik	1.01	0.61	0.63
52696	Zwint	1.05	0.61	0.81
58865	Tdh	1.01	0.67	0.86
68221	1700049M11Rik	0.99	0.74	0.91
68842	Tulp4	1.03	0.87	1.29
69367	Glr2	1.01	0.74	0.86
74551	1810010O14Rik	0.99	0.90	1.01
77424	9530002K18Rik	0.98	0.76	0.82
78287	Zfyve20	1.00	0.89	0.95
113865	V1rc8	1.03	0.88	0.88
171245	V1rh1	1.06	0.82	0.94
171247	Vmn1r199	1.01	0.73	0.78
171257	V1ri6	1.04	0.75	0.87
171271	Vmn1r220	1.05	0.81	0.88
213081	Wdr19	1.01	0.73	0.90
22360	Vmp	1.04	0.84	0.92
230796	Wdte1	1.02	0.71	0.74
252908	V1ri8	1.04	0.76	0.78
27973	Vkorc1	1.03	0.77	0.79
54636	Wdr45	1.03	0.73	0.74
69568	Vkorc1l1	1.01	0.64	0.65
113848	Vmn1r42	0.99	0.71	0.87
113864	V1rc7	1.03	0.82	0.99
171198	Vmn1r28	0.98	0.76	0.88
212190	Ubx3	1.04	0.68	0.83
217379	Ubx4	1.00	0.71	0.99
22269	Upk2	1.02	0.61	0.81
22270	Upk3a	0.99	0.80	0.86
69136	Tusc1	1.06	0.69	0.90
70450	Unc13d	1.01	0.89	1.24
72565	Uaca	1.03	0.62	0.63
80385	Tusc2	1.05	0.89	1.23
215627	Zbtb8	1.08	0.76	0.79
22631	Ywhaz	1.06	0.77	0.79
54367	Zfp326	1.10	0.90	1.27
231659	G431004K08Rik	1.09	0.88	1.03
67230	2810439M05Rik	1.08	0.73	0.84
12189	Brca1	1.02	0.93	1.28
208104	B930074I24	1.00	0.94	1.28
216874	Camta2	1.01	0.94	0.99
232855	BC023179	1.00	1.04	1.30
235048	BC050092	1.01	0.90	1.05
235956	Zfp825	1.00	0.88	1.00
244219	BC030314	1.01	1.09	1.13
319792	9130023H24Rik	1.03	0.84	1.15
381066	Zfp948	1.01	0.84	1.13
66830	Nacc1	1.01	0.97	1.21
78783	Brpf1	1.02	0.93	1.03
406222	Krt74	1.03	0.93	1.01
71994	Cnn3	1.03	0.89	1.20
102162	Taf5l	1.06	0.86	1.05
74469	Taf7l	1.02	0.99	1.06
328280	Rslan24	1.05	1.02	1.10

20288	Msr1	1.14	0.79	0.81
239029	4933430J11	1.21	0.65	0.65
18171	Nr1i2	1.14	0.68	0.72
257891	Olfr479	1.14	0.54	0.61
258016	Olfr453	1.14	0.62	0.77
258222	Olfr310	1.19	0.71	0.75
258270	Olfr448	1.11	0.60	0.62
258293	Olfr437	1.10	0.74	0.77
258302	Olfr420	1.14	0.79	0.80
258436	Olfr458	1.12	0.61	1.01
258490	Olfr492	1.19	0.43	0.43
258529	Olfr313	1.15	0.56	0.57
258530	Olfr311	1.16	0.60	0.70
258648	Olfr237-ps1	1.18	0.68	0.71
258713	Olfr430	1.14	0.61	0.61
258926	Olfr476	1.13	0.69	0.72
257908	Olfr115	1.21	0.84	1.01
257899	Olfr1000	1.20	0.71	0.79
257916	Olfr1031	1.16	0.66	0.67
18442	P2ry2	1.13	0.72	0.78
259112	Olfr979	1.12	0.50	0.53
102607	Snx19	1.11	0.77	0.78
14700	Gng10	1.07	0.98	1.11
19385	Ranbp1	1.16	0.51	0.56
19387	Rangap1	1.15	0.40	0.45
20403	ltsn2	1.11	0.82	1.09
227800	Rabgap1	1.20	0.48	0.51
236573	E430029F06	1.09	0.86	1.00
243362	Stard13	1.07	0.79	0.94
244962	Snx14	1.24	0.69	0.75
380711	Garnl4	1.08	0.83	0.83
50780	Rgs3	1.14	0.82	0.87
56395	C78915	1.12	0.79	0.95
56784	Ralgapa1	1.09	0.82	1.00
70497	Arhgap17	1.11	0.79	0.91
73910	Arhgap18	1.15	0.80	0.93
76117	Arhgap15	1.13	0.85	0.88
79264	Krit1	1.07	0.76	0.84
99326	Garnl3	1.13	0.71	0.72
107435	Hat1	1.07	0.78	1.33
216454	BC089597	1.04	0.78	0.93
77805	A930014I12Rik	1.06	0.88	1.04
114143	Atp6v0b	1.05	0.87	1.00
232906	6430596G11Rik	1.05	0.80	0.81
68449	1110003P22Rik	1.05	0.84	0.93
17110	Lzp-s	1.06	0.29	0.53
17766	Nudt1	1.05	0.90	0.97
18010	Neu1	1.07	0.98	1.11
207806	Gm608	1.07	0.92	1.17
212442	Lactb2	1.06	0.35	0.65
215951	Lace1	1.08	0.33	0.58
223254	Farp1	1.05	0.85	1.06
226090	MGC28180	1.08	0.79	1.10
227377	Farp2	1.06	0.91	0.99

227619	Man1b1	1.05	0.38	0.63
23956	Neu2	1.07	0.94	1.09
268395	Mpg	1.05	0.91	1.16
30959	Ddx25	1.07	0.89	1.09
320685	Dctd	1.09	0.77	0.80
52633	Nit2	1.07	0.78	0.89
59007	Ngly1	1.09	0.94	1.06
67328	Lyz1	1.07	0.38	0.66
71567	Mcmdc1	1.09	0.90	1.13
72831	Dhx30	1.05	0.81	0.93
80907	Lactb	1.05	0.36	0.64
83456	Mov10l1	1.08	0.90	1.02
101497	Al194308	1.06	0.97	1.24
102075	4931414L13Rik	1.04	0.92	1.00
107338	Gbf1	1.04	1.01	1.34
109151	Chd9	1.03	0.92	1.02
11938	Atp2a2	1.04	0.89	1.04
11941	Atp2b2	1.05	0.92	1.13
11981	Atp9a	1.11	1.13	1.31
16801	Arhgef1	1.03	1.00	1.22
209224	Cova1	1.07	0.93	1.03
213484	BC036718	1.04	0.82	0.89
213522	BC026778	1.03	0.32	0.63
216848	Chd3	1.02	0.81	1.02
217364	D230014K01Rik	1.04	0.82	0.88
224079	9330174J19Rik	1.11	1.03	1.10
227723	5830434P21Rik	1.04	0.83	0.84
229688	BC051070	1.03	0.92	0.94
230379	Acer2	1.07	0.86	0.94
243272	BC021875	1.03	0.46	0.73
319767	9030605H24Rik	1.06	1.04	1.10
320024	Aadacl1	1.02	0.52	0.57
320707	Atp2b3	1.02	0.93	1.11
381572	9430007A20Rik	1.06	0.87	1.01
50769	Atp8a2	1.06	1.01	1.07
52666	D10Ert610e	1.08	0.93	0.96
53404	Atoh7	1.06	1.10	1.50
54608	Abhd2	1.06	0.94	0.97
67239	Bxdc1	1.03	0.97	1.13
67772	Chd8	1.05	0.90	1.01
68126	Fahd2a	1.02	0.63	0.89
71562	Afmid	1.02	0.95	1.28
74018	Als2	1.04	1.08	1.14
80744	BC003993	1.02	0.54	0.71
83379	AV071179	1.04	0.97	1.27
21843	Tial1	1.04	0.78	0.81
219131	Phf11	1.05	0.70	0.71
547168	Rhox7	1.07	0.90	0.96
57317	Sfrs4	1.05	0.87	1.12
68927	Ptcd2	1.04	0.91	0.96
100609	9830109N13Rik	1.05	0.90	1.02
103284	Zc3h10	1.02	1.13	1.23
12877	Cpeb1	1.04	1.20	1.39
13831	Epc1	1.04	1.01	1.06

14359	Fxr1h	1.02	0.92	0.94
226049	Dmrt2	1.01	1.13	1.34
231044	Gbx1	1.03	0.98	1.13
231999	Plekha8	1.01	0.89	1.18
233904	BC010250	1.02	1.15	1.17
242620	Dmrta2	1.01	1.10	1.22
268741	5730589K01Rik	1.03	0.74	0.80
268859	A2bp1	1.06	1.02	1.33
320858	D930040M24Rik	1.02	0.89	1.06
494448	Cbx6	1.03	0.87	1.09
66408	Aptx	1.06	1.16	1.36
70127	Dpf3	1.02	0.97	1.14
217944	Rapgef5	1.06	0.84	0.90
26464	Vnn3	1.07	1.02	1.27
67229	Prpf18	1.06	0.97	1.02
67724	Pop1	1.07	0.78	0.86
72886	2900016D05Rik	1.06	0.94	1.11
74002	Psd2	1.07	0.94	0.97
14957	Hist1h1d	1.05	1.12	1.17
14958	H1f0	1.04	0.93	0.98
15078	H3f3a	1.02	0.92	1.06
15267	Hist2h2aa1	1.07	1.10	1.28
15371	Hmx1	1.07	1.23	1.75
15372	Hmx2	1.03	1.08	1.40
16815	Lbx2h	1.04	0.98	1.13
18080	Nin	1.02	0.89	1.02
18508	Pax6	1.06	1.11	1.29
223499	Gm83	1.04	0.88	0.91
228731	Nkx2-4	1.04	1.07	1.31
234988	Mbd3l2	1.01	1.13	1.45
237339	L3mbtl3	1.02	1.20	1.29
243529	H1fx	1.03	0.99	0.99
246738	ORF28	1.04	0.93	1.02
260423	Hist1h3f	1.05	1.12	1.41
27354	Nbn	1.02	0.44	0.78
319158	Hist1h4i	1.05	1.10	1.31
382035	Pabpn1l	1.07	1.03	1.09
433762	LOC433762	1.05	1.04	1.41
50708	Hist1h1c	1.05	1.17	1.39
56335	Mettl3	1.03	0.42	0.69
56702	Hist1h1b	1.02	1.13	1.17
80838	Hist1h1a	1.03	1.02	1.18
97908	Hist1h3g	1.03	1.08	1.16
30928	Zfp238	1.06	0.75	0.89
67876	1500041J02Rik	1.07	0.77	0.83
69029	1500032L24Rik	1.02	0.79	0.99
69770	1600002K03Rik	1.07	0.66	0.78
75188	1700009J07Rik	1.03	0.75	0.98
75462	1700001C19Rik	1.02	0.72	0.95
76568	1500035H01Rik	1.05	0.82	1.04
78304	1500034E06Rik	1.02	0.78	0.90
78330	1500032D16Rik	1.02	0.80	0.88
66183	1110032A04Rik	1.07	0.79	0.90
66195	1110058A15Rik	1.07	0.82	0.87

68659	1110032E23Rik	1.08	0.87	0.99
68731	Rbfa	1.09	0.74	0.88
68796	1110039B18Rik	1.07	0.58	0.61
73730	1110008K04Rik	1.08	0.86	0.97
74165	1110004B15Rik	1.12	0.84	1.00
381629	0610007C21Rik	1.00	0.72	1.01
55978	lft20	1.02	0.72	1.05
56700	0610031J06Rik	1.03	0.70	0.80
57247	Zfp276	1.03	0.74	1.04
59052	Mettl9	1.00	0.75	1.06
66048	0610009E20Rik	1.00	0.78	0.96
66074	0610041E09Rik	1.02	0.85	0.93
66089	Rmnd5b	1.03	0.68	0.96
66910	Tmem107	1.06	0.66	0.78
67441	0610042E07Rik	1.01	0.89	0.98
68212	0610007H07Rik	1.02	0.67	0.84
68314	0610008F07Rik	0.99	0.80	0.88
68323	0610006K04Rik	1.02	0.84	0.88
68421	0910001K20Rik	1.02	0.86	0.98
68550	1110002N22Rik	1.00	0.86	0.99
71691	Pnmal1	1.01	0.81	1.03
77038	Arfgap2	1.05	0.80	0.91
109082	1110064L07Rik	1.13	0.79	1.02
231238	2310045A20Rik	1.06	0.82	1.00
65971	Tbata	1.07	0.87	0.96
66374	2310011J03Rik	1.06	0.88	0.94
71897	2310010M24Rik	1.08	0.91	0.94
66934	1700022L09Rik	1.06	0.88	1.02
67317	1700022I11Rik	1.08	0.90	1.02
69479	1700029J07Rik	1.06	0.99	1.43
73274	1700034P14Rik	1.05	0.89	1.08
73299	1700041G16Rik	1.05	0.93	1.26
75564	1700027N10Rik	1.09	0.83	1.14
76416	Znrd1as	1.08	0.93	0.96
108735	2010005O13Rik	1.15	0.83	0.96
109129	2010311D03Rik	1.12	0.73	0.82
233545	2210018M11Rik	1.08	0.84	0.87
53951	2310002B06Rik	1.11	0.88	0.90
56786	Tmem9b	1.14	0.90	0.94
66343	Tmem177	1.12	0.89	1.01
66349	2310004L02Rik	1.08	0.85	1.06
66353	2310007A19Rik	1.17	0.99	1.00
66358	2310004I24Rik	1.16	0.65	0.71
66359	Fam36a	1.08	0.95	0.96
66488	Fam136a	1.10	0.80	0.88
66526	2210012G02Rik	1.04	0.88	0.94
66528	2210020M01Rik	1.16	1.05	1.10
66549	Aggf1	1.08	0.80	0.87
67017	2010011I20Rik	1.17	0.97	1.16
67038	2010109I03Rik	1.11	0.86	0.96
67298	Gprasp1	1.11	0.81	0.92
67484	Eepd1	1.13	0.99	1.02
67495	Tmem167b	1.11	0.90	0.97
67620	2310006J04Rik	1.10	0.90	0.95

67899	Cmc1	1.10	0.90	1.02
69147	2200002J24Rik	1.08	0.89	0.93
69457	2310005G13Rik	1.10	0.94	0.96
69520	Lce3f	1.12	0.80	0.90
69542	2300002M23Rik	1.06	0.84	0.94
69871	2010007H12Rik	1.08	0.88	1.09
69876	2010013E08Rik	1.14	0.98	1.08
69882	2010321M09Rik	1.10	0.93	1.15
69893	2010305A19Rik	1.12	0.99	1.00
69894	2010107G23Rik	1.19	0.79	0.96
70082	2210402C18Rik	1.18	0.91	1.05
70088	2310005N01Rik	1.14	0.87	0.93
70160	Vps36	1.14	0.86	0.97
70163	2210415F13Rik	1.09	0.73	0.73
70178	2210412D01Rik	1.18	0.87	0.97
70257	2010107E04Rik	1.06	0.89	0.96
71886	2310002L09Rik	1.14	0.99	1.01
71912	2300003C06Rik	1.15	0.81	0.95
72084	2010319C14Rik	1.10	0.97	1.10
72098	2010300G19Rik	1.05	0.93	0.97
72103	2010301N04Rik	1.13	0.87	0.87
72123	2010109K11Rik	1.14	0.94	1.01
72357	2210016L21Rik	1.05	1.04	1.07
74175	2300002G24Rik	1.10	0.90	0.95
74243	2210009G21Rik	1.12	0.88	0.95
75691	Anks6	1.09	0.98	1.13
76425	Gid8	1.04	1.07	1.09
76527	2010004A03Rik	1.11	1.04	1.05
98682	2210010L05Rik	1.16	0.68	0.71
67291	3110023B02Rik	1.24	0.88	0.92
108755	2610208E05Rik	1.12	1.03	1.25
108909	2610208M17Rik	1.16	0.84	1.10
214459	2610318I01Rik	1.19	0.93	1.24
54614	2610317D23Rik	1.15	1.10	1.47
66459	2610022G08Rik	1.15	0.87	1.09
66460	2610042O14Rik	1.16	0.98	1.23
67171	Dram2	1.18	0.92	1.07
68032	2610318K02Rik	1.15	0.94	1.18
69900	Mfsd11	1.14	0.85	1.12
70297	Gcc2	1.17	0.83	0.94
70333	Cd3eap	1.13	1.00	1.16
70420	2610034B18Rik	1.20	1.03	1.31
70466	Ckap2l	1.19	0.95	1.18
72137	Wdsub1	1.17	0.93	1.14
72139	2610044O15Rik	1.14	1.00	1.25
72141	Adpgk	1.12	0.86	1.13
72155	2610510J17Rik	1.13	1.04	1.24
72201	2600013N14Rik	1.16	0.99	1.23
72503	2610507B11Rik	1.13	0.78	0.98
72519	2610319K07Rik	1.12	1.01	1.12
76375	2610034H20Rik	1.12	0.81	1.07
76915	2610034E18Rik	1.19	1.02	1.17
66985	2400009B11Rik	1.17	0.90	0.98
108900	2700049P18Rik	1.14	0.99	1.17

230582	Cyb5rl	1.08	0.95	1.23
269633	2810046M22Rik	1.11	1.01	1.09
66310	2810410M20Rik	1.09	0.90	1.32
67217	2810055F11Rik	1.10	0.95	1.02
68020	2810002N01Rik	1.12	0.93	1.26
68026	2810417H13Rik	1.12	0.70	0.83
70211	2810407A14Rik	1.12	0.92	1.08
72174	2810423G08Rik	1.18	1.05	1.19
72195	Supt7l	1.07	0.89	1.11
72522	2610528J18Rik	1.11	0.66	0.69
72543	2610528K11Rik	1.10	0.67	0.77
72649	Tmem209	1.10	0.83	1.02
72669	2810032G03Rik	1.07	0.82	1.05
78833	2700085M18Rik	1.08	0.95	1.15
67745	4930583K01Rik	1.10	0.82	1.11
73167	3110043J09Rik	1.14	0.82	1.01
74383	Ubap2l	1.11	0.64	0.68
99887	4930577M16Rik	1.10	0.85	1.00
67574	4833435D08Rik	1.13	0.66	0.76
78757	4921505C17Rik	1.15	0.86	1.05
225392	Rel2	1.08	0.95	1.16
233826	4732427B05	1.11	0.99	1.14
245843	4632417D23	1.09	0.60	0.64
66701	4633402N23Rik	1.10	0.82	1.13
69823	3830421F13Rik	1.06	0.88	1.09
76863	4833420K19Rik	1.07	1.02	1.09
77043	4632433K11Rik	1.06	0.80	1.06
77056	Tmco4	1.06	0.98	1.27
67592	4930524B15Rik	1.17	0.75	0.89
75283	4930556L07Rik	1.16	0.66	0.77
109212	6720460F02Rik	1.20	1.06	1.09
71406	5430416O09Rik	1.15	0.92	1.00
108654	4933403F05Rik	1.11	0.91	1.04
244178	4933400K24Rik	1.10	0.84	0.99
381622	5031410I06Rik	1.17	0.99	1.14
66775	4933428I03Rik	1.12	1.01	1.06
71323	5133400D11Rik	1.14	0.85	0.95
75991	5033405K12Rik	1.11	0.77	0.91
244886	Al118078	1.16	0.91	1.09
64074	Smoc2	1.07	0.75	0.82
216724	Rufy1	1.08	0.54	0.56
83564	Rnh2	1.08	0.73	0.83
19328	Rab12	1.07	0.84	0.85
19362	Rad51ap1	1.09	0.61	0.62
245195	Retnlg	1.04	0.67	0.73
245688	Rbbp7	1.05	0.90	1.18
69903	Rasip1	1.08	0.63	0.70
70052	Prpf4	1.06	0.92	0.98
76938	Rbm17	1.05	0.56	0.56
24056	Sh3bp5	1.09	0.73	0.78
27387	Sh2d3c	1.07	0.86	0.89
68723	S100a18	1.08	0.75	0.77
20409	Ostf1	1.08	0.59	0.63
242737	Oog4	1.05	0.74	0.86

258225	Ofr913	1.05	0.86	1.14
258500	Ofr944	1.05	0.61	0.75
68767	Wash	1.05	0.59	0.63
257898	Ofr867	1.10	0.68	0.71

Table 5-2. PANTHER Identified receptor/receptor activity hits.

Entrez Gene ID	Gene Symbol	Gene Name	Screen Survival		
			20min	2.0hr	10.0hr
11539	Adora1	Adenosine receptor A1	1.17	0.74	0.74
12766	Cxcr3	C-X-C chemokine receptor type 3	1.08	1.01	1.30
12801	Cnr1	Cannabinoid receptor 1	1.10	0.93	1.03
12813	Col10a1	Collagen alpha-1(X) chain	1.07	0.82	0.88
13051	Cx3cr1	CX3C chemokine receptor 1	1.16	0.94	1.03
13488	Drd1a	D(1A) dopamine receptor	1.13	1.15	1.23
13490	Drd3	D(3) dopamine receptor	1.16	1.08	1.20
13491	Drd4	D(4) dopamine receptor	1.16	0.85	1.09
13609	Edg1	Sphingosine 1-phosphate receptor 1	1.17	0.99	1.30
13617	Ednra	Endothelin-1 receptor	1.13	0.65	0.70
14062	F2r	Proteinase-activated receptor 1	1.15	0.96	1.22
14065	F2rl3	Proteinase-activated receptor 4	1.14	1.04	1.28
14293	Fpr1	fMet-Leu-Phe receptor	1.30	1.23	1.39
14294	Fprl1	Formyl peptide receptor-related sequence 1	1.12	1.00	1.19
14527	Gcgr	Glucagon receptor	1.18	0.78	0.82
14602	Ghrhr	Growth hormone-releasing hormone receptor	1.09	0.94	0.98
14652	Glp1r	Glucagon-like peptide 1 receptor	1.11	0.82	0.85
14715	Gnrhr	Gonadotropin-releasing hormone receptor	1.15	0.95	1.03
14744	Gpr65	Psychosine receptor	1.12	0.84	0.90
14747	Cmklr1	Chemokine-like receptor 1	1.16	0.87	1.04
15370	Nr4a1	Nuclear receptor subfamily 4 group A member 1	1.06	0.63	0.77
15551	Htr1b	5-hydroxytryptamine receptor 1B	1.12	0.94	1.14
16639	Klra8	Killer cell lectin-like receptor 8	1.08	1.08	1.09
16995	Ltb4r1	Leukotriene B4 receptor 1	1.10	0.88	1.02
18171	Nr1i2	Nuclear receptor subfamily 1 group I member 2	1.14	0.68	0.72
18227	Nr4a2	Nuclear receptor subfamily 4 group A member 2	1.07	1.06	1.60
18441	P2ry1	P2Y purinoceptor 1	1.10	0.45	0.52
18442	P2ry2	P2Y purinoceptor 2	1.13	0.72	0.78
19214	Ptgdr	Prostaglandin D2 receptor	1.13	0.71	0.75
19220	Ptgfr	Prostaglandin F2-alpha receptor	1.06	0.48	0.59
19222	Ptgir	Prostacyclin receptor	1.01	0.80	1.15
19228	Pthr1	Parathyroid hormone/parathyroid hormone-related peptide receptor	1.03	0.99	1.39
19401	Rara	Retinoic acid receptor alpha	1.09	0.86	0.91
20288	Msr1	Macrophage scavenger receptor types I and II	1.14	0.79	0.81
20605	Sstr1	Somatostatin receptor type 1	1.03	0.76	0.87

20607	Sstr3	Somatostatin receptor type 3	1.05	1.04	1.13
20608	Sstr4	Somatostatin receptor type 4	1.06	0.68	0.96
20609	Sstr5	Somatostatin receptor type 5	1.00	0.78	1.22
21337	Tacr2	Substance-K receptor	1.01	0.86	1.03
21338	Tacr3	Neuromedin-K receptor	1.05	0.63	0.68
21833	Thra	Thyroid hormone receptor alpha	1.22	0.87	1.01
21834	Thrb	Thyroid hormone receptor beta	0.99	0.92	1.16
21907	Nr2e1	Nuclear receptor subfamily 2 group E member 1	1.06	0.44	0.50
21926	Tnf	Tumor necrosis factor	1.09	0.52	0.54
22045	Trhr	Thyrotropin-releasing hormone receptor	1.00	1.10	1.56
22337	Vdr	Vitamin D3 receptor	1.11	0.59	0.60
22354	Vipr1	Vasoactive intestinal polypeptide receptor 1	1.04	0.95	1.32
22355	Vipr2	Vasoactive intestinal polypeptide receptor 2	1.03	0.76	0.95
23957	Nr0b2	Nuclear receptor subfamily 0 group B member 2	1.06	1.01	1.41
23958	Nr2e3	Photoreceptor-specific nuclear receptor	1.10	0.49	0.58
50908	C1s	Complement C1s-A subcomponent	1.08	0.86	0.91
50928	Klrg1	Killer cell lectin-like receptor subfamily G member 1	1.09	0.85	0.86
52389	D7Ert68 0e	MCG21623, isoform CRA_b	1.16	0.96	1.29
52614	Emr4	EGF-like module-containing mucin-like hormone receptor-like 4	1.11	1.06	1.34
54160	Copg2	Granzyme A	1.00	0.99	1.36
56544	V2R2	Vomer nasal type-2 receptor 1	1.05	0.77	1.13
56696	Gpr132	Probable G-protein coupled receptor 132	1.09	0.96	1.21
57385	P2ry4	P2Y purinoceptor 4	1.02	0.78	1.12
64095	Gpr35	G-protein coupled receptor 35	1.11	0.68	0.69
67168	P2y5	Lysophosphatidic acid receptor 6	1.06	0.80	0.89
68897	Disp1	Protein dispatched homolog 1	1.10	1.06	1.07
70839	P2ry12	P2Y purinoceptor 12	1.01	0.86	1.02
71326	Trem1	Trem-like transcript 1 protein	1.00	0.70	0.83
71991	Ckn1	DNA excision repair protein ERCC-8	1.07	0.93	1.00
78560	Gpr124	G-protein coupled receptor 124	1.28	1.10	1.10
80910	Gpr84	G-protein coupled receptor 84	1.17	0.97	1.06
84111	Gpr87	G-protein coupled receptor 87	1.09	0.87	0.96
84112	Sucnr1	Succinate receptor 1	1.02	0.88	1.23
94109	Csmd1	CUB and sushi domain-containing protein 1	1.04	1.05	1.05
94226	Edg8	Sphingosine 1-phosphate receptor 5	1.18	1.19	1.53
97998	Deptor	Rod outer segment membrane protein 1	1.06	1.08	1.10
101533	1200016 C12Rik	Kallikrein 1-related peptidase b9	1.06	0.94	1.01
170757	Eltd1	EGF, latrophilin seven transmembrane domain-containing protein 1	1.23	0.81	0.87

213527	Pthr2	Parathyroid hormone 2 receptor	1.06	1.05	1.80
216749	Nmur2	Neuromedin-U receptor 2	1.10	0.84	0.85
226278	Prlhr	Prolactin-releasing peptide receptor	1.12	1.06	1.51
227288	Il8ra	C-X-C chemokine receptor type 1	1.10	0.77	0.90
229323	Gpr171	Probable G-protein coupled receptor 171	1.14	0.78	0.93
233571	P2ry6	P2Y purinoceptor 6	1.02	0.82	1.08
238252	Gpr135	Probable G-protein coupled receptor 135	1.17	0.75	0.79
239029	4933430J 11	Anthrax toxin receptor-like	1.21	0.65	0.65
239853	Gpr128	Probable G-protein coupled receptor 128	1.17	0.85	0.85
243083	Tmprss11 f	Transmembrane protease serine 11F	1.11	0.84	1.06
243084	A030012 E10	Transmembrane protease serine 11E	1.03	0.89	1.27
243277	E230012 M21	Probable G-protein coupled receptor 133	1.16	0.99	1.42
245688	Rbbp7	Histone-binding protein RBBP7	1.05	0.90	1.18
257891	Olfr479	Olfactory receptor Olfr479	1.14	0.54	0.61
257898	Olfr867	Olfactory receptor 867	1.10	0.68	0.71
258302	Olfr420	Olfactory receptor	1.14	0.79	0.80
258713	Olfr430	Olfactory receptor	1.14	0.61	0.61
258925	Olfr20	Olfactory receptor	1.07	0.76	0.81
269053	Gpr152	Probable G-protein coupled receptor 152	1.16	0.90	0.98
321019	Ebi2	G-protein coupled receptor 183	1.14	0.78	0.85
387285	Hcrtr2	Orexin receptor type 2	1.15	0.92	1.00
435845	Tmprss11 c	Neurobin	1.17	0.73	0.74
436440	Gpr31c	12-(S)-hydroxy-5,8,10,14-eicosatetraenoic acid receptor	1.14	0.79	0.83

CHAPTER 6:
DISCUSSION AND FUTURE DIRECTIONS

Research Summary

I demonstrated that *Y. pestis* survival within the macrophage is a dynamic process and several host proteins are directly involved in YCV biogenesis. My data, summarized in Fig. 6-1, demonstrates that within 20 mins post-infection *Y. pestis* prevents lysosome fusion through recruitment of Rab1b and Rab4a to arrest YCV acidification. By 80 mins post-infection the maturing YCV associates with Rab1b, Rab4a and Rab11b. In addition to recruitment of Rab proteins involved in endocytic recycling to the YCV, *Y. pestis* infection also stalls the host recycling process, and this is necessary for late stage bacterial replication. My data suggests that stalling of the recycling process can be directly attributed to sequestering Rab11b on the YCV, as overexpression of Rab11b restores recycling and prevents bacterial replication. These data provide a significant improvement in our understanding of the early colonization of the macrophage and trafficking events leading the maturation of the YCV into a replicative niche.

Implications of My Research and Future Directions

Developing new pathway analysis techniques for RNAi screens through mapping interactions

Our identification and enrichment for host cell trafficking processes and ultimately the impact of the endocytic recycling pathway on *Y. pestis* survival was due in part to our novel approach to genomic screening data. To the best of my knowledge, to date all RNAi genomic screens have focused their post-screen efforts using pathway and ontology analysis software to understand their validated data [130-142], and not to explore their datasets in a biological context during validation. As such, we initially used MetaCore pathway analysis software to determine enrichment within our validated gene hits. However, due to the limited number of input genes (135), we were unable to identify specific pathways with any degree of confidence. In many instances, the significantly enriched networks only contained a single gene that skewed the p-value due to the weight of the gene within the identified network. Whereas another networks would contain multiple genes, but the combined p-value was not sufficient to warrant significance by the pathway analysis software. Part of this is the nature of RNAi genomic screens versus microarray analysis, which

pathway analysis programs were developed for. RNAi does not have 100% penetrance, meaning the targeted gene is usually only inhibited to an undefined degree. In contrast, a microarray has 100% penetrance, meaning the impact upon the phenotype of interest can be completely dictated by the experimental design (e.g., gene deletion or growth condition). As such, enrichment for a pathway based on gene p-value is difficult to interpret in the context of an RNAi screen. Furthermore, statistical weight is assigned to each cellular component based on their interconnectedness with other cellular proteins. As a result, transcriptional and global pathway regulators have larger statistical weight when included in the user's dataset. As such, a dataset could be significantly skewed by the number of transcriptional or global regulators within the dataset, resulting in analysis missing important pathways. Therefore, we shifted our bioinformatic analysis to Gene Ontology (GO) clustering to generate and build maps of interacting gene partners based on our validated and primary screen hits. These initial interaction maps then served to guide our subsequent experiments.

Curated pathways are also limited to the quality and known knowledge of the genes within the pathways. This limitation ultimately skews screen analysis toward what is known or predicted. Thus, we chose to build maps of interacting partners within our validated and primary screen hits to avoid any bias inherent to current analysis software. This allowed our networks to self-enrich through inclusion of additional nodes that strengthened the interactions between input datasets. Moving forward, one could use this process to further understand the relationship between various subsets identified in our validated dataset. Also one could use this process to understand bacterial invasion through mapping invasion hits to our survival hits. Furthermore, we can begin development of an application using these simple rules to allow fellow pathway explorers to build maps of their datasets.

Are Rab1b and Rab4a only required to avoid YCV acidification?

Y. pestis recruits Rab1b and Rab4a within 20 mins post-infection of the macrophage to prevent YCV acidification (chapters 3 and 4;[61]). These findings show *Y. pestis* survival within the macrophage hinges on early subversion of phagolysosome maturation. However, it is unclear if Rab1b and Rab4a are required only to prevent YCV acidification or if they are also essential for *Y.*

pestis YCV biogenesis/survival post-phagolysosome subversion. To address this, one could use chemical inhibitors, such as ammonium chloride, to block vacuole acidification in Rab1b and Rab4a siRNA treated macrophages and then monitor survival of *Y. pestis*. If either of these Rabs are required to manipulate the macrophages in subsequent steps after preventing YCV acidification, *Y. pestis* bacterial survival will still be inhibited in RNAi treated cells. In contrast, if these Rabs are strictly recruited to block acidification, ammonium chloride treatment should restore bacterial survival in RNAi treated cells. In the event treatment does not restore virulence, further characterization of the YCV biogenesis process in these cells will need to be performed.

Does the Timing of Rab Recruitment Impact YCV Maturation?

Rab GTPase trafficking occurs in coordinated and sequential fashion to efficiently move the vesicle to its intended destination along an endocytic pathway within the cell (see reviews [102, 185, 289, 290]). For example, Rabs 5, 7 and 9 are recruited in a specific sequence to achieve phagosome fusion with the lysosome [94, 95, 98-101]. Disrupting the recruitment of one protein results in failure to recruit subsequent Rabs, terminating phagolysosome maturation [94, 95, 98-101]. We have shown *Y. pestis* quickly subverts/arrests phagolysosome maturation and prevents YCV acidification within 20 mins of entry into the macrophage by recruiting Rab1b and Rab4a (chapter 3 and 4; [61]). However, we have not determined if recruitment of either of these proteins is required for subsequent recruitment of Rab11b. Using RNAi to inhibit Rab1b and Rab4a, one could determine if Rab11b is still recruited to the YCV in the absence of these other Rab proteins. These experiments can be further extended to identify if loss of any of the other validated Rab proteins impact recruitment. Moreover, future studies using CRISPR/CAS systems to integrate multiple fluorescently tagged Rabs1b, 4a & 11b and live cell imaging could provide a powerful tool to monitor Rab GTPase timing and bacterial trafficking in real-time. Importantly, live cell imaging could also incorporate tagged markers for cellular processes such as autophagy, receptors, and/or the phagolysosome to allow for real-time analysis of: 1) *Y. pestis* trafficking Rab interactions that lead to autophagy, recycling endosome maturation and phagolysosome avoidance, 2) *Y. pestis* time and spatial dependent recruitment of Rabs and host markers to support autophagy, recycling endosome maturation and phagolysosome avoidance 3) *Y. pestis* time dependent modeling of

trafficking and replication requirements during YCV maturation, and 4) identification and data to develop computational systems to demonstrate/animate Rab GTPase mediated trafficking events *in silico*. Understanding the timing of Rab GTPase recruitment events may also reveal if one Rab protein is targeted by *Y. pestis* to influence the recruitment of others, resulting in prioritizing potential Rab proteins for subsequent studies to understand how *Y. pestis* recruits these proteins to the YCV.

How does *Y. pestis* recruit Rab GTPases to the YCV?

Efforts to identify *Y. pestis* proteins responsible for intracellular survival by targeting the bacterium itself using mutagenic screens have had limited success, and have only identified the PhoP/Q regulon as required [86, 291-293]. We have identified nine Rab GTPases that appear to be required for *Y. pestis* survival (Rabs 1b, 2b, 3d, 4a, 19, 20, 23, 30, & 40b). Based on their cellular location and similarity of GTP binding domains, these Rabs can be classified into five subfamilies: Subclass 1: Rab23; Subclass 9: Rab20; Subclass 11: Rab2b, Rab4a; Subclass 12: Rab19, Rab30; or Subclass 13: Rab1b, Rab3d, Rab40b [294-297]. Our enrichment for Rab GTPases involved with host endocytic recycling suggests *Y. pestis* makes a bacterial effector that recognizes a specific motif within these Rab GTPases [294-297]. Using Rab1b, Rab4a and Rab11b as “bait”, immunoprecipitation could be performed to pull down *Y. pestis* proteins that potential interact with these Rabs. The bacterial proteins would then be identified by MS/MS. Mutations in these genes could then be made and tested for Rab recruitment, intracellular survival, and virulence in the mouse model. It should be noted that *Y. pestis* may indirectly recruit Rab proteins through interactions with host Rab effectors. In this scenario, *Y. pestis* proteins may not precipitate via Rab pull down. In the event that no proteins are identified via pull downs, transposon mutagenesis could be used to identify *Y. pestis* mutants that do not recruit Rabs to the early YCV (using high content screening). Host targets of these *Y. pestis* proteins could then be identified by immunoprecipitation of eukaryotic lysates.

How do *Y. pestis* interactions with the host cell recycling pathway contribute to intracellular survival?

Cross talk between endocytic recycling and autophagy is a potential cellular mechanism for sensing disruptions within trafficking pathways or inadequate homeostatic signals from receptors involved in maintaining cellular metabolism [298]. Furthermore, recent studies have indicated that Rab11b may be an important mediator of this cross talk [254]. *Y. pestis* has been shown to associate with autophagosomes; however, the contribution of autophagy to *Y. pestis* replication is yet to be determined [59, 88, 89]. During the first 8 h of infection, *Y. pestis* induces autophagy within infected cells, as indicated by the conversion of LC3-I to LC3-II [59, 299]. Pujol et al. showed that *Y. pestis* avoids clearance by xenophagy, resides in autophagosomes, but does not require autophagy to survive in macrophages up to 8 h post infection [59]. Studies with *Y. pseudotuberculosis*, the closest relative to *Y. pestis*, have shown autophagy is required for bacterial replication [88, 89]. Additionally, Moreau et al. have shown that induction of autophagy with rapamycin increased metabolic activity of *Y. pseudotuberculosis* within the YCV, and abolishing autophagy induction using Atg4b C74A (enzymatically inactive Atg4b) prevented the recruitment of LC3 to the YCV [88]. Therefore, it is reasonable to hypothesize that by stalling the host recycling pathway, *Y. pestis* may disrupt metabolic signals resulting in the host cell, becoming quiescent and inducing autophagic flux in the cell. This hypothesis could explain how *Y. pestis* induces autophagy. To test if autophagy is specifically required for bacterial replication independent of host cell recycling, one could treat *Y. pestis* infected Rab11b overexpressing macrophages with rapamycin to chemically induce autophagy independent of recycling inhibition. If autophagy is required for *Y. pestis* replication, induction of autophagy using rapamycin in *Y. pestis* infected Rab11b overexpressing cells would restore bacterial replication to wildtype levels. However, it is possible that autophagy is not required for *Y. pestis* replication/survival. In this case induction of autophagy will not restore bacterial replication in Rab11b overexpressing cells. Furthermore, these results would suggest bacterial replication is dependent on an unknown recycling endosome maturation event, and induction of autophagy within infected cells is a byproduct of the infection.

Extending our Rab11b studies suggests a universal mechanism for intracellular pathogens

In addition to *Y. pestis*, a variety of other pathogens appear to target Rab11 (a/b) [107, 130, 131, 140-142, 191, 194, 215-217, 240, 246, 248, 300-312]. Anthrax toxins were shown to disrupt recycling in *Drosophila* wing discs, and overexpression of Rab11 restored wildtype morphology [248, 313]. This theme has been observed for Tetanus and Shiga toxin B through their disruption and association with markers for recycling endosomes [240, 309, 310]. While these toxins are secreted from their respected pathogens, neither *Bacillus anthracis*, *Shigella flexneri* or *Clostridium tetani* appear to reside in a pathogen containing vacuole (PCV) [103, 314]. However, the targeting of Rab11 by intracellular pathogens indicates a potentially universal mechanism supporting survival (summary in Table 6-1). Future studies determining if these pathogens target Rab11 to disrupt host cellular recycling processes to promote survival need to be conducted. Perhaps diverting/stalling Rab11 naturally driven processes through the dilution/sequestration/inactivation of Rab GTPase protein available to the cell would allow these organisms to establish their replicative niches, by modulating downstream innate cellular defenses, such as autophagy [254, 315].

Does stalling of host recycling potentially impact pro-inflammatory responses?

Y. pestis infection produces very little pro-inflammatory response early during infection, but at latter stages there is a dramatic spike in inflammation [1, 316-322]. This phenomena is also observed in transcriptome analysis of monocytes/ macrophages infected with *Y. pestis* lacking the pCD1 virulence plasmid and T3SS secreted Yops [321], which are potent modulators of the inflammasome and pro-inflammatory apoptosis [323-325]. Rab11 trafficking has also been shown to impact many host proteins involved in innate immunity. For example, efficient signaling and recycling of TLR4 requires Rab11a and CD14 [71, 326, 327]. Moreover, it is known that Rab11 is required for both loading/storing MHC I within recycling endosomes, but also for recruitment of MHC I to endosomes engaged in active TLR4 signaling [328, 329]. Finally, Weigert et al. found dominant negative forms of Rab11 and Rab22a prevented MHC I recycling [330]. One can view these findings as two separate but integral events for TLR4 and MHC I signaling as mediated by Rab11 trafficking processes: 1) pre-priming recycling endocytic compartments with MHC I and recycling/trafficking MHC I to the plasma membrane, and 2) TLR4 engaged signaling promoting

recruitment of MHC I via Rab11 to initiate an innate immune response (perhaps autophagy/xenophagy). Due to the requirement for Rab11 in TLR4 and MHC I cellular processes, one can speculate that *Y. pestis* sequestration of Rab11b may also be disrupting TLR4 and MHC I signaling cascades. This disruption could potentially contribute to the anti-inflammatory nature of *Y. pestis* infection.

To determine if TLR4 signaling is disrupted, one could adapt our TfR recycling assay to monitor TLR4 recycling and TLR4 retention in macrophages infected with *Y. pestis* and compare to infection with *E. coli* K12 or *S. Typhimurium*. Given our previous findings that TfR is retained due to disruption of host recycling, we expect to see retention of TLR4 in *Y. pestis* infected cells and inefficient recycling of TLR4. These results would suggest that *Y. pestis* infected macrophages may be further inhibited in their ability to respond to LPS through TLR4 signaling. To determine if MHC I presentation is disrupted, one could pulse *Y. pestis* infected macrophages with Ova SIINFEKL peptide. Using flow cytometry, one can compare MHC I expression of *Y. pestis* infected cells to uninfected cells. If *Y. pestis* disrupts MHC I presentation, one would expect to see diminished surface expression of MHC I specifically in *Y. pestis* infected cells. Furthermore, classical T-cell activation assays could be used to determine if MHC antigen presentation is disrupted by *Y. pestis* infection.

An extension of these studies would be to adoptively transfer *Y. pestis* infected wildtype and Rab11b overexpressing macrophages into mice. Herein, one could determine if stalling cellular host recycling by *Y. pestis* contributes to: 1) dampening the early pro-inflammatory response of infected hosts via cytokine response, 2) dissemination of *Y. pestis*, or 3) overall animal survival. The results of these studies will provide biological significance for stalling host cell recycling in *Y. pestis* infected macrophages within the context of *in vivo* pathogenesis of plague. Moreover, these adoptive macrophage studies could have novel insight into the overall contribution of *Y. pestis* intracellular survival within the macrophage in terms of disease progression. Overall, these studies would be the first to determine if *Y. pestis* disruption of host endocytic recycling leads to the dampening of pro-inflammatory response of an infected host.

Does *Y. pestis* use eukaryotic receptors to target the recycling pathway?

The first step of any pathogen to colonize a host cell is adherence and invasion. We identified 96 potential receptors that exhibit a *Y. pestis* invasion phenotype from our RNAi genome-wide screen. Of the 96 identified receptors exhibiting a *Y. pestis* invasion phenotype, we hit Edg1 (Sphingosine 1-phosphate receptor 1). This receptor has been shown to inhibit bacterial dissemination from the draining lymph node *in vivo* [49]. Furthermore, St. John et al. demonstrated that chemical ablation of Edg1 reduced *Y. pestis* burden in CD11b (macrophage) and CD11c (dendritic) cell types in the popliteal and iliac lymph nodes [49]. Due to these previous findings, Edg1 should be prioritized for further characterization using experiments detailed in chapter 5.

Interestingly, recycling endosomes are hallmarked by very little acidification, and remain at ~ pH 6.4 to prevent degradation of vacuole contents in order to recycle these reusable cellular components [244, 331]. Therefore, the ability of *Y. pestis* to inhibit YCV acidification could be directly linked to the receptor it uses for invasion, if this receptor targets the endosome to the recycling pathway. Several chemokine and scavenger receptors were identified as potential *Y. pestis* receptors. These receptors have been shown to associate with recycling endosomes, and potentially have common motifs or interacting partners [332, 333]. Using our validated screen hits as a focal point, one could map network interactions to the 96 receptors to determine if a common pathway emerges. In support of this, we identified Arfgap2, an interacting partner of Arf1, within our invasion dataset [288]. Arf1 interacts with Rab4a to facilitate recycling endosome trafficking from the early endosome [238, 244, 334]. These findings indicate that *Y. pestis* entry and/or early survival may directly link to the pathogen's ability to traffic into the host recycling pathway.

It is possible that *Y. pestis* uses multiple receptors for invasion, or binds to a cluster of receptors associated within a lipid raft. In this case, there may be several receptors that inhibit *Y. pestis* invasion, but the efficiency of each individual receptor to inhibit invasion would matter. As such, one could use chemical inhibitors to further determine the general mechanism for internalization of *Y. pestis*. Overall, identifying a receptor that prevents uptake of *Y. pestis* is advantageous. Once identified, one could define the bacterial proteins that facilitate this through

screening a transposon library or using bacterial outer membrane preparations in pull-down assays with tagged versions of the receptors. Through the identification of these bacterial proteins one could generate deletion mutations of *Y. pestis* and assess the contribution invasion has on pathogenesis. Importantly, these bacterial proteins could serve as potential targets to develop new therapeutics or vaccines to inhibit macrophage invasion.

Is spatial location within the cell important for intracellular survival?

Using live cell microscopy, we have observed dynamic YCV movement occurring during the first 8 hours of infection (unpublished data). We have also observed that *Y. pestis* tends to replicate only in YCVs that traffic to the perinuclear region (unpublished data). In contrast, bacteria that remain spatially halfway between the plasma membrane and perinuclear region appear to be degraded, presumably within phagolysosomes. Recently, Johnson et al. have shown that heterogeneity exists in lysosomes within the cell [335]. Their results demonstrate the further from the plasma membrane the more efficient the acidification process is through accumulation (increased density) of vATPase and Rab7 [335]. Intriguingly, this data suggests that spatial and temporal areas of the cell are more capable of mounting innate immune responses than others. Looking at cellular location and similarity of GTP binding domains of the nine validated Rabs (Rabs 1b, 2b, 3d, 4a, 19, 20, 23, 30, & 40b) we noticed enrichment for the Golgi/ ERGIC perinuclear space, indicating that recruitment of these Rabs to the YCV may result in trafficking towards the Golgi/ ERGIC space. These observations suggest that *Y. pestis* survival and avoidance of the phagolysosome may be directly linked to trafficking of the bacteria to the perinuclear region. Using markers for lysosomes (vATPase, Rab7, Rab9 & Cathepsin D) and image analysis software, one could determine the spatial requirements for *Y. pestis* survival/replication. Moreover, using RNAi techniques and markers for the Golgi/ERGIC space, one could determine trafficking events and spatial location requirements for *Y. pestis* replication. If temporal and spatial location are essential for *Y. pestis* replication/survival, we would expect to see differences in recruitment of Rab GTPases and phagolysosome markers to perinuclear YCVs in contrast to their counterparts closer to the plasma membrane.

Potential Biological Impact of *Y. pestis* Low Calcium Response in Macrophages

Y. pestis has a growth phenomenon termed the “Low Calcium Response” (LCR) discovered in the late 1940-50s [1, 75, 82, 336, 337]. The LCR is characterized as a biological requirement for Ca^{2+} for growth at 37°C in broth media, and no supplementation for growth at 26°C (see review [1]). Furthermore, consecutive passages at 37°C in the absence of Ca^{2+} results in loss of the pCD1 plasmid, which encodes the T3SS, and attenuation in mice [336, 337]. To date, there is little known about the biological relevance for the LCR [1, 338-341]. Szatmari and colleagues recently demonstrated that Rab11b interacts with Hook, a negative regulator of endosome maturation, to facilitate crosstalk between recycling endosomes and induction of autophagy [254]. Furthermore, autophagy triggers an influx of calcium into the nascent autophagic vesicle, and Rab11b is required for the effective fusion and docking during this transition [342, 343]. These observations suggests that *Y. pestis* induction of autophagy may result in the induction of Ca^{2+} influx into the YCV and subsequently trigger bacterial replication. To determine if calcium influx occurs in the YCV, cells could be infected with fluorescent *Y. pestis* strain and pulsed with a calcium fluoro dye to monitor the changes in YCV Ca^{2+} concentration over time. Simultaneously one could determine when the LCR is induced during a macrophage infection by monitoring the expression levels of *lcrF* (a gene whose expression changes during the LCR) during macrophage infection using a bioluminescent transcriptional reporter. If *lcrF* expression is dependent on Ca^{2+} influx, then we would expect induction of *lcrF* expression to occur after influx of calcium into the YCV. In the event that Ca^{2+} influx and *lcrF* expression changes are observed, one could then determine if Rab11b recruitment prevents the induction of LCR. In either case, these experiments would clearly demonstrate a biological role for LCR of *Y. pestis* in bacterial replication during bacterial survival within the macrophage. In addition to growth at 37°C, *Y. pestis* secretion of the T3SS Yops effector proteins is also regulated by calcium and the *lcrF* (see review [344]). If indeed LCR responses are triggered with Ca^{2+} influx into the YCV, one could also determine if *Y. pestis* T3SS expression is also triggered by Ca^{2+} influx. If expression is induced during intracellular infection, studies to determine if secretion of the Yop effectors occurs in response to Ca^{2+} influx could be performed.

These studies would provide a novel insight into how *Y. pestis* regulates mammalian specific virulence factors, and senses the transition into the mammalian host. This would also suggest that *Y. pestis* modulation of mammalian expressed virulence factors is not solely dependent on temperature shift. Findings may explain why *in vitro* growth of *Y. pestis* require calcium. This also suggests that spontaneous loss of pCD1 in naturally occurring environmental isolates is a response of *Y. pestis* adapting to an environment with little potential for transmission to a mammalian host. Furthermore, to our knowledge there is not a calcium driven immune response to *Y. pestis* within the flea midgut. Potentially, the influence of a sustained calcium event and a 37°C temperature shift is the necessary trigger for *Y. pestis* to sense intracellular survival in a mammal vs extracellular survival within the flea.

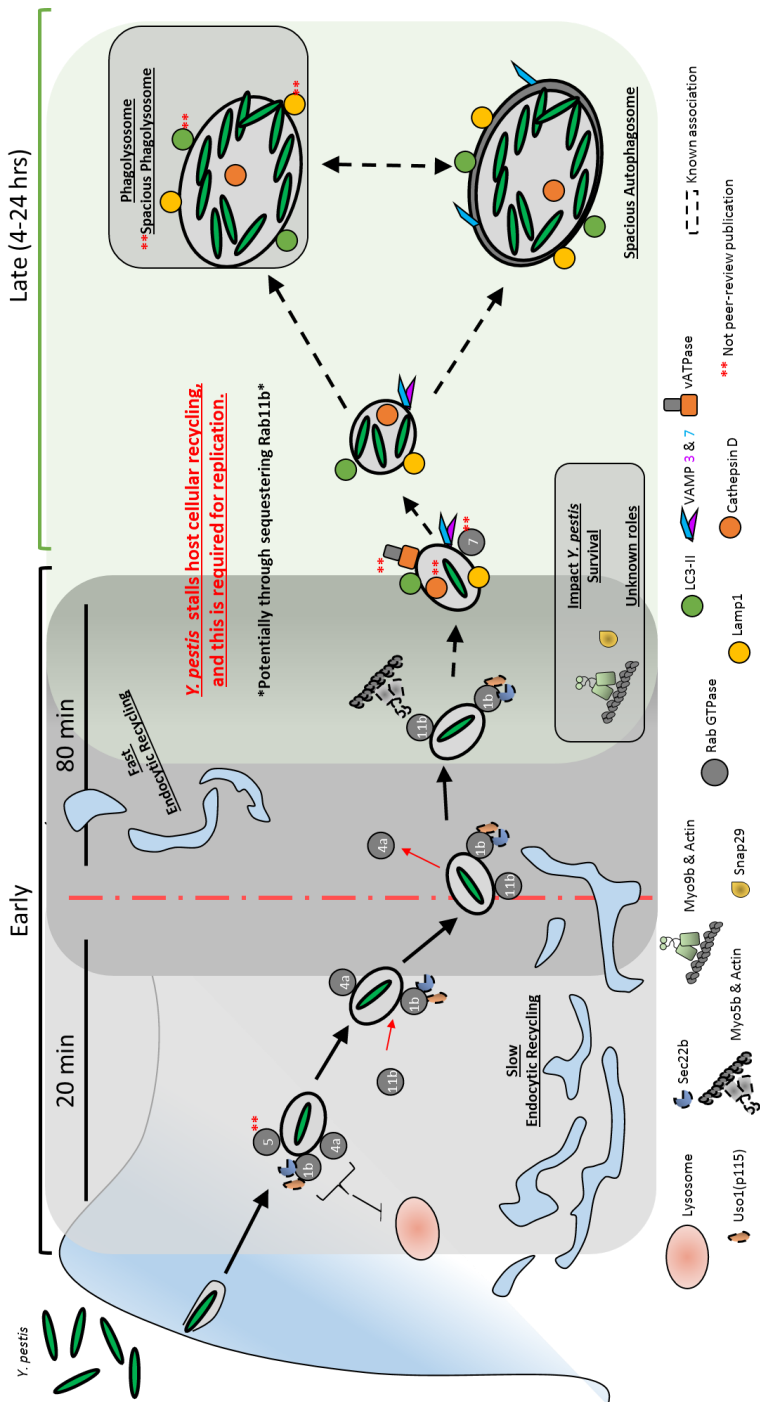


Figure 6-1. Summary model of our findings

Tables

Table 6-1. Rab11 (a/b) pathogen & toxin association.

Rab11 (a/b) Pathogen & Toxin Association		
Pathogen	Rab11 (a/b) loss impact on replication/survival?	Ref.
<i>C. burnetii</i>	Small vacuoles	[131, 215, 217, 300-302]
<i>L. pneumophila</i>	?; is on the LCV	[304]
<i>L. monocytogenes</i>	Inhibits	[130, 141]
<i>S. aureus</i>	?; has dynamic co-localization	[108]
<i>S. flexneri</i>	Inhibits vacuole rupture	[305, 306]
<i>S. typhimurium</i>	Partially inhibits; required for efficient maturation	[307]
<i>Mycobacterium sp</i>	Inhibits?; cell type specificity?	[142, 311]
<i>Anaplasma sp</i>	Inhibits	[191, 216]
<i>Chlamydia sp</i>	Inhibits	[140, 194, 246]
Andes virus	Inhibits	[312]
Hantavirus (new world)	Inhibits	[312]
Respiratory syncytial virus	?	[303]
Toxin	Rab11 (a/b) overexpression rescue phenotype?	Ref.
Anthrax (EF & LF)	Yes, for EF toxin only	[248]
Cholera	Yes	[308]
Tetanus	Yes	[240, 309]
Shiga B	Yes	[310]

REFERENCES

1. Perry, R.D. and J.D. Fetherston, *Yersinia pestis*--etiologic agent of plague. Clin Microbiol Rev, 1997. **10**(1): p. 35-66.
2. Langer, W.L., *THE BLACK DEATH*. Sci Am, 1964. **210**: p. 114-21.
3. Konkola, K., *More than a coincidence? The arrival of arsenic and the disappearance of plague in early modern Europe*. J Hist Med Allied Sci, 1992. **47**(2): p. 186-209.
4. CDC - Maps & Statistics - Plague. [Website] 23 Apr. 2013 [cited 2013 04 May]; Available from: <<http://www.cdc.gov/plague/maps/>>.
5. Butler, T., *Plague gives surprises in the first decade of the 21st century in the United States and worldwide*. Am J Trop Med Hyg, 2013. **89**(4): p. 788-93.
6. Natalie Kwit, D.C.N., MD; Kiersten Kugeler, PhD; Jeannine Petersen, PhD; Lydia Plante, MSPH; Hayley Yaglom, MPH; Vicki Kramer, PhD; Benjamin Schwartz, MD; Jennifer House, DVM; Leah Colton, PhD; Amanda Feldpausch, MPH; Cherie Drenzek, DVM; Joan Baumbach, MD; Mark DiMenna, PhD; Emily Fisher, MD; Emilio Debess, DVM; Danielle Buttke, DVM; Matthew Weinburke, MPH; Christopher Percy, MD; Martin Schriefer, PhD; Ken Gage, PhD; Paul Mead, MD, *Human Plague — United States, 2015*, in *MMWR Morbidity and Mortality Weekly Report*. 2015: Centers for Disease Control and Prevention.
7. CDC, *Possession, Use, and Transfer of Select Agents and Toxins; Biennial Review; Final Rule*. 2012: Federal Register. p. 61083-61115.
8. Hull, H.F., J.M. Montes, and J.M. Mann, *Septicemic plague in New Mexico*. J Infect Dis, 1987. **155**(1): p. 113-8.
9. Doll, J.M., et al., *Cat-transmitted fatal pneumonic plague in a person who traveled from Colorado to Arizona*. Am J Trop Med Hyg, 1994. **51**(1): p. 109-14.
10. von Reyn, C.F., et al., *Epidemiologic and clinical features of an outbreak of bubonic plague in New Mexico*. J Infect Dis, 1977. **136**(4): p. 489-94.
11. Crook, L.D. and B. Tempest, *Plague. A clinical review of 27 cases*. Arch Intern Med, 1992. **152**(6): p. 1253-6.
12. Conrad, F.G., F.R. LeCocq, and R. Krain, *A recent epidemic of plague in Vietnam*. Arch Intern Med, 1968. **122**(3): p. 193-8.
13. Butler, T., *The black death past and present. 1. Plague in the 1980s*. Trans R Soc Trop Med Hyg, 1989. **83**(4): p. 458-60.
14. Inglesby, T.V., et al., *Plague as a biological weapon: medical and public health management. Working Group on Civilian Biodefense*. Jama, 2000. **283**(17): p. 2281-90.
15. Abbott, R.C., and Rocke, T.E. , *Plague: U.S. Geological Survey Circular 1372*. 2012: p. 79 p.
16. Achtman, M., et al., *Microevolution and history of the plague bacillus, Yersinia pestis*. Proc Natl Acad Sci U S A, 2004. **101**(51): p. 17837-42.
17. Chain, P.S., et al., *Insights into the evolution of Yersinia pestis through whole-genome comparison with Yersinia pseudotuberculosis*. Proc Natl Acad Sci U S A, 2004. **101**(38): p. 13826-31.
18. Parkhill, J., et al., *Genome sequence of Yersinia pestis, the causative agent of plague*. Nature, 2001. **413**(6855): p. 523-7.
19. Williamson, E.D. and P.C. Oyston, *The natural history and incidence of Yersinia pestis and prospects for vaccination*. J Med Microbiol, 2012. **61**(Pt 7): p. 911-8.

20. Butler, T., *Plague history: Yersin's discovery of the causative bacterium in 1894 enabled, in the subsequent century, scientific progress in understanding the disease and the development of treatments and vaccines*. Clin Microbiol Infect, 2014. **20**(3): p. 202-9.
21. Bos, K.I., et al., *A draft genome of Yersinia pestis from victims of the Black Death*. Nature, 2011. **478**(7370): p. 506-10.
22. Seifert, L., et al., *Genotyping Yersinia pestis in Historical Plague: Evidence for Long-Term Persistence of Y. pestis in Europe from the 14th to the 17th Century*. PLoS One, 2016. **11**(1): p. e0145194.
23. Harbeck, M., et al., *Yersinia pestis DNA from Skeletal Remains from the 6(th) Century AD Reveals Insights into Justinianic Plague*. PLoS Pathog, 2013. **9**(5): p. e1003349.
24. Muhlenkamp, M., et al., *Yersinia adhesin A (YadA)--beauty & beast*. Int J Med Microbiol, 2015. **305**(2): p. 252-8.
25. Bialas, N., et al., *Bacterial cell surface structures in Yersinia enterocolitica*. Arch Immunol Ther Exp (Warsz), 2012. **60**(3): p. 199-209.
26. Mikula, K.M., R. Kolodziejczyk, and A. Goldman, *Yersinia infection tools-characterization of structure and function of adhesins*. Front Cell Infect Microbiol, 2012. **2**: p. 169.
27. Cowan, C., et al., *Invasion of epithelial cells by Yersinia pestis: evidence for a Y. pestis-specific invasin*. Infect Immun, 2000. **68**(8): p. 4523-30.
28. Gillenius, E. and C.F. Urban, *The adhesive protein invasin of Yersinia pseudotuberculosis induces neutrophil extracellular traps via beta1 integrins*. Microbes Infect, 2015.
29. Grassl, G.A., et al., *Interaction of Yersinia enterocolitica with epithelial cells: invasin beyond invasion*. Int J Med Microbiol, 2003. **293**(1): p. 41-54.
30. Suomalainen, M., et al., *Using every trick in the book: the Pla surface protease of Yersinia pestis*. Adv Exp Med Biol, 2007. **603**: p. 268-78.
31. Zhang, S.S., et al., *Plasminogen activator Pla of Yersinia pestis utilizes murine DEC-205 (CD205) as a receptor to promote dissemination*. J Biol Chem, 2008. **283**(46): p. 31511-21.
32. Trosky, J.E., A.D. Liverman, and K. Orth, *Yersinia outer proteins: Yops*. Cell Microbiol, 2008. **10**(3): p. 557-65.
33. Viboud, G.I. and J.B. Bliska, *Yersinia outer proteins: role in modulation of host cell signaling responses and pathogenesis*. Annu Rev Microbiol, 2005. **59**: p. 69-89.
34. Caulfield, A.J. and W.W. Lathem, *Substrates of the plasminogen activator protease of Yersinia pestis*. Adv Exp Med Biol, 2012. **954**: p. 253-60.
35. Hinnebusch, B.J., E.R. Fischer, and T.G. Schwan, *Evaluation of the role of the Yersinia pestis plasminogen activator and other plasmid-encoded factors in temperature-dependent blockage of the flea*. J Infect Dis, 1998. **178**(5): p. 1406-15.
36. Easterbrook, T.J., et al., *Studies on the immunogenicity of the Pla protein from Yersinia pestis*. Contrib Microbiol Immunol, 1995. **13**: p. 214-5.
37. Hu, P., et al., *Structural organization of virulence-associated plasmids of Yersinia pestis*. J Bacteriol, 1998. **180**(19): p. 5192-202.
38. Lindler, L.E., et al., *Complete DNA sequence and detailed analysis of the Yersinia pestis KIM5 plasmid encoding murine toxin and capsular antigen*. Infect Immun, 1998. **66**(12): p. 5731-42.
39. Drozdov, I.G., et al., *Virulent non-capsulate Yersinia pestis variants constructed by insertion mutagenesis*. J Med Microbiol, 1995. **42**(4): p. 264-8.
40. Chouikha, I. and B.J. Hinnebusch, *Yersinia-flea interactions and the evolution of the arthropod-borne transmission route of plague*. Curr Opin Microbiol, 2012.

41. Chouikha, I. and B.J. Hinnebusch, *Yersinia--flea interactions and the evolution of the arthropod-borne transmission route of plague*. *Curr Opin Microbiol*, 2012. **15**(3): p. 239-46.
42. Hinnebusch, B.J., *The evolution of flea-borne transmission in Yersinia pestis*. *Curr Issues Mol Biol*, 2005. **7**(2): p. 197-212.
43. Williamson, E.D. and P.C. Oyston, *Protecting against plague: towards a next-generation vaccine*. *Clin Exp Immunol*, 2013. **172**(1): p. 1-8.
44. Sun, W. and R. Curtiss, *Rational considerations about development of live attenuated Yersinia pestis vaccines*. *Curr Pharm Biotechnol*, 2013. **14**(10): p. 878-86.
45. Kartman, L., M.I. Goldenberg, and W.T. Hubbert, *Recent observations on the epidemiology of plague in the United States*. *Am J Public Health Nations Health*, 1966. **56**(9): p. 1554-69.
46. Hinnebusch, B.J., *Bubonic plague: a molecular genetic case history of the emergence of an infectious disease*. *J Mol Med (Berl)*, 1997. **75**(9): p. 645-52.
47. Hinnebusch, B.J. and D.L. Erickson, *Yersinia pestis biofilm in the flea vector and its role in the transmission of plague*. *Curr Top Microbiol Immunol*, 2008. **322**: p. 229-48.
48. Hinnebusch, B.J., R.D. Perry, and T.G. Schwan, *Role of the Yersinia pestis hemin storage (hms) locus in the transmission of plague by fleas*. *Science*, 1996. **273**(5273): p. 367-70.
49. St John, A.L., et al., *S1P-Dependent Trafficking of Intracellular Yersinia pestis through Lymph Nodes Establishes Buboes and Systemic Infection*. *Immunity*, 2014. **41**(3): p. 440-50.
50. Hinnebusch, B.J., et al., *Role of the Yersinia pestis Ail protein in preventing a protective polymorphonuclear leukocyte response during bubonic plague*. *Infect Immun*, 2011. **79**(12): p. 4984-9.
51. Spinner, J.L., et al., *Yersinia pestis survival and replication within human neutrophil phagosomes and uptake of infected neutrophils by macrophages*. *J Leukoc Biol*, 2013.
52. Ye, Z., et al., *Gr1+ cells control growth of YopM-negative yersinia pestis during systemic plague*. *Infect Immun*, 2009. **77**(9): p. 3791-806.
53. Janssen, W.A. and M.J. Surgalla, *Plague bacillus: survival within host phagocytes*. *Science*, 1969. **163**(3870): p. 950-2.
54. Straley, S.C. and P.A. Harmon, *Growth in mouse peritoneal macrophages of Yersinia pestis lacking established virulence determinants*. *Infect Immun*, 1984. **45**(3): p. 649-54.
55. Straley, S.C. and P.A. Harmon, *Yersinia pestis grows within phagolysosomes in mouse peritoneal macrophages*. *Infect Immun*, 1984. **45**(3): p. 655-9.
56. Oyston, P.C., et al., *The response regulator PhoP is important for survival under conditions of macrophage-induced stress and virulence in Yersinia pestis*. *Infect Immun*, 2000. **68**(6): p. 3419-25.
57. Pujol, C. and J.B. Bliska, *The ability to replicate in macrophages is conserved between Yersinia pestis and Yersinia pseudotuberculosis*. *Infect Immun*, 2003. **71**(10): p. 5892-9.
58. Lukaszewski, R.A., et al., *Pathogenesis of Yersinia pestis infection in BALB/c mice: effects on host macrophages and neutrophils*. *Infect Immun*, 2005. **73**(11): p. 7142-50.
59. Pujol, C., et al., *Yersinia pestis can reside in autophagosomes and avoid xenophagy in murine macrophages by preventing vacuole acidification*. *Infect Immun*, 2009. **77**(6): p. 2251-61.
60. Bliska, J., *Survival and Trafficking of Yersinia pestis in Non-acidified Phagosomes in Murine Macrophages*, in *The Challenge of Highly Pathogenic Microorganisms*, A. Shafferman, A. Ordentlich, and B. Velan, Editors. 2010, Springer Netherlands. p. 31-44.

61. Connor, M.G., et al., *Yersinia pestis* Requires Host *Rab1b* for Survival in Macrophages. PLoS Pathog, 2015. **11**(10): p. e1005241.
62. Ponnusamy, D. and K.D. Clinkenbeard, *Yersinia pestis* intracellular parasitism of macrophages from hosts exhibiting high and low severity of plague. PLoS One, 2012. **7**(7): p. 27.
63. Pujol, C. and J.B. Bliska, *Turning Yersinia pathogenesis outside in: subversion of macrophage function by intracellular yersiniae*. Clin Immunol, 2005. **114**(3): p. 216-26.
64. Marketon, M.M., et al., *Plague bacteria target immune cells during infection*. Science, 2005. **309**(5741): p. 1739-41.
65. Balada-Llasat, J.M. and J. Meccas, *Yersinia has a tropism for B and T cell zones of lymph nodes that is independent of the type III secretion system*. PLoS Pathog, 2006. **2**(9): p. e86.
66. Merritt, P.M., et al., *Yersinia pestis* targets neutrophils via complement receptor 3. Cell Microbiol, 2014.
67. Knirel, Y.A. and A.P. Anisimov, *Lipopolysaccharide of Yersinia pestis, the Cause of Plague: Structure, Genetics, Biological Properties*. Acta Naturae, 2012. **4**(3): p. 46-58.
68. Telepnev, M.V., et al., *Tetraacylated lipopolysaccharide of Yersinia pestis can inhibit multiple Toll-like receptor-mediated signaling pathways in human dendritic cells*. J Infect Dis, 2009. **200**(11): p. 1694-702.
69. Maeshima, N. and R.C. Fernandez, *Recognition of lipid A variants by the TLR4-MD-2 receptor complex*. Front Cell Infect Microbiol, 2013. **3**: p. 3.
70. Poltorak, A., et al., *Defective LPS signaling in C3H/HeJ and C57BL/10ScCr mice: mutations in Tlr4 gene*. Science, 1998. **282**(5396): p. 2085-8.
71. Zanoni, I., et al., *CD14 controls the LPS-induced endocytosis of Toll-like receptor 4*. Cell, 2011. **147**(4): p. 868-80.
72. Andrews, G.P., et al., *Fraction 1 capsular antigen (F1) purification from Yersinia pestis CO92 and from an Escherichia coli recombinant strain and efficacy against lethal plague challenge*. Infect Immun, 1996. **64**(6): p. 2180-7.
73. Soliakov, A., et al., *The structure of Yersinia pestis Caf1 polymer in free and adjuvant bound states*. Vaccine, 2010. **28**(35): p. 5746-54.
74. Tito, M.A., et al., *Macromolecular organization of the Yersinia pestis capsular F1 antigen: insights from time-of-flight mass spectrometry*. Protein Sci, 2001. **10**(11): p. 2408-13.
75. Cavanaugh, D.C. and R. Randall, *The role of multiplication of Pasteurella pestis in mononuclear phagocytes in the pathogenesis of flea-borne plague*. J Immunol, 1959. **83**: p. 348-63.
76. Bacot, A.W. and C.J. Martin, *LXVII. Observations on the mechanism of the transmission of plague by fleas*. J Hyg (Lond), 1914. **13**(Suppl): p. 423-39.
77. Du, Y., E. Galyov, and A. Forsberg, *Genetic analysis of virulence determinants unique to Yersinia pestis*. Contrib Microbiol Immunol, 1995. **13**: p. 321-4.
78. Chromy, B.A., et al., *Proteomic characterization of Yersinia pestis virulence*. J Bacteriol, 2005. **187**(23): p. 8172-80.
79. Karlyshev, A.V., et al., *Caf1R gene and its role in the regulation of capsule formation of Y. pestis*. FEBS Lett, 1992. **305**(1): p. 37-40.
80. Vagima, Y., et al., *Circumventing Y. pestis Virulence by Early Recruitment of Neutrophils to the Lungs during Pneumonic Plague*. PLoS Pathog, 2015. **11**(5): p. e1004893.

81. Spinner, J.L. and B.J. Hinnebusch, *The life stage of Yersinia pestis in the flea vector confers increased resistance to phagocytosis and killing by murine polymorphonuclear leukocytes*. Adv Exp Med Biol, 2012. **954**: p. 159-63.
82. Burrows, T.W. and G.A. Bacon, *The basis of virulence in Pasteurella pestis: the development of resistance to phagocytosis in vitro*. Br J Exp Pathol, 1956. **37**(3): p. 286-99.
83. Grabenstein, J.P., et al., *The response regulator PhoP of Yersinia pseudotuberculosis is important for replication in macrophages and for virulence*. Infect Immun, 2004. **72**(9): p. 4973-84.
84. Finegold, M.J., *Pneumonic plague in monkeys. An electron microscopic study*. Am J Pathol, 1969. **54**(2): p. 167-85.
85. Zhang, Y. and J.B. Bliska, *Role of macrophage apoptosis in the pathogenesis of Yersinia*. Curr Top Microbiol Immunol, 2005. **289**: p. 151-73.
86. Grabenstein, J.P., et al., *Characterization of phagosome trafficking and identification of PhoP-regulated genes important for survival of Yersinia pestis in macrophages*. Infect Immun, 2006. **74**(7): p. 3727-41.
87. Klein, K.A., *Elucidation of mechanisms of Yersinia pestis survival in macrophages by examination of phagosomal acidification and negative selection screening*, in *Genetics*. 2009, Stony Brook University: The official electronic file of this thesis or dissertation is maintained by the University Libraries on behalf of The Graduate School at Stony Brook University. p. 116.
88. Moreau, K., et al., *Autophagosomes can support Yersinia pseudotuberculosis replication in macrophages*. Cell Microbiol, 2010. **12**(8): p. 1108-23.
89. Ligeon, L.A., et al., *Role of VAMP3 and VAMP7 in the commitment of Yersinia pseudotuberculosis to LC3-associated pathways involving single- or double-membrane vacuoles*. Autophagy, 2014. **10**(9).
90. Bozue, J., et al., *The role of the phoPQ operon in the pathogenesis of the fully virulent CO92 strain of Yersinia pestis and the IP32953 strain of Yersinia pseudotuberculosis*. Microb Pathog, 2011. **50**(6): p. 314-21.
91. Rust, J.H., Jr., et al., *The role of domestic animals in the epidemiology of plague. I. Experimental infection of dogs and cats*. J Infect Dis, 1971. **124**(5): p. 522-6.
92. Desjardins, M., et al., *Biogenesis of phagolysosomes proceeds through a sequential series of interactions with the endocytic apparatus*. J Cell Biol, 1994. **124**(5): p. 677-88.
93. Roberts, E.A., et al., *Higher order Rab programming in phagolysosome biogenesis*. J Cell Biol, 2006. **174**(7): p. 923-9.
94. Kinchen, J.M. and K.S. Ravichandran, *Phagosome maturation: going through the acid test*. Nat Rev Mol Cell Biol, 2008. **9**(10): p. 781-95.
95. Vieira, O.V., R.J. Botelho, and S. Grinstein, *Phagosome maturation: aging gracefully*. Biochem J, 2002. **366**(Pt 3): p. 689-704.
96. Sarantis, H., et al., *Yersinia entry into host cells requires Rab5-dependent dephosphorylation of PI(4,5)P(2) and membrane scission*. Cell Host Microbe, 2012. **11**(2): p. 117-28.
97. Luzio, J.P., N.A. Bright, and P.R. Pryor, *The role of calcium and other ions in sorting and delivery in the late endocytic pathway*. Biochem Soc Trans, 2007. **35**(Pt 5): p. 1088-91.
98. Luzio, J.P., S.R. Gray, and N.A. Bright, *Endosome-lysosome fusion*. Biochem Soc Trans, 2010. **38**(6): p. 1413-6.
99. Luzio, J.P., et al., *ESCRT proteins and the regulation of endocytic delivery to lysosomes*. Biochem Soc Trans, 2009. **37**(Pt 1): p. 178-80.

100. Luzio, J.P., P.R. Pryor, and N.A. Bright, *Lysosomes: fusion and function*. Nat Rev Mol Cell Biol, 2007. **8**(8): p. 622-32.
101. Luzio, J.P., et al., *Membrane traffic to and from lysosomes*. Biochem Soc Symp, 2005(72): p. 77-86.
102. Stein, M.P., M.P. Muller, and A. Wandinger-Ness, *Bacterial pathogens commandeer Rab GTPases to establish intracellular niches*. Traffic, 2012. **13**(12): p. 1565-88.
103. Brumell, J.H. and M.A. Scidmore, *Manipulation of rab GTPase function by intracellular bacterial pathogens*. Microbiol Mol Biol Rev, 2007. **71**(4): p. 636-52.
104. Hilbi, H., et al., *Beyond Rab GTPases: activates the small GTPase Ran to promote microtubule polymerization, pathogen vacuole motility, and infection*. Small GTPases, 2014. **5**(1).
105. Bloom, B.R. and C.J. Murray, *Tuberculosis: commentary on a reemergent killer*. Science, 1992. **257**(5073): p. 1055-64.
106. Deretic, V., *Autophagy, an immunologic magic bullet: Mycobacterium tuberculosis phagosome maturation block and how to bypass it*. Future Microbiol, 2008. **3**(5): p. 517-24.
107. Seto, S., et al., *Dissection of Rab7 localization on Mycobacterium tuberculosis phagosome*. Biochem Biophys Res Commun, 2009. **387**(2): p. 272-7.
108. Seto, S., K. Tsujimura, and Y. Koide, *Rab GTPases regulating phagosome maturation are differentially recruited to mycobacterial phagosomes*. Traffic, 2011. **12**(4): p. 407-20.
109. Fratti, R.A., et al., *Role of phosphatidylinositol 3-kinase and Rab5 effectors in phagosomal biogenesis and mycobacterial phagosome maturation arrest*. J Cell Biol, 2001. **154**(3): p. 631-44.
110. Fratti, R.A., et al., *Mycobacterium tuberculosis glycosylated phosphatidylinositol causes phagosome maturation arrest*. Proc Natl Acad Sci U S A, 2003. **100**(9): p. 5437-42.
111. Santos, J.C. and J. Enninga, *At the crossroads: communication of bacteria-containing vacuoles with host organelles*. Cell Microbiol, 2016.
112. Price, C.T., A.M. Richards, and Y. Abu Kwaik, *Nutrient generation and retrieval from the host cell cytosol by intra-vacuolar Legionella pneumophila*. Front Cell Infect Microbiol, 2014. **4**: p. 111.
113. Chen, Y., et al., *Structural basis for Rab1 de-AMPylation by the Legionella pneumophila effector SidD*. PLoS Pathog, 2013. **9**(5): p. e1003382.
114. Del Campo, C.M., et al., *Structural basis for PI(4)P-specific membrane recruitment of the Legionella pneumophila effector DrrA/SidM*. Structure, 2014. **22**(3): p. 397-408.
115. Hardiman, C.A. and C.R. Roy, *AMPylation is critical for Rab1 localization to vacuoles containing Legionella pneumophila*. MBio, 2014. **5**(1): p. e01035-13.
116. Horenkamp, F.A., et al., *Legionella pneumophila subversion of host vesicular transport by SidC effector proteins*. Traffic, 2014. **15**(5): p. 488-99.
117. Ingmundson, A., et al., *Legionella pneumophila proteins that regulate Rab1 membrane cycling*. Nature, 2007. **450**(7168): p. 365-9.
118. Kagan, J.C., et al., *Legionella subvert the functions of Rab1 and Sec22b to create a replicative organelle*. J Exp Med, 2004. **199**(9): p. 1201-11.
119. Machner, M.P. and R.R. Isberg, *Targeting of host Rab GTPase function by the intravacuolar pathogen Legionella pneumophila*. Dev Cell, 2006. **11**(1): p. 47-56.
120. Mishra, A.K., et al., *The Legionella pneumophila GTPase activating protein LepB accelerates Rab1 deactivation by a non-canonical hydrolytic mechanism*. J Biol Chem, 2013. **288**(33): p. 24000-11.

121. Muller, M.P., et al., *The Legionella effector protein DrrA AMPylates the membrane traffic regulator Rab1b*. Science, 2010. **329**(5994): p. 946-9.
122. Murata, T., et al., *The Legionella pneumophila effector protein DrrA is a Rab1 guanine nucleotide-exchange factor*. Nat Cell Biol, 2006. **8**(9): p. 971-7.
123. Neunuebel, M.R., et al., *Legionella pneumophila LidA affects nucleotide binding and activity of the host GTPase Rab1*. J Bacteriol, 2012. **194**(6): p. 1389-400.
124. Schoebel, S., et al., *Protein LidA from Legionella is a Rab GTPase supereffector*. Proc Natl Acad Sci U S A, 2011. **108**(44): p. 17945-50.
125. Tan, Y. and Z.Q. Luo, *Legionella pneumophila SidD is a deAMPyase that modifies Rab1*. Nature, 2011. **475**(7357): p. 506-9.
126. Zhu, Y., et al., *Structural mechanism of host Rab1 activation by the bifunctional Legionella type IV effector SidM/DrrA*. Proc Natl Acad Sci U S A, 2010. **107**(10): p. 4699-704.
127. Campanacci, V., et al., *Structure of the Legionella effector AnkX reveals the mechanism of phosphocholine transfer by the FIC domain*. Embo j, 2013. **32**(10): p. 1469-77.
128. Mihai Gazdag, E., et al., *Mechanism of Rab1b deactivation by the Legionella pneumophila GAP LepB*. EMBO Rep, 2013. **14**(2): p. 199-205.
129. Tan, Y., R.J. Arnold, and Z.Q. Luo, *Legionella pneumophila regulates the small GTPase Rab1 activity by reversible phosphorylation*. Proc Natl Acad Sci U S A, 2011. **108**(52): p. 21212-7.
130. Kuhbacher, A., et al., *Genome-Wide siRNA Screen Identifies Complementary Signaling Pathways Involved in Listeria Infection and Reveals Different Actin Nucleation Mechanisms during Listeria Cell Invasion and Actin Comet Tail Formation*. MBio, 2015. **6**(3): p. e00598-15.
131. McDonough, J.A., et al., *Host Pathways Important for Coxiella burnetii Infection Revealed by Genome-Wide RNA Interference Screening*. MBio, 2013. **4**(1): p. 00606-12.
132. Ooi, Y.S., et al., *Genome-Wide RNAi Screen Identifies Novel Host Proteins Required for Alphavirus Entry*. PLoS Pathog, 2013. **9**(12): p. e1003835.
133. Thornbrough, J.M., et al., *Human genome-wide RNAi screen for host factors that modulate intracellular Salmonella growth*. PLoS One, 2012. **7**(6): p. 11.
134. Zhou, H., et al., *Genome-wide RNAi screen in IFN-gamma-treated human macrophages identifies genes mediating resistance to the intracellular pathogen Francisella tularensis*. PLoS One, 2012. **7**(2): p. e31752.
135. Akimana, C., S. Al-Khodor, and Y. Abu Kwaik, *Host factors required for modulation of phagosome biogenesis and proliferation of Francisella tularensis within the cytosol*. PLoS One, 2010. **5**(6): p. e11025.
136. Kumar, D., et al., *Genome-wide analysis of the host intracellular network that regulates survival of Mycobacterium tuberculosis*. Cell, 2010. **140**(5): p. 731-43.
137. Jayaswal, S., et al., *Identification of host-dependent survival factors for intracellular Mycobacterium tuberculosis through an siRNA screen*. PLoS Pathog, 2010. **6**(4): p. e1000839.
138. Qin, Q.M., et al., *RNAi screen of endoplasmic reticulum-associated host factors reveals a role for IRE1alpha in supporting Brucella replication*. PLoS Pathog, 2008. **4**(7): p. e1000110.
139. Krishnan, M.N., et al., *RNA interference screen for human genes associated with West Nile virus infection*. Nature, 2008. **455**(7210): p. 242-5.
140. Derre, I., et al., *RNAi screen in Drosophila cells reveals the involvement of the Tom complex in Chlamydia infection*. PLoS Pathog, 2007. **3**(10): p. 1446-58.

141. Agaisse, H., et al., *Genome-wide RNAi screen for host factors required for intracellular bacterial infection*. *Science*, 2005. **309**(5738): p. 1248-51.
142. Philips, J.A., E.J. Rubin, and N. Perrimon, *Drosophila RNAi screen reveals CD36 family member required for mycobacterial infection*. *Science*, 2005. **309**(5738): p. 1251-3.
143. Sharma, S. and A. Rao, *RNAi screening: tips and techniques*. *Nat Immunol*, 2009. **10**(8): p. 799-804.
144. Echeverri, C.J. and N. Perrimon, *High-throughput RNAi screening in cultured cells: a user's guide*. *Nat Rev Genet*, 2006. **7**(5): p. 373-84.
145. Sledz, C.A. and B.R. Williams, *RNA interference and double-stranded-RNA-activated pathways*. *Biochem Soc Trans*, 2004. **32**(Pt 6): p. 952-6.
146. Elbashir, S.M., W. Lendeckel, and T. Tuschl, *RNA interference is mediated by 21- and 22-nucleotide RNAs*. *Genes Dev*, 2001. **15**(2): p. 188-200.
147. Brummelkamp, T.R., R. Bernards, and R. Agami, *A system for stable expression of short interfering RNAs in mammalian cells*. *Science*, 2002. **296**(5567): p. 550-3.
148. Boutros, M., F. Heigwer, and C. Laufer, *Microscopy-Based High-Content Screening*. *Cell*, 2015. **163**(6): p. 1314-25.
149. Birmingham, A., et al., *Statistical methods for analysis of high-throughput RNA interference screens*. *Nat Methods*, 2009. **6**(8): p. 569-75.
150. Malo, N., et al., *Statistical practice in high-throughput screening data analysis*. *Nat Biotechnol*, 2006. **24**(2): p. 167-75.
151. Sun, Y., et al., *Development of bioluminescent bioreporters for in vitro and in vivo tracking of Yersinia pestis*. *PLoS One*, 2012. **7**(10): p. e47123.
152. Pujol, C., et al., *Replication of Yersinia pestis in interferon gamma-activated macrophages requires ripA, a gene encoded in the pigmentation locus*. *Proc Natl Acad Sci U S A*, 2005. **102**(36): p. 12909-14.
153. Andrews, G.P. and A.T. Maurelli, *mxIA of Shigella flexneri 2a, which facilitates export of invasion plasmid antigens, encodes a homolog of the low-calcium-response protein, LcrD, of Yersinia pestis*. *Infect Immun*, 1992. **60**(8): p. 3287-95.
154. Close, D., et al., *The evolution of the bacterial luciferase gene cassette (lux) as a real-time bioreporter*. *Sensors (Basel)*, 2012. **12**(1): p. 732-52.
155. Meighen, E.A., *Molecular biology of bacterial bioluminescence*. *Microbiol Rev*, 1991. **55**(1): p. 123-42.
156. Butler, T., *Plague and Other Yersinia Infections*. *Current Topics in Infectious Disease*, ed. W.B.G.I.a.T.C. Merigan. 1983, New York: Plenum Medical Book Company. 1-220.
157. Kauppi, A.M., et al., *Targeting bacterial virulence: inhibitors of type III secretion in Yersinia*. *Chem Biol*, 2003. **10**(3): p. 241-9.
158. Pan, N.J., et al., *Targeting type III secretion in Yersinia pestis*. *Antimicrob Agents Chemother*, 2009. **53**(2): p. 385-92.
159. Trcek, J., T.M. Fuchs, and K. Trulzsch, *Analysis of Yersinia enterocolitica invasion expression in vitro and in vivo using a novel luxCDABE reporter system*. *Microbiology*, 2010. **156**(Pt 9): p. 2734-45.
160. Uliczka, F., et al., *Monitoring of gene expression in bacteria during infections using an adaptable set of bioluminescent, fluorescent and colorigenic fusion vectors*. *PLoS One*, 2011. **6**(6): p. e20425.
161. Strong, P.C., et al., *Identification and characterisation of a novel adhesin Ifp in Yersinia pseudotuberculosis*. *BMC Microbiol*, 2011. **11**: p. 85.
162. Trcek, J., K. Berschl, and K. Trulzsch, *In vivo analysis of Yersinia enterocolitica infection using luxCDABE*. *FEMS Microbiol Lett*, 2010. **307**(2): p. 201-6.

163. Thorslund, S.E., et al., *The RACK1 signaling scaffold protein selectively interacts with Yersinia pseudotuberculosis virulence function*. PLoS One, 2011. **6**(2): p. e16784.
164. Nham, T., et al., *Imaging of bubonic plague dynamics by in vivo tracking of bioluminescent Yersinia pestis*. PLoS One, 2012. **7**(4): p. e34714.
165. Warawa, J.M., et al., *Bioluminescent diagnostic imaging to characterize altered respiratory tract colonization by the burkholderia pseudomallei capsule mutant*. Front Microbiol, 2011. **2**: p. 133.
166. Massey, S., et al., *In vivo Bioluminescence Imaging of Burkholderia mallei Respiratory Infection and Treatment in the Mouse Model*. Front Microbiol, 2011. **2**: p. 174.
167. Bina, X.R., M.A. Miller, and J.E. Bina, *Construction of a bioluminescence reporter plasmid for Francisella tularensis*. Plasmid, 2010. **64**(3): p. 156-61.
168. Miller, M.A., et al., *Visualization of murine intranasal dosing efficiency using luminescent Francisella tularensis: effect of instillation volume and form of anesthesia*. PLoS One, 2012. **7**(2): p. e31359.
169. Lawrenz, M.B., *Model systems to study plague pathogenesis and develop new therapeutics*. Front Microbiol, 2010. **1**: p. 119.
170. Lane, M.C., et al., *Expression of flagella is coincident with uropathogenic Escherichia coli ascension to the upper urinary tract*. Proc Natl Acad Sci U S A, 2007. **104**(42): p. 16669-74.
171. Choi, K.H., et al., *A Tn7-based broad-range bacterial cloning and expression system*. Nat Methods, 2005. **2**(6): p. 443-8.
172. Bland, D.M., et al., *Novel genetic tools for diaminopimelic acid selection in virulence studies of Yersinia pestis*. PLoS One, 2011. **6**(3): p. e17352.
173. Harrell, M.I., B.M. Iritani, and A. Ruddell, *Lymph node mapping in the mouse*. J Immunol Methods, 2008. **332**(1-2): p. 170-4.
174. Van den Broeck, W., A. Derore, and P. Simoons, *Anatomy and nomenclature of murine lymph nodes: Descriptive study and nomenclatory standardization in BALB/cAnNCrl mice*. J Immunol Methods, 2006. **312**(1-2): p. 12-9.
175. Lathem, W.W., et al., *Progression of primary pneumonic plague: a mouse model of infection, pathology, and bacterial transcriptional activity*. Proc. Natl. Acad. Sci. USA, 2005. **102**(49): p. 17786-91.
176. Lathem, W.W., et al., *A plasminogen-activating protease specifically controls the development of primary pneumonic plague*. Science, 2007. **315**(5811): p. 509-13.
177. Sodeinde, O.A., et al., *A surface protease and the invasive character of plague*. Science, 1992. **258**(5084): p. 1004-7.
178. Welkos, S.L., A.M. Friedlander, and K.J. Davis, *Studies on the role of plasminogen activator in systemic infection by virulent Yersinia pestis strain C092*. Microb Pathog, 1997. **23**(4): p. 211-23.
179. Sebbane, F., et al., *Role of the Yersinia pestis plasminogen activator in the incidence of distinct septicemic and bubonic forms of flea-borne plague*. Proc Natl Acad Sci U S A, 2006. **103**(14): p. 526-30.
180. Galen, J.E., et al., *Optimization of plasmid maintenance in the attenuated live vector vaccine strain Salmonella typhi CVD 908-htrA*. Infect. Immun., 1999. **67**(12): p. 6424-33.
181. Cathelyn, J.S., et al., *RovA, a global regulator of Yersinia pestis, specifically required for bubonic plague*. Proc. Natl. Acad. Sci. USA, 2006. **103**(36): p. 13514-9.
182. Pujol, C. and J.B. Bliska, *The ability to replicate in macrophages is conserved between Yersinia pestis and Yersinia pseudotuberculosis*. Infect. Immun., 2003. **71**(10): p. 5892-9.

183. Lawrenz, M.B., J.D. Lenz, and V.L. Miller, *A novel autotransporter adhesin is required for efficient colonization during bubonic plague*. Infect. Immun., 2009. **77**(1): p. 317-26.
184. Gonzalez, R.J., et al., *Dissemination of a highly virulent pathogen: tracking the early events that define infection*. PLoS Pathog, 2015. **11**(1): p. e1004587.
185. Bhui, T. and J.K. Roy, *Rab proteins: the key regulators of intracellular vesicle transport*. Exp Cell Res, 2014. **328**(1): p. 1-19.
186. Sturgill-Koszycki, S., U.E. Schaible, and D.G. Russell, *Mycobacterium-containing phagosomes are accessible to early endosomes and reflect a transitional state in normal phagosome biogenesis*. EMBO J, 1996. **15**(24): p. 6960-8.
187. Via, L.E., et al., *Arrest of mycobacterial phagosome maturation is caused by a block in vesicle fusion between stages controlled by rab5 and rab7*. J Biol Chem, 1997. **272**(20): p. 13326-31.
188. Campoy, E.M., F.C. Zoppino, and M.I. Colombo, *The early secretory pathway contributes to the growth of the Coxiella-replicative niche*. Infect Immun, 2011. **79**(1): p. 402-13.
189. Derre, I. and R.R. Isberg, *Legionella pneumophila replication vacuole formation involves rapid recruitment of proteins of the early secretory system*. Infect Immun, 2004. **72**(5): p. 3048-53.
190. Dong, N., et al., *Structurally distinct bacterial TBC-like GAPs link Arf GTPase to Rab1 inactivation to counteract host defenses*. Cell, 2012. **150**(5): p. 1029-41.
191. Huang, B., et al., *The Anaplasma phagocytophilum-occupied vacuole selectively recruits Rab-GTPases that are predominantly associated with recycling endosomes*. Cell Microbiol, 2010. **12**(9): p. 1292-307.
192. Huang, J., et al., *Antibacterial autophagy occurs at PI(3)P-enriched domains of the endoplasmic reticulum and requires Rab1 GTPase*. Autophagy, 2011. **7**(1): p. 17-26.
193. Neunuebel, M.R., et al., *De-AMPylation of the small GTPase Rab1 by the pathogen Legionella pneumophila*. Science, 2011. **333**(6041): p. 453-6.
194. Rzomp, K.A., et al., *Rab GTPases are recruited to chlamydial inclusions in both a species-dependent and species-independent manner*. Infect Immun, 2003. **71**(10): p. 5855-70.
195. Hardiman, C.A., et al., *The role of Rab GTPases in the transport of vacuoles containing Legionella pneumophila and Coxiella burnetii*. Biochem Soc Trans, 2012. **40**(6): p. 1353-9.
196. Tisdale, E.J., et al., *GTP-binding mutants of rab1 and rab2 are potent inhibitors of vesicular transport from the endoplasmic reticulum to the Golgi complex*. J Cell Biol, 1992. **119**(4): p. 749-61.
197. Touchot, N., et al., *Biochemical properties of the YPT-related rab1B protein. Comparison with rab1A*. FEBS Lett, 1989. **256**(1-2): p. 79-84.
198. Plutner, H., et al., *Rab1b regulates vesicular transport between the endoplasmic reticulum and successive Golgi compartments*. J Cell Biol, 1991. **115**(1): p. 31-43.
199. Ao, X., L. Zou, and Y. Wu, *Regulation of autophagy by the Rab GTPase network*. Cell Death Differ, 2014. **21**(3): p. 348-58.
200. Huang, J. and J.H. Brummell, *Bacteria-autophagy interplay: a battle for survival*. Nat Rev Microbiol, 2014.
201. Mukhopadhyay, A., J.A. Quiroz, and A.W. Wolkoff, *Rab1a regulates sorting of early endocytic vesicles*. Am J Physiol Gastrointest Liver Physiol, 2014. **306**(5): p. G412-24.
202. Mukhopadhyay, A., et al., *Proteomic analysis of endocytic vesicles: Rab1a regulates motility of early endocytic vesicles*. J Cell Sci, 2011. **124**(Pt 5): p. 765-75.

203. Arasaki, K., D.K. Toomre, and C.R. Roy, *The Legionella pneumophila effector DrrA is sufficient to stimulate SNARE-dependent membrane fusion*. Cell Host Microbe, 2012. **11**(1): p. 46-57.
204. Arasaki, K. and C.R. Roy, *Legionella pneumophila promotes functional interactions between plasma membrane syntaxins and Sec22b*. Traffic, 2010. **11**(5): p. 587-600.
205. Misselwitz, B., et al., *RNAi screen of Salmonella invasion shows role of COPI in membrane targeting of cholesterol and Cdc42*. Mol Syst Biol, 2011. **7**: p. 474.
206. Galen, J.E., et al., *Optimization of plasmid maintenance in the attenuated live vector vaccine strain Salmonella typhi CVD 908-htrA*. Infect Immun, 1999. **67**(12): p. 6424-33.
207. Kagan, J.C. and C.R. Roy, *Legionella phagosomes intercept vesicular traffic from endoplasmic reticulum exit sites*. Nat Cell Biol, 2002. **4**(12): p. 945-54.
208. Itoh, T., et al., *Screening for target Rabs of TBC (Tre-2/Bub2/Cdc16) domain-containing proteins based on their Rab-binding activity*. Genes Cells, 2006. **11**(9): p. 1023-37.
209. Satoh, A., et al., *Golgin-84 is a rab1 binding partner involved in Golgi structure*. Traffic, 2003. **4**(3): p. 153-61.
210. Martinez, O. and B. Goud, *Rab proteins*. Biochim Biophys Acta, 1998. **1404**(1-2): p. 101-12.
211. Horwitz, M.A. and F.R. Maxfield, *Legionella pneumophila inhibits acidification of its phagosome in human monocytes*. J Cell Biol, 1984. **99**(6): p. 1936-43.
212. Sturgill-Koszycki, S. and M.S. Swanson, *Legionella pneumophila replication vacuoles mature into acidic, endocytic organelles*. J Exp Med, 2000. **192**(9): p. 1261-72.
213. Ortiz Sandoval, C. and T. Simmen, *Rab proteins of the endoplasmic reticulum: functions and interactors*. Biochem Soc Trans, 2012. **40**(6): p. 1426-32.
214. Liu, S. and B. Storrie, *Are Rab proteins the link between Golgi organization and membrane trafficking?* Cell Mol Life Sci, 2012. **69**(24): p. 4093-106.
215. Gutierrez, M.G., et al., *Autophagy induction favours the generation and maturation of the Coxiella-replicative vacuoles*. Cell Microbiol, 2005. **7**(7): p. 981-93.
216. Niu, H., M. Yamaguchi, and Y. Rikihisa, *Subversion of cellular autophagy by Anaplasma phagocytophilum*. Cell Microbiol, 2008. **10**(3): p. 593-605.
217. Newton, H.J., J.A. McDonough, and C.R. Roy, *Effector protein translocation by the Coxiella burnetii Dot/Icm type IV secretion system requires endocytic maturation of the pathogen-occupied vacuole*. PLoS One, 2013. **8**(1): p. e54566.
218. Wieland, H., F. Goetz, and B. Neumeister, *Phagosomal acidification is not a prerequisite for intracellular multiplication of Legionella pneumophila in human monocytes*. J Infect Dis, 2004. **189**(9): p. 1610-4.
219. Benes, P., V. Vetvicka, and M. Fusek, *Cathepsin D--many functions of one aspartic protease*. Crit Rev Oncol Hematol, 2008. **68**(1): p. 12-28.
220. Saftig, P. and J. Klumperman, *Lysosome biogenesis and lysosomal membrane proteins: trafficking meets function*. Nat Rev Mol Cell Biol, 2009. **10**(9): p. 623-35.
221. Xu, H. and D. Ren, *Lysosomal Physiology*. Annu Rev Physiol, 2015. **77**: p. 57-80.
222. Machner, M.P. and R.R. Isberg, *A bifunctional bacterial protein links GDI displacement to Rab1 activation*. Science, 2007. **318**(5852): p. 974-7.
223. Mukherjee, S., et al., *Modulation of Rab GTPase function by a protein phosphocholine transferase*. Nature, 2011. **477**(7362): p. 103-6.
224. Abu Kwaik, Y., B.I. Eisenstein, and N.C. Engleberg, *Phenotypic modulation by Legionella pneumophila upon infection of macrophages*. Infect Immun, 1993. **61**(4): p. 1320-9.

225. Al-Khodor, S., et al., *A Dot/Icm-translocated ankyrin protein of Legionella pneumophila is required for intracellular proliferation within human macrophages and protozoa*. Mol Microbiol, 2008. **70**(4): p. 908-23.
226. Pedersen, L.L., et al., *HtrA homologue of Legionella pneumophila: an indispensable element for intracellular infection of mammalian but not protozoan cells*. Infect Immun, 2001. **69**(4): p. 2569-79.
227. Gibson, D.G., et al., *Enzymatic assembly of DNA molecules up to several hundred kilobases*. Nat Methods, 2009. **6**(5): p. 343-5.
228. Livak, K.J. and T.D. Schmittgen, *Analysis of relative gene expression data using real-time quantitative PCR and the 2(-Delta Delta C(T)) Method*. Methods, 2001. **25**(4): p. 402-8.
229. Kinder, S.A., et al., *Cloning of the YenI restriction endonuclease and methyltransferase from Yersinia enterocolitica serotype O8 and construction of a transformable R-M+ mutant*. Gene, 1993. **136**(1-2): p. 271-5.
230. Kugeler, K.J., et al., *Epidemiology of human plague in the United States, 1900-2012*. Emerg Infect Dis, 2015. **21**(1): p. 16-22.
231. Paskewitz, S.M., *Transmission factors for insect-vectored microorganisms*. Trends Microbiol, 1997. **5**(5): p. 171-3.
232. Hinnebusch, B.J., *Biofilm-dependent and biofilm-independent mechanisms of transmission of Yersinia pestis by fleas*. Adv Exp Med Biol, 2012. **954**: p. 237-43.
233. Shannon, J.G., C.F. Bosio, and B.J. Hinnebusch, *Dermal Neutrophil, Macrophage and Dendritic Cell Responses to Yersinia pestis Transmitted by Fleas*. PLoS Pathog, 2015. **11**(3): p. e1004734.
234. Finegold, M.J., et al., *Studies on the pathogenesis of plague. Blood coagulation and tissue responses of Macaca mulatta following exposure to aerosols of Pasteurella pestis*. Am J Pathol, 1968. **53**(1): p. 99-114.
235. Quan, S.F., T.H. Chen, and K.F. Meyer, *Protective action of antibiotics against the toxin of Pasteurella pestis in mice*. Proc Soc Exp Biol Med, 1950. **75**(2): p. 548-9.
236. Bindea, G., J. Galon, and B. Mlecnik, *CluePedia Cytoscape plugin: pathway insights using integrated experimental and in silico data*. Bioinformatics, 2013. **29**(5): p. 661-3.
237. Bindea, G., et al., *ClueGO: a Cytoscape plug-in to decipher functionally grouped gene ontology and pathway annotation networks*. Bioinformatics, 2009. **25**(8): p. 1091-3.
238. Grant, B.D. and J.G. Donaldson, *Pathways and mechanisms of endocytic recycling*. Nat Rev Mol Cell Biol, 2009. **10**(9): p. 597-608.
239. Li, F. and R.D. Vierstra, *Autophagy: a multifaceted intracellular system for bulk and selective recycling*. Trends Plant Sci, 2012. **17**(9): p. 526-37.
240. Daro, E., et al., *Rab4 and cellubrevin define different early endosome populations on the pathway of transferrin receptor recycling*. Proc Natl Acad Sci U S A, 1996. **93**(18): p. 9559-64.
241. Van Der Sluijs, P., et al., *The small GTP-binding protein rab4 is associated with early endosomes*. Proc Natl Acad Sci U S A, 1991. **88**(14): p. 6313-7.
242. van der Sluijs, P., et al., *Expression and properties of Rab4 and its effector rabaptin-4 in endocytic recycling*. Methods Enzymol, 2001. **329**: p. 111-9.
243. Lapierre, L.A., et al., *Myosin vb is associated with plasma membrane recycling systems*. Mol Biol Cell, 2001. **12**(6): p. 1843-57.
244. Maxfield, F.R. and T.E. McGraw, *Endocytic recycling*. Nat Rev Mol Cell Biol, 2004. **5**(2): p. 121-32.
245. Moulder, J.W., *Interaction of chlamydiae and host cells in vitro*. Microbiol Rev, 1991. **55**(1): p. 143-90.

246. Rejman Lipinski, A., et al., *Rab6 and Rab11 regulate Chlamydia trachomatis development and golgin-84-dependent Golgi fragmentation*. PLoS Pathog, 2009. **5**(10): p. e1000615.
247. Heuer, D., et al., *Chlamydia causes fragmentation of the Golgi compartment to ensure reproduction*. Nature, 2009. **457**(7230): p. 731-5.
248. Guichard, A., et al., *Anthrax toxins cooperatively inhibit endocytic recycling by the Rab11/Sec15 exocyst*. Nature, 2010. **467**(7317): p. 854-8.
249. Beemiller, P., A.D. Hoppe, and J.A. Swanson, *A phosphatidylinositol-3-kinase-dependent signal transition regulates ARF1 and ARF6 during Fcγ receptor-mediated phagocytosis*. PLoS Biol, 2006. **4**(6): p. e162.
250. Chesneau, L., et al., *An ARF6/Rab35 GTPase cascade for endocytic recycling and successful cytokinesis*. Curr Biol, 2012. **22**(2): p. 147-53.
251. Hurtado-Lorenzo, A., et al., *V-ATPase interacts with ARNO and Arf6 in early endosomes and regulates the protein degradative pathway*. Nat Cell Biol, 2006. **8**(2): p. 124-36.
252. Macia, E., et al., *Arf6 negatively controls the rapid recycling of the beta2 adrenergic receptor*. J Cell Sci, 2012. **125**(Pt 17): p. 4026-35.
253. Repella, T.L., et al., *Arf6-Dependent Intracellular Trafficking of Pasteurella multocida Toxin and pH-Dependent Translocation from Late Endosomes*. Toxins, 2011. **3**(3): p. 218-41.
254. Szatmari, Z., et al., *Rab11 facilitates cross-talk between autophagy and endosomal pathway through regulation of Hook localization*. Mol Biol Cell, 2014. **25**(4): p. 522-31.
255. Stark, C., et al., *BioGRID: a general repository for interaction datasets*. Nucleic Acids Res, 2006. **34**(Database issue): p. D535-9.
256. Szklarczyk, D., et al., *STRING v10: protein-protein interaction networks, integrated over the tree of life*. Nucleic Acids Res, 2015. **43**(Database issue): p. D447-52.
257. Shannon, P., et al., *Cytoscape: a software environment for integrated models of biomolecular interaction networks*. Genome Res, 2003. **13**(11): p. 2498-504.
258. Mi, H., et al., *PANTHER version 10: expanded protein families and functions, and analysis tools*. Nucleic Acids Res, 2016. **44**(D1): p. D336-42.
259. Schindelin, J., et al., *Fiji: an open-source platform for biological-image analysis*. Nat Methods, 2012. **9**(7): p. 676-82.
260. Cossart, P. and C.R. Roy, *Manipulation of host membrane machinery by bacterial pathogens*. Curr Opin Cell Biol, 2010. **22**(4): p. 547-54.
261. Ribet, D. and P. Cossart, *How bacterial pathogens colonize their hosts and invade deeper tissues*. Microbes Infect, 2015. **17**(3): p. 173-83.
262. Deuretzbacher, A., et al., *Beta1 integrin-dependent engulfment of Yersinia enterocolitica by macrophages is coupled to the activation of autophagy and suppressed by type III protein secretion*. J Immunol, 2009. **183**(9): p. 5847-60.
263. Isberg, R.R., D.L. Voorhis, and S. Falkow, *Identification of invasins: a protein that allows enteric bacteria to penetrate cultured mammalian cells*. Cell, 1987. **50**(5): p. 769-78.
264. Kreibich, S., et al., *Autophagy Proteins Promote Repair of Endosomal Membranes Damaged by the Salmonella Type Three Secretion System 1*. Cell Host Microbe, 2015. **18**(5): p. 527-37.
265. Kolodziejek, A.M., C.J. Hovde, and S.A. Minnich, *Yersinia pestis Ail: multiple roles of a single protein*. Front Cell Infect Microbiol, 2012. **2**: p. 103.
266. Falkow, S., *Bacterial entry into eukaryotic cells*. Cell, 1991. **65**(7): p. 1099-102.
267. Leo, J.C. and M. Skurnik, *Adhesins of human pathogens from the genus Yersinia*. Adv Exp Med Biol, 2011. **715**: p. 1-15.

268. Elvin, S.J., et al., *Evolutionary genetics: Ambiguous role of CCR5 in Y. pestis infection*. Nature, 2004. **430**(6998): p. 417.
269. Ng, L.C., et al., *The response of murine macrophages to infection with Yersinia pestis as revealed by DNA microarray analysis*. Adv Exp Med Biol, 2003. **529**: p. 155-60.
270. Zhang, P., et al., *Human dendritic cell-specific intercellular adhesion molecule-grabbing nonintegrin (CD209) is a receptor for Yersinia pestis that promotes phagocytosis by dendritic cells*. Infect Immun, 2008. **76**(5): p. 2070-9.
271. Meccas, J., et al., *Evolutionary genetics: CCR5 mutation and plague protection*. Nature, 2004. **427**(6975): p. 606.
272. Yang, K., et al., *Host Langerin (CD207) is a receptor for Yersinia pestis phagocytosis and promotes dissemination*. Immunol Cell Biol, 2015. **93**(9): p. 815-24.
273. Yang, K., et al., *Host Langerin (CD207) is a receptor for Yersinia pestis phagocytosis and promotes dissemination*. Immunol Cell Biol, 2015.
274. Razi, M., E.Y. Chan, and S.A. Tooze, *Early endosomes and endosomal coatomer are required for autophagy*. J Cell Biol, 2009. **185**(2): p. 305-21.
275. Styers, M.L., et al., *Depletion of beta-COP reveals a role for COP-I in compartmentalization of secretory compartments and in biosynthetic transport of caveolin-1*. Am J Physiol Cell Physiol, 2008. **294**(6): p. C1485-98.
276. Schliwa, M., *Action of cytochalasin D on cytoskeletal networks*. J Cell Biol, 1982. **92**(1): p. 79-91.
277. Azouz, N.P., et al., *Decoding the regulation of mast cell exocytosis by networks of Rab GTPases*. J Immunol, 2012. **189**(5): p. 2169-80.
278. Baltierra-Uribe, S.L., et al., *Mycobacteria entry and trafficking into endothelial cells*. Can J Microbiol, 2014. **60**(9): p. 569-77.
279. Croxatto, A. and G. Greub, *Early intracellular trafficking of Waddlia chondrophila in human macrophages*. Microbiology, 2010. **156**(Pt 2): p. 340-55.
280. Finlay, B.B. and S. Falkow, *Comparison of the invasion strategies used by Salmonella cholerae-suis, Shigella flexneri and Yersinia enterocolitica to enter cultured animal cells: endosome acidification is not required for bacterial invasion or intracellular replication*. Biochimie, 1988. **70**(8): p. 1089-99.
281. Garcia-del Portillo, F., et al., *Salmonella typhimurium induces selective aggregation and internalization of host cell surface proteins during invasion of epithelial cells*. J Cell Sci, 1994. **107 (Pt 7)**: p. 2005-20.
282. Guerra, C.R., et al., *Cryptococcus neoformans is internalized by receptor-mediated or 'triggered' phagocytosis, dependent on actin recruitment*. PLoS One, 2014. **9**(2): p. e89250.
283. Hsu, C.R., et al., *Klebsiella pneumoniae translocates across the intestinal epithelium via Rho GTPase- and phosphatidylinositol 3-kinase/Akt-dependent cell invasion*. Infect Immun, 2015. **83**(2): p. 769-79.
284. Kuhn, M., *The microtubule depolymerizing drugs nocodazole and colchicine inhibit the uptake of Listeria monocytogenes by P388D1 macrophages*. FEMS Microbiol Lett, 1998. **160**(1): p. 87-90.
285. Levenhagen, M.A., et al., *The role of cytoskeleton, components of inositol phospholipid signaling pathway and iron in Ehrlichia canis in vitro proliferation*. Vet Res Commun, 2012. **36**(3): p. 195-9.
286. Macdonald, L.J., et al., *Coxiella burnetii exploits host cAMP-dependent protein kinase signalling to promote macrophage survival*. Cell Microbiol, 2013. **13**(10): p. 12213.

287. Mi, H., et al., *Large-scale gene function analysis with the PANTHER classification system*. Nat Protoc, 2013. **8**(8): p. 1551-66.
288. Watson, P.J., et al., *Gamma-COP appendage domain - structure and function*. Traffic, 2004. **5**(2): p. 79-88.
289. Stenmark, H., *Rab GTPases as coordinators of vesicle traffic*. Nat Rev Mol Cell Biol, 2009. **10**(8): p. 513-25.
290. Stenmark, H. and V.M. Olkkonen, *The Rab GTPase family*. Genome Biol, 2001. **2**(5): p. Reviews3007.
291. Chauvaux, S., et al., *Transcriptome analysis of Yersinia pestis in human plasma: an approach for discovering bacterial genes involved in septicemic plague*. Microbiology, 2007. **153**(Pt 9): p. 3112-24.
292. Klein, K.A., et al., *A transposon site hybridization screen identifies galU and wecBC as important for survival of Yersinia pestis in murine macrophages*. J Bacteriol, 2012. **194**(3): p. 653-62.
293. Ponnusamy, D., et al., *High-throughput signature-tagged mutagenic approach to identify novel virulence factors of Yersinia pestis CO92 in a mouse model of infection*. Infect Immun, 2015.
294. Pereira-Leal, J.B. and M.C. Seabra, *Evolution of the Rab family of small GTP-binding proteins*. J Mol Biol, 2001. **313**(4): p. 889-901.
295. Pereira-Leal, J.B. and M.C. Seabra, *The mammalian Rab family of small GTPases: definition of family and subfamily sequence motifs suggests a mechanism for functional specificity in the Ras superfamily*. J Mol Biol, 2000. **301**(4): p. 1077-87.
296. Schwartz, S.L., et al., *Rab GTPases at a glance*. J Cell Sci, 2007. **120**(Pt 22): p. 3905-10.
297. Diekmann, Y., et al., *Thousands of rab GTPases for the cell biologist*. PLoS Comput Biol, 2011. **7**(10): p. e1002217.
298. Longatti, A. and S.A. Tooze, *Recycling endosomes contribute to autophagosome formation*. Autophagy, 2012. **8**(11): p. 1682-3.
299. Alem, F., et al., *Host response during Yersinia pestis infection of human bronchial epithelial cells involves negative regulation of autophagy and suggests a modulation of survival-related and cellular growth pathways*. Front Microbiol, 2015. **6**: p. 50.
300. Larson, C.L., et al., *Coxiella burnetii effector protein subverts clathrin-mediated vesicular trafficking for pathogen vacuole biogenesis*. Proc Natl Acad Sci U S A, 2013. **110**(49): p. E4770-9.
301. Larson, C.L., et al., *Coxiella burnetii Effector Proteins That Localize to the Parasitophorous Vacuole Membrane Promote Intracellular Replication*. Infect Immun, 2015. **83**(2): p. 661-70.
302. Newton, H.J., et al., *A screen of Coxiella burnetii mutants reveals important roles for Dot/Icm effectors and host autophagy in vacuole biogenesis*. PLoS Pathog, 2014. **10**(7): p. e1004286.
303. Brock, S.C., J.R. Goldenring, and J.E. Crowe, Jr., *Apical recycling systems regulate directional budding of respiratory syncytial virus from polarized epithelial cells*. Proc Natl Acad Sci U S A, 2003. **100**(25): p. 15143-8.
304. Hoffmann, C., et al., *Functional analysis of novel Rab GTPases identified in the proteome of purified Legionella-containing vacuoles from macrophages*. Cell Microbiol, 2013.
305. Mounier, J., et al., *Shigella effector IpaB-induced cholesterol relocation disrupts the Golgi complex and recycling network to inhibit host cell secretion*. Cell Host Microbe, 2012. **12**(3): p. 381-9.

306. Mellouk, N., et al., *Shigella* subverts the host recycling compartment to rupture its vacuole. *Cell Host Microbe*, 2014. **16**(4): p. 517-30.
307. Smith, A.C., et al., *Interaction of the Salmonella-containing vacuole with the endocytic recycling system*. *J Biol Chem*, 2005. **280**(26): p. 24634-41.
308. Guichard, A., et al., *Cholera toxin disrupts barrier function by inhibiting exocyst-mediated trafficking of host proteins to intestinal cell junctions*. *Cell Host Microbe*, 2013. **14**(3): p. 294-305.
309. Galli, T., et al., *Tetanus toxin-mediated cleavage of cellubrevin impairs exocytosis of transferrin receptor-containing vesicles in CHO cells*. *J Cell Biol*, 1994. **125**(5): p. 1015-24.
310. Wilcke, M., et al., *Rab11 regulates the compartmentalization of early endosomes required for efficient transport from early endosomes to the trans-golgi network*. *J Cell Biol*, 2000. **151**(6): p. 1207-20.
311. Halaas, O., et al., *Intracellular Mycobacterium avium intersect transferrin in the Rab11(+) recycling endocytic pathway and avoid lipocalin 2 trafficking to the lysosomal pathway*. *J Infect Dis*, 2010. **201**(5): p. 783-92.
312. Rowe, R.K., J.W. Suszko, and A. Pekosz, *Roles for the recycling endosome, Rab8, and Rab11 in hantavirus release from epithelial cells*. *Virology*, 2008. **382**(2): p. 239-49.
313. Guichard, A., V. Nizet, and E. Bier, *RAB11-mediated trafficking in host-pathogen interactions*. *Nat Rev Microbiol*, 2014. **12**(9): p. 624-34.
314. Ray, K., et al., *Life on the inside: the intracellular lifestyle of cytosolic bacteria*. *Nat Rev Microbiol*, 2009. **7**(5): p. 333-40.
315. Xu, Y., et al., *Toll-like receptor 4 is a sensor for autophagy associated with innate immunity*. *Immunity*, 2007. **27**(1): p. 135-44.
316. Pechous, R.D., et al., *In vivo transcriptional profiling of Yersinia pestis reveals a novel bacterial mediator of pulmonary inflammation*. *MBio*, 2015. **6**(1): p. e02302-14.
317. Sivaraman, V., et al., *Yersinia pestis activates both IL-1beta and IL-1 receptor antagonist to modulate lung inflammation during pneumonic plague*. *PLoS Pathog*, 2015. **11**(3): p. e1004688.
318. Agar, S.L., et al., *Characterization of the rat pneumonic plague model: infection kinetics following aerosolization of Yersinia pestis CO92*. *Microbes Infect*, 2009. **11**(2): p. 205-14.
319. Agar, S.L., et al., *Characterization of a mouse model of plague after aerosolization of Yersinia pestis CO92*. *Microbiology*, 2008. **154**(Pt 7): p. 1939-48.
320. Comer, J.E., et al., *Transcriptomic and innate immune responses to Yersinia pestis in the lymph node during bubonic plague*. *Infect Immun*, 2010. **78**(12): p. 5086-98.
321. Das, R., et al., *Study of proinflammatory responses induced by Yersinia pestis in human monocytes using cDNA arrays*. *Genes Immun*, 2007. **8**(4): p. 308-19.
322. Du, Z., et al., *Transcriptomic Response to Yersinia pestis: RIG-I Like Receptor Signaling Response Is Detrimental to the Host against Plague*. *J Genet Genomics*, 2014. **41**(7): p. 379-96.
323. Schoberle, T.J., et al., *Uncovering an Important Role for YopJ in the Inhibition of Caspase-1 in Activated Macrophages and Promoting Yersinia pseudotuberculosis Virulence*. *Infect Immun*, 2016.
324. Zheng, Y., et al., *YopJ-Induced Caspase-1 Activation in Yersinia-Infected Macrophages: Independent of Apoptosis, Linked to Necrosis, Dispensable for Innate Host Defense*. *PLoS One*, 2012. **7**(4): p. e36019.
325. Brodsky, I.E., et al., *A Yersinia effector protein promotes virulence by preventing inflammasome recognition of the type III secretion system*. *Cell Host Microbe*, 2010. **7**(5): p. 376-87.

326. Husebye, H., et al., *The Rab11a GTPase controls Toll-like receptor 4-induced activation of interferon regulatory factor-3 on phagosomes*. *Immunity*, 2010. **33**(4): p. 583-96.
327. Czerkies, M., et al., *An interplay between scavenger receptor A and CD14 during activation of J774 cells by high concentrations of LPS*. *Immunobiology*, 2013. **218**(10): p. 1217-26.
328. Nair-Gupta, P., et al., *TLR signals induce phagosomal MHC-I delivery from the endosomal recycling compartment to allow cross-presentation*. *Cell*, 2014. **158**(3): p. 506-21.
329. Nair-Gupta, P. and J.M. Blander, *An updated view of the intracellular mechanisms regulating cross-presentation*. *Front Immunol*, 2013. **4**: p. 401.
330. Weigert, R., et al., *Rab22a regulates the recycling of membrane proteins internalized independently of clathrin*. *Mol Biol Cell*, 2004. **15**(8): p. 3758-70.
331. van Ijzendoorn, S.C., *Recycling endosomes*. *J Cell Sci*, 2006. **119**(Pt 9): p. 1679-81.
332. Neel, N.F., et al., *Chemokine receptor internalization and intracellular trafficking*. *Cytokine Growth Factor Rev*, 2005. **16**(6): p. 637-58.
333. Haasken, S., et al., *Macrophage scavenger receptor 1 (Msr1, SR-A) influences B cell autoimmunity by regulating soluble autoantigen concentration*. *J Immunol*, 2013. **191**(3): p. 1055-62.
334. D'Souza, R.S., et al., *Rab4 orchestrates a small GTPase cascade for recruitment of adaptor proteins to early endosomes*. *Curr Biol*, 2014. **24**(11): p. 1187-98.
335. Johnson, D.E., et al., *The position of lysosomes within the cell determines their luminal pH*. *J Cell Biol*, 2016. **212**(6): p. 677-92.
336. Fukui, G.M., et al., *Studies on the relation of cultural conditions and virulence of Pasteurella pestis*. *J Bacteriol*, 1957. **74**(6): p. 714-7.
337. Higuchi, K., L.L. Kupferberg, and J.L. Smith, *Studies on the nutrition and physiology of Pasteurella pestis. III. Effects of calcium ions on the growth of virulent and avirulent strains of Pasteurella pestis*. *J Bacteriol*, 1959. **77**(3): p. 317-21.
338. Barve, S.S. and S.C. Straley, *lcrR, a low-Ca²⁺-response locus with dual Ca²⁺-dependent functions in Yersinia pestis*. *J Bacteriol*, 1990. **172**(8): p. 4661-71.
339. Fowler, J.M., et al., *Growth of calcium-blind mutants of Yersinia pestis at 37 degrees C in permissive Ca²⁺-deficient environments*. *Microbiology*, 2009. **155**(Pt 8): p. 2509-21.
340. Perry, R.D., et al., *DNA sequencing and analysis of the low-Ca²⁺-response plasmid pCD1 of Yersinia pestis KIM5*. *Infect Immun*, 1998. **66**(10): p. 4611-23.
341. Skrzypek, E. and S.C. Straley, *Differential effects of deletions in lcrV on secretion of V antigen, regulation of the low-Ca²⁺ response, and virulence of Yersinia pestis*. *J Bacteriol*, 1995. **177**(9): p. 2530-42.
342. Fader, C.M., et al., *Induction of autophagy promotes fusion of multivesicular bodies with autophagic vacuoles in k562 cells*. *Traffic*, 2008. **9**(2): p. 230-50.
343. Savina, A., et al., *Rab11 promotes docking and fusion of multivesicular bodies in a calcium-dependent manner*. *Traffic*, 2005. **6**(2): p. 131-43.
344. Schwiesow, L., et al., *The Yersinia type III secretion system master regulator LcrF*. *J Bacteriol*, 2015.

APPENDIX

Below are the acknowledgments and distribution permissions for each of the previously-published chapters (chapters I and III). Both published chapters are in PLOS (public library of science) open-access journals, which apply the Creative Commons Attribution (CC BY; creativecommons.org) license to all published materials. Under this license, anyone may reproduce, distribute, or reuse these articles as long as the author and original source are cited properly.

Chapter II

Acknowledgements

We thank M. Chelsea Lane and Harry Mobley for pGEN-*luxCDABE* plasmid, Herb Schweizer for the Tn7 system, Eric Weening and Virginia Miller for pUC18r6k-mini-Tn7(kanEW) plasmid, and Bill Goldman for the $\Delta p/a$ strain. We would also like to thank the vivarium staff and the BIO-Imaging Core at the Center for Predictive Medicine for support during these experiments and Jonathan Warawa for sharing the *Pto/C* template DNA, advice on in vivo imaging, and critical review of this manuscript. We also acknowledge helpful discussions throughout these studies with the faculty members of the Center for Predictive Medicine

Chapter III

Acknowledgements

We thank James Galen (University of Maryland) and Harry Mobley (University of Michigan) for pGEN222 and pGEN-*P_{EM7}::DsRED* and Dr. Shintaro Seto (Hamamatsu University School of Medicine) for pEGFP-Rab1B. The following reagent was obtained through BEI Resources, NIAID, NIH: *Yersinia pestis*, Strain KIM Derivative 19 (D19), NR-4681. We also thank Donghoon Chung for advice during these studies and Maria Gutierrez for helpful discussions.

DEPARTMENT OF MICROBIOLOGY AND IMMUNOLOGY CHAIRMAN'S
CITATION



■ DEPARTMENT OF
MICROBIOLOGY AND
IMMUNOLOGY
School of Medicine
University of Louisville
Louisville, Kentucky 40292
Office: 502-852-5351
Fax: 502-852-7531

April 13, 2016

Mr. Michael Connor
Ph.D. Candidate
Department of Microbiology and Immunology

Dear Michael,

The Department of Microbiology and Immunology recognizes your dedication and hard work, which as communicated to me by your thesis advisor Dr. Matthew Lawrenz, has resulted in the publication of 2 first author papers in *PLOS Pathogens* and *Frontiers in Microbiology*. I am also aware of your pending first author paper and a second author publication in *Plos One*.

This level of productivity is indeed exceptional and sets a commendable example for all our students. I wish you continued success in your future endeavors.

Congratulations!

Sincerely,

Nejat Egilmez, Ph.D.
Professor and Chairman
Department of Microbiology and Immunology

CURRICULUM VITAE

Michael Graylin Connor

Work: Center for Predictive Medicine
Dept. of Microbiology and Immunology
505 S Hancock Street Rm 633
Louisville, KY 40202

Home: 734 Bermuda Lane
Louisville, KY 40213

Born: February 10, 1988 Atlanta Georgia USA

Email: connormg@gmail.com
mgconn01@louisville.edu

Education

Ph.D Microbiology and Immunology, May 2016
University of Louisville, Louisville KY

Mentor: Matthew B. Lawrenz

Dissertation: "Identification of host factors required for *Yersinia pestis* macrophage Intracellular survival and their impact on vacuole maturation, acidification and trafficking"

M.S. Microbiology and Immunology, May 2012
University of Louisville, Louisville KY

Mentor: Matthew B. Lawrenz

B.S. Biology Pre-Health, May 2010
Lees-McRae College, Banner Elk NC

Peer-reviewed Manuscripts (* denotes co-first author)

1. Jason Nathaniel Payne*, Hitesh Kumar Waghwani*, **Michael G Connor***, Sarah Tockstein, Harsh Moolani, William Robert Hamilton, Vivek Badwaik, Fenil Chavda, Matthew B Lawrenz, Rajalingam Dakshinamurthy. (2016) Novel Synthesis of Kanamycin Conjugated Gold Nanoparticles with Potent Antibacterial Activity. *In press*. Front. Microbiol. Antimicrobials, Resistance and Chemotherapy. Manuscript ID: 177773.
1. **Connor MG**, Pulsifer AR, Price CT, Abu Kwaik Y, Lawrenz MB (2015) *Yersinia pestis* Requires Host Rab1b for Survival in Macrophages. PLoS Pathog 11(10): e1005241. doi:10.1371/journal.ppat.1005241
2. Sun Y, **Connor MG**, Pennington JM, Lawrenz MB (2012) Development of Bioluminescent Bioreporters for In Vitro and In Vivo Tracking of *Yersinia pestis*. PLoS ONE 7(10): e47123. doi:10.1371/journal.pone.0047123

Oral presentations and invited lectures

1. 2015-07-24 2nd Midwest Membrane Trafficking and Signaling Symposium, Louisville, KY.
“*Y. pestis* Exploits Host Rab GTPases for Intracellular Survival”
2. 2015-07-28 Guest Research Presentation, Dr. Virginia Miller, University of North Carolina, Chapel Hill, NC.
“Genome-wide RNAi High-throughput Screen Identifies Host Trafficking as Critical for *Y. pestis* Intracellular Survival”
3. 2015-04-09 Microbiology & Immunology Seminar Series. University of Louisville, Louisville, KY.
“RNAi High-throughput Screen Identifies Host Endocytic Trafficking as Critical for *Y. pestis* Intracellular Survival”
4. 2015-03-25 Bioinformatics Seminar Series. University of Louisville, Louisville, KY.
“Identifying How *Y. pestis* exploits the Host Macrophage”
5. 2014-10-31 Graduate School Research Symposium Series. University of Louisville, Louisville, KY.
“Understanding How Plague Manipulates the Host Macrophage”
6. 2013-10-31 Microbiology & Immunology Seminar Series. University of Louisville, Louisville, KY.
“Exploiting the Host. Using a RNAi High-throughput Screen to Identify Host Factors Exploited by *Y. pestis* for Macrophage Survival”
7. 2012 Center for Predictive Medicine Retreat. University of Louisville, Louisville, KY.
“Unlocking *Yersinia pestis* Intracellular Survival”

Posters and other scientific contributions (selected for talk)**

1. 2015 Midwest Microbial Pathogenesis Conference, Indianapolis, IN.
“*Yersinia pestis* exploits the host endosome recycling pathway for intracellular survival”; Michael G. Connor, Amanda R. Pulsifer, Eric Rouchka, Donghoon Chung, Matthew B. Lawrenz.
2. **2015 2nd Midwest Membrane Trafficking and Signaling Symposium, Louisville, KY.
“*Y. pestis* Exploits Host Rab GTPases for Intracellular Survival”; Connor M. G, Pulsifer A. R, and M.B. Lawrenz.
3. 2014 Gordon Research Conference, Toxins and Microbial Pathogenesis, Waterville Valley, NH.
“RNAi High-Throughput Screen Identifies Novel Host Factors Exploited By *Y. pestis* For Intracellular Survival”; Michael G. Connor, Donghoon Chung, Matthew B. Lawrenz.
4. 2014 Gordon Research Conference, Toxins and Microbial Pathogenesis, Waterville Valley, NH.
“Host Rab1B Is Required for *Yersinia pestis* Intracellular Survival”; Michael G. Connor, Amanda R. Pulsifer, Jarrod M. Pennington and Matthew B. Lawrenz.
5. 2014 Midwest Membrane Trafficking and Signaling Symposium, Louisville, KY.
“Host Rab1B Is Required for *Yersinia pestis* Intracellular Survival”; Michael G. Connor, Amanda R. Pulsifer, Jarrod M. Pennington and Matthew B. Lawrenz.
6. 2013 11th International Conference on *Yersinia*, Suzhou, China.

- “Development of a High Throughput Assay to Identify Host Factors Required for *Yersinia pestis* Survival in Macrophages”; Michael G. Connor, Yanwen Sun, Donghoon Chung, and Matthew B. Lawrenz.
7. 2013 Midwest Microbial Pathogenesis Conference, Columbus, OH.
“Unlocking *Yersinia pestis* intracellular survival from the host’s perspective using an RNAi high throughput screen”; Michael G. Connor, Yanwen Sun, Donghoon Chung, and Matthew B. Lawrenz.
 8. 2013 Research Louisville, Louisville, KY.
“Unlocking *Yersinia pestis* intracellular survival from the host’s perspective using an RNAi high throughput screen”; Michael G. Connor, Yanwen Sun, Donghoon Chung, and Matthew B. Lawrenz (Finalist for Best Graduate Student Poster).
 9. 2012 Research Louisville, Louisville, KY.
“Developing a bioluminescent high throughput siRNA screen for *Yersinia pestis*”; Michael G. Connor, Yanwen Sun, Jarrod M. Pennington, Donghoon Chung, and Matthew B. Lawrenz.
 10. 2009 SEPEEG, Dahlonega, GA.
“Measure Correlation Between Levels of Genetic Variation and Infestation by the Hemlock Woolly Adelgid in Stands of Carolina Hemlock”; Michael G. Connor, Jennifer C. Hurd and Stephanie Stewart.
 11. 2009 REU symposium, Athens, GA.
“*Natronolimnobius ‘aegyptiacus’*: A Novel Poly-extremophilic Archaeon Isolated from the Alkaline, Hypersaline Lakes of Wadi An Natrun, Egypt”; Michael G. Connor, Karen J. Bowers, Noha M. Mesbah, Felipe Sarmiento and Juergen Wiegel.

Fellowships

2011-2013 University of Louisville IPIBS Graduate Fellowship

Awards

2016 Department of Microbiology and Immunology Chairman’s Citation
 2015 Graduate School Travel Award: Midwest Microbial Pathogenesis Conference (MMPC)
 2014 University of Louisville Grant Writing Academy
 2014-2016 University of Louisville SIGS Tuition Match Award
 2013 Graduate School Travel Award: Midwest Microbial Pathogenesis Conference (MMPC)
 2013 Research Louisville Top Poster Finalist: “Unlocking *Yersinia pestis* Intracellular Survival from the Host’s Perspective Using a RNAi High Throughput Screen”

Service and memberships

2015 Kentucky Science Fair Judge
 2015 Louisville Regional Science Fair Judge
 2015 duPont Manual Science Fair Judge
 2014 - Present Animal House Shelter Volunteer

2011-Present American Society for Microbiology (ASM)
 2014-Present The American Society for Cell Biology (ASCB)

Employment

Ph.D Candidate

Microbiology & Immunology Ph.D Thesis Research
Dr. Lawrenz Lab, Center for Predictive Medicine; Louisville, KY

Title: Identification of host factors exploited by *Yersinia pestis* for survival in the macrophage.

Goal: Develop and complete a genome-wide RNAi high-throughput screen to identify host factors exploited by *Yersinia pestis* for survival within the macrophage.

2011–Present

Ph.D Rotation Student

Microbiology & Immunology Ph.D Rotation
Dr. Mitchell Lab, Institute for Cellular Therapeutics; Louisville, KY

Task: Learn flow cytometry, primary cell culture, and Dendritic cell differentiation procedures.

2012

Ph.D Rotation Student

Microbiology & Immunology Ph.D Rotation
Dr. Lawrenz Lab, Center for Predictive Medicine; Louisville, KY

Task: Develop a high-throughput RAW264.7 macrophage *Y. pestis* infection assay.

2011

Laboratory Technologist I

Products and Molecular Genetics Laboratory Technologist I
Bryce Burkhardt, LabCorp; RTP, NC

Task: Produce oligomers and diagnostic testing reagents for commercial molecular genetics testing in a GLP compliant laboratory.

2010–2011

Researcher

Lees-McRae College: NC Biotech Grant Researcher
Dr. Chrissy Spencer, Lees-McRae College; Banner Elk, NC

Title: Measure Correlation Between Levels of Genetic Variation and Infestation by the Hemlock Woolly Adelgid in Stands of Carolina Hemlock.

Goal: Identify heterozygosity of Carolina Hemlock tree stands in relationship to Hemlock Woolly Adelgid infestation.

2009–2010

Summer Researcher

REU Researcher
Dr. Juergen Wiegel, University of Georgia; Athens, GA

Title: Characterization of a novel polyextremophile, *Natronolimnobius* 'aegyptiacus'.

Goal: Characterize the growth range of the novel polyextremophile *Natronolimnobius* 'aegyptiacus'.

2009